Fire Resistance of Light Timber Framed Walls and Floors

A thesis submitted in partial fulfilment of the

requirements for the Degree of

Doctor of Philosophy in Fire Engineering

in the

University of Canterbury

by

Geoffrey Charles Thomas

University of Canterbury

1996

Table of Contents

Abstract

The structural fire resistance of light timber frame walls and floors has traditionally been determined by using standard fire resistance tests to provide a Fire Resistance Rating (FRR). The required FRR was prescribed by building codes and had little relation to likely fire severity. More recently, simple formulae have been used to determine an appropriate FRR given the ventilation parameters of a compartment, the likely fuel load and to a lesser extent the thermal properties of the compartment boundaries.

The work described in this thesis determines the validity of these formulae for light timber frame walls and floors and other materials.

It is shown that, computer modelling can be used to determine the thermal and structural performance of light timber frame walls and floors exposed to fire. The COMPF-2 program can be used with modification to model compartment fires. The thermal behaviour of cavity walls and floors exposed to fire can be modelled accurately using the TASEF program. The structural behaviour of light timber frame walls and floors exposed to fire can be modelled using a general purpose finite element program, such as ABAQUS.

The temperature dependent thermal properties used in the thermal model and the temperature dependent mechanical properties used in the structural model may not be absolutely accurate values, but are effective values that are (modifications of known values within a reasonable range) determined in the calibration process.

A simple temperature based failure criterion has been devised for the structural response of light timber frame walls and floors exposed to fires.

This study shows that simple time equivalent formulae are not suitable for the prediction of such a complex and variable phenomenon as the response of structures to fire.

For accurate prediction of structural response under fire exposure, a more rigorous computer based analysis can be used to give much more reliable results than a simple time equivalent method.

Chapter 1 Introduction

The objective of this study was to determine whether available computer models can be utilised to predict the behaviour of light timber framed walls and floors when exposed to fires other than the standard ISO-834 furnace test. The study also investigates the validity of formulae used to predict the response of structures to compartment fires expressed as an equivalent time of exposure to the standard fire test.

1.1 Previous Work in this Field

The author (Thomas 1991) undertook a feasibility study of building a six storey hostel in timber. The six storey hostel was feasible and economically advantageous over a concrete building. Acoustic separation was harder to achieve, requiring extra layers of gypsum plaster board in excess of those required for fire resistance. The structural limitation was the axial capacity of studs that had been tested using the ISO-834 (ISO 1975) fire test with 10 kN on each 150*50 mm stud. With the extra layers of protection required for acoustic reasons and the likely less severe fire exposure due to a real compartment fire, this capacity could be increased, hence a more economic design would result as a larger stud spacing would be used.

A review of current literature was undertaken in order to avoid repeating work already done and to determine which of the sub-models require further work. The literature review is incorporated as part of the relevant Chapters, to make this dissertation more readable.

1.1.1 Methods of Determining Fire Resistance

Until now, the fire resistance of light timber framed walls and floors has generally been determined using wall assemblies exposed under controlled conditions to the ISO-834 standard fire test. With the advent of performance based codes in New Zealand (NZBIA 1992) and overseas, the need for the prediction of the structural performance of light

timber frame walls exposed to real fires was perceived. Collier (1996) has developed a design method for extrapolating test results for light timber framed walls exposed to the ISO-834 standard test. Gammon (1987) and Mehaffey (Mehaffey et al 1994, Cuerrier 1993, Mehaffey 1991) have developed computer models to predict the response of light timber framed walls to the ASTM standard fire test (ASTM 1985). Cramer (1995) has developed an analytical model for predicting the performance of floor/ceiling assemblies, taking account of partial composite action and load-sharing, during fire exposure. Clancy (Clancy 1994, Young and Clancy 1996) are in the process of developing a thermal and structural model of light timber framed walls.

Clancy (1996) is developing a probabilistic model for light timber framed assemblies exposed to real compartment fires.

The use of the ISO-834 test for the determination of fire resistance has major flaws, mainly that the thermal load on an element of building structure in a real fire may be significantly different from that in a test, due to different temperature histories, and different convective and radiative boundary conditions. These conditions may also vary from furnace to furnace.

To enhance the use of structural light timber frame assemblies in multi-unit residential, motel/hotel type buildings a simple time equivalent formula relating the ISO-834 test results to significant compartment fire parameters would be highly desirable. This formula would probably be similar to the CIB time equivalent formula for steel members. This formula is described in the next Section.

1.2 Time Equivalence

For the purposes of this dissertation the equivalent fire severity is the time at which the worst (either maximum or minimum) value of a specified parameter at a characteristic location in a structure exposed to a 'real' compartment fire, is reached in a furnace test. The most common parameter used in determining equivalent fire severity is the time at which load bearing capacity reaches a minimum. The other common parameter is maximum temperature.

For example, if an element of structure exposed to a real compartment fire is heated to such an extent that it loses a maximum of 50% of its cold strength and in an ISO-834

test the same element loses 50% of its strength after 45 minutes; then the real compartment fire is said to have an equivalent fire severity of 45 minutes, as shown in Figure 1.1.

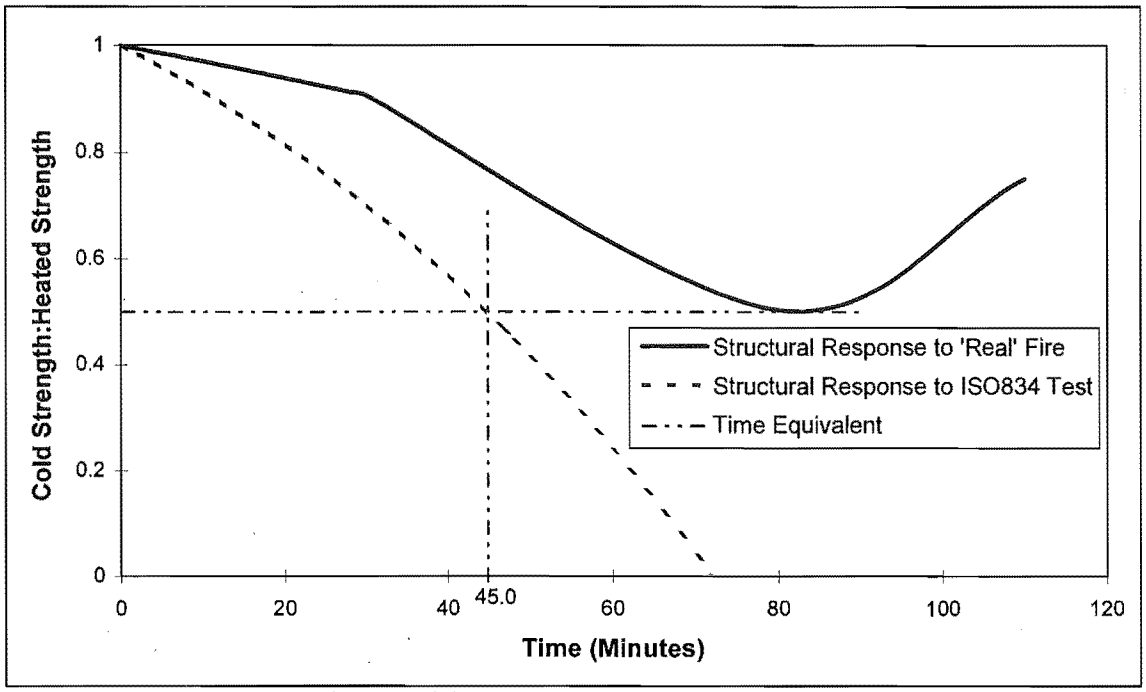

Figure 1.1 Definition of Structural Time Equivalence.

For temperature, the equivalent time of fire exposure is the time that the element would have to be exposed to the ISO-834 furnace test, for the temperature at some critical location to reach the maximum temperature obtained during exposure to a real fire.

The two temperature locations chosen for the thermal analysis part of the work in this dissertation, are shown in Figure 1.2. These locations are also those used in furnace tests at BRANZ (Collier 1991a).

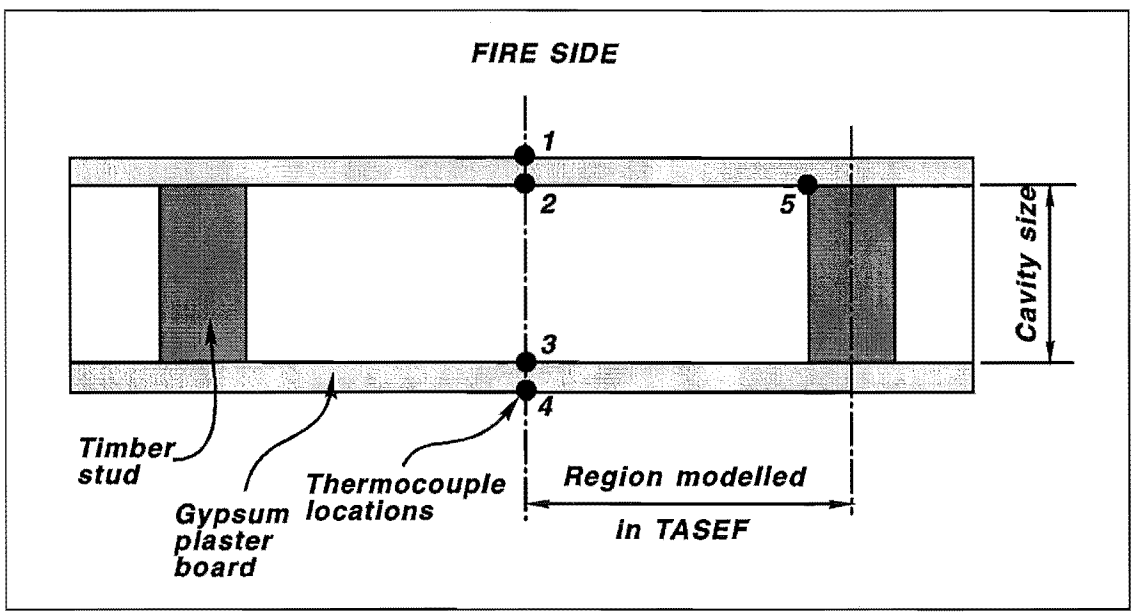

Figure 1.2 Section of Light Timber Framed Wall

Position 5, where charring of the timber would first occur.

Position 4, on the ambient side, where an insulation failure would occur.

Charring first occurs on the centreline of the stud, but the temperature at this location was not measured in test data used in this study. The difference between the first onset of charring and the criteria used here is of little significance.

It can be seen in Figure 1.3 that for the charring criterion at point 5, a maximum temperature of 732°C occurs when the assembly is exposed to a time-temperature curve characteristic of a real fire. The time at which this temperature is reached during an ISO-834 test is 99.5 minutes, which is the equivalent fire severity.

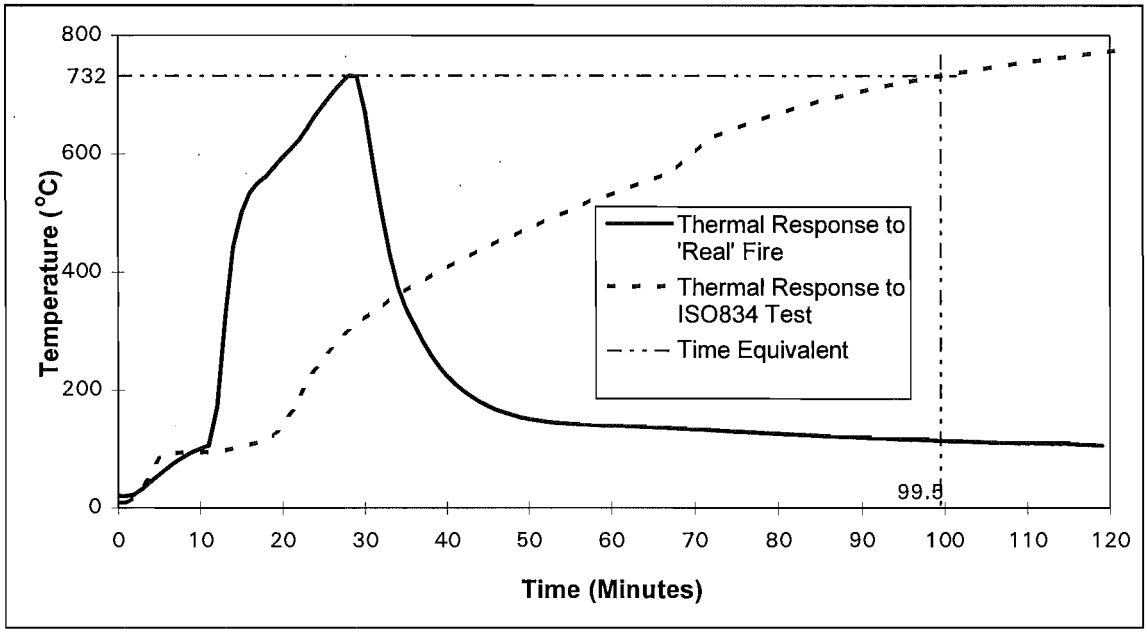

Figure 1.3 Definition of Temperature Time Equivalence.

1.2.1 The CIB Time Equivalence Formula

The formula referred to as the CIB (Conseil International du Batiment) formula (Thomas 1986) is an empirical expression for the equivalent fire severity, based on experiments on insulated steel members exposed to fires in concrete lined compartments. It is derived from a simpler formula devised by Law (1977). The concept of equivalent time is described in Schleich (1993). This formula depends on the ventilation parameters of the compartment and the fuel load and is given by Equation 1.1:-

$$t_e = cwQ_f \qquad (1.1)$$

where:- t_e is the equivalent time of exposure to an ISO-834 test (minutes)

c is a parameter to account for different compartment linings, it is roughly inversely proportional to the thermal inertia of the compartment linings and is further described in Section 2.1.2.

w is the ventilation factor:-

$$w = A_f \Big/ \left(A_w A_t H_v^{1/2}\right)^{1/2} \qquad (1.2)$$

where:- A_f is the floor area of the compartment (m^2)

A_w is the total window area (m^2)

A_t is the total area of the bounding surfaces of the compartment (m^2)

H_v is the height of the windows (m)

Q_f is the fuel load in (MJ/m^2 of floor area)

In this work A_t is assumed to include the window area.

1.2.2 The Eurocode Formula

The CIB formula has the limitation of only being valid for compartments with no horizontal openings such as ceiling vents. It was later modified to allow for horizontal openings and is described in Eurocode (1993). The formula is the same and uses Equation 1.1 and 1.2, however the ventilation factor is modified. It has been used to develop tables in the approved documents of the New Zealand Building Code (NZBIA 1992) as described in Buchanan (1994). The modified ventilation factor w is:-

$$w = \left(\frac{6.0}{H_c}\right)^{0.3}\left[0.62 + \frac{90(0.4-\alpha_v)}{1+b_v\alpha_h}\right] \quad > 0.5 \qquad (1.3)$$

where:- H_c is the compartment height (m)

$$\alpha_v = A_v / A_f \qquad 0.05 \le \alpha_v \le 0.25 \tag{1.4}$$

$$\alpha_h = A_h / A_f \qquad \alpha_h \le 0.20 \tag{1.5}$$

$$b_v = 12.5\left(1 + 10\alpha_v - \alpha_v^2\right)\Big) \tag{1.6}$$

A_f is the floor area of the compartment (m^2)

A_v is the area of vertical openings (m^2)

A_h is the area of horizontal openings (m^2)

When this formula is used the values for ***c*** are slightly reduced.

If horizontal openings are not present and the compartment height is 3.0 m, then the Equation reduces to:-

$$w = 1.231\left[0.62 + 90(0.4 - \alpha_v)^4\right] \quad > 0.5 \tag{1.7}$$

These two versions of the formula are used with different values of the coefficient **c** which allows for both the thermal characteristics of the compartment boundary and to some extent a correlation coefficient.

The values used in this study are given in the Fire Engineering Design Guide (Buchanan 1994). A value of 0.067 is used for the general case in the New Zealand Building Code acceptable solution C3/AS1 (NZBIA 1992). The values in the New Zealand Building Code are higher than those used in the Eurocode (1993) as shown in Table 1.1. Kirby's values were suggested for the Eurocode after large-scale tests by Kirby et al (1994) showed that the values in the Eurocode were unconservative.

Source	Formula	$\sqrt{k\ \rho\ c}$			
		>2500	720 to 2500	<720	General
CIB W14 (Thomas, P.H. 1986)	CIB	0.050	0.070	0.090	
Eurocode (1993)	Eurocode	0.040	0.055	0.070	0.060
Kirby et al (1994)	Eurocode	0.050	0.070	0.090	
FEDG (Buchanan 1994)	Eurocode	0.045	0.055	0.080	0.067

Table 1.1 Values for *c* used in the Time Equivalent Formulae

These four combinations of the values for ***c*** and the two formulas are hereinafter referred to as the CIB, Eurocode, Kirby and BIA formulae respectively. The CIB formula and the BIA formula are used in this dissertation for comparison purposes. The Eurocode may be altered to Kirby's suggested values.

1.2.3 Comparison of The CIB and Eurocode Formulae

For the compartment geometry of 5.0 by 5.0 by 3.0 metres high chosen for this project using the BIA formula for time equivalence results in a value which is up to 10% lower than that given using Equation 1.2 and the appropriate values for c. Equation 1.7 does not allow for the effects of variable compartment and window geometry. Equation 1.2 includes a term for the height of the window, and the wall area of the compartment. Equations 1.2 and 1.7 give significantly different results when compartments with unusual layouts are considered. The window height in particular has a significant effect on the ventilation, namely that the flow through a vertical opening is proportional to the product of the area and the square root of the opening height.

1.3 Methodology

The methodology developed in this thesis has been to use numerical computer models to predict expected temperatures in real compartment fires, and to carry out thermal and structural analysis of light timber framed walls and floors exposed to such fires.

No tests were carried out by the author apart from the house burn described in Chapter 7. Data for the models was found in literature and modified where appropriate within reasonable bounds. Given the large variation in testing methods and results for many properties by many different researchers it would be arrogant to assume that any methods used by the author and results from these test methods would be any better than those found by other researchers.

The models used are freely available. It was decided that it was not possible to develop computer models from scratch because of the complexity required and to produce the results required. In some cases models were modified and the structural model was modified by the use of user coded sub-routines.

1.3.1 Compartment Fire Model

Time - temperature curves and/or heat flux curves were developed using COMPF-2, a compartment fire model developed by Babrauskas and Williamson (1978a and 1979) and based on Harmathy's work (Harmathy 1983, Harmathy and Mehaffey 1982, 1983

and 1987). This program requires ventilation parameters, fuel loads and thermal properties of compartment boundaries as input data. The output data from this model are used as input to the finite element model of the wall assembly described in Section 2.3.1.

1.3.2 Heat Transfer Model

A finite element heat transfer model of a wall assembly was developed using TASEF (Sterner and Wickstrom 1990). TASEF is a two dimensional model designed for fire problems. Input data for thermal properties has been found in the literature, notably Gammon (1987) , Fuller (1990) and from FORINTEK (Mehaffey 1991 and Currier 1993). The model was subjected to an ISO-834 fire and the results compared with real fire tests performed at the Building Research Association of New Zealand (BRANZ) in Wellington. Some knowledge of furnace characteristics was required and the results will be more relevant to the furnace used for calibration of the model than other test furnaces.

This modelling is more difficult than for steel or concrete structures because of the non-homogeneity of the assembly. The assembly is composed of at least two different materials, three if char is regarded as a different material, and enclosed voids.

1.3.3 Structural Models

The structural model used was ABAQUS (Hibbitt et al 1994), a general purpose finite element program. This program allowed the use of user-coded sub-routines to modify the program to suit the user's requirements.

The structural part of this program was used, and compared with the results from furnace tests on walls and floors tested at BRANZ and a large series of beam tests carried out by König at Trätek, in Sweden (König 1995).

Composite action between the gypsum plasterboard lining and the timber structure was considered, as was that between the particleboard floor and floor joists.

1.3.4 Time Equivalents and Simplified Design Method

The results from the combination of the three models above were used to calculate time equivalents and compared with the values found using formula. The accuracy is discussed and an alternative design method is proposed.

1.4 Layout of the Dissertation

In general the layout is: compartment fire model, thermal model for walls, the house fire test, structural model of König's beam tests, structural model of walls, thermal model of floors, structural model of floors and then discussion and results.

The first page of each Chapter is preceded by a coloured page. Each Chapter starts on an odd numbered page so the previous even numbered page may be blank.

Chapter 2 Fire Severity Models

2.1 Introduction

This Chapter is concerned with the severity of real fires and their temperature histories. Harmathy (1979) proposes that temperature histories are unrealistic in describing a post-flashover fire. The time duration and the average penetration heat flux are more important in determining the severity of exposure to fire of structural components. His report emphasises the need for fire engineering design, highlights the pitfalls of traditional prescriptive approaches and describes a method of determining fire severity parameters by calculation. The heat transfer characteristics of the barriers around the compartment are included in the determination of fire severity, but Harmathy does not give an indication of the magnitude of this effect. The conductivity and thermal diffusivity of compartment barriers will affect the temperature history in a compartment.

2.1.1 Fire Severity

Fire severity can be quantified in two ways:-

(i) By the time-temperature curve of the fire

(ii) By the amount of energy (heat flux) that is input to the structure under consideration.

As used in this dissertation, fire severity is the impact a post-flashover compartment fire has on a structure. This may be in terms of thermal performance, that is the ability of a compartment boundary to minimise heat transfer to an adjoining compartment. This is described in the ISO-834 test protocol as an insulation failure. On the other hand it may be in terms of a structural failure, where collapse of the structure occurs or loss of integrity allows flame or hot gases to pass through the assembly. These are described in

the ISO-834 test protocol as a structural or integrity failure respectively. Two fires with identical time-temperature curves will not have the same severity on different elements, for example a steel column and a concrete wall (except by coincidence). Similarly a fire in compartments with identical geometry, ventilation and fuel load, will have a different severity on identical steel columns, if the compartment linings are concrete in one case and gypsum plasterboard in the other.

As there is a very large amount of standard (ISO-834) test data available, it is highly desirable to compare the fire severity of a compartment fire with that of the standard fire resistance test. The first method was comparing the area under the time-temperature curve (Babrauskas and Williamson 1978d). Comparing area under the curve is not a suitable method as the heat energy that is input into structural walls is not directly proportional to the temperature. It is mostly due to radiation and hence is proportional to the temperature difference raised to the fourth power. A simple integration over time will therefore underestimate the severity of short hot fires and overestimate the severity of long cooler fires. The other method is by using some form of time equivalence formula, that is, an empirical equation relating key parameters to an equivalent time of exposure to an ISO-834 test. The most commonly used formula is the CIB formula described in Section 1.2.4. Methods of comparing heat flux are referenced in Section 2.2, below.

2.1.2 Ventilation Controlled Fires

In the Swedish method, (Magnusson and Thelandersson 1970), the fire severity is determined by ventilation parameters and the fuel load density for specific compartment lining materials and layout. These assumptions are also inherent in the CIB time equivalent formula (Section 1.2.1). The assumption that a compartment fire will be ventilation controlled is probably reasonable for small compartments with a "normal" range of ventilation parameters and typical fuels. This assumption has not been justified by sufficient experimental results or by any analytical procedure. It appears to be commonly assumed, but never discussed.

In the CIB formula (Section 1.2.1) the factor C takes this into account. The factor C is a function of the thermal inertia Γ of the lining material.

$$\Gamma = \sqrt{k\rho C_p} \tag{2.1}$$

where:- k is the thermal conductivity of the lining material (W/m.K)

ρ is the density of the lining material (kg/m^3)

C_p is the specific heat of the lining material (J/kg.K)

Table 2.1 gives values of c as a function of Γ.

Γ (W^{2}s/m^{4}K)	Typical Construction	c
<720	Insulating Material	0.08
720 to 2500	Concrete or Plasterboard	0.055
>2500	Thin Steel	0.045

Table 2.1 (from NZBIA 1992)

As can been seen in the Table c is not strongly a function of Γ. It takes a very large change in Γ to alter c significantly, hence minor changes in the lining materials are not very significant when using the CIB formula.

2.1.3 Repeatability

Harmathy states that the agreement between two compartment fire tests identically set up will not necessarily be better than 20% (Babrauskas and Williamson 1975), hence repeatability is poor.

Fang (1981), reports on a series of four compartment tests, which were as close to identical as practically possible. The coefficient of variation for the measurement with the most repeatability was 6% on room gas temperatures. It was 11% for heat flux. After flashover the correlation between tests was very poor. Despite furnishings and linings being supplied by the same firm, variations of up to 15% of the mass of the items was noted. The accuracy of predictions of temperature histories is unlikely to be better than 15-20%. Reproduceability is likely to be a more significant problem. Even in the standard ISO-834 furnace test and the standard ISO-9705 room test large variability (>15%) between test furnaces and compartments has been reported. The variation is likely to be even larger for compartment fire tests.

2.2 Fire Severity Literature

2.2.1 Harmathy Method

Harmathy and Mehaffey (1983) reviewed the different available post-flashover fire models. These models have only changed in detail since then. They list the different models with regard to various criteria and suggest that Harmathy's normalised heat load concept is the most useful and accurate. The normalised heat load concept involves the normalisation of heat load over the thermal inertia of the compartment boundaries and assumes the boundaries are a semi-infinite slab. The boundary is sufficiently thick for no heat loss from the boundary material to the ambient side of the boundary to occur for the duration of the fire. This is a valid assumption for a thick concrete slab (Harmathy and Mehaffey 1987), but it is a problem for thin sheet material such as plasterboard. Harmathy and Mehaffey (1987) state that the properties of the lining are insignificant for short duration fires, hence for relatively short duration:-

> "ventilation controlled fires the designer may use judgement in choosing the effective value of the thermal absorptivity of the surface layer, depending on the nature of the substratum".

Hence it may be appropriate to normalise the heat load according to another parameter or parameters for light framed structures. This approach is that used by Barnett (1989) for steel structures.

2.2.2 Barnett Thesis

Barnett (1989 and 1991) describes previous work on post-flashover fires in some detail. He describes the limitations of fire resistance testing, such as repeatability with one furnace or between furnaces. This is due to many factors, such as the method of operation, thermal restraint of beams, flame emissivity and furnace linings. These problems, and the fact that the ASTM E-119 or ISO-834 time-temperature curves do not represent real fires, is used to justify the use of analytical models for realistic fire engineering design. He summarises the development of ventilation control parameters for the behaviour of ventilation controlled fires. He states "the heat release rate can be accurately determined for a ventilation control fire because the mass loss rate of

charring fuels is not affected greatly by re-radiation to the fuel surface", (Barnett 1989, p 23). No satisfactory method has been found for predicting the burning rate of fuel-bed controlled fires. Modelling such a fire as ventilation controlled results in the maximum temperatures calculated being higher than the maximum temperature that would actually be reached in a real fire. This is conservative. However, this would also result in a shorter calculated duration, which may be unconservative. The fire severity in terms of the effect on structural elements may be more severe during a long colder fire than a short hot fire. This is because of the time effects. During a short hot fire there may not be enough time for heat to penetrate far enough into a structural element to cause damage, despite the fact that the gas temperatures are very high. The layout and type of combustibles within a compartment is impossible to predict at the design stage.

There are descriptions of several methods to calculate the fire resistance of steel beams and columns used in Sweden, Australia and France. Barnett's method is then described. It is based on Harmathy's normalised heat load model, which is described well in the thesis.

The computer program, COMPF-2 (Babrauskas 1979), for modelling post-flashover fires, is described in Barnett's thesis and later in this Chapter. Barnett modelled compartments using COMPF-2 and fitted a polynomial curve to the time-temperature curve output. This procedure was carried out for different opening factors and compartment boundary materials with differing thermal properties for a time of 5000 seconds (1 hour 23 minutes). This curve was compared with two room fire tests with a variation of about 15%. The normalised heat load can then be calculated for this curve and compared with that for a test fire to give a time equivalence. The temperature in a protected steel structural element can then be predicted by modelling the insulation as a semi-infinite slab. This is subject to a limit on the Fourier number and hence limits the time this is valid for thin insulation. The solution is invalid when the heat penetrates into the steel.

This is similar to the problem for cavity walls, when modelling the wall as a semi-infinite slab becomes inadequate when heat starts to be lost from the ambient side of the exposed lining board. An approximate solution and a finite element analysis solution is also given and compared. These give good agreement for times of less than 18 minutes and thickness of insulation greater than 25 mm. For unprotected steel a J factor is

introduced as a substitute for thermal inertia. The use of thermal inertia as a parameter is not valid as the section can not be realistically modelled as a semi-infinite slab. J varies with time and geometry of the steel section. For design purposes Barnett's approach has the advantage that it can be used to predict resistance to the standard fire and hence can be used to satisfy prescriptive codes.

2.3 The Swedish Time - Temperature Curves

2.3.1 Model Description

The Swedish time-temperature curves are a series of time temperature curves for compartment fires first published by Magnusson and Thelandersson (1970). They are based on the heat balance in an enclosed compartment and the heat transfer through bounding surfaces. Two equations for heat balance and heat flux through boundaries are solved simultaneously to give the compartment temperature and the heat released in the compartment.

An example of a set of curves is shown in Figure 2.1.

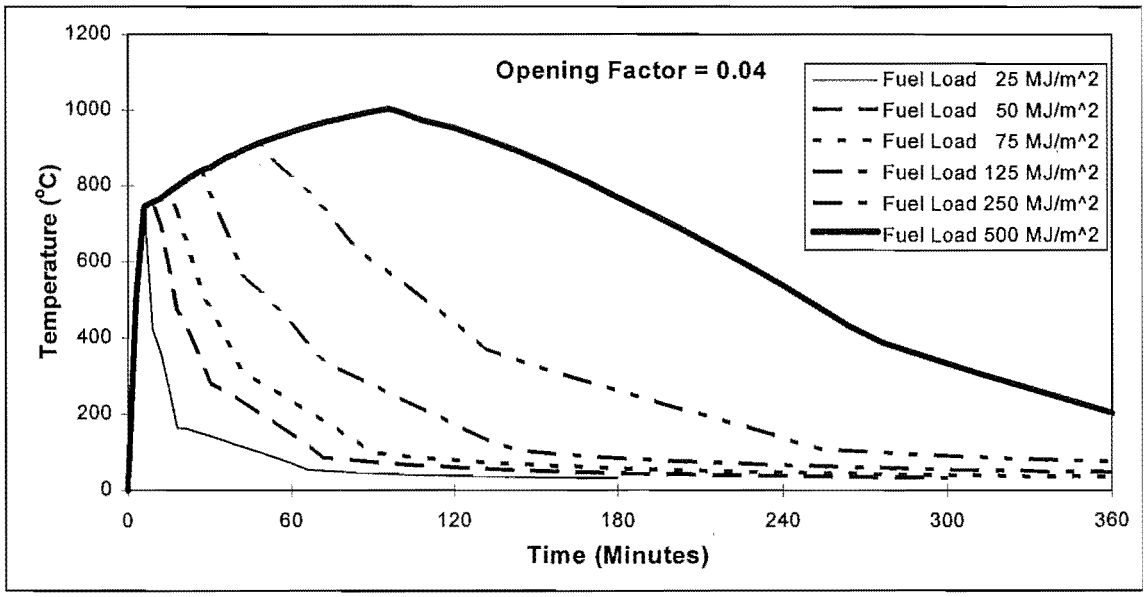

Figure 2.1 Swedish Time-Temperature Curves for a Type A Compartment

2.3.1.1 Fuel Load

The fuel load is defined in this Section and in Figure 2.1, as being per unit area of total bounding surfaces as described in Magnusson and Thelandersson (1970), not per unit floor area as is more usual. Elsewhere in this thesis it is expressed per unit floor area.

2.3.1.2 Ventilation

Within each series of curves there is a set for a range of opening factors from 0.01 to 0.12. This opening factor, V, is given by:-

$$V = A_w H_v^{1/2} / A_t \tag{2.2}$$

where:- A_W is the window area (m^2)

H_v is the height of the window (m)

A_t is the total bounding surface area of the compartment, including the window area (m^2)

For each opening factor, there is a range of curves for different fuel loads. However the published results do not give the same range of fuel loads for each opening factor.

2.3.1.3 Lining Materials

Series of curves were developed for compartments with differing linings. Figure 2.1 is for a type A compartment, that is, a compartment lined with normal weight concrete. There are series of curves for different compartment types with boundaries with differing thermal properties, known as type B to type G. Most of these types consist mainly of normal or light weight concrete, however for a type G compartment, the lining is mostly gypsum plasterboard on steel studs and some lightweight concrete on some sides. They are described in Chapter 7 of Magnusson and Thelandersson (1970).

2.3.2 Assumptions Inherent in the Method

The assumptions inherent in the development of these curves are as follows:-

(i) The time history of the rate of heat release from the fire was determined by trial and error. A heat balance was carried out to determine gas temperatures. The final shape of the heat release curves are those that gave the best fit with the test results. The tests were carried out by other researchers and some principle measurements including the mass loss rate were not reported.

(ii) All of the energy contained within the fuel is released within the compartment during the course of the fire.

(iii) The maximum heat release rate is calculated using a maximum burning rate for cellulosic fuels, which is dependent solely on the ventilation and given by:-

$$R_{\max} = 5.5 A_v H_v^{1/2} \tag{2.3}$$

where:- $R_{\max}$ is the maximum rate of fuel consumption (kg wood/min.)

A_v is the total area of the windows (m^2)

H_v is the height of the windows (m)

(iv) The duration of the fully developed (ventilation limited) phase is given by dividing 60% of the total amount of fuel present by Equation (2.3), the burning rate.

(v) The assumed duration of the fully developed phase in the model is taken to be slightly less than given by (iv).

(vi) The maximum burning rate is independent of the quantity, geometry or layout of the fuel.

(vii) The remainder of the energy content of the fuel (43% or more depending on the difference between the assumed and calculated value used for duration of the fully developed phase in (iv)and(v)), is liberated after the fully developed phase, in the decay phase of the fire.

(viii) The fire has a slower temperature decrease during the decay phase if the duration of the fully developed phase is longer.

(ix) The correlation with tests in compartments lined with normal and lightweight concrete can be extrapolated to compartments lined with a mixture of steel and concrete or a mixture of gypsum plasterboard and concrete (series F and G, Magnusson and Thelandersson 1970 Chapter 7), using the appropriate thermal properties of the lining materials.

These assumptions are all described in Magnusson and Thelandersson (1970) and Böhm (1977) reviews their findings and describes his own similar tests.

2.4 COMPF-2

2.4.1 Model Description

COMPF-2 is a computer program with a more rigorous approach to calculating gas temperatures during a compartment fire than the Swedish time-temperature curves. It was developed by Babrauskas and Williamson (1975), who describe the background to fire resistance testing and the development of standard fire test curves. They describe the development of the mathematical model and correlation with experiments. The variation with experimental results is up to 20%. This value seems to be a realistic limit on accuracy of theoretical models. The program is a development of Harmathy's work, but it allows for compartment linings of finite thickness. Babrauskas and Williamson (1978a) describe the basis of the theoretical model more concisely.

A later paper, Babrauskas and Williamson (1979) describes the application of the model. This paper includes a description of the effects of changes in the main variables. The main variables are scale effects, window radiation, losses through walls and heat transfer coefficients. The program uses a heat balance to calculate the gas temperatures, described in Chapters 2 and 3 of Babrauskas (1979). The program solves two simultaneous equations for the heat balance in the compartment and the conduction through the walls. The equations used are similar to those used by Magnusson and Thelandersson (1970), but the simplifying assumptions they used were not used in COMPF-2. The heat balance contains terms for heat loss due to convection and radiation to the compartment walls, ceiling and floor, radiation through the window, energy required to heat the combustion gases, energy lost in unburnt pyrolysates and energy produced by combustion.

2.4.1.1 Rate of Pyrolysis

The rate of pyrolysis is dependent on either:-

(i) The ventilation of the compartment.

(ii) The fuel surface, that is the maximum regression rate of the fuel.

(iii) The porosity, in the case of a crib.

The pyrolysis rate is determined by theory for liquid pool fires, using Nilsson's (1974) formulas for crib fires and by assuming a user specified constant surface regression rate for a given size and shape (and hence shape factor) for other solid fuel fires.

It should be noted that the pyrolysis rate or mass loss rate is not the same as the burning rate of combustion or heat release rate. The first two are the rate at which the fuel is decomposed into combustible gaseous products. The burning rate is the rate at which these gaseous products react with oxygen within the compartment. The burning rate is always less than or equal to the pyrolysis rate. The heat release rate is similar to the burning rate, but is expressed in terms of a rate of energy release or power, whereas the other rates are normally expressed as a mass per unit time.

2.4.2 Assumptions Inherent In COMPF-2

A program manual for COMPF-2 (Babrauskas 1979) describes briefly the theoretical background. The main assumptions in the model are described in the manual and are as follows:-

(i) The compartment is assumed to be well stirred, that is, the compartment is the same temperature throughout. This means the model is a "single zone" model with the compartment assumed to be at a constant temperature throughout for the purposes of calculating a heat balance.

(ii) The model is quasi-steady, that is, the terms in the heat balance equation relating to the change of mass and heat energy of the gas in the compartment are ignored. The change in mass is small as the observed pressure increase during a fire in a typical ventilated fire is small. The increase in temperature, and hence heat energy contained in the gas, is negligible compared with the total heat released by the fire as the heat capacity of combustion gases and air is relatively low.

(iii) Air supply and fire gas outflow are due to buoyancy driven convection. The model has been modified to allow for multiple vents in vertical walls by calculating an effective window area and window height but does not allow for horizontal openings.

(iv) The burning rate is limited by rates of air or fuel supply, not by chemical reaction kinetics.

(v) Walls are modelled as a homogeneous solid of finite thickness. This differs from Harmathy's model, where bounding surfaces are assumed to be semi-infinite slabs. Thermal properties may be temperature dependent. The properties of a non-homogeneous cavity wall can not be input directly.

COMPF-2 also features "pessimisation", the process by which one or more variables is adjusted to create the worse possible fire for the variables which are specified. It is defined in Babrauskas and Williamson (1979) as :-

"being analogous to, but inverse to optimisation"

This process is justified by assuming that not all variables will be constant during the life of the building. The three main variables are the ventilation, fuel load and properties of the compartment boundaries. The paper recommends that the wall properties be specified, as they are least likely to be significantly altered and have the least effect. The fuel load should be specified, because it is less variable and has a less marked effect on the time-temperature curve. Ventilation is the most likely to change and has the biggest effect on the time-temperature curve. If this process is followed then there is a large reduction in the number of design cases which need to be considered. If a fire that has cellulosic fuel is pessimised over pyrolysis, then the resulting heat release rate varies little from a ventilation controlled fire with a constant pyrolysis rate.

2.4.3 Effect of Fuel Geometry

In COMPF-2 the fuel pyrolysis rate is determined using one of four methods in three subroutines. One is for a hydrocarbon pool fire. The method for both wood cribs or wood sticks is contained in the second subroutine. In the third subroutine, the pyrolysis rate is pessimised.

The crib subroutine utilises Nilsson's formulas for crib fires (Nilsson 1974). When using this subroutine the fuel geometry specified can have a significant effect on the time-temperature curve of the fire. A "stick" fire is controlled by this subroutine, but crib porosity does not limit the pyrolysis rate for a stick fire.

If a fire is fuel surface controlled, the temperatures will be lower than for a ventilation controlled fire, everything else being equal. Increasing the ventilation will lower the temperatures. If the fire is ventilation controlled, increasing the ventilation will increase the temperatures, resulting in a more severe, but shorter duration fire.

The effect of fuel geometry is highlighted in Figure 2.2, for a compartment with a fuel load of 400 MJ/m^2 and a opening factor of 0.15. The fuel surface regression rate is specified as 36 mm per hour. It can be seen that by increasing the size of the sticks, the pyrolysis rate reduces as the fire becomes fuel bed controlled to a greater degree. This results in a longer and cooler fire. All fires other than the pessimised option, are fuel bed controlled towards the end. This is because the fuel bed controlled pyrolysis rate decreases with the amount of exposed fuel surface area. This area decreases at a rate proportional to the square root of the mass remaining for a two dimensional stick.

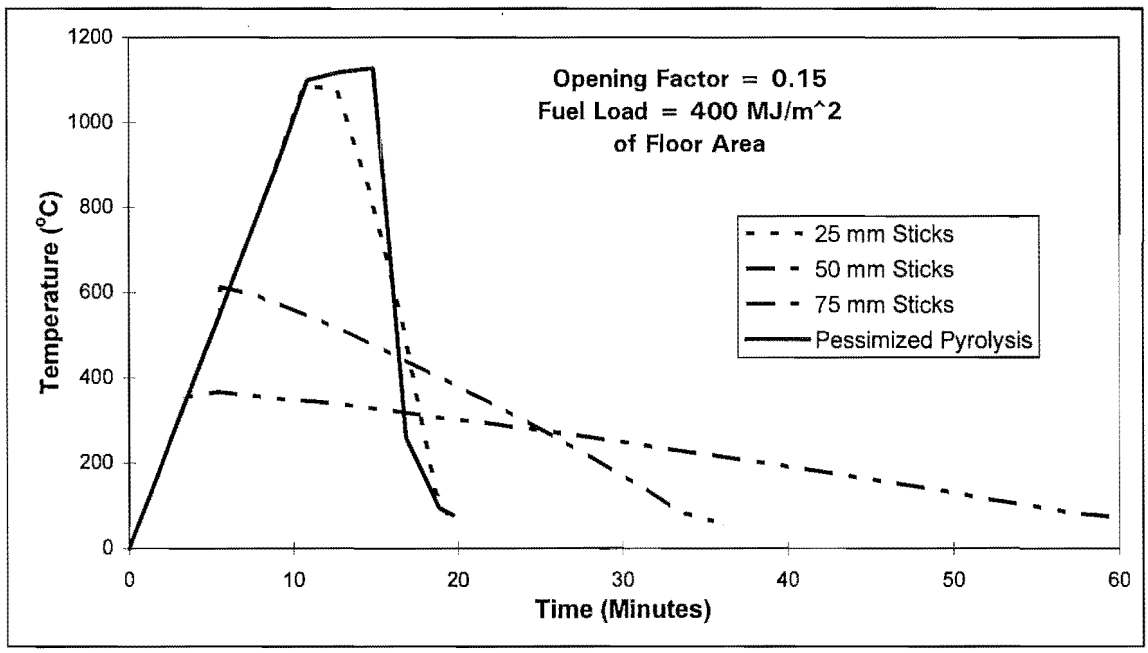

Figure 2.2 Effect of Fuel Geometry on the Time-Temperature Curve

The third option in COMPF-2 is pessimising the fuel pyrolysis rate. In this process the pyrolysis rate is continuously adjusted to give the highest possible temperature at each time step, and hence produces the most severe fire for a defined ventilation and compartment. It can be seen in Figure 2.2 that the pessimised fire produces higher temperatures for a longer time than the crib or stick fire, with a very rapid decay phase.

2.5 Comparison Between The Swedish Time - Temperature Curves and COMPF-2

This Section describes a comparison of the Swedish time-temperature curves for compartment fires derived by Magnusson and Thelandersson (1970) and the output from COMPF-2 (Babrauskas 1979).

2.5.1 Assumptions Made in the Comparison

2.5.1.1 Magnusson and Thelandersson

The curves derived by Magnusson and Thelandersson (1970) have been used for the comparison. The following assumptions were made:-

(i) Time-temperature curves for their "type A" (concrete) compartment are used , that is, one characterised by a bounding material with a thermal conductivity of 0.81 W/m.K and the product of heat capacity and density of 1.67 MJ/m^{3}K.

(ii) The values for opening factor, V (Equation 2.2) used are 0.02, 0.04, 0.08 and 0.12.

(iii) The fuel load is given by Magnusson and Thelandersson in kCal/m^2 of the total bounding area of the compartment. This has been converted to kg/m^2 of wood equivalent per unit floor area, for input to COMPF-2, assuming a calorific value of wood equivalent of 15 MJ/kg. The value of 15 MJ/kg is also input to COMPF-2. The fuel loads chosen vary depending on the ventilation parameter. From the curves produced by Magnusson and Thelandersson (1970), the third lowest, third highest and highest fuel load were chosen, for each of the opening factors given in (ii) above. Subsequently it was found that Magnusson and Thelandersson appeared to have used a value of about 17 MJ/kg for the calorific value of wood. This difference is of no importance as the values for the Swedish Curves are given in MCal/m2 of bounding surface area not in terms of mass and the input to COMPF-2 was back calculated from energy values to give the same fuel load in terms of energy per unit area (kg/m^2).

2.5.1.2 COMPF-2

The fires were modelled using COMPF-2 assuming the following:-

(i) A room size of 5 m by 5m, and a height of 3 m, as shown in Figure 2.3. This room size was chosen as being the largest reasonable limit for a light timber framed building. The fire severity would be less severe in a very small compartment because the bounding area is larger compared with the enclosed volume. The results from this study is expected to be valid for compartments ranging in size from about 20 m^3 to 200 m^3 and could be extended to larger compartments with larger safety factors.

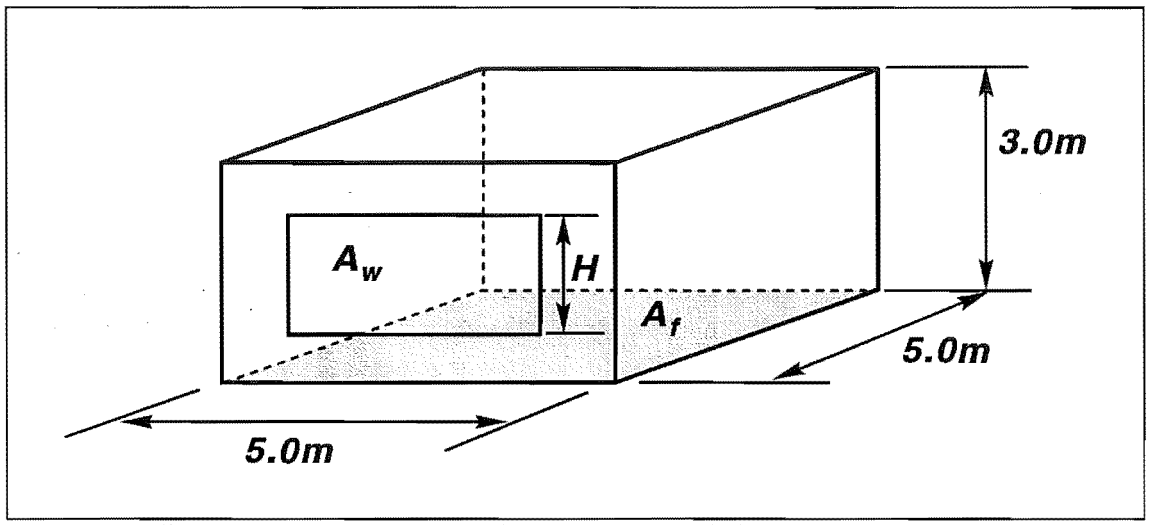

Figure 2.3 Layout of the Compartment Modelled in COMPF-2

(ii) Thermal properties of the bounding surfaces as described above.

(iii) The opening factors as described above.

(iv) The fuel loads as described above.

(v) The window height was assumed to be 1.0 metre, hence the total window width is 2.2, 4.4, 8.8 and 13.2 metres for the four different ventilation factors. The Swedish curves are for differing opening factors and hence the shape of the window is irrelevant. In COMPF-2, the only term affected by the window shape is the window radiation. This term ranges from 5 to 20% of the total heat energy produced and is directly proportional to the window area. Leaving the ventilation factor constant and altering window shape within reasonable limits does not greatly affect the area of the window, so the effect on the heat balance will be at worst 8% and in most cases less than 5%.

(vi) The percentage of pyrolysates burned is 70% in most cases and 85% for series 8, (see Table 2.2).

(vii) Chemical composition of fuel is that for wood.

(viii) For crib fires the pyrolysis rates are for 23, 100 and 150 mm sticks, with a clear spacing between sticks of three times the stick size, as used by Böhm (1977).

(ix) The crib shape factor (clear stick spacing/crib height) is inversely proportional to the fuel load, as the crib height is altered to increase the value for fuel load.

(x) When comparing results the start of the COMPF-2, data was offset 6 minutes allowing for the fact that the Swedish temperature curves start with a temperature equal to ambient at time zero, while COMPF-2 starts with a heat balance and hence a temperature significantly higher than ambient at time zero, which is indicative of the start of the fully developed stage of the fire.

2.5.2 Comparison for Crib Fires

Table 2.2 summarises the fuel loads, ventilation factors and crib geometry for each run of each series.

Fuel and Ventilation Parameters			Duration of Fully Developed Phase of Fire (Minutes)							
			Hand Calcs	Swedish Curves	COMPF2					
Series					6	7	8	9	10	11
Stick Size (mm)					23	100	23	100	150	*
Fuel Geometry					Crib	Crib	Crib	Crib	Stick	Stick
% Pyrolysites Burned					70	85	70	70	70	70
Run	Vent. Factor	Fuel Load (MJ/m^2)								
1	0.02	38	30	18			18	82		
2	0.02	125	100	60			58	87		
3	0.02	250	200	120			116	130		
4	0.04	75	30	18	18	82	18	82	122	41
5	0.04	250	100	60	58	87	58	87	122	81
6	0.04	500	200	120	116	130	116	130	122	122
7	0.08	150	30	18			21	82		
8	0.08	500	100	60			69	87		
9	0.08	1000	200	120			138	130		
10	0.12	225	30	18			31	82		
11	0.12	750	100	60			104	87		
12	0.12	1500	200	120			207	130		
								* Varies with Fuel Load		

Table 2.2 Summary of COMPF-2 Runs and Duration of Fully developed phase.

Series 6, 7, 8 and 9 are crib fires and series 10 and 11 are stick fires. Series 1 to 5 are not reported here. Table 2.2 also shows a comparison of the duration of the fully developed phase of compartment fires for the following:-

(i) Swedish time-temperature curves.

(ii) Hand calculations assuming a maximum ventilation controlled burning rate (Equation 2.3). The total fuel load divided by the burning rate gives the duration.

(iii) The COMPF-2 runs.

The comparison between COMPF-2 and the Swedish curves is shown in Figures 2.4 to 2.13. Initial runs showed that the main difference between COMPF-2 results and the Swedish curves was in the decay phase of the fire. Another significant difference was that the Swedish curves have smoother transitions between the growth, peak burning and decay phases of the fire.

2.5.3 Decay Phase

Magnusson and Thelandersson assume that the rate of temperature decrease during the decay period is inversely related to the duration of the fully developed phase of the fire, that is the longer the fully developed phase, the slower the rate of temperature decrease. In their model they modified the rate of burning in the decay phase to give a good correlation with experiments using wooden cribs. Similar results are described by Lie (1988).

The decay phase in the Swedish Curves requires some discussion. Magnusson and Thelandersson assume that the entire energy content of the fuel is liberated during the fire (p20 Magnusson and Thelandersson 1970). They appear to calculate a duration of fully developed phase as a time slightly less than that required for 57% of the fuel's energy to be released at the constant, ventilation controlled burning rate as given by Equation (2.3). The remainder of the fuel is assumed to burn during the decay phase of the fire, at a reducing rate. This rate has been modified to correlate with test results, for fires of up to one hour duration, but has been extrapolated for fires of up to six hours duration. The rate of burning during the decay phase has no theoretical justification, and can not be compared with mass loss rates as these were not recorded for the tests that Magnusson and Thelandersson used. Böhm (1977, p84-5) has reservations about these assumptions.

In real compartment fires, the energy that is not released during the fully developed phase can be accounted for in several ways, that is:-

(i) Unburnt pyrolysates, are carried out through the windows with combustion gases.

(ii) Gaseous products of incomplete combustion are carried out through the windows with combustion gases.

(iii) Solid products of incomplete combustion remain in the compartment.

(iv) Some fuel is not burnt due to being protected by char or non-combustible materials.

Most of the unburnt pyrolysates and gaseous products of incomplete combustion, such as carbon monoxide will have left the compartment via the windows. Some of the pyrolysates will burn outside the compartment and appear as flames projecting from the windows, and hence the energy from these pyrolysates is not released within the compartment. Solid products of incomplete combustion (mainly elemental carbon and tars) and other unburnt fuel, may smoulder for some time, but will not release a large quantity of heat at a significant rate. The assumption made in the input data to COMPF-2, that 70% of the energy contained in the fuel is released is to allow for energy lost to the system due to (i) to (iv) above. Kawagoe and Sekine (1963) assume that 72% of the dry fuel's energy is released. Magnusson and Thelandersson's assumption that all the energy is released in the compartment is inconsistent with their assumption of ventilation control.

Most of the tests used by Magnusson and Thelandersson were carried out in compartments lined with thick concrete. The lining in most cases was thermally thick, and hence heat loss through the walls did not occur. Heat input to the walls could only be released back into the compartment resulting in a long cooling period. In compartments with light weight walls this would not be the case. The time-temperature curves in Appendix G of Böhm (1977) for polyethylene fires show a much faster rate of heat decrease than for wood fires. The decay phase in Böhm's tests (Appendix F) is more rapid than that for the Swedish curves. Some of the slow rate of temperature decrease measured in tests may be attributable to the fact that heavy shielded thermocouples will cool at a slower rate than the gas temperature.

Despite these problems with the Swedish curves, in most cases they will result in a conservative design for protected steel members as the severity of the fire they model is likely to be less than that predicted using the Swedish curves in the type A (concrete) compartment.

2.5.4 Crib Size

For some COMPF-2 runs, the 23 mm crib was chosen to match that given in Böhm (1977), since details of the cribs in the tests described by Magnusson and Thelandersson were not given and Böhm refers to Magnusson and Thelandersson's curves. With the 23 mm cribs the fire was only fuel bed controlled for a opening factor of 0.02. By prescribing a fuel that switches from ventilation control to fuel bed control at about the time the decay period starts according to the Swedish curve, then a slower decay period, similar to that of the Swedish curves would be achieved. For other runs a 100 mm crib size was chosen, so that the fire would be fuel bed controlled in compartments with opening factors of 0.02 or greater.

2.5.5 Fire Duration

The duration of the fully developed phase is summarised in Table 2.2.

2.5.5.1 Ventilation Controlled Fires

Series 6 and series 8 fire curves were developed using COMPF-2 and assuming a stick size of 23 mm in cribs.

The values for fire duration calculated analytically and shown in Table 2.2 are slightly longer than those calculated by Magnusson and Thelandersson. This is because they reduced the duration of the fully developed phase slightly in order to correlate with test results (pp 62-3 Magnusson and Thelandersson 1970).

The COMPF-2 results for series 6 and 8 are identical and hence the plots for series 8 overlay those for series 6 and can not be distinguished in the graph, as shown in Figure 2.4. The only difference between series 6 and 8 is the crib shape factor (Table 2.3), which affects the porosity controlled burning rate. Since the porosity controlled rate is higher than the ventilation controlled burning rate in both series, the ventilation governs.

Table 2.3 is used to show which of the three parameters; crib porosity, ventilation or the fuel surface, controls the burning rate. The lowest value governs. The porosity value varies directly with the crib shape factor and is constant. The ventilation value is governed by the size and shape of the windows, and is also constant throughout the

duration of the fire. The fuel surface control value is dependent on the fuel remaining and decreases proportional to the square root of the mass of fuel remaining, for a two dimensional fuel. All fires will be fuel bed controlled just before all the fuel is burnt, because as the mass of fuel remaining tends to zero then so does the fuel surface controlled burning rate.

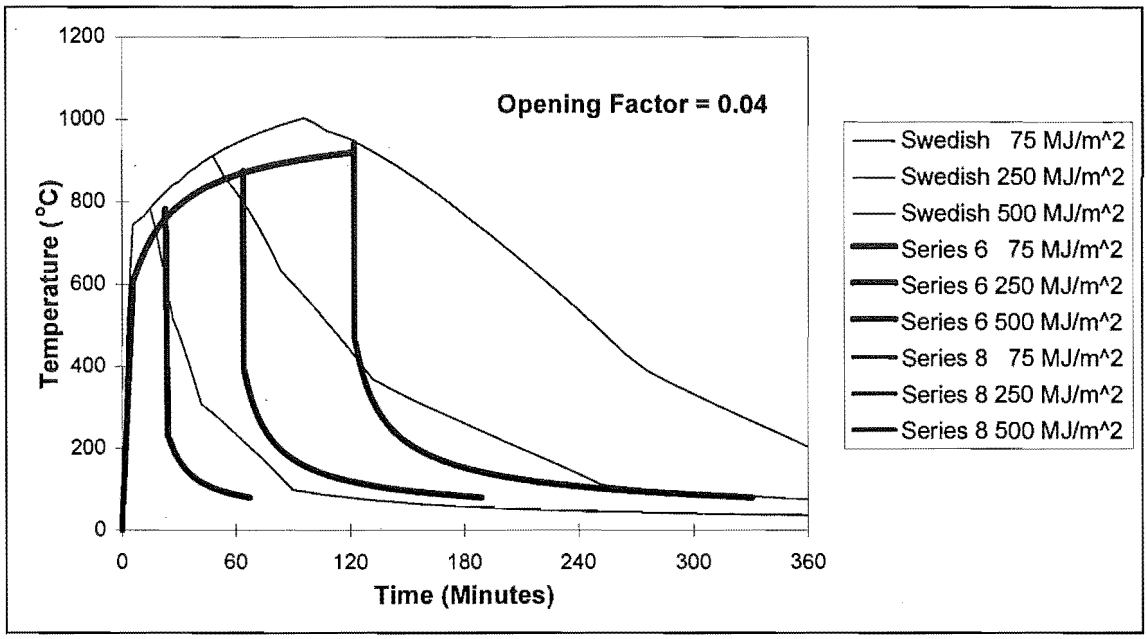

Figure 2.4 Comparison Between Series 6 and 8

For the series 6 and 8 fires, Table 2.3 shows that the fires are all ventilation controlled, except for the 75 MJ/m^2 fires which become fuel surface controlled when less than 20% of the mass of the fuel remains.

Fuel Load MJ/m^2(A_t)	Crib Shape Factor	Rate of Burning,governed by:- Porosity (MW)	Vent. (MW)	Fuel Surface Control (MW) M/M_o= 1.00	0.90	0.80	0.70	0.60	0.50	0.40	0.30	0.20	0.10
Series 6													
75	0.1249	19.9	8.0	23.7	22.5	21.2	19.8	18.4	16.8	15.0	13.0	10.6	7.5
250	0.0375	19.9	8.0	79.0	75.0	70.7	66.1	61.2	55.9	50.0	43.3	35.3	25.0
500	0.0187	19.9	8.0	158.1	149.9	141.4	132.2	122.4	111.8	100.0	86.6	70.7	50.0
Series 8													
75	0.0842	13.4	8.0	23.7	22.5	21.2	19.8	18.4	16.8	15.0	13.0	10.6	7.5
250	0.0253	13.4	8.0	79.0	75.0	70.7	66.1	61.2	55.9	50.0	43.3	35.3	25.0
500	0.0126	13.4	8.0	158.1	149.9	141.4	132.2	122.4	111.8	100.0	86.6	70.7	50.0

Table 2.3 Parameters Governing Burning Rate Series 6 and 8

The maximum temperature reached in the COMPF-2 curves (Figure 2.4) occurs later than for the Swedish curves because of the initial temperature rise added to the COMPF-2 curve (Section 2.5.1.2). The comparison between the Swedish and COMPF-2 curves is reasonable, given the problems with repeatability and accuracy discussed previously. Hence the duration is similar to that calculated by the author and Magnusson and Thelandersson.

2.5.5.2 Fuel Bed Controlled Fires

Series 9 fire curves are developed for cribs consisting of 100 mm sticks.

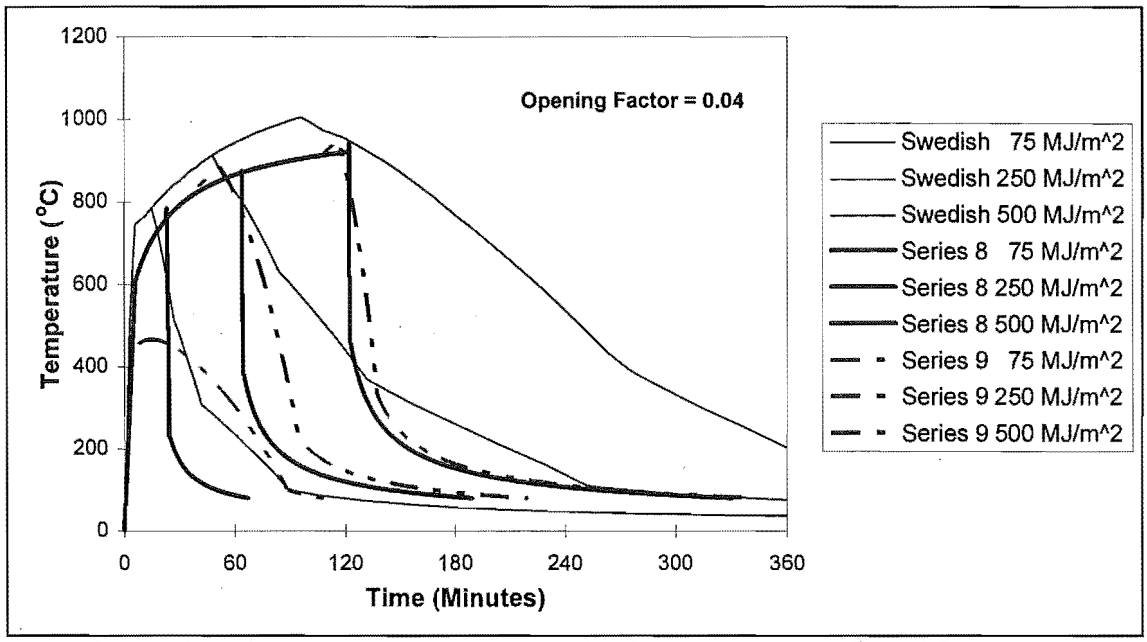

Figure 2.5 Comparison Between Series 8 and 9 and the Swedish Curves

The duration of the fully developed phase for series 9 (Figure 2.5) is significantly longer for the two fires with fuel loads of 75 MJ/m^2 and 250 MJ/m^2 and slightly longer for the 500 MJ/m^2 fire, than for the same fires in series 8. The other difference is that the decay phase is more gradual. The maximum temperature reached by the 75 MJ/m^2 fire in series 9 is much lower than for the same fuel load fire in series 8. This is because the fire is highly ventilation controlled throughout the duration of the fire as shown in Table 2.4.

Fuel Load	Crib Shape	Rate of Burning,governed by:-												
		Porosity	Vent.	Fuel Surface Control (MW)										
MJ/m^2(A_t)	Factor	(MW)	(MW)	M/M_0=	1.00	0.90	0.80	0.70	0.60	0.50	0.40	0.30	0.20	0.10
Series 7 & 9														
75	0.8827	32.4	8.0		2.3	2.1	2.0	1.9	1.7	1.6	1.4	1.2	1.0	0.7
250	0.2648	32.4	8.0		7.5	7.1	6.7	6.3	5.8	5.3	4.8	4.1	3.4	2.4
500	0.1324	32.4	8.0		15.1	14.3	13.5	12.6	11.7	10.6	9.5	8.2	6.7	4.8

Table 2.4 Parameters Governing Burning Rate Series 7 and 9

The 250 MJ/m^2 fire is fuel bed controlled throughout the fire, while the 500 MJ/m^2 fire is fuel bed controlled only after 70% of the fuel is burnt. The degree of fuel surface control accounts for the variation from the series 8 to the series 9 curves for each value of fuel load. The comparison with between series 9 and the Swedish curves is poor for the fire with a fuel load of 75 MJ/m^2, and better for the other two, as their decay phase is longer, but not nearly as long as for the Swedish curves.

2.5.5.3 Crib Shape Factor

The crib shape factor is the ratio of the clear horizontal spacing between the sticks of the crib to the total crib height. In all the crib runs, the spacing is three times the stick thickness. Hence the shape factor is lower for broad low cribs than for narrow tall cribs for the same fuel load energy density (FLED). Series 6 differs from 8 (Figure 2.4) only in the shape parameter of the crib. It is about 50% higher for the 6 series. Since these fires are ventilation controlled, as shown in Table 2.3, this does not make any difference. The crib shape factor is directly proportional to the burning rate for porosity control, so if porosity control governs, then the shape factor is significant. Porosity control has a similar effect to ventilation control of a fire.

2.5.5.4 Percentage of Pyrolysates Burned

The percentage of pyrolysates burnt is the dimensionless ratio of the amount of energy released in the compartment by burning fuel to the pyrolysates produced by the decomposition of the fuel. It is to some extent a measure of combustion efficiency and is described in Section 2.4.1.

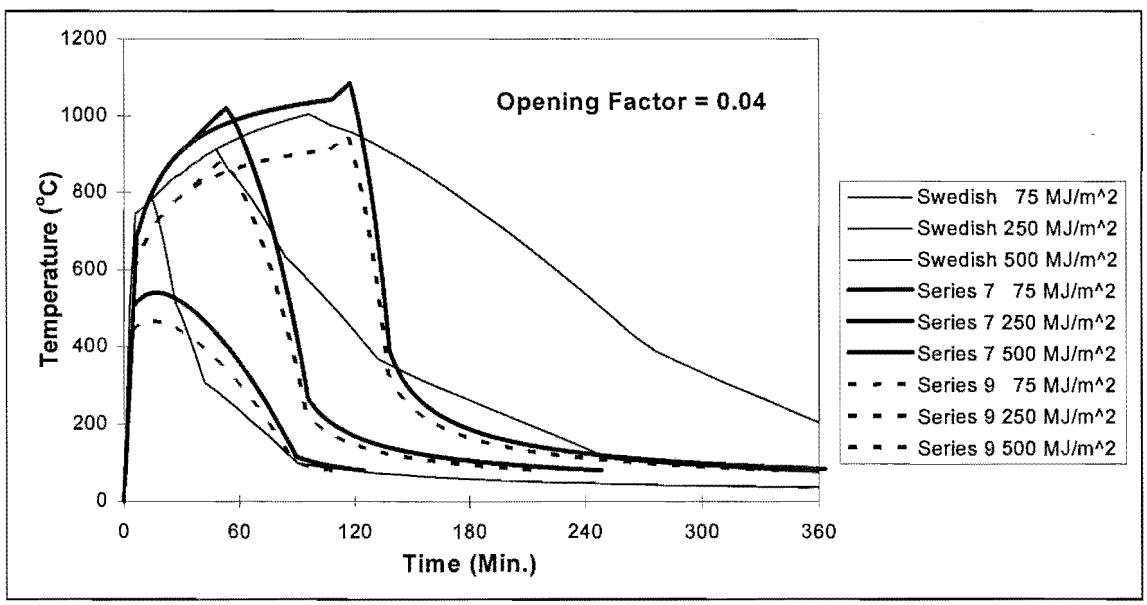

Figure 2.6 Comparison Between Series 7 and 9 and The Swedish Curves

Series 7 and 9 (Figure. 2.6) differ only in the percentage of pyrolysates burned, 85% for series 7 and 70% for series 9. Hence maximum temperatures of about 100°C higher are reached in the series 7 runs, with 85% of pyrolysates burnt, than for fires with 70% of the pyrolysates burnt in series 9. The duration of the fully developed phase is the same (Table 2.2), for both series.

2.5.6 Other Comparisons Between the Models

2.5.6.1 23 mm Cribs

For series 8 fires, the 23 mm stick size cribs, for low and medium ventilation, (Figures. 2.7, 2.8, 2.9) have good agreement with the Swedish curves until the end of the fully developed phase.

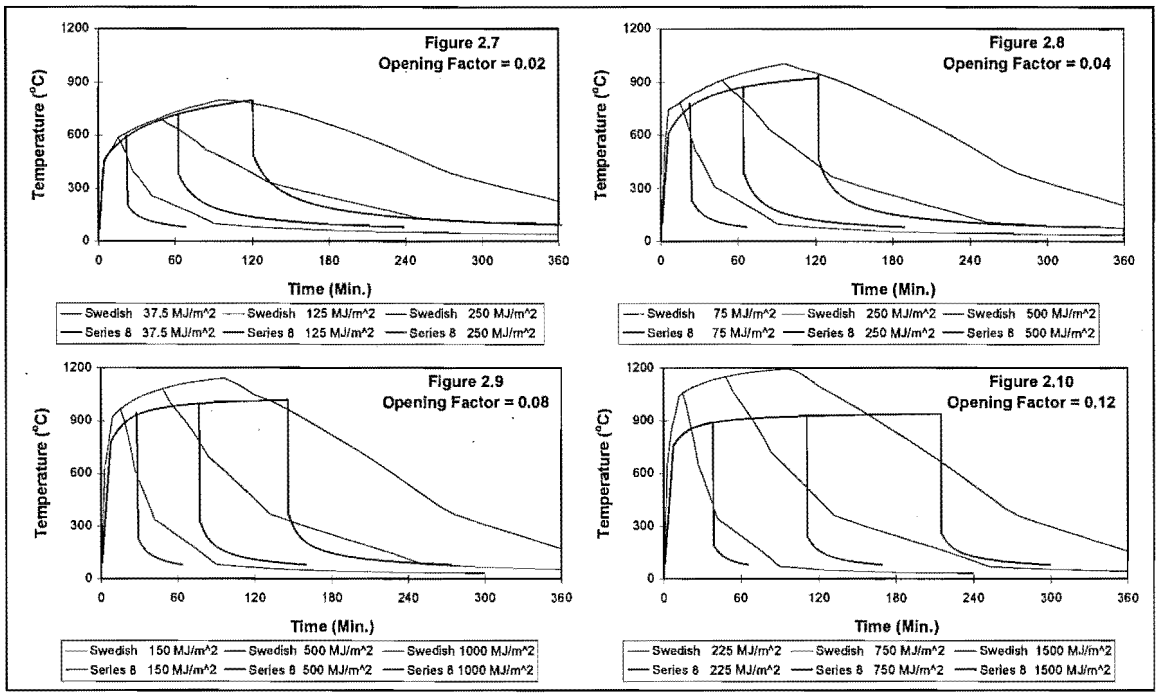

Figures 2.7 to 2.10 Comparison Between Series 8 and the Swedish Curves

For high opening factors, Figure 2.10 shows a longer fully developed phase and lower temperatures, because the fire is crib porosity controlled (see Table 2.5). The values of heat output for the porosity controlled case is lower than that for ventilation control. The length of the fully developed phase is also similar to that calculated by hand (Table 2.2).

Fuel Load	Crib Shape	Rate of Burning,governed by:-											
		Porosity	Vent.	Fuel Surface Control (MW)									
$MJ/m^2(A_t)$	Factor	(MW)	(MW)	M/M_o= 1.00	0.90	0.80	0.70	0.60	0.50	0.40	0.30	0.20	0.10
Series 8													
37.5	0.1684	13.4	4.0	11.9	11.2	10.6	9.9	9.2	8.4	7.5	6.5	5.3	3.7
125	0.0505	13.4	4.0	39.5	37.5	35.3	33.1	30.6	27.9	25.0	21.6	17.7	12.5
250	0.0253	13.4	4.0	79.0	75.0	70.7	66.1	61.2	55.9	50.0	43.3	35.3	25.0
75	0.0842	13.4	8.0	23.7	22.5	21.2	19.8	18.4	16.8	15.0	13.0	10.6	7.5
250	0.0253	13.4	8.0	79.0	75.0	70.7	66.1	61.2	55.9	50.0	43.3	35.3	25.0
500	0.0126	13.4	8.0	158.1	149.9	141.4	132.2	122.4	111.8	100.0	86.6	70.7	50.0
150	0.0421	13.4	15.9	47.4	45.0	42.4	39.7	36.7	33.5	30.0	26.0	21.2	15.0
500	0.0126	13.4	15.9	158.1	149.9	141.4	132.2	122.4	111.8	100.0	86.6	70.7	50.0
1000	0.0063	13.4	15.9	316.1	299.9	282.7	264.5	244.9	223.5	199.9	173.1	141.4	100.0
225	0.0281	13.4	23.9	71.1	67.5	63.6	59.5	55.1	50.3	45.0	39.0	31.8	22.5
1000	0.0084	13.4	23.9	237.1	224.9	212.0	198.4	183.6	167.6	149.9	129.9	106.0	75.0
1500	0.0042	13.4	23.9	474.2	449.8	424.1	396.7	367.3	335.3	299.9	259.7	212.0	474.2

Table 2.5 Parameters Governing Burning Rate, Series 8

2.5.6.2 100 mm Cribs

Series 9, the 100 mm stick size cribs, shown in Figures 2.11 to 2.14, differ from series 8, in that the fires are fuel bed controlled for the entire duration of the fire except for the fire which has the highest fuel load for each ventilation value.

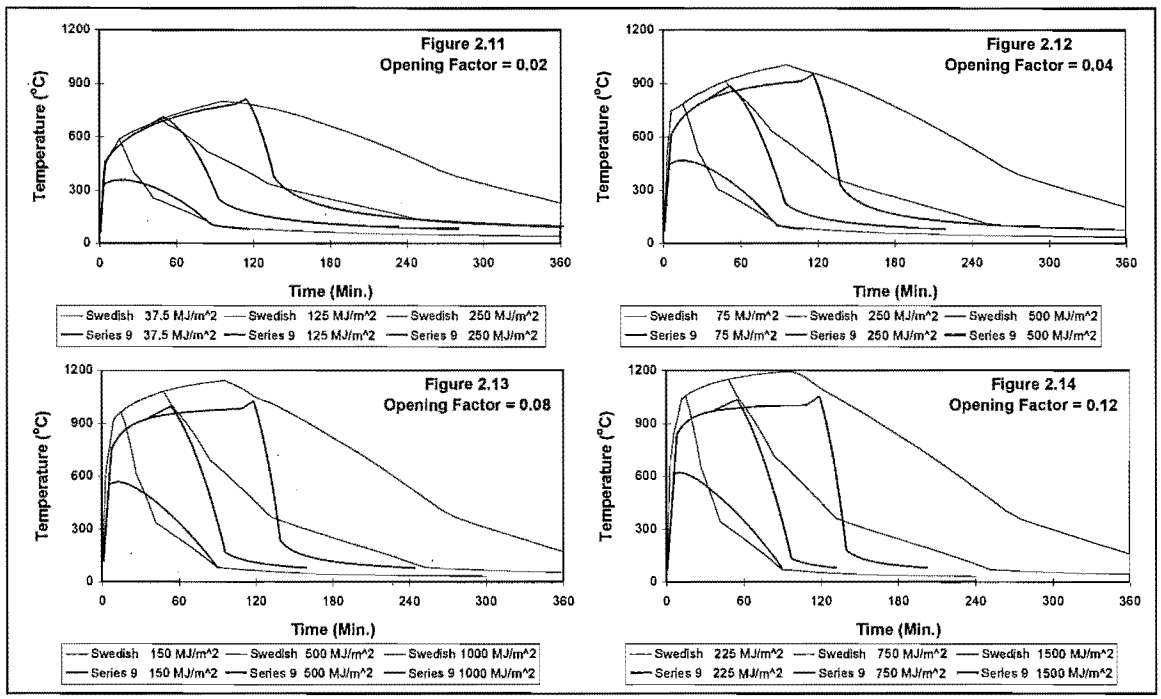

Figures 2.11 to 2.14 Comparison Between Series 9 and the Swedish Curves

Hence the duration of the fire is not affected by the opening factor. The parameters affecting the burning rate are shown in Table 2.6

Fuel Load	Crib Shape	Rate of Burning,governed by:-											
		Porosity	Vent.	Fuel Surface Control (MW)									
$MJ/m^2(A_t)$	Factor	(MW)	(MW)	M/M_o= 1.00	0.90	0.80	0.70	0.60	0.50	0.40	0.30	0.20	0.10
Series 9													
37.5	1.7654	32.4	4.0	1.1	1.1	1.0	0.9	0.9	0.8	0.7	0.6	0.5	0.4
125	0.5296	32.4	4.0	3.8	3.6	3.4	3.1	2.9	2.7	2.4	2.1	1.7	1.2
250	0.2648	32.4	4.0	7.5	7.1	6.7	6.3	5.8	5.3	4.8	4.1	3.4	2.4
75	0.8827	32.4	8.0	2.3	2.1	2.0	1.9	1.7	1.6	1.4	1.2	1.0	0.7
250	0.2648	32.4	8.0	7.5	7.1	6.7	6.3	5.8	5.3	4.8	4.1	3.4	2.4
500	0.1324	32.4	8.0	15.1	14.3	13.5	12.6	11.7	10.6	9.5	8.2	6.7	4.8
150	0.4413	32.4	15.9	4.5	4.3	4.0	3.8	3.5	3.2	2.9	2.5	2.0	1.4
500	0.1324	32.4	15.9	15.1	14.3	13.5	12.6	11.7	10.6	9.5	8.2	6.7	4.8
1000	0.0662	32.4	15.9	30.1	28.6	26.9	25.2	23.3	21.3	19.0	16.5	13.5	9.5
225	0.2942	32.4	23.9	6.8	6.4	6.1	5.7	5.2	4.8	4.3	3.7	3.0	2.1
1000	0.0883	32.4	23.9	22.6	21.4	20.2	18.9	17.5	16.0	14.3	12.4	10.1	7.1
1500	0.0441	32.4	23.9	45.2	42.8	40.4	37.8	35.0	31.9	28.6	24.7	20.2	45.2

Table 2.6 Parameters Governing Burning Rate Series 9

The runs with the lowest fuel load in each set are so severely fuel controlled that the initial burning rate is much lower than in series 8 and the temperatures reached are significantly lower.

In both series 8 and 9 the temperatures predicted by COMPF-2 were higher than the Swedish curves for an opening factor of 0.02 (Figures 2.7, 2.11) roughly equal for a

opening factor of 0.04 (Figures 2.8, 2.12) and lower for higher opening factors (Figures 2.9, 2.10, 2.13, 2.14).

2.5.7 Heat Input To Walls

In general, the effects of ventilation and fuel load are what is normally expected; that is, higher opening factors cause a hotter and shorter fire and higher fuel loads cause a longer fire. Table 2.7 shows the total heat input into the walls for series 8, 9, 10 and 11, over the full duration of the fire. It is higher for the longer, cooler fires typical of the fuel bed controlled fires in series 9, provided the opening factor is low (0.04 or less).

Series			8	9	10	11
Stick Size (mm)			23	100	150	*
% Pyrolysites Burned			70	70	70	70
Run	Vent. Factor	Fuel Load (MJ/m^2)	Heat Input to Walls			
			kJ/m^2	kJ/m^2	kJ/m^2	kJ/m^2
1	0.02	38	14	16		
2	0.02	125	40	42		
3	0.02	250	68	68		
4	0.04	75	20	20	18	24
5	0.04	250	51	53	56	50
6	0.04	500	82	82	68	68
7	0.08	150	29	23		
8	0.08	500	66	58		
9	0.08	1000	99	87		
10	0.12	225	34	24		
11	0.12	750	72	57		
12	0.12	1500	107	85		
* Varies with Fuel Load						

Table 2.7 Heat Input to Walls of Compartment

At higher opening factors the short, hotter, ventilation controlled fires in series 8 appear more severe. At higher opening factors the proportion of heat flow through the window is higher and hence heat flow into the wall is lower. The heat input into the walls is by convection, with a value proportional to the temperature difference between the compartment walls and the gas temperature, and radiation which is proportional to the temperature difference raised to the power of four. Radiation through the window is a minor component of heat loss and the heat loss due to mass flow through the window is roughly proportional to the temperature of the gas, as the flow is buoyancy driven. Hence if the fire temperature is higher the proportion of total heat input into the wall is higher.

In series 8, as for all ventilation controlled fires, if the ventilation increases, then the gas temperature increases (Babrauskas and Williamson 1979) and therefore so will the proportion of heat input to the walls. With fuel bed controlled fires such as series 9, if

the ventilation is increased, then temperatures will decrease as the burning rate will not alter, but there is more energy lost by convective flow through the window, which cools the compartment. The gas temperature and hence heat input to the walls is therefore lower. The difference in temperature is about 10% for fires with low ventilation and up to 30% for fires with high ventilation.

2.5.8 COMPF-2 Runs Assuming Stick Burning

Series 10 and 11 are described in Tables 2.2, and 2.8 and are portrayed graphically in Figure 2.15.

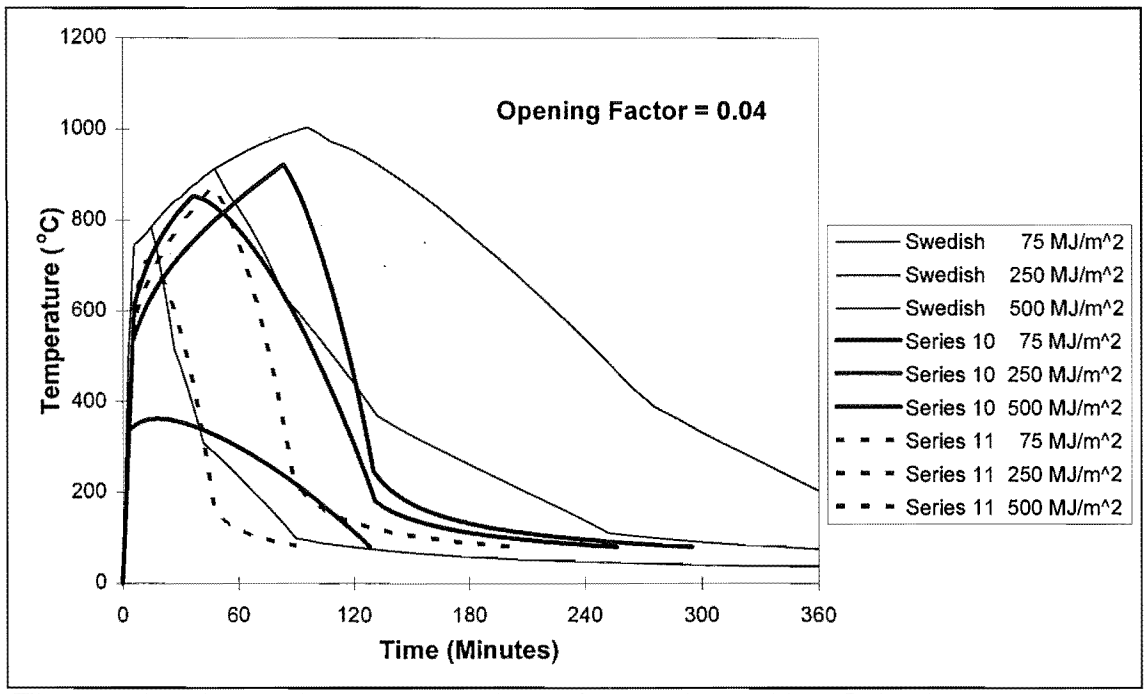

Figure 2.15 Comparison Between Series 10 and Series 11 and the Swedish Curves

Runs 10 and 11 use the stick burning option in COMPF-2. The difference between this and the crib burning option is that porosity control is not a factor. Series 10 was developed using 150 mm sticks. In series 11 the fuel size was varied with fuel load in an attempt to produce curves that are similar to the Swedish curves and was chosen arbitrarily as:-

50 mm for a fuel load of 300 kJ/m^2

100 mm for a fuel load of 1000 kJ/m^2

150 mm for a fuel load of 2000 kJ/m^2

The curves for the 500 MJ/m^2 fire in series 11 overlays the 500 MJ/m^2 fire in series 10, because they both have the same stick size in both series The fuel regression rate must

be specified for stick burning. This was chosen as 36 mm per hour. It can be seen in Table 2.8 that all series 10 and 11 fires are fuel surface controlled. As these series are stick fires, the crib shape factor and crib porosity control value do not exist.

Fuel Load $MJ/m^2(A_t)$	Crib Shape Factor	Rate of Burning,governed by:- Porosity (MW)	Vent. (MW)	Fuel Surface Control (MW) M/M_o = 1.00	0.90	0.80	0.70	0.60	0.50	0.40	0.30	0.20	0.10
Series 10													
75			8.0	1.2	1.1	1.1	1.0	0.9	0.8	0.7	0.6	0.5	0.4
250			8.0	3.9	3.7	3.5	3.3	3.0	2.8	2.5	2.2	1.8	1.2
500			8.0	7.9	7.5	7.0	6.6	6.1	5.6	5.0	4.3	3.5	2.5
Series 11													
75			8.0	6.8	6.5	6.1	5.7	5.3	4.8	4.3	3.7	3.1	2.2
250			8.0	7.5	7.1	6.7	6.3	5.8	5.3	4.8	4.1	3.4	2.4
500			8.0	7.9	7.5	7.0	6.6	6.1	5.6	5.0	4.3	3.5	2.5

Table 2.8 Parameters Governing Burning Rate Series 10 and 11

A shape factor of 2 was chosen. The shape factor depends on the dimensionality of the material, and has a value of 1,2 or 3, as follows:-

(i) Shape factor = 1; for slabs, items that are thin in one dimension, but large in the other two dimensions, examples are the top of a desk or the side of cupboard.

(ii) Shape factor = 2; for prismatic objects (sticks), items that are thin in two dimensions, but large in one dimension, examples are chair legs or table legs.

(iii) Shape factor = 3; for objects that are small in three dimensions, such as spheres or cubes.

The duration of the fully developed phase is the same for the three different fuel loads (Table 2.2). Fuel surface control governs throughout series 10 (Figure 2.14) and the shape of the curves is very similar to series 9 (Figure 2.12). This is because the stick size is similar (Table 2.2) and the crib fires (Table 2.3) are not porosity controlled. The series 9 fires, are all fuel surface controlled except at the start of the 500 MJ/m^2 fire, which is ventilation controlled. Crib fires will only vary significantly from other fires if they are porosity controlled or if the shape factor is not 2.

The results for series 11 are shown in Figure 2.15 Using a smaller fuel size for lower fuel loads results in a fire that initially burns much more rapidly and higher temperatures are reached. This is usually a more severe case as the heat input to the walls is much higher. This is reflected in the total heat input to the walls being higher for the 75 MJ/m^2 fire in series 11 than for the same size fire in series 10. The 250 MJ/m^2 fire however is less severe for series 11 than series 10. The temperatures reached in the 75 MJ/m^2 and the 250 MJ/m^2 fire are lower for series 10 than for series 11,

because the fuel surface controlled burning rate is much lower in series 10 than series 11.

2.6 Conclusions

2.6.1 The Swedish Time-Temperature Curves

The burning rate is ventilation controlled.

The length and shape of the decay phase is extrapolated from test results.

All the energy contained within the fuel is released within the compartment.

The shape of the curves are a direct result of the assumptions mentioned above and their affect on the shape of the mass loss rate versus time curves.

Correlations for concrete lined compartments can be extrapolated for other materials.

2.6.2 COMPF-2

The burning rate is governed by the lower of:-

(i) Ventilation control.

(ii) Fuel surface control.

(iii) Crib porosity control (for crib fires only).

The time-temperature curve is very sensitive to the fuel geometry for fuel bed-controlled wood fires (as sticks, slabs, blocks or cribs).

The decay phase is very short for fires that are ventilation controlled throughout the duration of the fire, or longer for fuel bed controlled fires.

COMPF-2 ignores radiation from the room back to the fuel (except for hydrocarbon pool fires) which may result in an underestimate of the pyrolysis rate. If the fire is pessimised over ventilation, then this may result in an overestimate of the fraction of fuel burnt compared with the input value.

The shape of the time-temperature curves are a result of the assumptions made in the program and assumptions regarding the mass loss rate as a function of time.

2.6.3 Comparison

The duration of the fully developed phase, and temperatures reached during the fully developed phase are very similar for ventilation controlled fires.

For large ventilation fires, COMPF-2 produces cooler fires than for the Swedish type A compartment.

It is possible to manipulate the stick size to get a fire that switches from ventilation control to fuel bed control, after about 60% of the fuel has burnt, and produce COMPF-2 time-temperature curves, that are similar to the Swedish curves. It is not possible to produce a decay phase using COMPF-2 that is as long or as hot as that in the Swedish curves. This is because COMPF-2 does not make the erroneous assumption that 100% of the fuel's energy is released within the compartment.

2.6.4 Recommendations for Future Work

The effect of fuel geometry needs to be looked at further.

More fuel load surveys need to be carried out and must include details on the shape and size of fuel as well as the fuel load.

A model that allows for multiple fuel types needs to be developed. This could be a development of COMPF-2. Ideally it should also include the effects of re-radiation to the fuel surface to solid fuels and accurately calculate pyrolysis rates from first principles, but this problem is extremely complex and difficult to solve.

In the long term, a computer program should be developed to produce fire curves for different occupancies and/or types of fuels, as well as for fuel loads, ventilation parameters and lining properties.

Chapter 3 Heat Transfer Through Walls

3.1 Literature Review

This Section is divided into two parts, the first is a review of wall models and the second is a review of models for heat transfer in wood alone.

3.1.1 Wall Models

Collier (1991a, 1991b, 1992 and 1994) has developed a design method for extrapolating test results for light timber framed walls exposed to the ISO-834 standard test. There are limits on the use of the extrapolation and the method requires a significant testing program.

Gammon (1987) attempted to predict the structural performance of light timber frame walls exposed to the ASTM E-119 fire as a time to failure and compared it with real fire tests. He wrote his own Fortran program for doing this, which is listed in his dissertation. He used a coarse mesh and ignored convection across the cavity in the wall. The analysis of heat transfer across the wall is adequate, but the structural model is simplistic. He considered a (Euler) buckling formula of the reduced section of each stud to calculate the time to structural failure. This is a very simplistic determination which ignores the effects of the linings on stability and strength.

König (1991, 1994) describes small scale tests carried out on light timber members in pure bending and subjected to an ISO-834 exposure. Some of the tests were of specimens lined with gypsum plasterboard, but the gypsum plasterboard was attached in such a way that it did not contribute to the strength of the stud. The timber members were exposed on one side only as the two long sides were insulated using rock wool.

The char front can be modelled as a straight line parallel to the exposed face. The depth of charring was found to vary linearly with time at a rate of about 1.4 mm per minute and hence could be predicted reasonably accurately. The compression strength appears to drop more rapidly with temperature than the strength in tension. This is probably due to the "steaming" effect, where creep occurs rapidly in timber under compression loading and containing steam. The properties found in small scale tests were used to make a reasonable prediction of the time to failure of full size wall tests when the ends of the studs were modelled as partial hinges (König and Kallsner 1988).

The most recent developments in this field are by Forintek Canada Corporation, (Mehaffey et al 1994, Currier 1993, Mehaffey 1991). This research group has been developing a computer model for the behaviour of light timber frame walls exposed to fire tests. They have achieved reasonable correlations using the following methodology:-

(i) Literature was reviewed to find thermo-physical and material properties of gypsum plasterboard. Other models such as Gammon were also reviewed.

(ii) The thermo-physical and mechanical properties of gypsum plasterboard and timber were found for elevated temperature ranges.

(iii) A two dimensional computer model for heat transfer was developed and correlated using a range of furnace tests. Initially a test on a solid wall composed of four layers of gypsum plasterboard board, was used to correlate the gypsum wallboard properties. The specific heat was measured using a differential scanning calorimeter. The conductivity was modified, by increasing it at a more rapid rate over 500^{O}C in order to mimic ablation of the board.

Clancey et al (1994) are in the process of developing a more sophisticated model which was to include mass transfer, but this was omitted in the final model. The main effect of mass transfer is to result in a rapid initial temperature increase on the ambient side of the void as moisture evaporated from the lining on the fire side of the cavity condenses on the lining on the other side of the void. This moisture then has to be re-evaporated before the temperature on the ambient side of the void increases much above 100^{o}C. However, as the energy transferred when the moisture is condensed is equal to that

require to evaporate the moisture again, the net effect on the temperature profile at that point is nil at temperatures of interest, over 120°C.

3.1.2 Heat and Mass Transfer in Wood

Fredlund (1988) describes a computer based finite element model used to calculate multiple parameters for a slab of wood exposed to a known radiant heat flux on one surface. The parameters are temperature, pore pressure, density, mass loss rate, moisture content and rate of regression of the char interface. The model is essentially one dimensional, but incorporates mass transfer as well as heat transfer. The report includes a review of thermal properties of wood and char.

3.2 TASEF

Heat transfer through cavity walls is modelled using TASEF (Version 3.0), a two dimensional heat transfer model developed for fire problems at the Swedish National Testing Institute (Sterner and Wickstrom 1990).

The wall section modelled is shown in Figure 3.1.

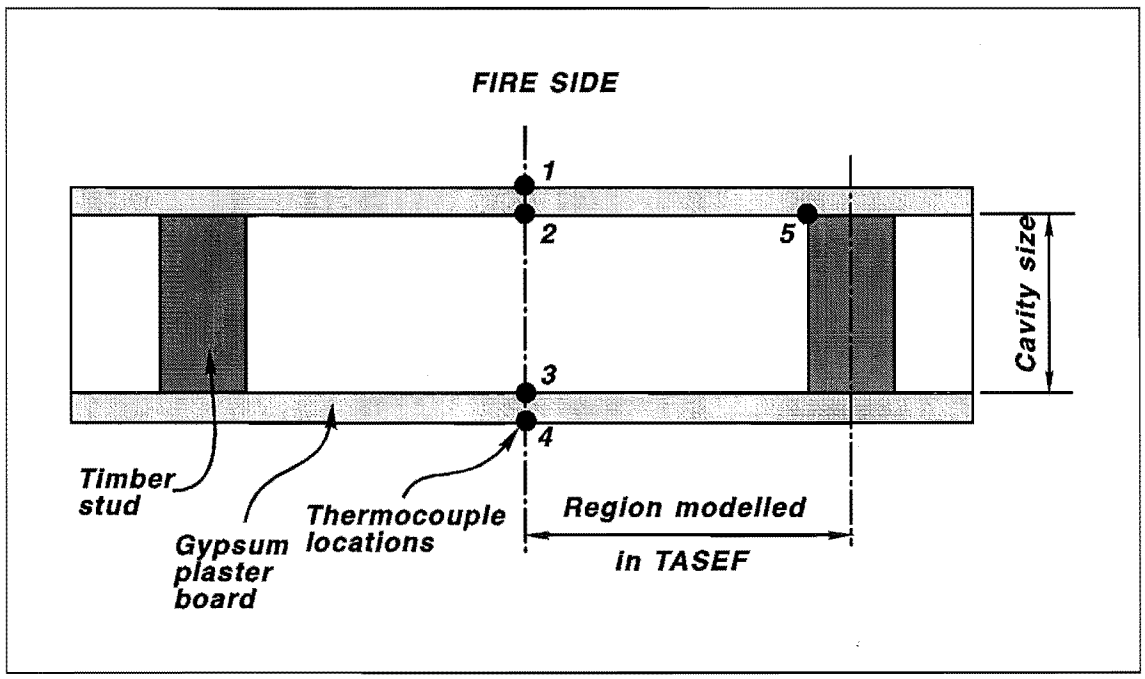

Figure 3.1 Section of Light Timber Framed Wall

3.2.1 The Heat Balance in TASEF

TASEF was developed for use for fire problems and uses a forward difference time integration scheme. It has sub-routines to analyse heat transfer by convection and radiation across voids. It does not model mass transfer within an assembly but does allow for combinations of material types. Thermal inertia and thermal conductivity can be specified as temperature dependent. The element heat balance is subject to the following equation:-

$$\frac{\partial}{\partial x}\left(k\frac{\partial T}{\partial x}\right)+\frac{\partial}{\partial y}\left(k\frac{\partial T}{\partial y}\right)-\frac{\partial\left(\rho C_p T\right)}{\partial t}+Q=0 \tag{3.1}$$

Where:- x, y are co-ordinates (m)

T is temperature (K)

k is thermal conductivity (kW/m.K)

ρ is density (kg/m^3)

C_p is specific heat (kJ/kg.K)

t is time (s)

Q is internally generated heat (kW/m^3)

This can be summarised as the net heat flow in to the element in the x and y directions (the first two terms) less the increase in internal energy (the third term) plus any internal heat generation from chemical reactions or say electrical heating elements is equal to zero.

3.2.2 Heat Transfer at Boundaries

The heat transfer across boundaries is given by:-

$$q=\varepsilon\sigma\left(T_g^4-T_s^4\right)+\beta\left(T_g-T_s\right)^\gamma \tag{3.2}$$

Where:-q is the rate of heat transfer (W/m^2)

ε is the resultant emissivity of the gas and the boundary (dimensionless)

σ is the Stefan -Boltzmann constant ($5.67*10^{-8}$ W/m^2K^4)

β is the convection coefficient (W/m^2K^{γ})

γ is the convection power, usually 1.33 (dimensionless)

T_g is the absolute gas temperature (K)

T_s is the absolute surface temperature (K)

TASEF , however does not allow for temperature dependent values of ε, β and γ. The values for β and γ do not have a large effect on the overall heat transfer if they are within the range recommended in the TASEF manual.

On the fire side of the assembly the first term, that is, the radiation term governs. This is because the temperatures are large and the temperatures are raised to the fourth power. The second or convective term is often ignored in determining the heat flux from the furnace into the test wall. It may be significant in small furnaces, less than about two square metres (Sultan et al 1986). However on the cold side of the assembly the convection term governs (Sterner and Wickstrom 1990). This was confirmed by a sensitivity analysis of the finite element model. The most critical value on the fire side is the emissivity as this alters the radiation term.

3.2.2.1 Heat Transfer At the Void Boundaries

The heat transfer in the void is very significant as this determines the charring and hence load capacity of the timber members. When using the temperature differences across the void found in real fire tests, then convection governs across the void.

There is little information about the heat flow through cavities in light timber framed walls. This information may be gained from a furnace test using calorimeters and radiometers to measure precisely the net heat flux and components of heat flux through a wall assembly. The characteristics of the measuring equipment may result in results that are difficult to reproduce.

TASEF assumes the void is a vacuum for radiation purposes. In reality some radiation is absorbed by void gases and is then re-emitted. The proportion of radiative heat flux absorbed by the void gases increases as the test progresses because steam and smoke are present in the cavity. This radiation absorbed heats the gas in the void. Since almost all of the heat absorbed by the gas is re-emitted and the specific heat for the void gases is low, it does not affect the overall result. As a result of this simplification however TASEF does underpredict the void temperature.

3.3 Assumptions Used in This Analysis

The finite element model of walls was developed assuming the following:-

(i) Mass transfer, that is, movement of moisture in the assembly is ignored. It only has a significant effect at temperatures below 120 C.

(ii) The emissivities emissivity and convection coefficients are constant, that is, not time or temperature dependent This reduces the complexity of the analysis.

(iii) The emissivities and convection coefficients are the same for the gypsum plasterboard on both sides of the cavity and for the timber. This again reduces the number of variables in the analysis.

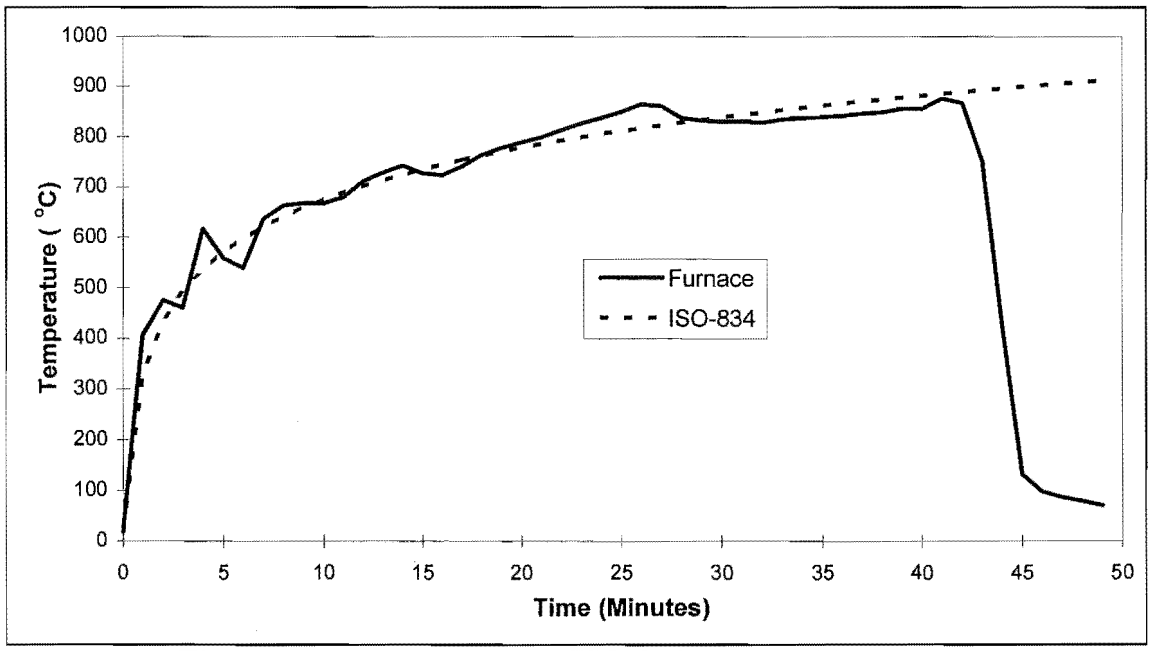

Figure 3.2 Actual and Ideal ISO-834 Furnace Test Curve

(iv) The ISO-834 test curve is used as specified, rather than the actual furnace temperatures. The data supplied by BRANZ on fire tests includes furnace temperatures.

Figure 3.2 is a plot of the furnace temperature (average of twelve thermocouples) and the ISO-834 test curve over time. There is a variation from the ISO-834 curve. The real curve can be used, but does not make a significant difference in the results.

3.4 Specific Heat and Enthalpy of Gypsum Plasterboard

These properties were determined from a literature review and checked using calculation methods where possible.

3.4.1 Literature on Specific Heat

Dry gypsum, that is, with no free moisture, contains 21% water by weight, that is bound in a crystal matrix. This water is released and evaporates during heating. Some free moisture is also present in gypsum boards. This free moisture is also driven off as steam.

3.4.1.1 Harmathy

A value of specific heat of 0.84 kJ/kg.K is given in Drysdale (1985) for ambient temperatures. This compares well with Harmathy (1988), who gives a value of 0.88 kJ/kg.K, with a peak of 7.32 kJ/kg.K at about 100°C, a trough of 0.25 kJ/kg.K at about 350°C and a rapid increase over 550°C. Although it is difficult to measure off a graph, the width of the 100°C peak appears to be 60 to 65°C. Hence the energy required to drive the moisture off is (7.32-0.88)*62.5/2 = 201 kJ/kg of gypsum board. This value is rather low.

3.4.1.2 Andersson and Jansson

Andersson and Jansson (1987) do not report a base specific heat value as such, but report that 75% of the bound water starts to evaporate at 100°C requiring 515 kJ/kg for this process to occur (reaction 1, Figure 3.3 and Equation 3.1). The remaining 25% of water of crystallisation is driven off at around 210°C. This process is again endothermic and requires 185 kJ/kg of gypsum for completion (reaction 2, Figure 3.3 and Equation 3.2). A base value of 0.7 kJ/kg.K was deduced for specific heat from an enthalpy curve.

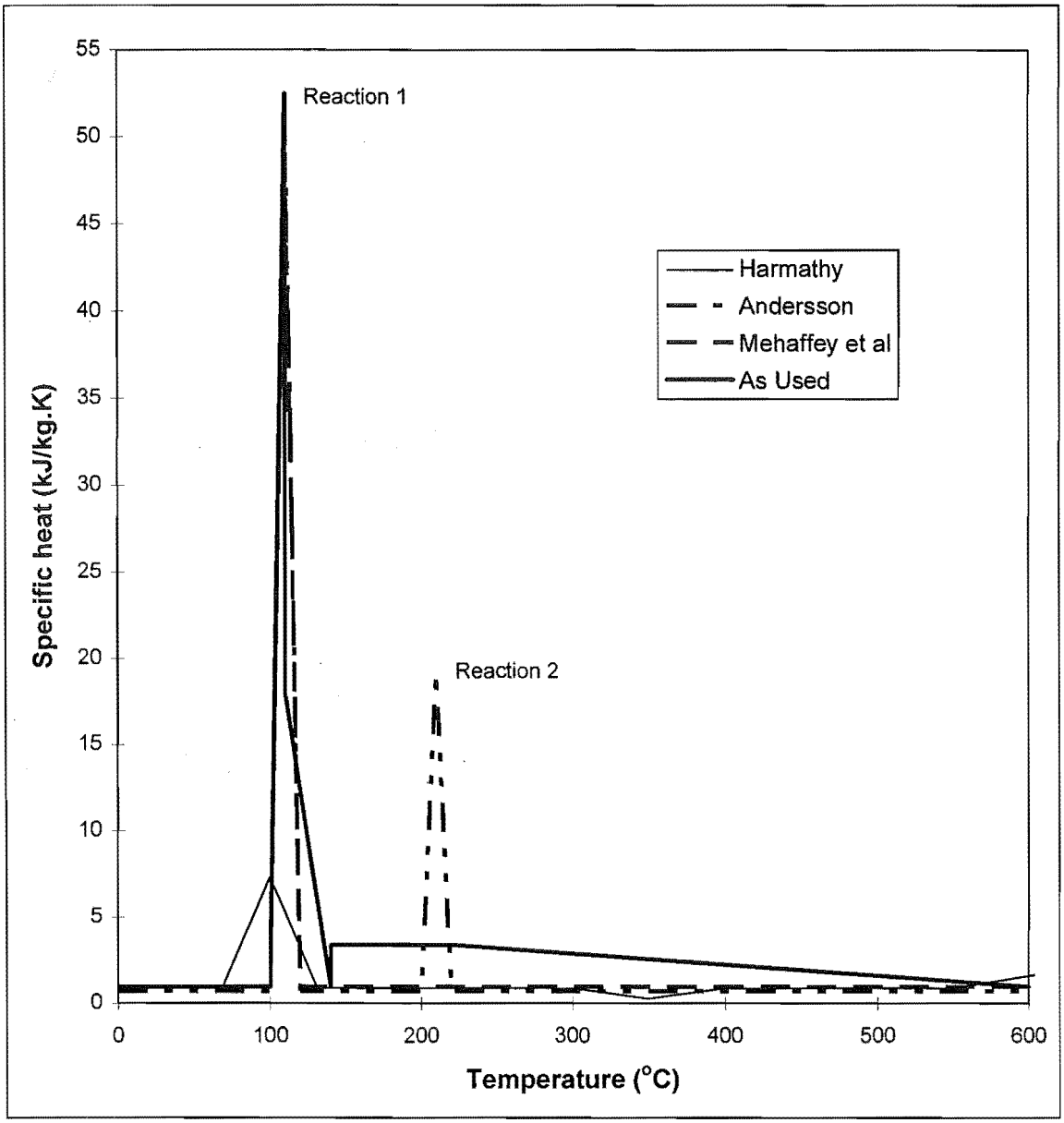

Figure 3.3 Comparison of Specific Heat Values from Different Researchers

3.4.1.3 Mehaffey et al

Mehaffey et al (1994) utilised a differential scanning calorimeter and obtained a base value of 0.95 kJ/kg.K for specific heat. Two scanning rates were used, 2°C/min and 20°C/min. For the slower scanning rate a peak of 29 kJ/kg.K at 95°C was found. A peak of 14 kJ/kg.K at 140°C resulted when the faster scanning rate was used. The area under both peaks is about 490 kJ/kg. Mehaffey et al used a symmetrical peak of 49.95 kJ/kg.K between 100°C and 120°C in their model. Mehaffey et al only measured specific heat up to 200°C and did not record the second peak at 210°C (reaction 2), where the remainder of the water of crystallisation is driven off. Figure 3.3 compares these values.

3.4.2 Chemistry and Specific Heat of Gypsum Plasterboard

The base value for specific heat of gypsum was chosen as 0.95 kJ/kg.K. This value is from Mehaffey et al. It is used because they describe the method used to reach this value and the method is sound. It compares well with the value of 1.08 kJ/kg.K for pure gypsum as selenite (CRC 1991). Gypsum Plasterboard is over 90% gypsum with small quantities of other materials such as glass and vermiculite.

3.4.2.1 Water of Crystallisation

During heating gypsum plaster undergoes two endothermic decomposition reactions in which the water of crystallisation is removed. These are denoted reaction 1 and reaction 2 in Figure 3.3.

3.4.2.2 The First Dehydration Reaction

In the first reaction, shown as the first peak in Figure 3.3, the enthalpy plot, gypsum is converted to calcium sulphate hemihydrate as follows:-

$$CaSO_4.2H_2O \rightarrow CaSO_4.\tfrac{1}{2}H_2O + \tfrac{3}{2}H_2O \qquad (3.3)$$

This reaction starts at about 100°C and is completed by about 120°C, but this range is affected by the rate of heating. This effect is shown by the different values given by Mehaffey et al (1994) for different scanning rate using a differential scanning calorimeter. The heat of this reaction is 112 kJ/kg of gypsum, assuming a β form of hemihydrate is formed and 100 kJ/kg for the α form. The heats of reactions are calculated using enthalpies from CRC (1991). Both forms are crystals, the β form has smaller crystals and is a higher energy form. As can be seen in the equation, 75% of the water of crystallisation is driven off. As the total water of crystallisation is 20.9% by mass, then 0.75 * 20.9 = 15.675% of the total mass is water. This water is then evaporated with an energy requirement of 0.15675 * 2260 = 354 kJ/kg of gypsum.

3.4.2.3 The Second Dehydration Reaction

In the second reaction, labelled reaction 2 in Figure 3.3, calcium sulphate hemihydrate is converted to calcium sulphate anhydrate as follows:-

$$CaSO_4.\tfrac{1}{2}H_2O \rightarrow CaSO_4 + \tfrac{1}{2}H_2O \qquad (3.4)$$

This reaction occurs at about 210°C according to Andersson and Jansson (1987) and 300°C according to others (Groves 1958). This value may also depend on the rate of heating. The heat of this reaction is 63.5 kJ/kg of gypsum, assuming a β form of anhydrate is formed from β-hemihydrate and 50 kJ/kg for the α-hemihydrate decomposing to α- anhydrate. The form of the anhydrate is the same as that of the hemihydrate it was derived from (Groves 1958). As can be seen in Equation 3.4, 25% of the water of crystallisation is driven off. As the total water of crystallisation is 20.9% by mass, then 0.25 * 20.9 = 5.225% of the total mass is water. This water is then evaporated with an energy requirement of 0.05225 * 2260 = 136 kJ/kg of gypsum.

3.4.2.4 Mehaffey et al's Method for Accounting for these Reactions

Mehaffey et al used the overall heat of reaction for the reaction shown in Equation 3.5:-

$$CaSO_4.2H_2O \rightarrow CaSO_4 + 2H_2O \qquad (3.5)$$

It was between 150 kJ/kg for α-anhydrate and 176 kJ/kg for β-anhydrate. They ignored the heat required to vaporise the 25% of water of crystallisation produced when the second part of the reaction (Equation 2.1) occurs. This method gives a total value of between 505 and 531 kJ/kg of gypsum. They also state that the energy required to undertake the first reaction (Equation 3.1) is over 455 kJ/kg, being 355 kJ/kg for the evaporation of moisture produced and between 100 and 112 kJ/kg for the heat of the reaction. It appears that these values bound the average value for the peak they found using a scanning calorimeter. They have ignored the effect of free moisture that was not removed during conditioning.

3.4.2.1 Effect of Free Moisture

The basic value of 0.950 kJ/kg.K does not include the effect of free moisture as the Mehaffey et al samples were conditioned at 40°C for 24 hours to remove most of the free moisture. If the free moisture that is removed is about 3 to 4% of total mass, the increase in specific heat due to free moisture is approximately 0.035/1.035 * (4.184 - 0.95) = 0.11 kJ/kg.K of gypsum.

In tests carried out at the University of Canterbury, samples of gypsum plasterboard were conditioned at 50°C for nine days and then heated to 180°C over a period of eight weeks. The initial moisture content after conditioning was between 22.4 and 23.3% of

dry mass or 18.0 and 18.7% of total mass. After 4 weeks at 105°C and 1 week at 120°C, the samples reached a minimum weight which remained constant after 3 weeks of 20°C incremental temperature rises to 180°C. As no decrease in moisture content was observed between 120°C and 180°C, it can be assumed that the second reaction (Equation 3.4) did not occur. In the first reaction (Equation 3.3) 15.675% of total mass is driven off as water. Therefore between 18.02 - 15.675 = 2.35% and 18.70 - 15.675 = 3.0% of the total mass is residual free water, that is not easily driven off. Gypsum plasterboard has an equilibrium moisture content of about 4-8%. This will vary depending on ambient conditions. The moisture that is removed by conditioning is easily removed and hence is ignored in calculating the specific heat.

3.4.3 Heats of Reaction and Effect on Specific Heat

The values of heat required to undertake the two reactions is taken from Andersson and Jansson (1987). The peaks are 515 and 185 kJ/kg of gypsum. The first (Equation 3.3) is assumed to occur between 100 and 120°C and the second (Equation 3.4) between 200 and 220°C.

3.4.3.1 The First Dehydration Reaction

Assuming that the α form of the hemihydrate is produced, then the peak at 110°C (reaction 1, Figure 3.3) has a value as follows:-

Heat of Reaction		100 kJ/kg
Evaporation of Water of Crystallisation	0.75 * 0.209 * 2260 =	354 kJ/kg
Evaporation of Residual Free Water	(0.0235 + 0303)/2* 2260 =	61 kJ/kg
TOTAL		**515 kJ/kg**

Assuming that the β form of the hemihydrate is produced, then the peak at 110°C (reaction 2, Figure 3.3) has a value as follows:-

Heat of Reaction		112 kJ/kg
Evaporation of Water of Crystallisation	0.75 * 0.209 * 2260 =	354 kJ/kg
Evaporation of Residual Free Water	(0.0235 + 0.0303)/2 * 2260 =	61 kJ/kg
TOTAL		**527 kJ/kg**

The value used for the first reaction, 515 kJ/kg is within the range given above.

3.4.3.2 The Second Dehydration Reaction

The peak at 210°C has a value between the following:-

Assuming that the α form of both hemihydrate and anhydrate is produced:-

Heat of Reaction		50 kJ/kg
Evaporation of Water of Crystallisation	0.25 * 0.209 * 2260 =	118 kJ/kg
TOTAL		**168 kJ/kg**

Assuming that the β form of both hemihydrate and anhydrate is produced:-

Heat of Reaction		64 kJ/kg
Evaporation of Water of Crystallisation	0.25 * 0.209 * 2260 =	118 kJ/kg
TOTAL		**182 kJ/kg**

The value used for the second reaction 185 kJ/kg, is slightly on the high side, but the overall value of 700 kJ/kg is within the range of 515 + 168 = 683 and 527 + 182 = 709. kJ/kg. A value on the low side for the first reaction, and high for the second may be appropriate as all the moisture may not be evaporated by 120°C.

3.4.4 The Enthalpy of Gypsum Plasterboard

TASEF utilises an enthalpy curve, rather than separate values for density and specific heat. This is a specific volume enthalpy and has the units W.Hr/m^3. Enthalpy is used to avoid numerical instabilities and to avoid missing a peak in the specific heat when the temperature values for an element in consecutive time steps are below and above the peak respectively. The enthalpy is the product of the specific heat, volume, density and temperature.

The initial density is determined by weighing a sample from a section of a sheet that was part of a furnace test sample. The reduction in density with temperature is from Harmathy (1988) and is shown in Figure 3.4. The mass loss is due to water being driven off. As gypsum plasterboard is about 24% by weight water, much of this water must remain as steam in the plasterboard, on account of the mass loss being less than 24%.

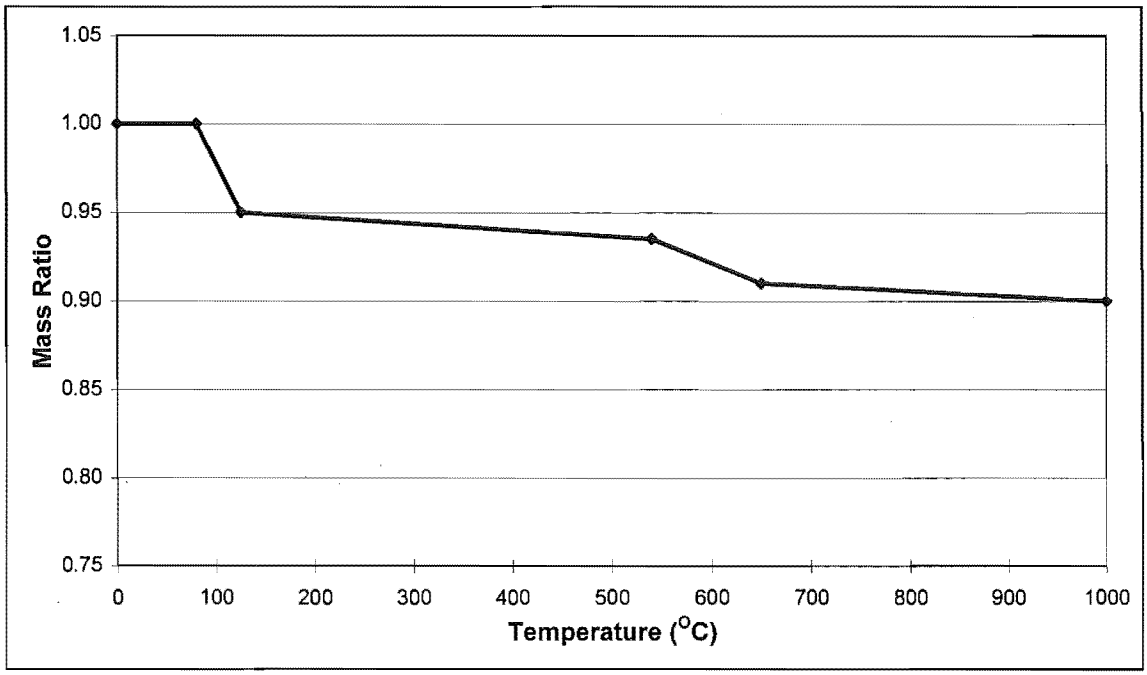

Figure 3.4 Mass Loss in Gypsum Plasterboard Undergoing Heating (Harmathy 1991)

The enthalpy curve is constructed from the initial density, mass ratio and specific heat. The enthalpy curve is shown in Figure 3.5 and compared with that used by other researchers.

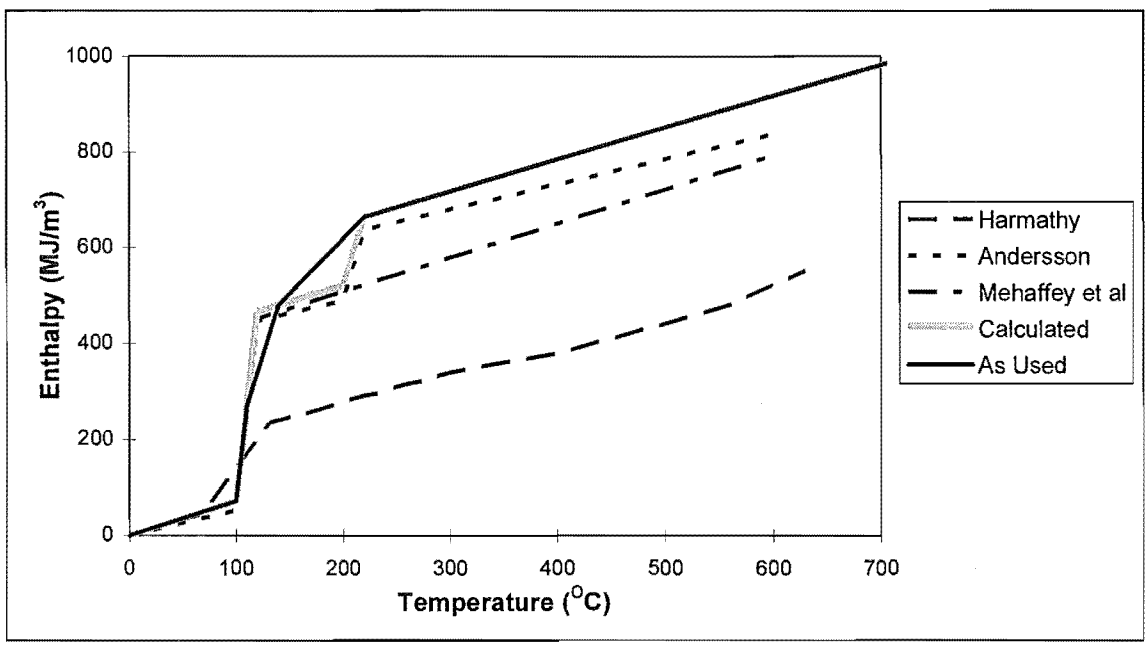

Figure 3.5 Enthalpy Curves for Gypsum Plasterboard

Harmathy's values are significantly lower than the others, but the values of specific heat used to calculate it were scaled off a graph, so it is not very accurate. Mehaffey et al's values are similar to Andersson and Jansson's values, but they exclude the second steep rise in enthalpy due to reaction 2 as described earlier and their base value is slightly higher. The values calculated are basically the same as Mehaffey et al's, but the second reaction is included. The enthalpy as used in the analysis is a smoothed version of the

calculated curve. The first peak in the enthalpy was modified to be between 100°C and 140°C with a peak at 110°C, but the area is the same on each side of 110°C. The second peak at 210°C was modified to be between 140°C and 220°C, but the area is the same on each side of 200°C. These modification create a smoother transition between the plateau at 100°C and the subsequent temperature rise.

3.5 Conductivity of Gypsum Plasterboard

3.5.1 Literature

Conductivity values for gypsum plasterboard are shown in Figure 3.6.

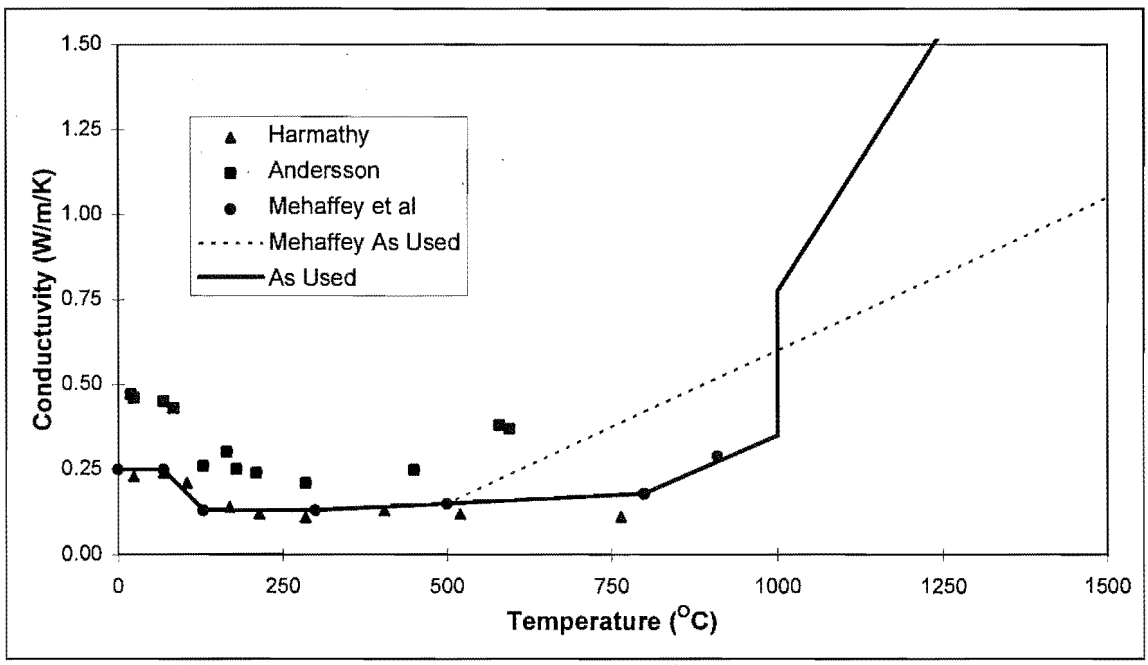

Figure 3.6 Conductivity values for Gypsum Plasterboard

The values given by symbols are measured values from Harmathy (1988), Andersson and Jansson (1987) and Mehaffey et al (1994).

3.5.1.1 Harmathy

It is not known how Harmathy's results were found.

3.5.1.2 Andersson and Jansson

Andersson and Jansson's values were found using the Transient Hot Strip (THS) method of measuring thermal conductivity. The THS method measures the resistance of a metal strip embedded in the material and from this a conductivity is derived.

3.5.1.3 Mehaffey et al

Mehaffey et al used a Kyoto Electronic model TC-31 thermal conductivity meter. This meter uses steady state analysis to determine conductivity. They tested 12.7 mm standard board and 15.9 mm type X fibre reinforced board. Mehaffey et al used modified values for conductivity over 500°C. They increased the value to 0.6 W/mK at 1000°C. This is to allow for the increased conductivity due to the opening of cracks in the gypsum at high temperatures and due to ablation. They state that their testing method prevents cracks from opening up in the board.

3.5.2 Ablation

Ablation is the process by which consecutive thin layers of a material are shed as a material undergoes heating. This occurs because the material undergoes chemical and physical changes during heating which reduce the bonding of the material to itself. Hence the altered material will fall off because it is not firmly attached to the unaltered material underneath. As gypsum is heated it is transformed into calcium anhydrate which has the appearance of a dry cohesionless powder, which will then fall off the board. This process is slowed if the board is reinforced with fibreglass. Ablation occurs at about 700°C for normal gypsum board and 1000°C for fibre reinforced board. Glass fibre reinforced gypsum plasterboard will ablate at temperatures over 900°C. The effect of ablation is more apparent when trying to correlate results from tests of boards varying greatly in thickness, since ablation has a more serious effect on a thinner board due to the fact that a higher proportion of the board is lost.

3.5.3 Conductivity Values

The values used in the analysis are derived from the Mehaffey et al value. This is because of several reasons:-

(i) The method of measurement is more direct, that is the derivation is less complex, than for Andersson and Jansson's THS method.

(ii) It is close in value to Harmathy's results, where as Andersson and Jansson's are isolated.

(iii) The composition of plasterboard in New Zealand is based on North American practice, and hence Harmathy's and Mehaffey et al's results will be more relevant, than Andersson and Jansson's, which are for boards produced in Europe. The exact composition of the board used is unknown due to commercial sensitivity. The effect of the composition is small as the boards are mostly gypsum, the rest being glass fibre, vermiculite and some impurities.

The conductivity used is as per the values measured by Mehaffey et al for Type X board, extrapolated to 1000°C. The conductivity then jumps to 0.775 W/mK at 1000°C and reaches 2.3 W/mK at 1500°C. These large values allow for ablation. The values have no theoretical justification, but they result in reasonable correlations with test data.

3.6 Thermo-Physical Properties of Wood and Char

Janssens (1994) has carried out a rigorous review of the thermo-physical properties of wood and char and investigated over 30 models for the prediction of temperature profiles and charring rates in wood. He found that none were suitable without major modification. Other sources, notably Gammon (1987) and Fredlund (1988) also contain a review of previous data.

3.7 Specific Heat of Wood and Char

3.7.1 Literature

Harmathy (1988) gives a plot of specific heat which is reproduced less accurately in Figure 3.7. Mehaffey et al (1994) describe the method behind their calculation of specific heat curve for wood, but they neglect to give a value for the specific heat of char, that is, the material present over 350°C. They referenced Lie (1992) in which it is given as 0.69 kJ/kg, so it is assumed that they used this value. Harmathy's values seem a little low compared with the others and the peak due to evaporation of moisture is ignored. This plot may be for oven-dry wood, but this is not stated. Fredlund gives values of specific heat for wood, char, water and pyrolysis gases, but it was not reported how these were combined.

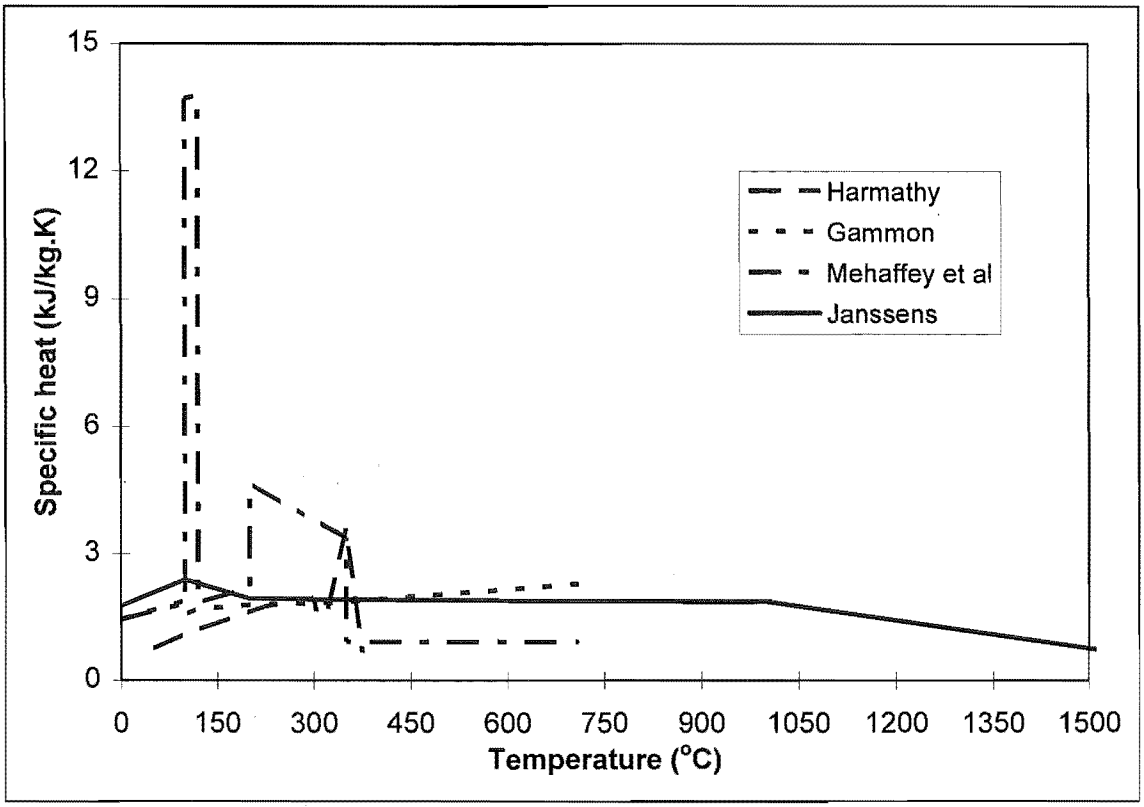

Figure 3.7 Specific Heat Values for Wood

3.7.1.1 Wood

For the specific heat of wood, Mehaffey et al, Gammon and Janssens' use an equation of the form:-

$$C_p = \left(\frac{a + bT_c + 4.187u}{1+u} \right) + \Delta c \qquad (3.6)$$

where:- C_p is specific heat (kJ/kg.K)

a, b are coefficients which are given different values by the three researchers

T_c is temperature (°C)

u is moisture content (kg/kg)

Δc is a correction to allow for bound moisture:-

$$\Delta c = (23.55T - 1326u + 2417)u \qquad (3.7)$$

This correction is only used by Janssens.

The following Table gives values of **a** and **b** used by the three researchers.

Model	Temperature Range (°C)	a	b
Gammon	< 100	1110	4.86
	> 100	1440	1.19
Mehaffey et al	< 350	1110	4.2
Janssens	< 200	1159	3.86

Table 3.1 Values for Specific Heat Coefficients

Janssens uses a lower value for **b** than the others, but this is more than compensated for by the use of the ΔC correction. In Figure 3.7, Janssens curve is higher below 100°C than both Gammon and Mehaffey et al. Once the moisture is driven off this term becomes zero and Equation 3.6 reduces to:-

$$C_p = a + bT_c \tag{3.8}$$

where the symbols are as for Equation 3.6.

3.7.1.2 Moisture Content

Mehaffey et al assume that the moisture is evaporated between 100 and 120°C. Janssens assumes that it is driven off between 100°C and 160°C, but does not add the energy required to convert moisture to steam to the specific heat. Mehaffey et al also assume that any water given off is still present as steam and requires 2.1 kJ/kg.K to heat it. This is ignored by Gammon and not mentioned by Janssens.

3.7.1.3 Char

Janssens assumes char properties over 800°C and wood properties below 200°C. Linear interpolation is used between these temperatures. Gammon used wood properties throughout and Mehaffey et al appear to use a specific heat of char of 0.69 kJ/kg.K above 350°C. The equation used by Janssens for char is:-

$$C_p = 714 + 2.32T - 8*10^{-4}T_c^2 - 3.69*10^{-7}T_c^3 \tag{3.9}$$

where:- C_p is the specific heat of char (kJ/kg.K)

T_c is temperature (°C)

3.7.1.4 Density

The mass of wood varies significantly with temperature. If char shrinkage is ignored then this equates to density as shown in figure 3.8.

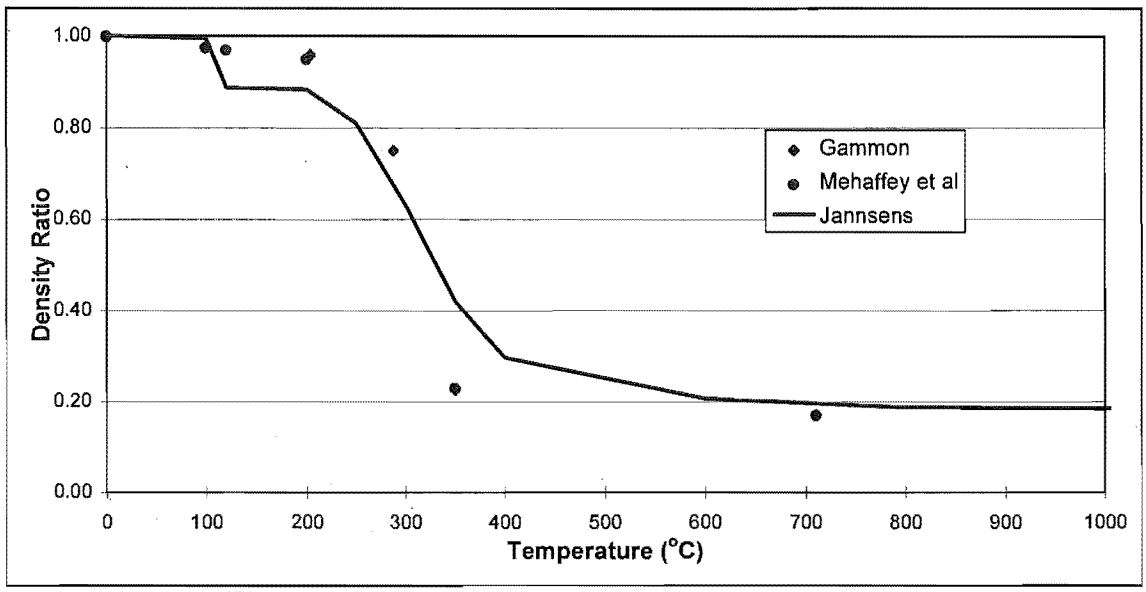

Figure 3.8 Density of Wood at High Temperatures

Since it is not known wether the specific heat values in Figure 3.7 were calculated assuming temperature dependent density or the initial density. Initial density was used in this study to calculate specific heat. Gammon uses temperature dependent density in order to calculate the enthalpy of wood. The density value normally used in this dissertation is air-dry density, normally at 12% moisture content. The test density is the density as tested, at a given moisture content. The oven-dry density is the nominal density of wood at 0% moisture content. The definition of the various terms for density of timber as used in this dissertation is defined in a report by Collins (1983).

3.7.2 Enthalpy Values Used

The values for specific heat used were those of Janssens (1994), because it is the most recent and his review is more rigorous than the others. Several additional assumptions were made:-

(i) Wood density is 450 kg/m^3 at 12% moisture content.

(ii) Moisture is evaporated between 100 and 120°C.

(iii) Initial density is used to calculate the enthalpy.

(iv) Steam is lost to the system after the moisture is evaporated. Obviously some of the steam will be lost, but the proportion that remains in the wood is difficult to determine and so is ignored.

(v) The enthalpy for partially charred wood (between 200 °C and 800 °C) is found by linear interpolation.

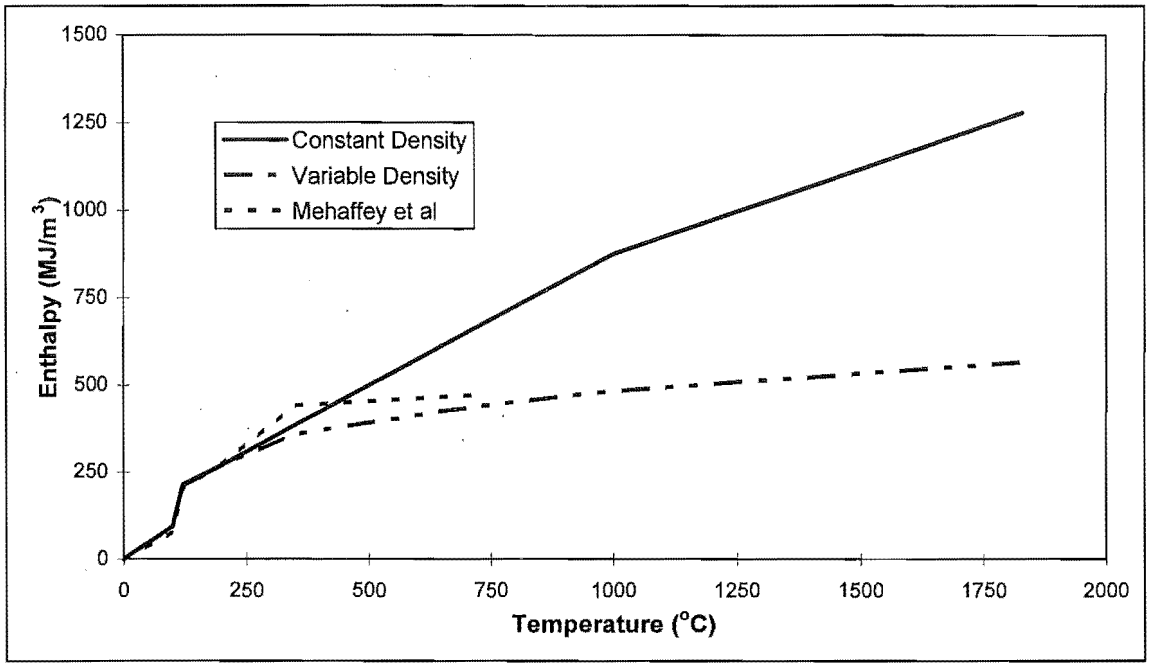

Figure 3.9 Enthalpy Curves for Wood and Char

The resulting curve for enthalpy as used is shown in Figure 3.9. For interest it is compared with the curve calculated using density varying with temperature and with the Mehaffey et al curve that includes the energy required for pyrolysis of wood and that required to heat the steam. Density has no significant effect below 350°C. Using the initial value of density to calculate enthalpy results in a better correlation with test data.

3.8 Conductivity of Wood

3.8.1 Literature

Conductivity values come from five sources, Janssens (1994), Gammon (1987), Fredlund (1988), Harmathy (1988) and Cuerrier (1993).

3.8.1.1 Janssens

Again Janssens has the most comprehensive review and most rigorous approach. Janssens calculates the conductivity from the oven dry density and moisture content. The details are outlined in his paper (Janssens 1994) and it is too involved to show details of all the formulae here.

Janssens assumes the wood is composed of layers of solid wood fibres and voids (and water at temperatures below 100°C). The conductivity is at a maximum if the layers are arranged in parallel and a minimum if they are arranged in series. The maximum and minimum values for conductivity are then derived from temperature dependent values for the conductivity of air, water and wood fibre and temperature dependent values of the proportion of wood, air and water in the wood. An interpolation factor is used to calculate the conductivity from the maximum and minimum values. This process is used up to 200°C.

Above 200°C a temperature dependent function for the conductivity of partially charred wood fibre is used instead of that for wood fibre. Temperature dependent values for bulk density of the wood are used to calculate the proportion of solid wood and voids. Bulk density is the density of the solid proportion of the material, that is, the mass per unit occupied space. The occupied volume being total volume less volume occupied by the voids in a porous material such as wood.

3.8.1.2 Fredlund

This process is also used by Fredlund (1988 and 1993). Fredlund reports two sets of results for wood and char (Figure 3.10). The results achieved are consistent with measured results for various densities and moisture contents at ambient temperatures.

3.8.1.3 Gammon

Gammon used a formula that relates the ambient conductivity linearly with moisture content and density. He assumes the conductivity at elevated temperatures is related to that at ambient by the ratio of temperature to the reference temperature of 302 K.

3.8.1.4 Harmathy

Harmathy (1988) shows measured values (Figure 3.10). These values are taken from a graph, so may not be very accurate.

3.8.1.5 Cuerrier

Cuerrier (1993) uses four measured values at 0°C and 200°C for wood and at 350°C and 1100°C for char.

3.8.2 Comparison of Values

3.8.3 Conductivity Values Used

The values found by different researchers are shown in Figure 3.10.

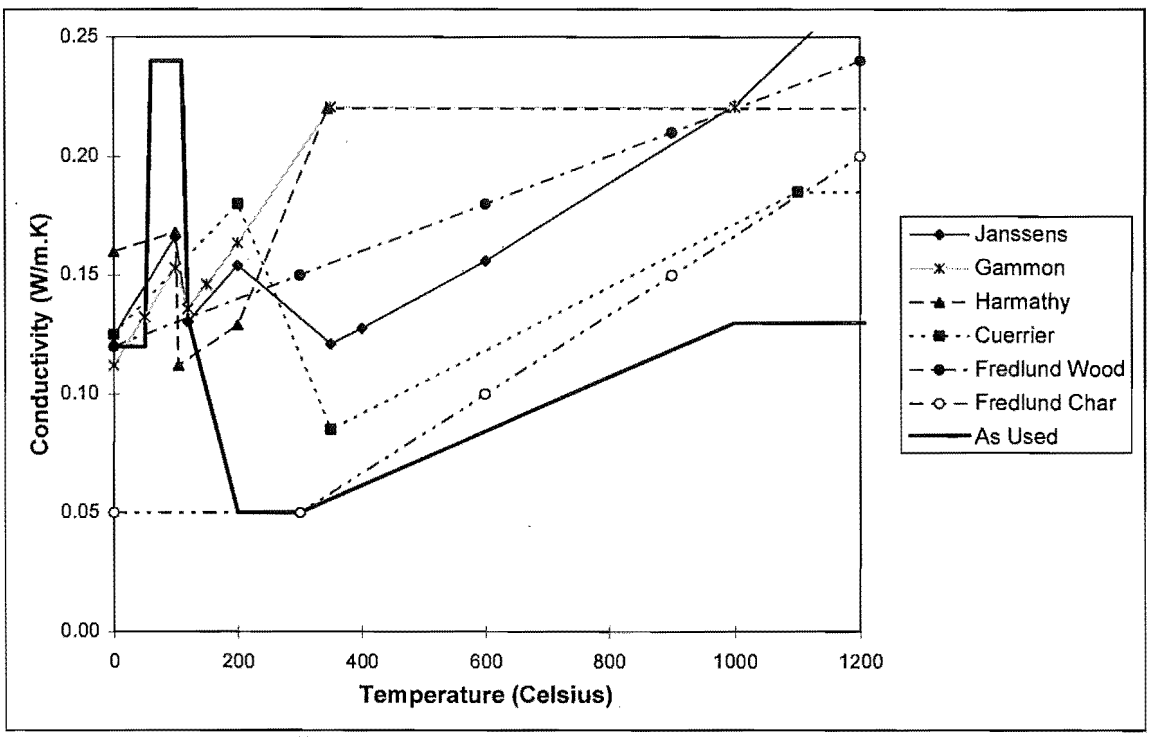

Figure 3.10 Conductivity Values for Wood

Conductivity values used were based on Fredlund's values below 120°C, but were doubled between 60°C and 110°C to allow for the increase in conductivity due to the evaporation of moisture, movement into the wood and subsequent condensation. This modification is necessary as moisture movement is not modelled. This process is known to contribute to conductivity, but to what extent is difficult to determine. Doubling the value cannot be justified by theory, but provides good correlation with experimental results. Between 200°C and 350°C Fredlund's values for char are used. Above 350°C a lower value has been used in order to achieve a better correlation with the temperatures within the studs measured during furnace tests.

The values for conductivity are altered to achieve correlation with test data, as it is harder to determine accurately than the specific heat. It should be noted that it is not necessary to modify the conductivity to allow for moisture movement in gypsum plasterboard. The effect of moisture movement is less apparent in a thin sheet of plasterboard than a block of wood.

3.9 Heat Transfer Coefficients

The walls were modelled by assuming the above values for thermo-physical properties were correct and by modifying the heat transfer coefficients to give reasonable agreement for all four tests. The heat transfer coefficients are varied within a range that is deemed reasonable, considering values from the literature.

3.9.1 Furnace Characteristics and The Standard Fire Tests

Before discussing values for radiative and convective heat transfer between the test furnace and the test specimen, some discussion on furnace characteristics is needed.

3.9.1.1 Temperature Measurement

The temperature of the furnace in the full size test may be up to 100°C higher than the thermocouple temperature throughout the test. The thermocouple actually records a lower temperature than that of the gas. This is due to losses in the stem of the thermocouple (Babrauskas and Williamson 1978b) and the effect of the furnace wall temperature and its radiation to the test wall (Gammon 1987 p 72-75). However the equation given in Gammon does not match the text, the equation implies that the thermocouple temperature is higher than the furnace temperature. The example C in Babrauskas and Williamson (1978b) shows that the furnace temperature is higher than the thermocouple temperature. The thermocouples will measure a temperature that is between that of the furnace gases, the specimen temperature and the temperature of the furnace walls. Assuming the test specimen is the same temperature and has the same emissivity as the furnace walls, the furnace temperature is a function of the thermocouple temperature, the furnace wall temperature, the furnace wall emissivity and the gas emissivity:-

$$T_f = \left[\frac{\varepsilon_f + \varepsilon_x(1-\varepsilon_f)}{\varepsilon_f} T_t^4 - \frac{\varepsilon_x(1-\varepsilon_f)}{\varepsilon_f} T_x^4 \right]^{1/4} \quad (3.10)$$

where:- T_f is the gas temperature (K)

T_t is the thermocouple temperature (K)

T_x is the furnace wall temperature (K)

ε_f is the gas emissivity (dimensionless)

ε_x is the furnace wall emissivity (dimensionless)

Assuming that the specimen temperature is the same as that of the walls of the furnace is reasonable if they have similar thermal properties. This is usually the case for concrete test specimens, but not for light timber framed walls and floors.

3.9.1.2 Thermocouple Lag

The time constant of the thermocouples also affects the results. Babrauskas and Williamson (1978b) report that the time constant for the thermocouples prescribed in the ASTM furnace test have a response time of 16 minutes at the start of the test, reducing to 2 minutes after a duration of 20 minutes. This corresponds to a temperature lag of 550°C initially and 50°C after 12 minutes. BRANZ uses thermocouples with a low thermal inertia and hence fast response so this problem is less significant. For a fast response thermocouple the lag is 400°C at the start of the test, reducing exponentially to about 50°C after 4 minutes and 5°C after 20 minutes (Babrauskas and Williamson 1978b). Gammon (1987) states that in smaller furnaces, that is, less than 2.0 m, the difference between the furnace temperature and the thermocouple temperature is smaller.

3.9.1.3 Comparisons Between Furnaces

As test furnaces differ in their geometry and linings, it is obvious that results from different furnaces can not be compared directly. This is apparent in comparing test results from the pilot furnace, a two by one metre furnace and the full size furnace (four metres by three metres) in the same laboratory at BRANZ. The BRANZ furnace is

fuelled by diesel, which burns with a sooty flame. The furnace gas has a higher effective emissivity than the gases in the commonly used natural gas fuelled furnaces. Possible sources of variability in results between test furnaces are given and quantified by Harmathy (1981). Thermal characteristics of test furnaces are described in Keltner and Moya (1990) and Sultan et al (1986). Keltner and Moya (1990) also describe the effectiveness of different methods of measuring the temperature and heat flux within a furnace, such as plate thermometers and Gardon heat flux gauges. The historical basis of testing is described by Babrauskas and Williamson (1978c and 1978d). Comparisons between the ISO and ASTM test are described by Harmathy and Sultan (1988). In essence these papers state that the fire resistance test is a historical method, that bears little relation to real fires, and there is a need for a method of reducing the variation between furnaces.

3.9.2 Emissivity on the Furnace Side of the Wall

Given the problems determining the actual gas temperature in a test furnace as described in the previous Section and the limitations of the program TASEF, it is difficult to determine an appropriate value for the furnace emissivity.

Equation 3.10 is derived from a more complex equation (Babrauskas and Williamson 1978b, Equation (1)) which gives the heat flux to a test specimen as a function of the specimen temperature, the furnace wall temperature, the furnace gas temperature and the emissivities of the furnace gas, the specimen and the furnace wall. Furthermore, the furnace gas temperature is a function of the specimen, furnace wall and measured thermocouple temperatures and the emissivities of all three. The solution is iterative and relies on assumptions about the emissivities of the specimen, furnace walls and the furnace gas. As the temperature of the exposed surface of the specimen and furnace walls is not measured, then assumptions also have to be made about these. By assuming the furnace walls and the specimen are at the same temperature and that the specimen temperature is given by a TASEF run and assuming that it does not change significantly for variation in the gas and furnace wall emissivities, an effective emissivity relating the heat flux to the specimen and thermocouple temperature can be calculated. By varying the gas emissivity from 0.34 to 0.7, and the furnace wall emissivity from 0.6 to 0.8 and assuming a specimen emissivity of 0.9 then an effective emissivity of between 0.7 and 1.05 is found. Given the number of assumptions made, the result is not reliable and a

value for emissivity greater than unity is an impossibility.

Gammon (1987) assumes that the furnace wall temperature is the same as the gas temperature. He also assumes the emissivity of the test specimen and the furnace walls as being 0.8 and 0.4 for the furnace gases. This gives an effective emissivity of 0.7.

The emissivity of soot is given by:-

$$\varepsilon_s = 1 - e^{-(BL)} \tag{3.11}$$

where:- ε_s is the soot emissivity (dimensionless)

B is the extinction coefficient (m^{-1})

L is the mean path length (m)

The SFPE handbook, (Tien et al 1988), gives the following equation for the emissivity of gas-soot mixtures:-

$$\varepsilon = \left(1 - e^{-(BL)}\right) + \varepsilon_g e^{-(BL)} \tag{3.12}$$

where:- ε_g is the gas emissivity (dimensionless)

B is the extinction coefficient (m^{-1})

L is the mean path length (m)

Gammon also gives this formula, although in a different form. It is unclear which formula Gammon has used. Gammon gives a value of 0.8 for the extinction coefficient. It can be deduced that he used a beam length of 0.65 metres to give a gas emissivity of 0.4 using Equation 3.11. If Gammon used Equation 3.10, assuming that he used an emissivity of 0.85, for carbon dioxide gas, as mentioned by him then the emissivity would be equal to four, which is not possible as the value can not be greater than unity. A reasonable assumption for the beam length, would be that for a cube (Atreya 1988). This gives a value of 0.60 of the furnace depth. Gammon's value gives a depth of 1.1 metres, which is reasonable. Drysdale, p75 (1985) gives a value of 0.43 for the extinction coefficient for diesel. The extinction coefficient will be less for diluted products of combustion but this is not taken into account here. Using Equation 3.10, a gas emissivity of 0.85 and a path length of 0.6 metres and an extinction coefficient of 0.43, then a gas emissivity of 0.88 is found. Using Babrauskas and Williamson's

method, and a furnace wall emissivity of 0.8 and a specimen emissivity of 0.9 then the resultant emissivity varies between 0.82 and 0.84 during a typical test.

Mehaffey et al (1994) assumes radiative heat transfer only between the furnace walls and the specimen as two parallel planes. The view factor is therefore 1.00 and assuming they have an emissivity of 0.9 for both the furnace walls and the test specimen, an effective emissivity of 0.82 is calculated using Equation 3.13:-

$$\varepsilon = \frac{1}{\left(1/\varepsilon_1 + 1/\varepsilon_2 - 1 \right)} \tag{3.13}$$

where:- ε_{eff} is the overall effective emissivity (dimensionless)

ε_1 is the emissivity of one surface (dimensionless)

ε_2 is the emissivity of another parallel surface (dimensionless)

This also assumes that the furnace wall temperature is the same as the thermocouple temperature. The furnace wall temperature will be lower than the thermocouple temperature, but this is compensated for by the additional radiative heat flux from the furnace gases.

The TASEF manual (Sterner and Wickstrom 1990), suggest values of effective emissivity between 0.6 and 1.0.

Given all of the above, it would be reasonable to assume that the furnace gases and walls can be modelled as a flat plate with a temperature equal to that of the ISO-834 test curve, that is similar to the thermocouple temperature, with an emissivity of between 0.7 and 1.0. Assuming it is radiating to the wall specimen which can be assumed to be another, parallel, flat plate with an emissivity of 0.9, then the overall effective emissivity is between 0.65 and 0.9.

3.9.2.1 Sensitivity Analysis

A sensitivity analysis was carried out for a typical wall assembly by running the wall model, with ISO-834 exposure, using overall emissivities of 0.6, 0.8 and 1.0 and leaving all other parameters the same. It can be seen in Figure 3.11 that the temperature of the

exposed surface of the wall varies little with a change in emissivity. Some convection heat transfer is included but the convection coefficients were not varied.

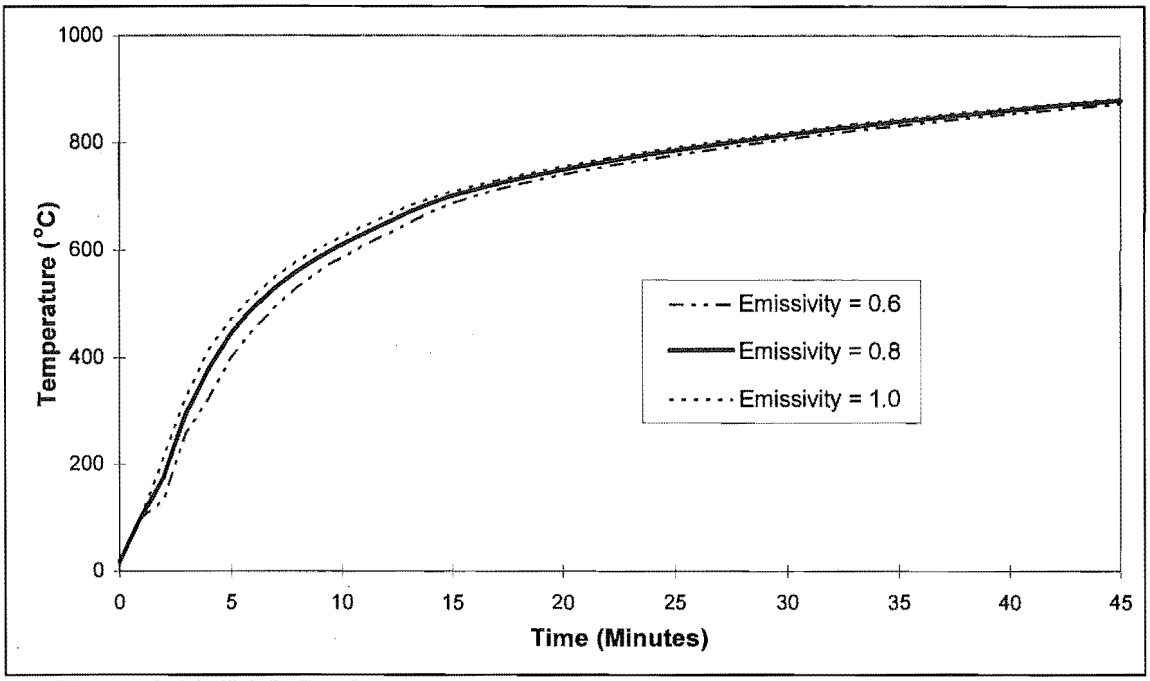

Figure 3.11 Wall Surface Temperature as a Function of Effective Emissivity

The same is true for net heat flux into the wall as shown in Figure 3.12.

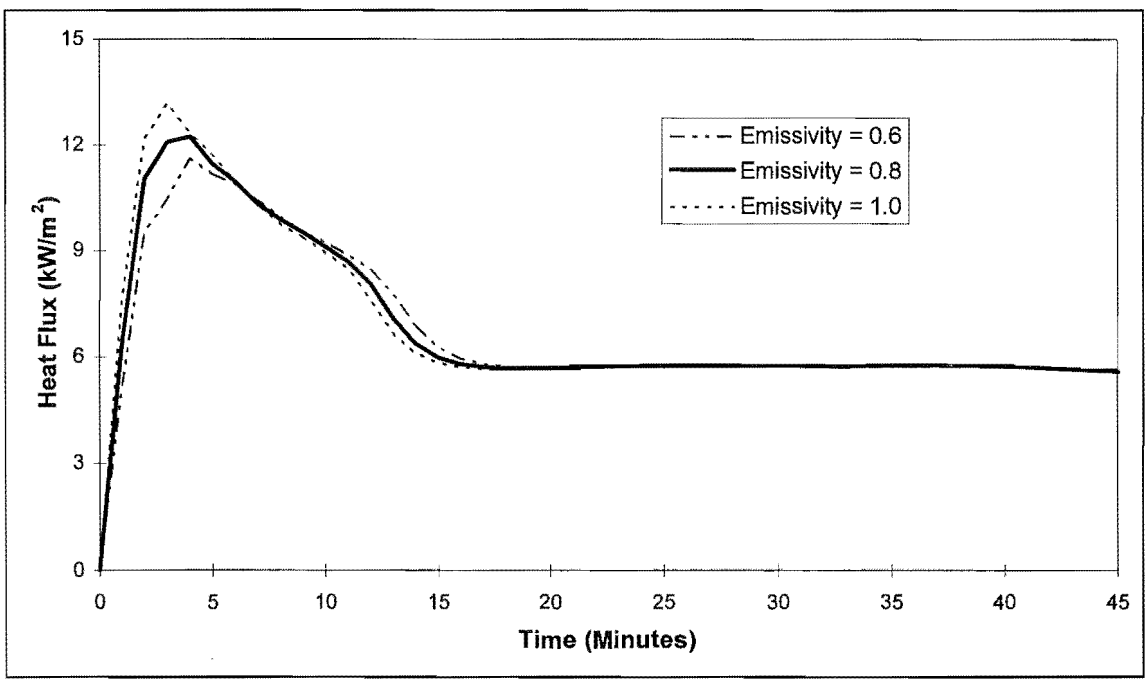

Figure 3.12 Net Heat Flux to Wall Surface as a Function of Effective Emissivity

The total net heat energy input to the wall assembly during the fire exposure is 18.51, 18.66 and 18.74 MJ/m2 respectively for emissivities of 0.6, 0.8 and 1.0. The difference is 1.2% at most.

3.9.2.2 Emissivity Value Used

Hence a value of 0.9 for the furnace emissivity is assumed , giving an overall effective value of 0.82. This is rounded to 0.8, the level of significance reflecting the accuracy of the value.

3.9.3 Convection Coefficients on The Furnace Side of the Wall

The convective coefficient is of little significance as the proportion of convective heat flux is negligible Williamson and Buchanan (1972), compared with the total heat flux.

Gammon (1987) bases his calculations for the convective heat transfer coefficient on thermodynamic considerations. This was based on the assumption of natural convection heat transfer, which is not correct as the convection is forced. The derivation in this section is not therefore appropriate. This error does not greatly affect the overall results as convection is a small part of the total heat flux to a wall. The effect on the time equivalent is negligible as the error affects both the compartment fire computer runs and the reference furnace run.

The coefficient is calculated using several dimensionless groups. **Nu** is the Nusselt number or the dimensionless heat transfer coefficient:-

$$Nu = hl / k_{air} = a(Ra)^b \tag{3.14}$$

where:-h is the convective heat transfer coefficient (W/m^2.K)

l is the characteristic dimension (m)

k_{air} is the conductivity of air:-

$$k_{air} = 0.0003266T^{0.7663} \tag{3.15}$$

where:-T is absolute mean air temperature (K)

a, b are coefficients that relate the Rayleigh number to the Nusselt number

Ra is the Rayleigh number:-

$$Ra = Gr.\Pr \tag{3.16}$$

Gr is the Grashof number, the ratio of buoyancy forces to viscous forces (dimensionless):-

$$Gr = \frac{g}{T}(T_w - T_\infty)\frac{l^3}{\upsilon^2} \tag{3.17}$$

where:- g is gravitational acceleration (m^2/s)

T_w is the fluid temperature next to wall surface (K or °C)

T_∞ is the bulk fluid temperature (K or °C)

υ is the kinematic viscosity (m^2/s)

$\Pr$ is the Prandtl number, the ratio of diffusion of momentum to the diffusion of heat (dimensionless):-

$$\Pr = \upsilon/\alpha \tag{3.18}$$

where:-α is the thermal diffusivity (m^2/s)

The Grashof and Prandtl numbers are highly temperature dependent, not only because of the temperature terms in the Grashof number, but because the kinematic viscosity and the thermal diffusivity of air is temperature dependent. Gammon reduces this dependence to a simple equation:-

$$Ra = 5.5.85 \times 10^{19} T^{-4.329}(T_\infty - T_o)\ ) \tag{3.19}$$

where:- T is absolute mean air temperature (K)

T_w is the fluid temperature next to wall surface (K or °C)

T_∞ is the bulk fluid temperature (K or °C)

There are two flow regimes, laminar and turbulent. The flow is regarded as turbulent if **Ra** is greater than 10^9. Rearranging Equation 3.12 gives:-

$$h = a\frac{k_{air}}{l}(Ra)^b \tag{3.20}$$

where the notation is as per Equation 3.15

Values of **a** and **b** vary depending on the source and are different for laminar and turbulent flow regimes. The three sources used are Gammon (1987), Atreya (1988) and Holman (1992). The values of **a** and **b** are as follows:-

Source	Flow Regime	a	b
Gammon	Laminar	0.555	0.25
	Turbulent	0.021	0.4
Atreya	Laminar	0.6	0.2
	Turbulent	0.17	0.25
Holman	Laminar	0.59	0.25
	Turbulent	0.1	0.33

Table 3.2 Values for The Coefficients c and d

In TASEF the convective heat transfer coefficient is derived from Equation 3.2 and is of the form:-

$$h = \beta(T_g - T_s)^{(\gamma - 1)} \tag{3.21}$$

Where:-h is the convective heat transfer coefficient (W/m^2.K)

β is the convection coefficient (W/m^{2}K$^\gamma$)

γ is the convection power, usually 1.33 or 1.25

T_g is the gas temperature (K)

T_s is the surface temperature (K)

Gammon states that in a fire test the flow regime is turbulent for the first five to ten minutes. After this time the flow regime is laminar, since the difference between the gas temperature and that of the surface of the test specimen becomes smaller. When calculating the value of the Rayleigh number in a typical test the flow is turbulent for the first six minutes. Since the Rayleigh number is a function of $\mathbf{T_g}$-$\mathbf{T_s}$, then the coefficient **b** corresponds to γ-**1**. From Table 3.2, **b** has a range of 0.2 to 0.4. A median

value of 0.33 is used. Using the values for the convective heat transfer coefficient calculated using Equation 3.17, assuming a value of **b** of 0.33 and Equation 3.18, values for the heat transfer coefficient β can be found. This value is an average calculated for the duration of the test back calculated from the heat transfer using values of the temperature of the furnace and wall surface during a TASEF run of the furnace test and hence can be directly compared. β is 0.45, 0.20 and 0.50, using Gammon, Atreya's and Holman's values for **a** and **b** respectively. The TASEF manual recommends a value of 1.0 for β and 1.25 for γ.

3.9.3.1 Sensitivity Analysis

The value used for β and γ makes little difference to either the surface temperature of the test wall (Figure 3.13), or to the net radiation flux to the test wall (Figure 3.14).

Mehaffey et al (1994) uses a constant value for the convective heat flux of 25 W/m^2.K

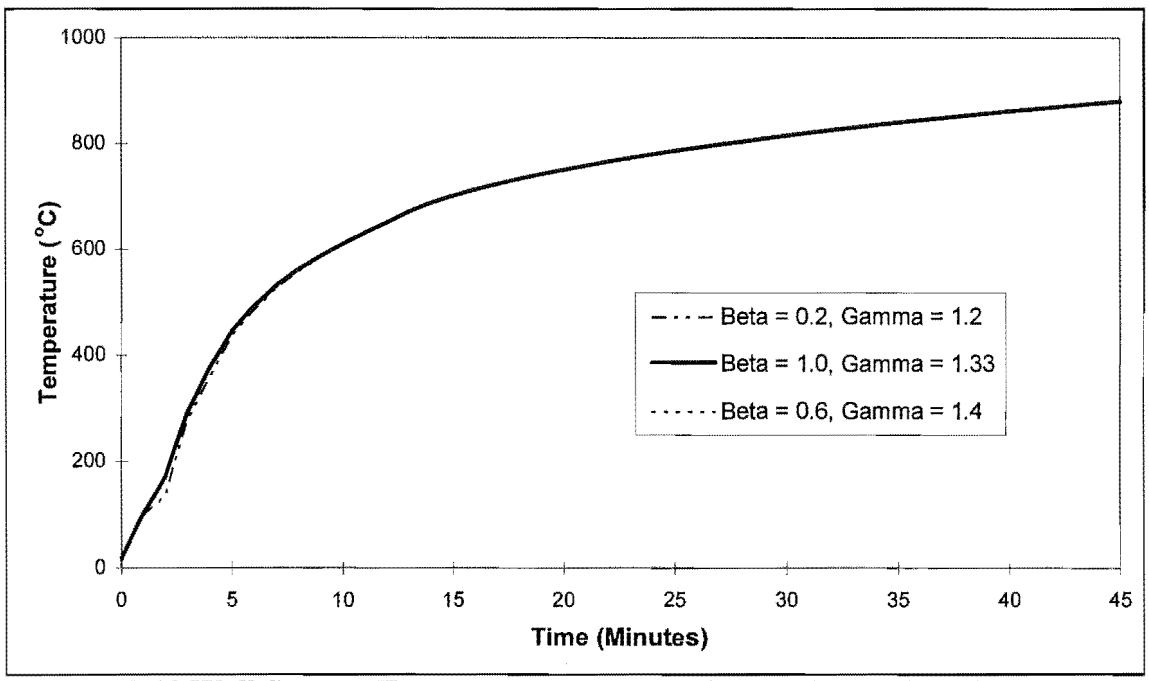

Figure 3.13 Wall Surface Temperature as a Function of Convection Coefficients

Furthermore the total net heat flux to the wall assembly is 18.65, 18.65, 18.77 and 21.63 MJ/m^2 respectively for the values for convective coefficients from Gammon, Atreya, Holman and Mehaffey et al respectively. The difference between the first three is less than 1%, but Mehaffey et al's value seems high (Figure 3.14).

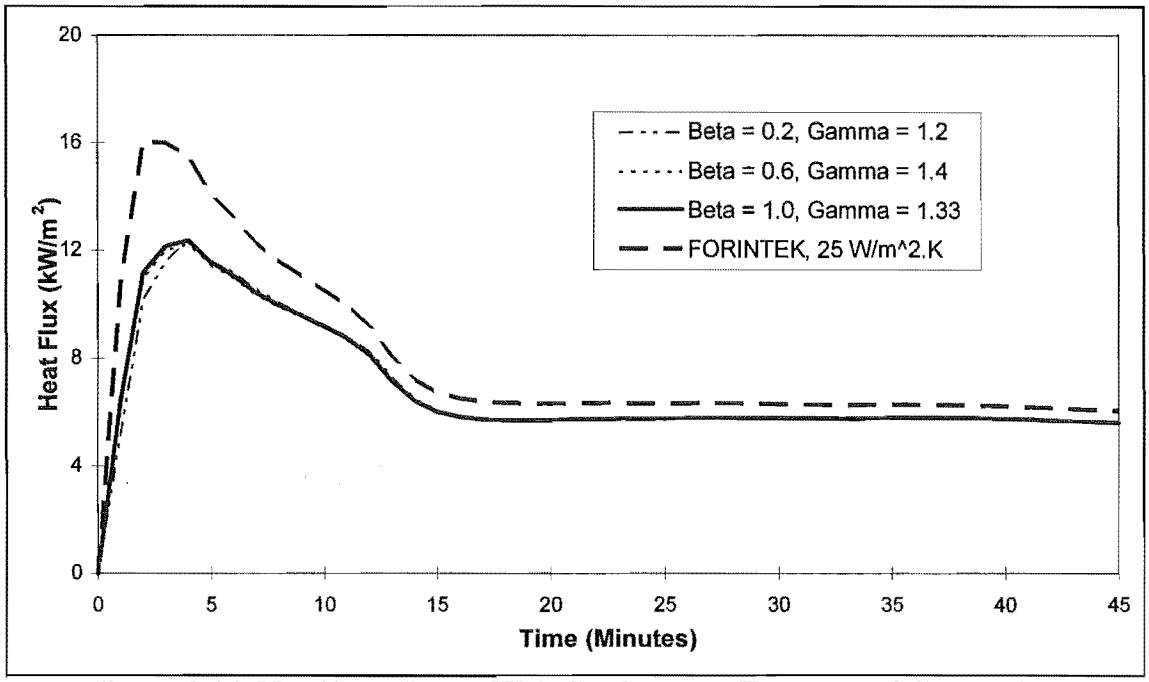

Figure 3.14 Net Heat Flux to Wall Surface as a Function of Convection Coefficients

3.9.3.2 Values Used for The Convection Coefficients

A value of for β of 1.0 and for γ of 1.33 is assumed in the model.

3.9.4 Emissivity on the Ambient Side of the Wall

The radiative heat flux from the unexposed side of the wall to the surroundings can be modelled as being between a plate and a hemispherical surface with an emissivity of 1.0. Given an emissivity of 0.9 for gypsum wallboard, then the resultant overall emissivity is 0.9. Gammon (1987) uses a value of 1.0, but ignores convective heat loss. Mehaffey et al (1994) assumes a value of 0.9 for the gypsum plasterboard and 1.0 for air. This is quite reasonable. It could be assumed that a lower value is more appropriate, as emissivity tends to increase with temperatures, due to the fact that the lower the temperature, the smaller the wavelength bandwidth of emitted radiation. TASEF uses a value of 0.6 in examples.

3.9.4.1 Sensitivity Analysis

The temperature of the unexposed surface of the wall varies little with variation in the emissivity as shown in Figure 3.15, except towards the end of the test. Varying the emmisivity from 0.6 to 0.8 would result in an insulation failure 3 minutes or 7% earlier.

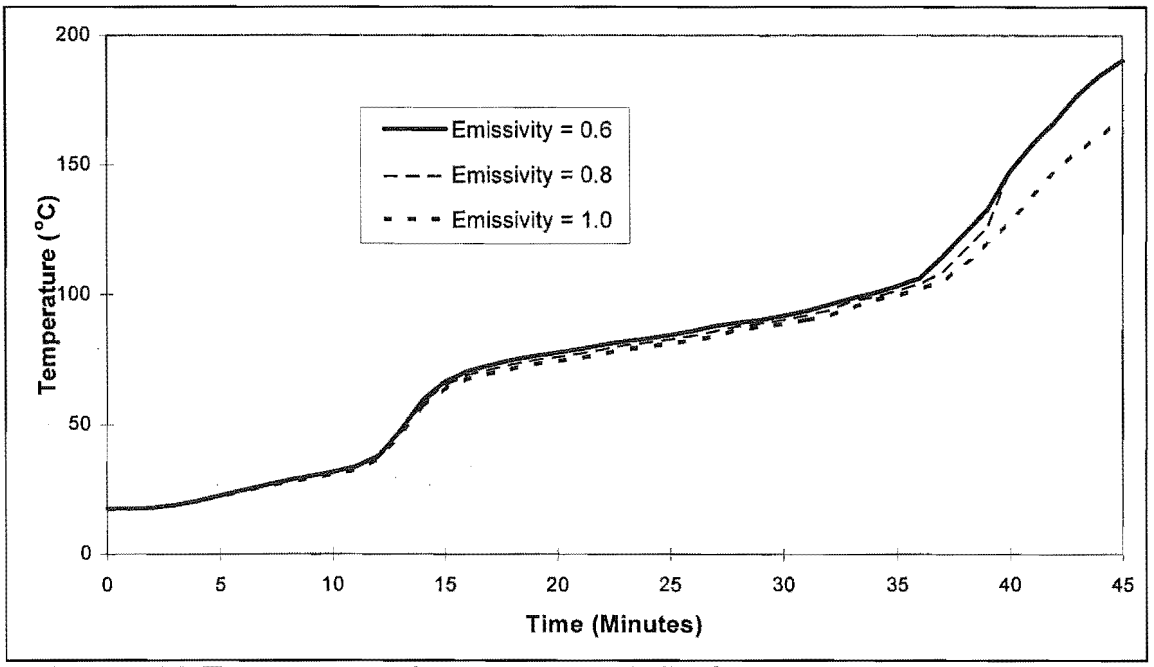

Figure 3.15 Temperature of Unexposed Wall Surface as a Function of Effective Emissivity

The heat flux from the wall surface varies more as shown in Figure 3.16. The total heat energy lost from the unexposed side of the wall during the test run is 2.69, 2.94 and 2.92 MJ/m^2 respectively for an emissivity of 0.6, 0.8 and 1.0, for a typical wall assembly. This is a difference of no more than 9%. The net heat energy absorbed by the wall assembly, that is heat energy in less heat energy out. The total energy input to the wall is about 19 MJ/m^2, so the difference is less than 2% and is not significant.

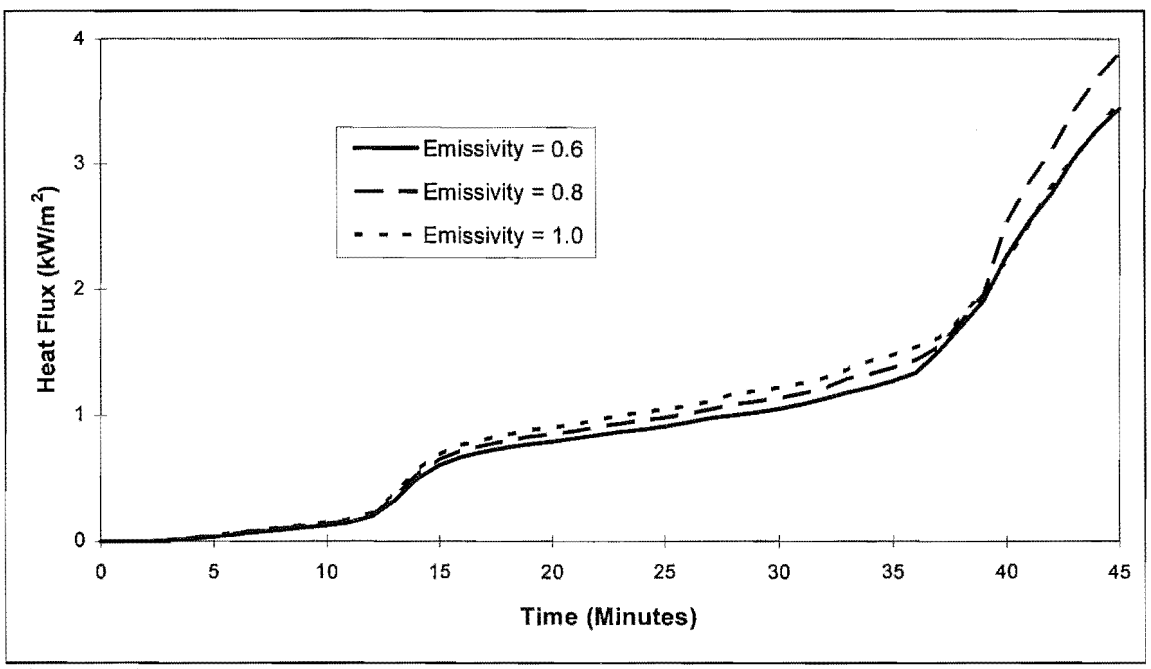

Figure 3.16 Net Heat Flux from Wall Surface as a Function of Effective Emissivity

3.9.4.2 Emissivity Value Used

The effective emissivity of the unexposed surface of the wall is assumed to be 0.6.

3.9.5 Convection Coefficients on the Ambient Side of the Wall

Repeating the process outlined in the previous Section, it can be shown that the flow regime on the unexposed side of the wall is turbulent, except for the first few minutes of a typical test. The value for the convection coefficients are irrelevant during the first few minutes of the test as the temperature of the cold side will have not risen above ambient.

From Table 3.2, the coefficient **b** (Equation 3.12) is 0.25, 0.33 or 0.4 in the turbulent flow regime. A median value of 0.33 is used and hence γ (Equations 3.2 and 3.18) is equal to 1.33. Using the values for the convective heat transfer coefficient calculated using Equation 3.17, assuming a value of **b** of 0.33 and Equation 3.21, values for the heat transfer coefficient β can be found. β varies from 0.1 to 1.7, 0.04 to 0.33 and 0.1 to 1.4, using Gammon, Atreya's and Holman's values for **a** and **b** respectively.

Mehaffey et al (1994) assume a constant value for the convective heat transfer coefficient of 9.0 $W/m^2.K$. Gammon (1987) ignores convective losses on the ambient side. TASEF recommends a value of 2.2 for β and 1.33 for γ.

3.9.5.1 Sensitivity Analysis

When the TASEF computer model of the a typical wall assembly is run with values for β ranging from 0.2 to 2.2 a significant variation in temperature is found (Figure 3.17), of approximately 45%.

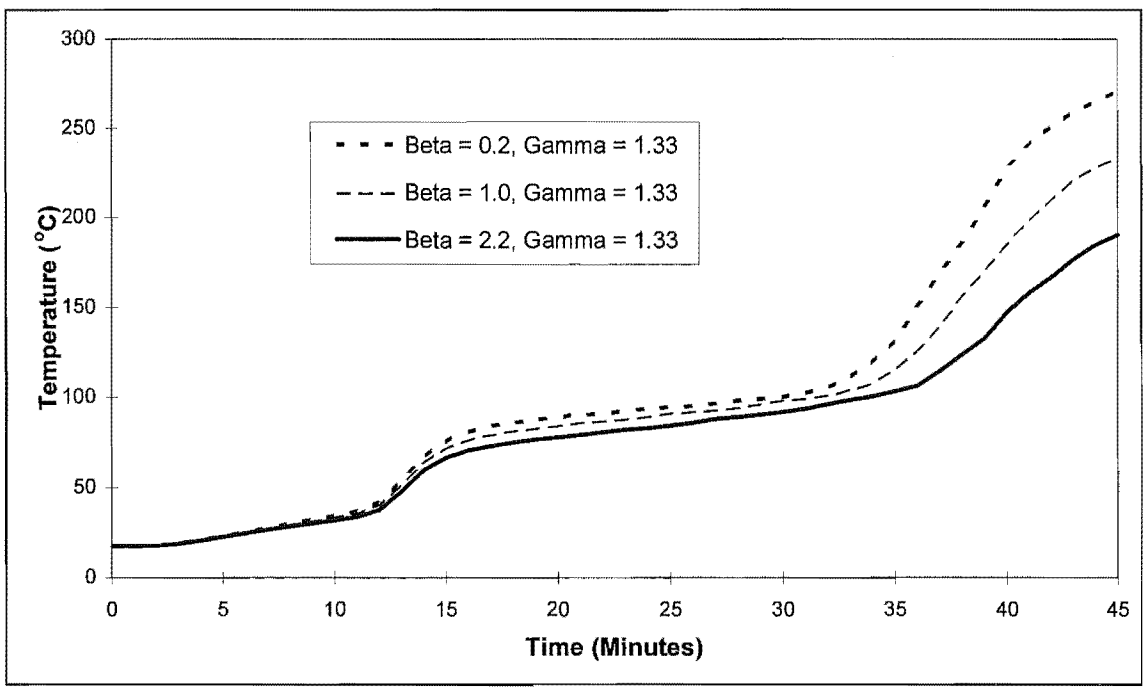

Figure 3.17 Temperature of Unexposed Wall Surface as a Function of the Convection Coefficients

This occurs towards the end of the test. The difference in time to an insulation failure is 5 minutes or 13%.

The heat flux from the wall surface also varies (Figure 3.18). The total heat energy lost from the unexposed side of the wall is 2.69, 2.28 and 1.92 MJ/m^2 respectively for an convection coefficient of 0.2, 1.0 and 2.2 respectively.

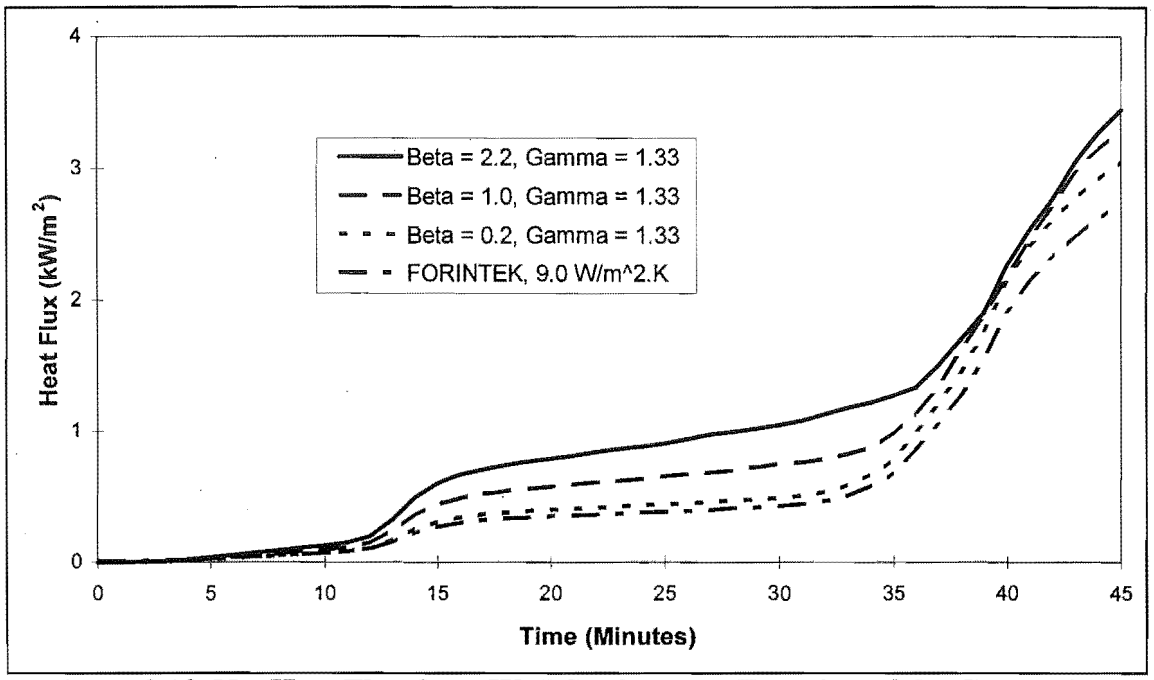

Figure 3.18 Net Heat Flux from Wall Surface as a Function of the Convective Coefficients

It is 1.71 MJ/m^2 assuming a constant value of 9.0 W/m^{2}K as did Mehaffey et al (1994). This is at most 40%, ignoring Mehaffey et al's value. This may initially seem significant, but of more interest is the net heat flux absorbed by the wall assembly, that is, heat flux in less heat flux out. The input heat flux is about 19 MW/m^2, so the difference is about 5%.

3.9.4.2 Values Used for The Convection Coefficients

A value of 2.2 for β and 1.33 for γ is used.

3.9.6 Combinations of Emissivity and Convection Coefficients on the Ambient Side of the Wall

Although varying either the emissivity or convection coefficients resulted in differences between the temperature on the unexposed side of the wall, the combinations used by various researchers show a smaller difference (Figure 3.19).

COMPF-2 is the compartment fire model described in Chapter 2. It has a fixed value for β and γ of 1.87 and 1.33 respectively for the unexposed side (Babrauskas 1979). The emissivity is the same as that for the wall material on the fire exposed side (Babrauskas 1979). This is 0.9 for gypsum plasterboard. These values were altered by modifying the program COMPF-2.

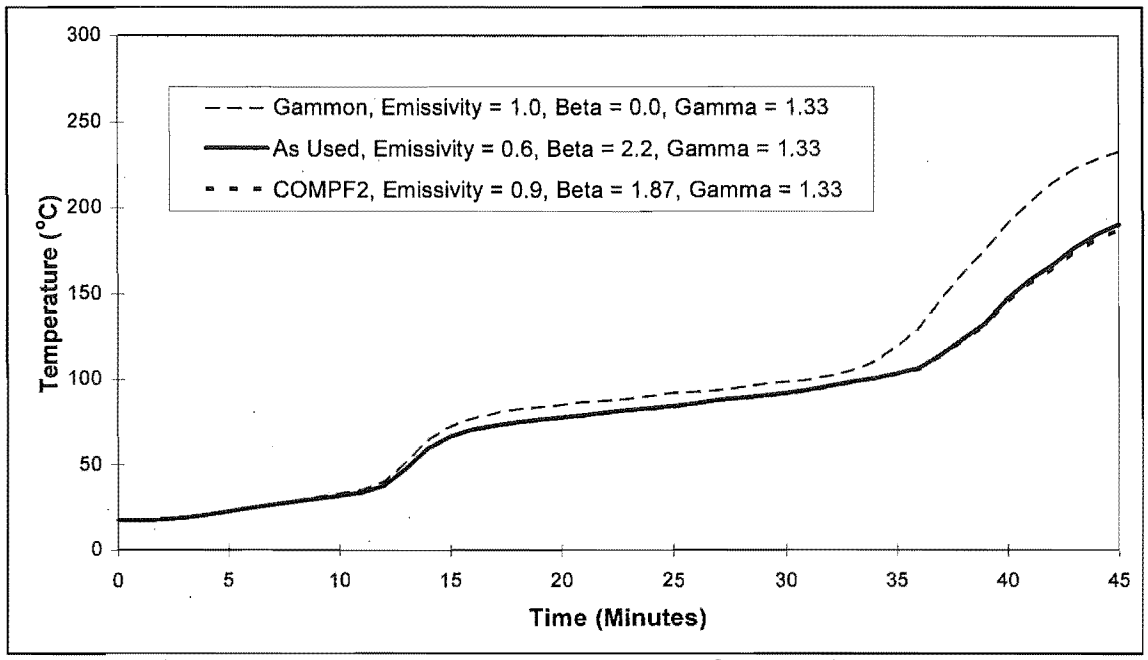

Figure 3.19 Temperature of Unexposed Wall Surface as a Function of the Heat Transfer Coefficients

Figure 3.20 shows the difference in heat energy for the various combinations used.

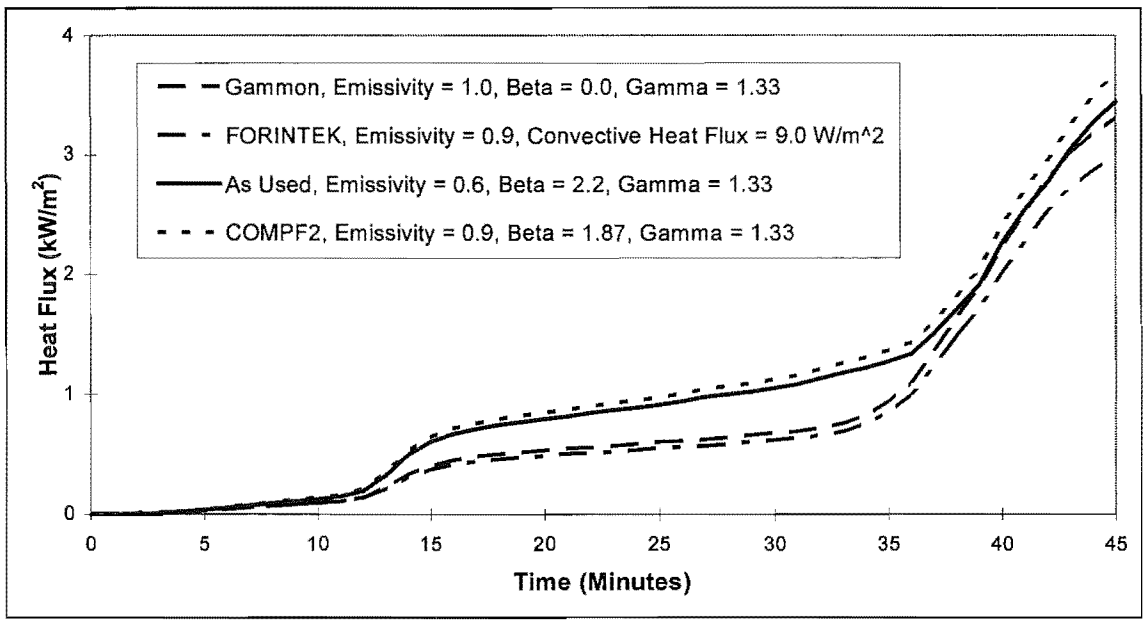

Figure 3.20 Net Heat Flux from Wall Surface as a Function of the Convective Coefficients

The total heat energy from the unexposed side is 2.23, 2.03, and 2.88 MJ/m^2 for Gammon's, Mehaffey et al's and the COMPF-2 values respectively. It is 2.69 for the

values assumed in this work. Again the difference is high, but not significant when compared with the net heat energy into the wall assembly.

3.9.7 Emissivity in the Cavity

In TASEF, radiation is modelled across the void only and the air within the void is assumed to be transparent to radiation. TASEF uses Hottel's crossed string method to calculate radiation view factors (Sterner and Wickstrom 1990). The void is assumed to be a vacuum for radiation purposes. This is a reasonable assumption at the start of exposure to fire or a furnace, but steam is driven out of the exposed lining and into the cavity after a few minutes. After the stud reaches about 300°C, pyrolysis products are present in the cavity. If these ignite, soot will also be present. These substances will reduce the radiation across the cavity. The primary mode of radiation heat transfer will be the hotter side radiating to the cavity gases which in turn radiate to the other sides of the cavity. The emissivity of the gases in compartments containing burning wood as cribs was found to be between 0.5 and 0.8 (Drysdale 1985). Hence the emissivity of burning wood pyrolysates in the cavity could be assumed to be in this range. Tien et al (1988) gives values for total emittance of water vapour and carbon dioxide as a function of partial pressure and path length. The mean path length is 0.9 of twice the thickness of an infinite slab (Tien et al 1988), that is, 0.16 m for a cavity 90 mm thick. at one atmosphere and 400 K the value is 0.25 for water and 0.05 for carbon dioxide. Atreya also gives the equation:-

$$\varepsilon_g \approx \varepsilon_{H_2O} + \frac{1}{2}\varepsilon_{CO_2} \tag{3.22}$$

where:- ε_g is the gas emissivity (dimensionless)

ε_{H_2O} is the emissivity of water (dimensionless)

ε_{CO_2} is the emissivity of carbon dioxide (dimensionless)

This gives a value of about 0.3 for gas emissivity. Using Equation 3.13 and an emissivity of 0.9 for gypsum plasterboard, then the emissivity can vary between 0.9 for a gas emissivity of 1.0 to 0.29 for a gas emissivity of 0.30. This assumes that the radiation interchange between the gypsum plasterboard and the void can be modelled as that between two parallel planes.

The other two sides of the void are composed of the wood stud. The emissivity of wood varies with the moisture content (Gammon 1987) according to the following equation:-

$$\varepsilon_w = 1.3u + 0.65 \tag{3.23}$$

where:- ε_w is wood emissivity (dimensionless)

u is moisture content (kg/kg)

At 12% moisture content the emissivity of wood is 0.81 and reduces to 0.65 as the moisture is driven off. Gammon also gives an emissivity for char of 0.85. Due to the variation of the void gas emissivity and for the sake of simplicity it is assumed that the effective emissivity between the wood and the void is the same as that between the gypsum plasterboard and the void.

3.9.7.1 Sensitivity Analysis

Figure 3.21 shows the variation in temperature due to variation in the emissivity value used. The Figure refers to the fire side of the void or cavity. The void has four sides, but due to symmetry the two wood sides are the same.

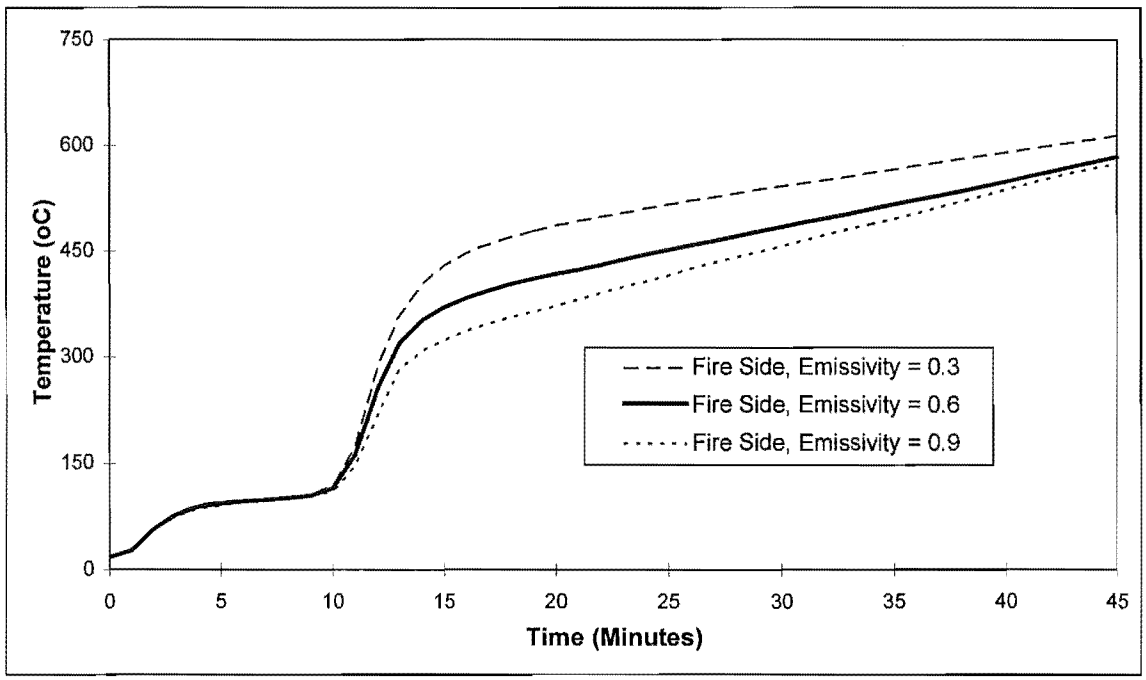

Figure 3.21 Variation in Temperature on the Fire Side of the Void as a Function of Emissivity

Similarly, Figure 3.22 shows the variation in temperature due to variation in the emissivity value used. This Figure refers to the stud side of the void or cavity.

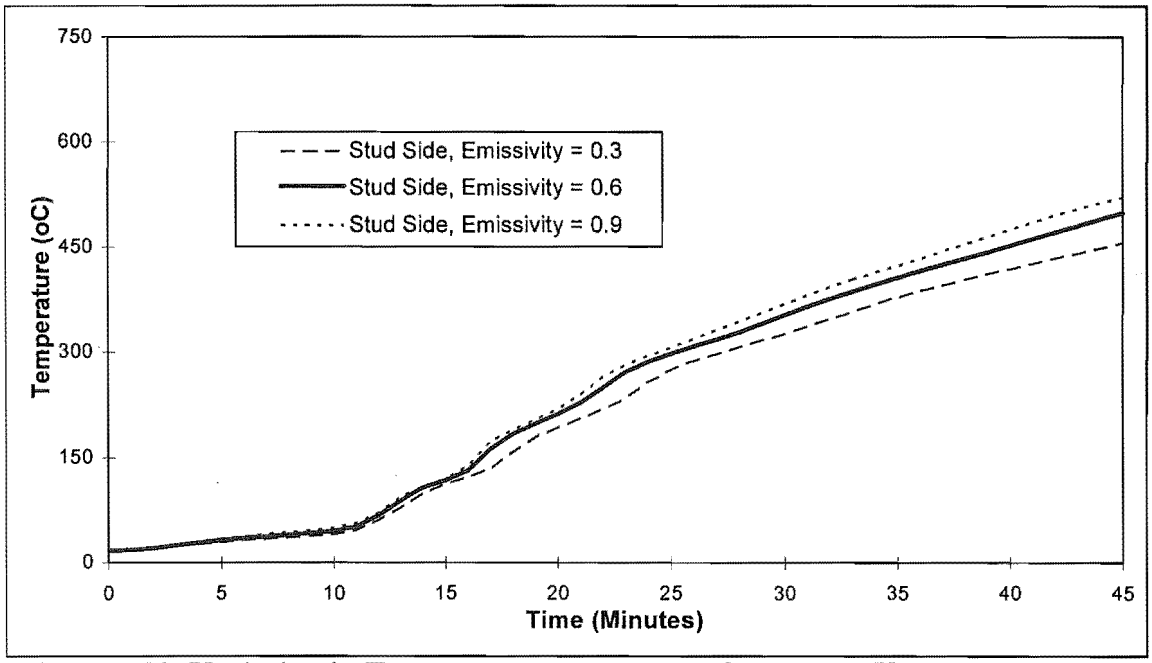

Figure 3.22 Variation in Temperature on the Stud Side of the Void as a Function of Emissivity

Figure 3.23 shows the variation in temperature and heat flux, due to variation in the emissivity value used on the ambient side of the void or cavity. The variation in temperature is not significant until the end of the test. The variation in heat flux is not reported here as it is not possible to find values accurately without producing a computer model of the radiation network.

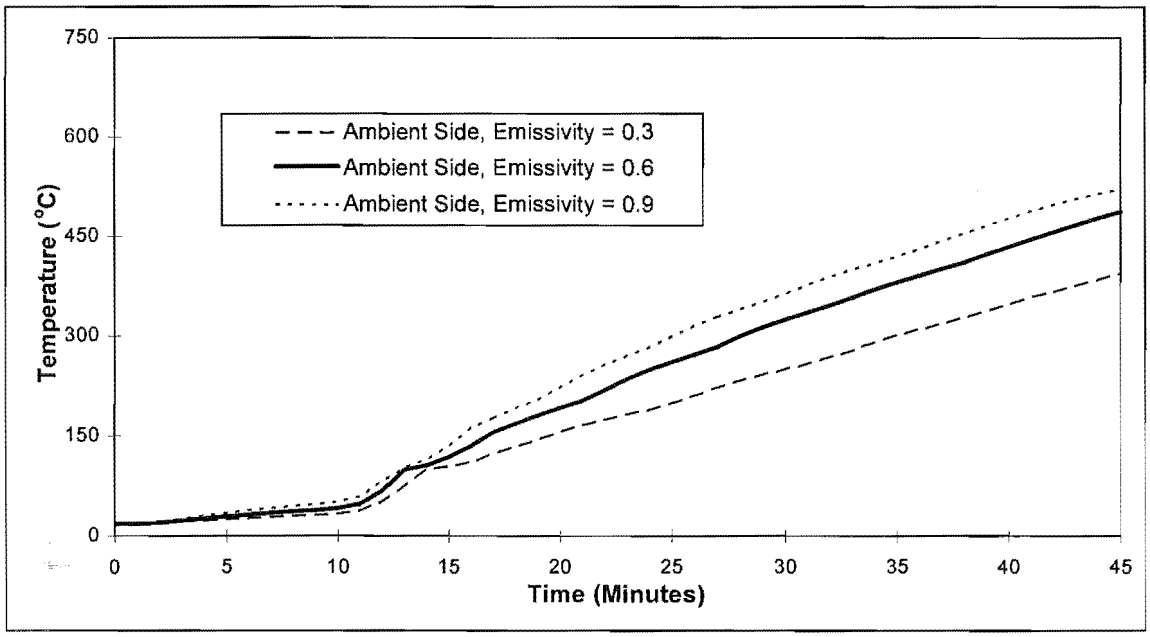

Figure 3.23 Variation in Temperature on the Ambient Side of the Void as a Function of Emissivity

3.9.7.2 Emissivity Value Used

An emissivity of 0.6 is used, because it is in the middle of the range and results in a good correlation with temperatures found in wall tests.

3.9.8 Convection Coefficients in the Void

Repeating the process outlined in the previous two Sections, to estimate the convection coefficients, it can be shown that the flow regime in the void is almost always turbulent as the Rayleigh number is over 10^9 for almost all of the duration of the test. Towards the end of the test the temperatures start to equalise and the flow becomes laminar.

From Table 3.2, the coefficient **b** (Equation 3.12) is 0.25, 0.33 or 0.4 in the turbulent flow regime. A median value of 0.33 is used and hence γ (Equations 3.2 and 3.18) is equal to 1.33. Using the values for the convective heat transfer coefficient calculated using Equation 3.17, assuming a value of **b** of 0.33 and Equation 3.18, values for the heat transfer coefficient β can be found.

Source	Beta, Fire Side of Void			Beta, Ambient Side of Void			Beta, Stud Side of Void			Beta, Overall
	Maximum	Minimum	Average	Maximum	Minimum	Average	Maximum	Minimum	Average	Average
Gammon	3.0	1.4	2.2	3.1	1.5	2.3	3.1	1.8	2.5	2.3
Atreya	0.80	0.50	0.65	0.80	0.50	0.65	0.80	0.55	0.68	0.66
Holman	3.1	1.6	2.4	3.1	1.7	2.4	3.1	1.9	2.5	2.4
Ince & Launder	1.5	0.7	1.1	1.5	0.8	1.1	1.5	0.8	1.1	1.1

Table 3.3 Values of β in the Void, Through Typical Test

Table 3.3 shows values of β, which is a maximum at the start of a test and reduces steadily throughout. The coefficients given are for a plate exposed to an unconfined air stream, except for Ince and Launder (1989), which is for convective heat flow in a cavity. The airstream is not unconfined in the cavity, and would be slower due to the small size of the cavity and the effect of interference between opposing flows. The flow pattern would be circular, air rising on the fire side of the cavity and sinking on the ambient side. Friction between these flows would slow them down. Hence a lower value for the convective coefficient β than used above is justified.

3.9.8.1 Sensitivity Analysis

The value of the convective coefficient has little effect on either temperatures or heat flux. The net heat flux values are not reported due to the problems of radiation described previously.

Mehaffey et al (1994) assumes a constant value for the convective heat transfer coefficient of 9.0 $W/m^2.K$. Gammon (1987) ignores convective losses on the ambient side. TASEF (Sterner and Wickstrom 1990) uses in examples a value of 1.5 for β and 1.33 for γ.

Figure 3.24 shows the variation in temperature, due to variation in the value of the convection coefficient, on the fire side of the void.

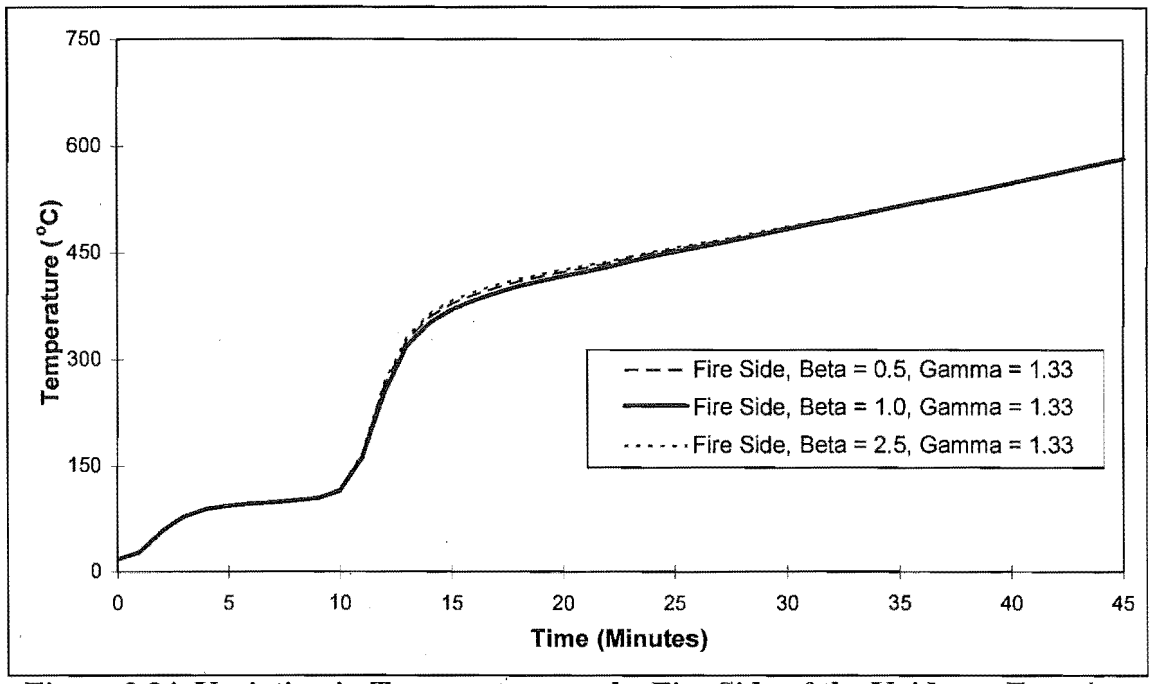

Figure 3.24 Variation in Temperature on the Fire Side of the Void as a Function of the Convection Coefficients

Figure 3.25 shows the variation in temperature due to variation in the value of the convection coefficient, for the stud side of the void.

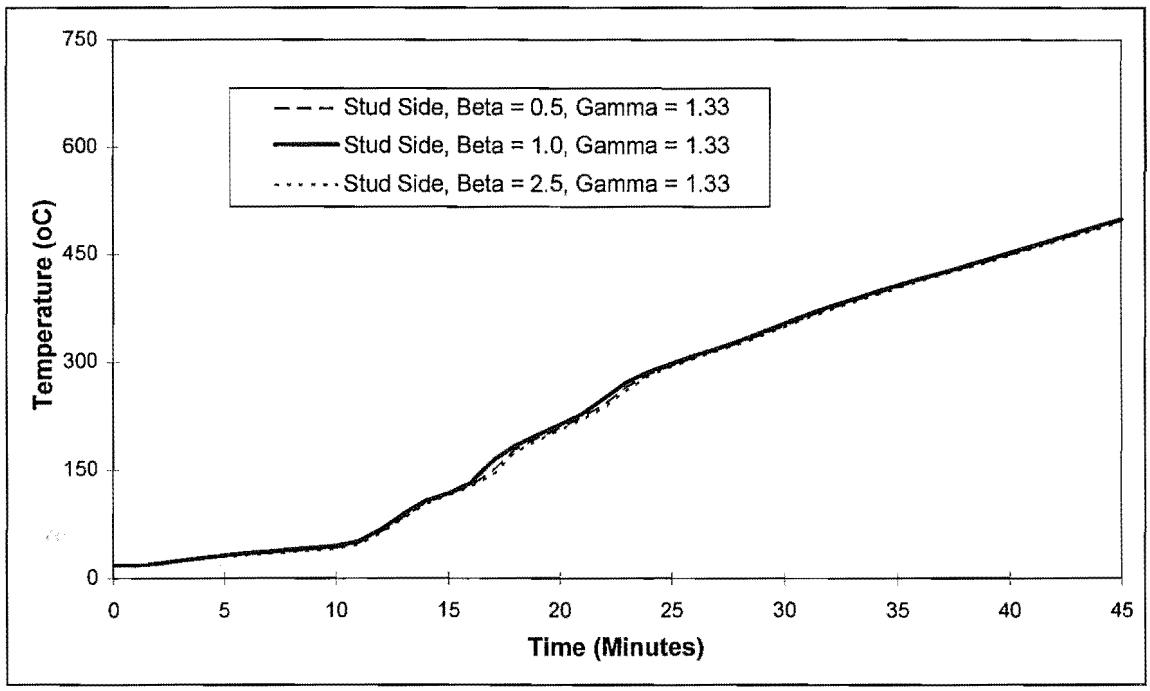

Figure 3.25 Variation in Temperature on the Stud Side of the Void as a Function of the Convection Coefficients

Figure 3.26 shows the variation in temperature due to variation in the emissivity value used, on the ambient side of the void or cavity.

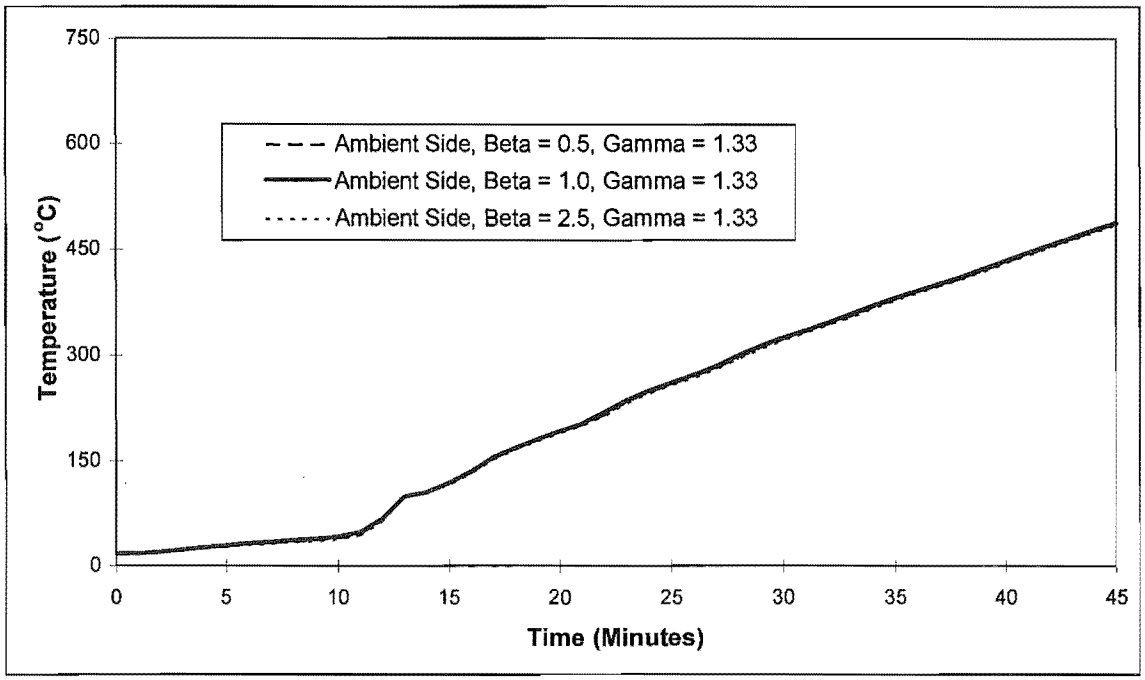

Figure 3.26 Variation in Temperature on the Ambient Side of the Void as a Function of the Convection Coefficients

3.9.8.2 Values Used for The Convection Coefficients

A value of 1.0 for β and 1.33 for γ is assumed within the cavity. This is close to the average value calculated using Ince and Launder's coefficients for convection in confined cavities.

3.9.9 Combinations of Emissivity and Convection Coefficients in the Void

Although varying either the emissivity or convection coefficients resulted in differences between the temperatures and heat fluxes around the cavity, the combinations used by various researchers show a smaller difference (Figures 3.27 to 3.29).

There is little variation in temperature due to the differences in the heat transfer coefficients used by Gammon (1987), Mehaffey et al (1994), or those used in this work.

The net heat flux values are not reported due to the problems with calculating radiation described previously. As the temperatures are very close, it is likely that the actual values of heat flux do not vary significantly.

Figure 3.27 shows the variation in temperature for the fire side of the void.

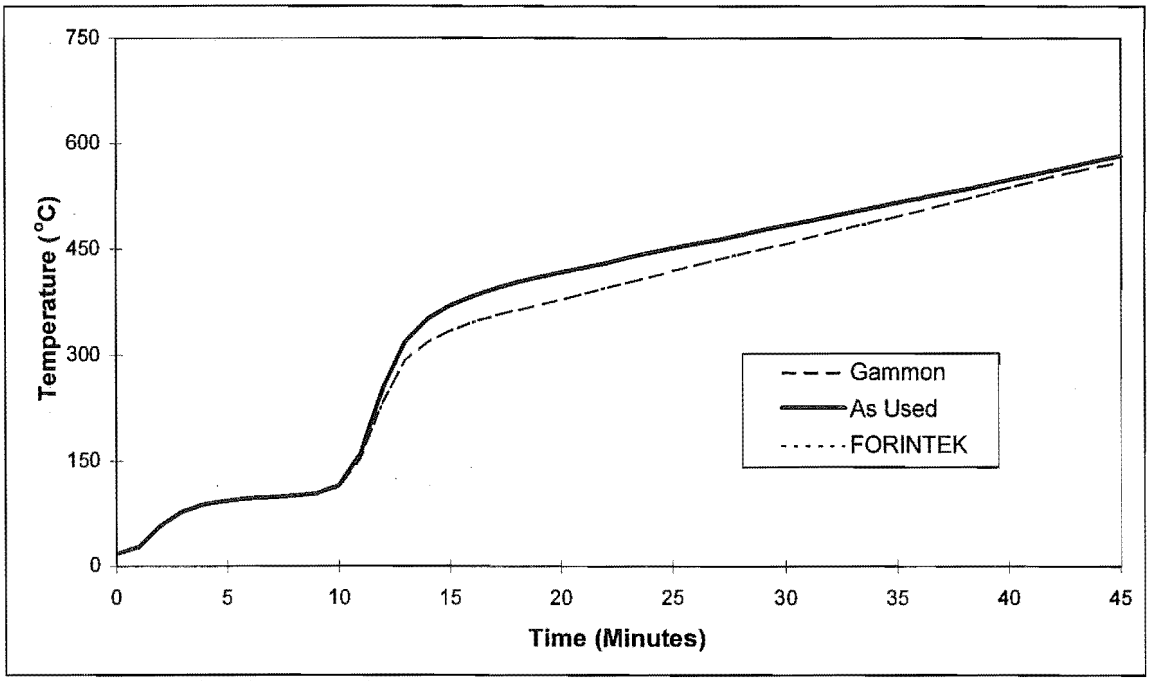

Figure 3.27 Variation in Temperature on the Fire Side of the Void as a Function of the Heat Transfer Coefficients

Figure 3.28 shows the variation in temperature for the stud side of the void.

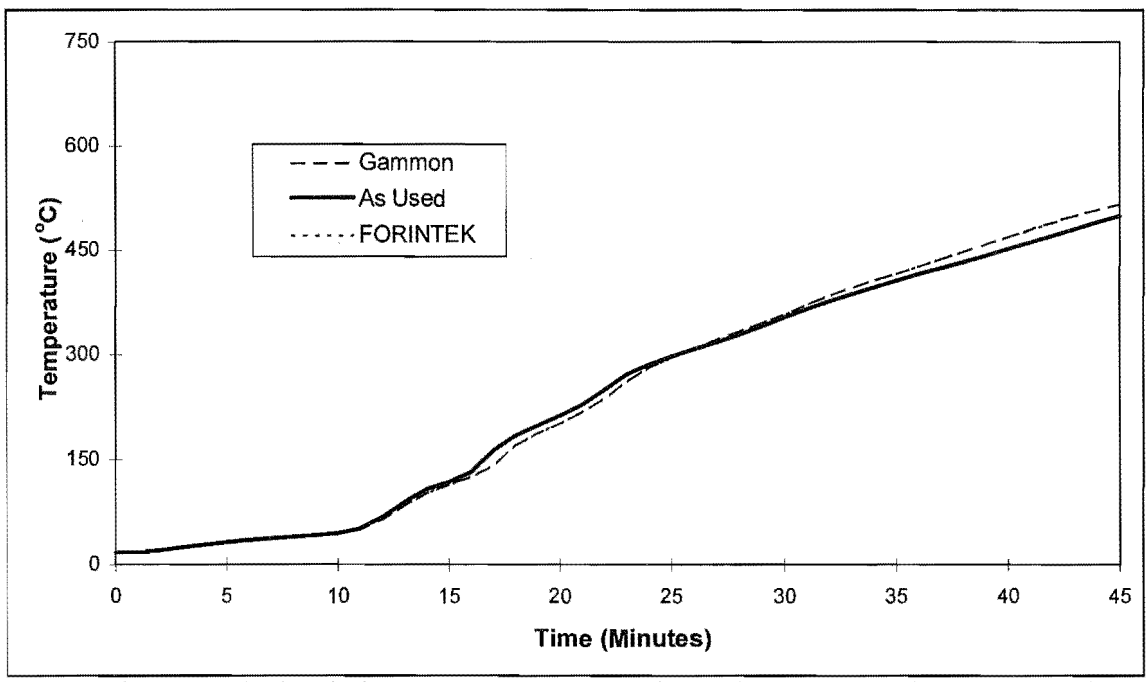

Figure 3.28 Variation in Temperature on the Stud Side of the Void as a Function of the Heat Transfer Coefficients

Figure 3.29 shows the variation in temperature for the ambient side of the void.

The choices that various researchers made about the emissivity within the void and the values for the convection coefficients have little effect.

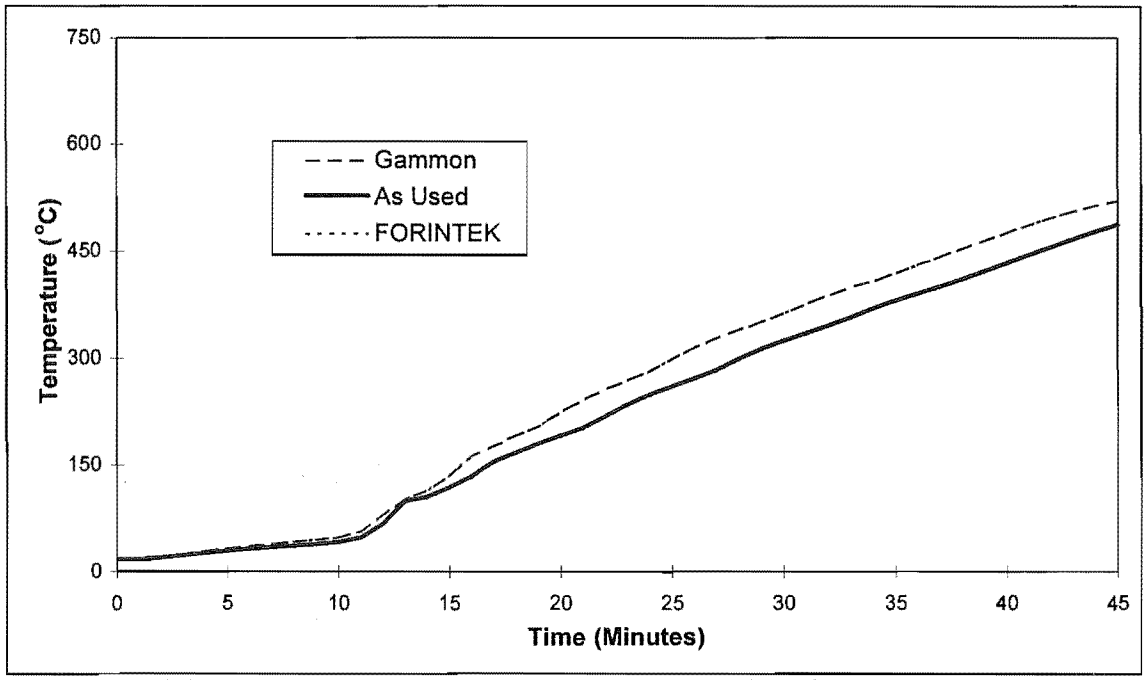

Figure 3.29 Variation in Temperature on the Ambient Side of the Void as a Function of the Heat Transfer Coefficients

3.9.10 Final Values for the Heat Transfer Coefficients

Table 3.4 summarises the values chosen for the heat transfer coefficients, for boundary elements. The heat transfer at boundaries is given by Equation 3.2.

Position	ε	β	γ
Fire Side	0.8	1.0	1.33
Lining, Fire Side of Cavity	0.6	1.0	1.33
Lining, Ambient Side of Cavity	0.6	1.0	1.33
Wood Stud Side of Cavity	0.6	1.0	1.33
Ambient Side	0.6	2.2	1.33

Table 3.4 Heat Transfer Coefficients

One mode of heat transfer that is not modelled is the evaporation of moisture from the exposed lining. This steam then condenses on the unexposed lining on the other side of the void, and on the stud. This results in a higher initial rate of heat transfer across the void. When the surface of the stud and the unexposed lining reach 100°C, this moisture then evaporates again. As the energy required to evaporate it is equal to that released when it condenses, then this anomaly self corrects.

3.10 Geometry of the Finite Element Mesh

The finite element mesh input into TASEF was chosen to maximise the accuracy of the model and at the same time minimising the complexity of the problem and hence run time. The memory used by TASEF is limited by the equation:-

$$25{,}000 < (18 + NE_y + 2) \times NN + 10 \times NE) \qquad (3.24)$$

where:- NN is the total number of nodes

NE is the total number of elements

NE_y is the number of elements across the model or the bandwidth

It is therefore desirable to have more nodes across the model, in the y-direction than in the x-direction, so the orientation of the mesh is as shown in Figure 3.30. Figure 3.30 is not to scale.

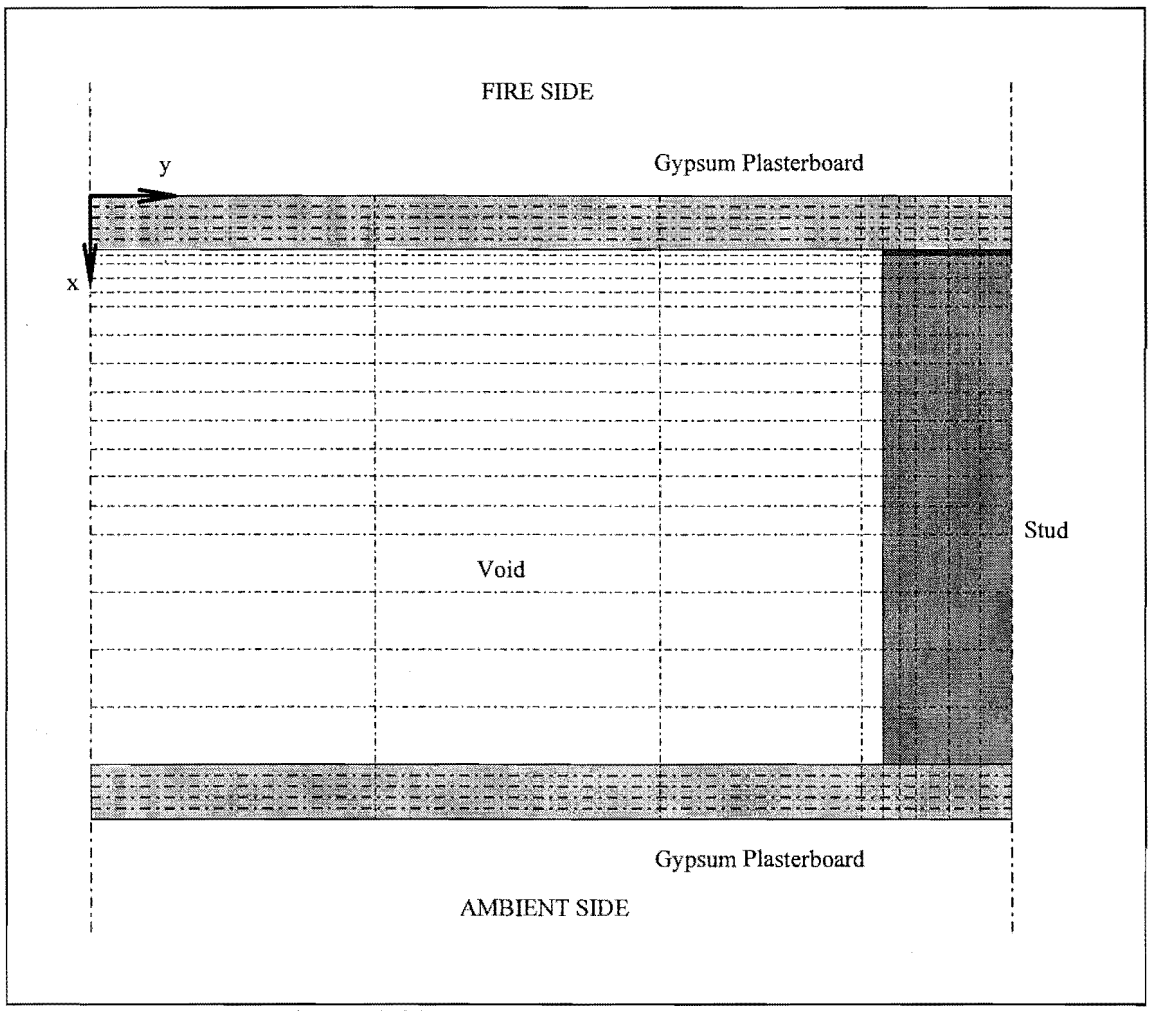

Figure 3.30 Layout of Finite Element Mesh

Table 3.5 gives the numerical coordinates of the X and Y lines and the size of the elements between them. Both Figure 3.30 and Table 3.5 are for a wall with a 9.5 mm thick gypsum plasterboard lining and a 90*45 mm stud. The size of the elements within the gypsum plasterboard are adjusted for different thicknesses. The same is true for different stud thicknesses. With a smaller stud depth, the number of X-lines (across page) is reduced.

There are few Y-lines on the left hand side, because the heat flow is mostly through the wall (down the page) and hence one dimensional. The spacing of the Y-lines through and close to the stud is much closer as the flow is more two dimensional here. The temperature gradients are also much bigger in the stud than in the void.

X (mm)	dX (mm)	X (mm)	dX (mm)	X (mm)	dX (mm)	Y (mm)	dY (mm)
0.000		19.500	2.500	79.500	10.000	0.000	
1.900	1.900	24.500	5.000	89.500	10.000	100.000	100.000
3.800	1.900	29.500	5.000	99.500	10.000	200.000	100.000
5.700	1.900	34.500	5.000	101.400	1.900	270.000	70.000
7.600	1.900	39.500	5.000	103.300	1.900	277.500	7.500
9.500	1.900	44.500	5.000	105.200	1.900	280.375	2.875
10.500	1.000	49.500	5.000	107.100	1.900	283.250	2.875
12.000	1.500	54.500	5.000	109.000	1.900	289.000	5.750
14.500	2.500	59.500	5.000			294.500	5.500
17.000	2.500	69.500	10.000			300.000	5.500

Table 3.5 Finite Element Grid and Spacing

The X-lines are more closely spaced in the gypsum plasterboard as the temperature gradients are steeper. The same is true with the stud on the fire side. The other side of the stud has a smaller temperature gradient and is of less interest as the temperatures do not get to a high enough level to significantly affect the wood.

In Figure 3.30 there is a dark grey area at the top of the stud. This is a region that is referred to as the "contact resistance" region. It has the same specific heat values as the rest of the stud and conductivity, until a temperature of 120°C is reached. At 150°C and above the conductivity used is the effective value for air at elevated temperatures through the cellular cavities in timber. This is given by Janssens' (1994) as:-

$$k_{air} = 0.024 + 7.05 \times 10^{-5} T_c - 1.59 \times 10^{-8} T_c^2 \qquad (3.22)$$

where:- k_{air} is the conductivity of air (W/m^2.K).

T_c is the temperature (°C).

The resulting values are shown in Figure 3.31.

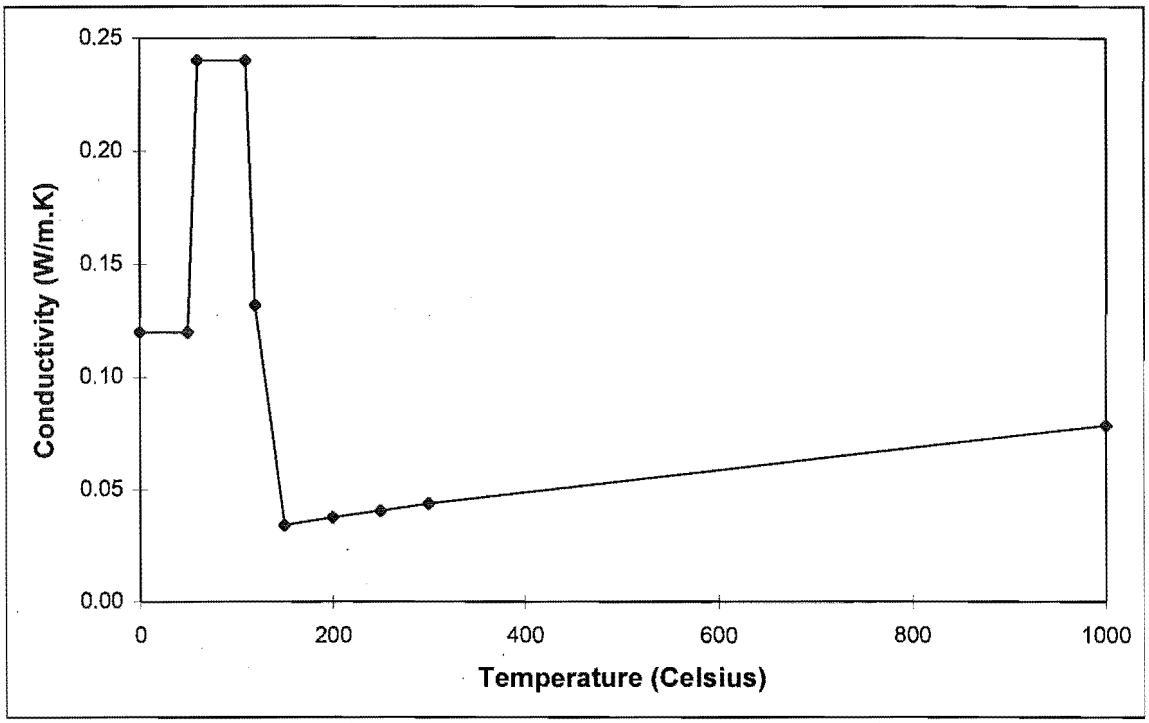

Figure 3.31 Conductivity of Contact Resistance Space

This region allows for the contact resistance of the gap between the stud and the gypsum plasterboard. This gap is small at low temperatures, but opens up at higher temperatures. Initially this opening is due to the fact that both gypsum plasterboard and wood shrink when heated as the moisture is driven off. The fastener, either a steel nail or screw expands when heated. Later, as the wood chars it contracts significantly (Janssens 1994) and the gap becomes much larger. A gap of only 1 mm appears to work well in the model throughout a typical test. A void could have been used to model this, but TASEF does not allow voids with an internal angle of greater than 180°C. TASEF does not allow two adjacent voids. A fictitious material could have been placed between the two voids, but this was not done.

Chapter 4 Calibration and Validation of the Finite Element Wall Model

After a reasonable range for the appropriate values for the thermal and physical properties of the wall and its component materials were found, the model was calibrated using ISO-834 tests on light timber framed wall systems. Subsequently the model was validated using similar tests and two furnace tests with non-standard time-temperature curves.

4.1 Test Data

Data from several fire resistance tests on load-bearing light timber frame walls were supplied by the Building Research Association of New Zealand (BRANZ). Some of these data were released with permission from Winstone Wallboards Ltd. The tests used are summarised in Table 4.1. Some were used to calibrate the model and the rest were used to validate it after reasonable comparisons had been reached.

Test Number	Lining Thickness (mm)	Stud Depth (mm)	Stud Width (mm)	Thermocouple Groups		Usage
				Disc	Stud	
FR1515A	14.5	90	45	4	2	Validation
FR1515B	14.5	90	45	4	2	Validation
FR1515C	14.5	90	45	4	2	Validation
FR1582A	9.5	69	45	2	2	Calibration
FR1582B	9.5	90	45	2	2	Calibration
FP1583A	9.5	69	45	3	1	Validation
FP1583B	9.5	90	45	3	1	Calibration
FR1611	12.5	69	45	4	2	Calibration
FR1777	16	90	35	4	1	Calibration
FP1970	9.5	90	45	3	1	Validation
FP1972	9.5	90	45	3	1	Validation
FR1868	19, 4*16, 19	n/a	n/a	n/a	n/a	Calibration

Table 4.1 Details of Wall Tests Used

Tests FR1515A, FR1515B and FR1515C were identical load-bearing tests, but the load per stud varied between tests. Test FR1868 included a portion of wall that was solid gypsum plasterboard. All walls had a 600 mm stud spacing.

These tests had more intensive instrumentation than is necessary or usual in a standard fire test. Test numbers starting with "FR" are full scale tests and tests starting with the prefix "FP" were carried out in the BRANZ pilot furnace. The full size furnace is three metres by four metres and the pilot furnace is 1.03 metres by 2.22 metres. The data includes information from thermocouples within the cavity and through the stud. There are thermocouples located in positions 2, 3, 4 and 5 in Figure 4.1 for most tests. These thermocouples are a 15 mm copper disc, shielded with a small piece of ceramic material behind them. There is between 2 and 4 sets of these in each wall tested except FR1868.

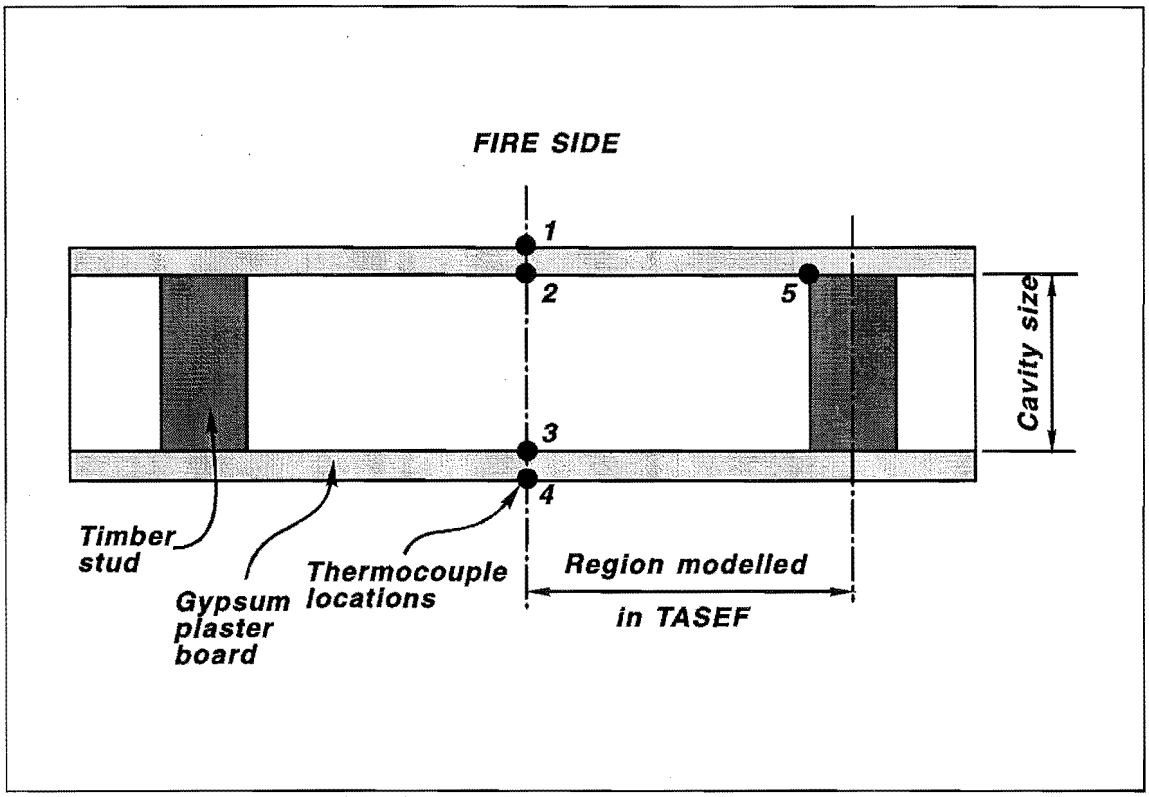

Figure 4.1 Section of Light Timber Framed Wall

There are also dummy studs instrumented with sheathed wire thermocouples throughout their cross-section. The layout of the thermocouples in the dummy studs is shown below in Figure 4.2.

For the tests used for calibration, there is a disc thermocouple at position 5 and wire thermocouples in positions 8 to 13 inclusive. This is not the case for FR1777, with a disc thermocouple in position 15 and wire thermocouples in positions 10, 11, 12 and 14 only.

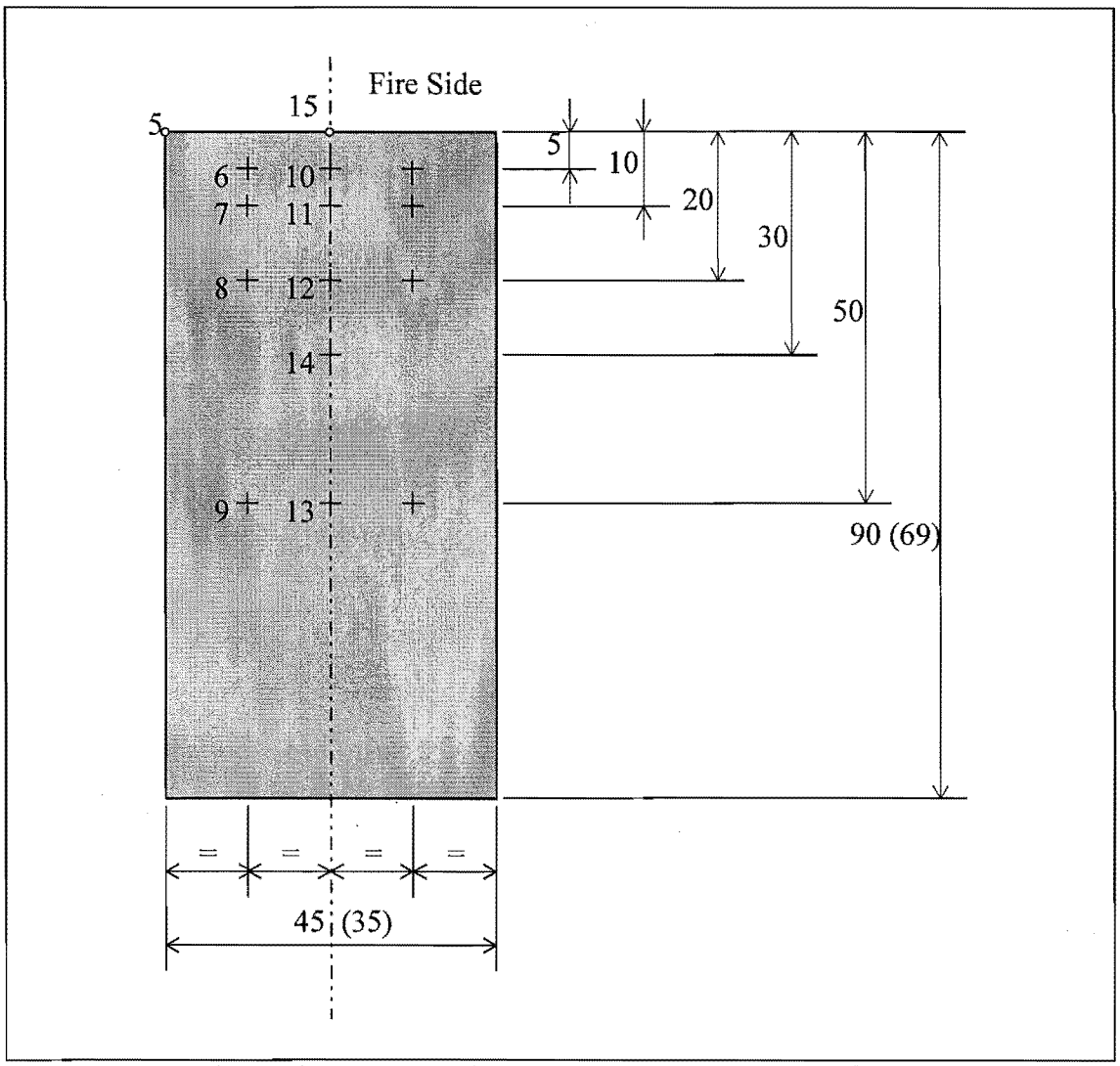

Figure 4.2 Layout of Thermocouples in Dummy Studs

As only one half of the stud is modelled, the temperatures on each side of the centreline were averaged. Average values for temperature were used when there were two or more identical groups of thermocouples within the wall.

4.2 Comparison with Tests

The model was initially developed to compare with test results through the centreline of the cavity and at the interface between the lining on the fire side of the assembly and the timber stud. That is, at positions 2, 3, 4 and 5 in Figure 4.1. The model was then extended to the temperature distribution in the stud. The calibration and validation of the model was carried out in the following order:-

(i) Calibration with test results from a solid gypsum plasterboard wall (FR1868).

(ii) Calibration with test results from a cavity wall (FR1582B).

(iii) Calibration with test results from several cavity walls, (FR1582A, FR1582B, FR1611 and FR1777), for a range of lining thicknesses and stud sizes.

(iv) Blind (with no prior knowledge of test results) validation with test results from another cavity wall, (FR1515A, FR1515B and FR1515C), using an average of the results from these three tests.

(v) Calibration of pilot furnace characteristics (FP1583A and FP1583B).

(vi) Validation using two non-standard tests (FP1970 and FP1972).

The resulting numerical values for thermo-physical properties are discussed in Sections 3.4 through 3.10. Throughout the calibration process, thermo-physical properties of the materials and heat transfer coefficients were modified in order to achieve good correlation between the fire tests and the computer model. Only the final values are given in Chapter 3.

4.2.1 Gypsum Plasterboard Wall

The model was initially calibrated with the test results for a solid gypsum plasterboard wall (FR1868). This wall was composed of two layers of 19 mm and 4 layers of 16 mm gypsum plasterboard with thermocouples located between the layers. The heat transfer in this wall is nearly one dimensional. One would expect that data from this test could be used to calibrate the thermal properties of gypsum plasterboard as there is no cavity to complicate the model, but this was not the case.

The conductivity was modified to give a high value at about 100°C. This mimics the increase in effective conductivity due to moisture movement which was not modelled. The thermal properties chosen using test FR1868 did not produce good comparisons with test data from cavity wall tests. This is because the moisture movement in the solid wall is different for a cavity wall. This effective increase in conductivity is only necessary in large volumes of materials, rather than in thin sheets. This adjustment to conductivity was necessary for the timber stud as described in Section 3.8.3.

4.3 Calibration with Cavity Walls

The model was calibrated using four cavity wall test results.

4.3.1 FR1582B

The first cavity wall used to develop the model was FR1582B. This is a wall made up of 90*45 mm studs at 600 mm centres, and one layer of 9.5 mm "Fyreline Gibraltar Board" on each side (this is also a very common assembly in New Zealand). This wall has a Fire Resistance Rating (FRR) of 30 minutes (Winstones 1992). The comparison between test and model results for this wall are shown in Figures 4.3 to 4.5 below.

4.3.1.1 Temperature Comparison Through the Wall

Figure 4.3 refers to positions 2,3 and 4 in Figure 4.1 and is for heat flow through the centre of the cavity, away from the studs and so the heat flow is primarily one-dimensional.

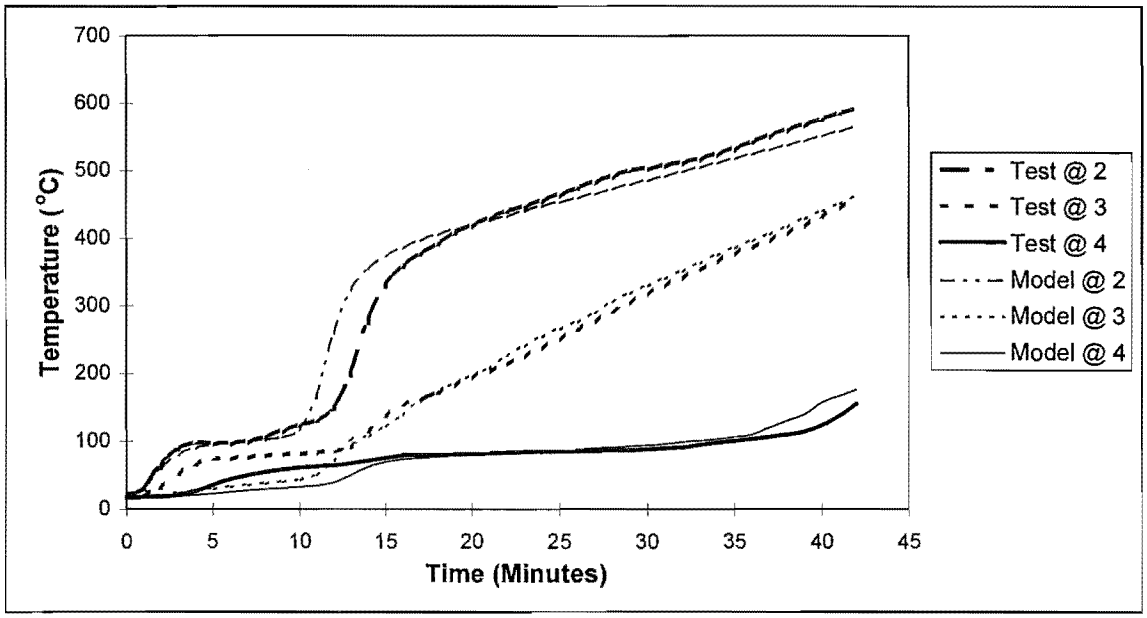

Figure 4.3 Test FR1582B Comparison with Model

The comparison is good, except for positions 3 and 4 at low temperatures. The heat transfer is higher than modelled because of the effect of moisture movement as described previously. The model tends to reduce in accuracy as the temperature of the hot side of the exposed lining approaches 1000°C. This discrepancy is due to the fact that surface recession or ablation of the plasterboard is not modelled.

4.3.1.2 Temperature Comparison in the Stud

Figure 4.4 shows the comparison at positions 5 to 9 in Figure 4.2. Position 5A is located on the corner of the stud, not against the gypsum plasterboard lining. The lining and the stud are separated by the "contact resistance" region as described in Section 3. It is 1 mm from the lining. This gives better comparison with test data. As this temperature is measured by a shielded disc thermocouple, the thermocouple and shield may affect the measurement.

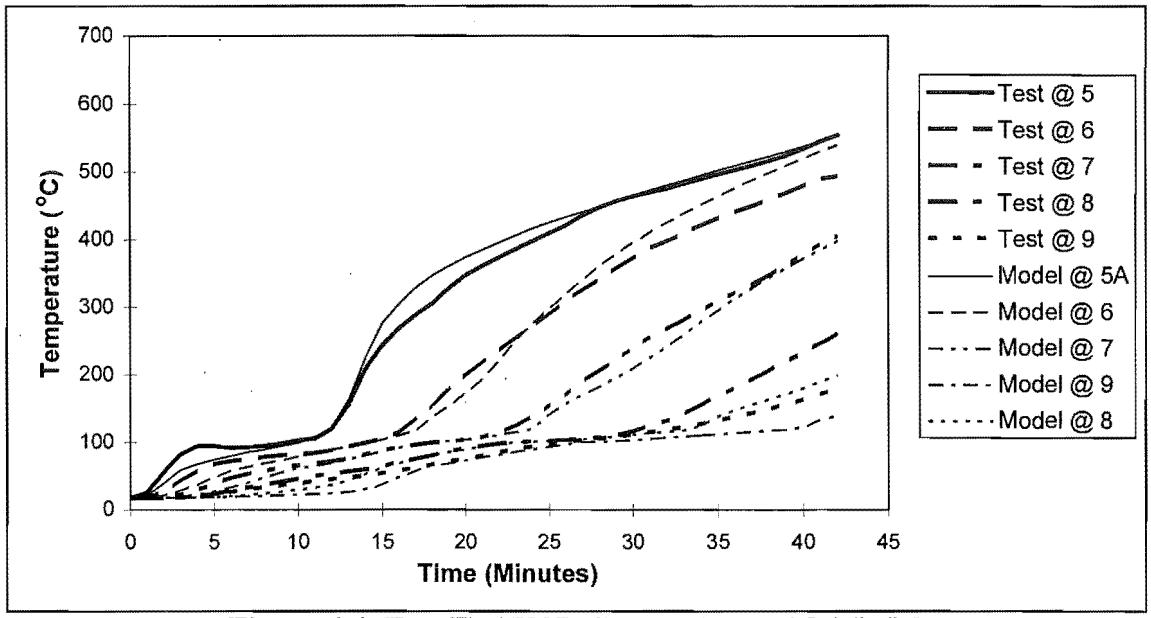

Figure 4.4 Test FR1582B Comparison with Model

The comparison at position 5 is reasonable. The temperature found using the model is a little high at position 6 and low at the others. Figure 4.5 refers to temperatures on the centreline of the stud, positions 10 to 13 inclusive in Figure 4.2.

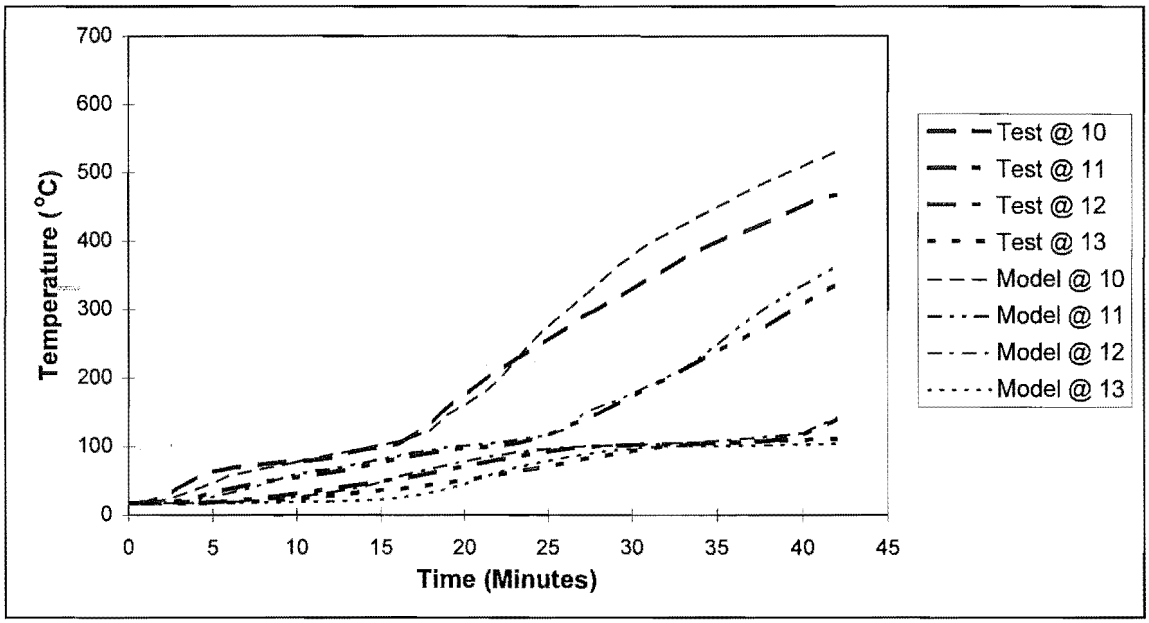

Figure 4.5 Test FR1582B Comparison with Model

The modelled temperature at position 10 is high as it is at position 6, however the comparison is good at the other locations. The model was calibrated to give a better comparison at the centreline (positions 10 to 13) of the studs, than at the quarter points (positions 6 to 9). The centreline temperature is more significant when looking at the amount of residual cross-section than the quarter point temperature. It is not possible to achieve a good comparison at both sets of points.

4.3.2 FR1582A

The same process was carried out for wall FR1582A. FR1582A is a wall made up of 69*45 mm studs at 600 mm centres, and one layer of 9.5 mm Fyreline Gibraltar Board on each side. This wall has a FRR of 30 minutes (Winstones 1992).

4.3.2.1 Temperature Comparison Through the Wall

The comparison between test and model results for this wall are shown in Figures 3.45 to 3.47 below. Figure 4.6 refers to positions 2, 3 and 4 in Figure 4.1.

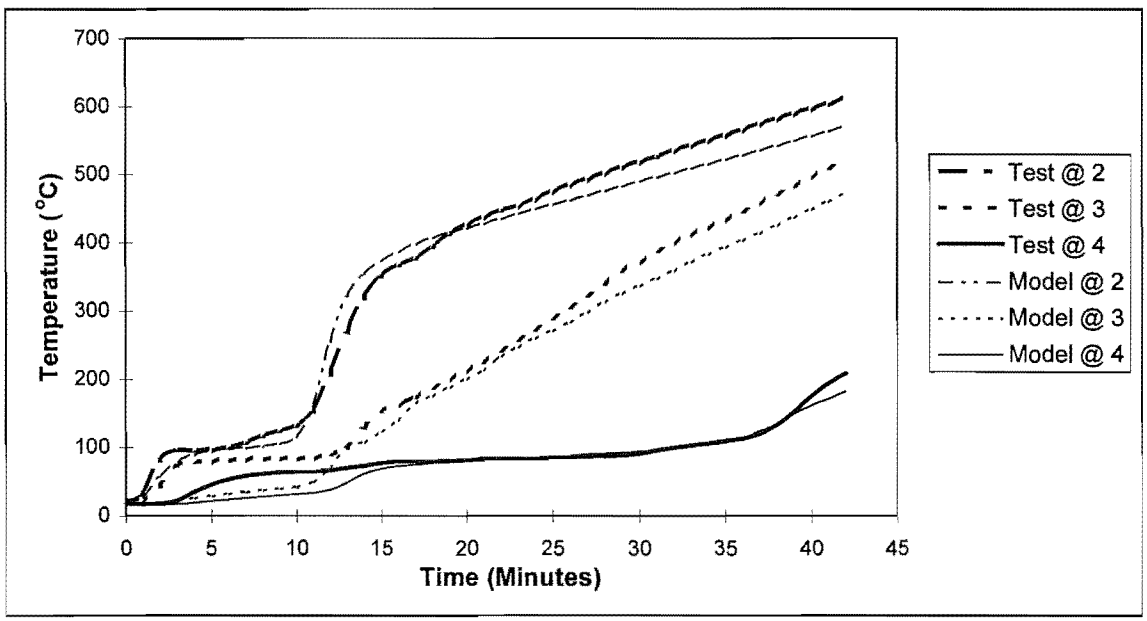

Figure 4.6 Test FR1582A Comparison with Model

The comparison is very similar to that for FR1582B. The discrepancies are the same as described previously and for the same reasons of moisture movement and ablation not being modelled.

4.3.2.2 Temperature Comparison in the Stud

Figure 4.7 shows the comparison at positions 5 to 9 (Figure 4.2).

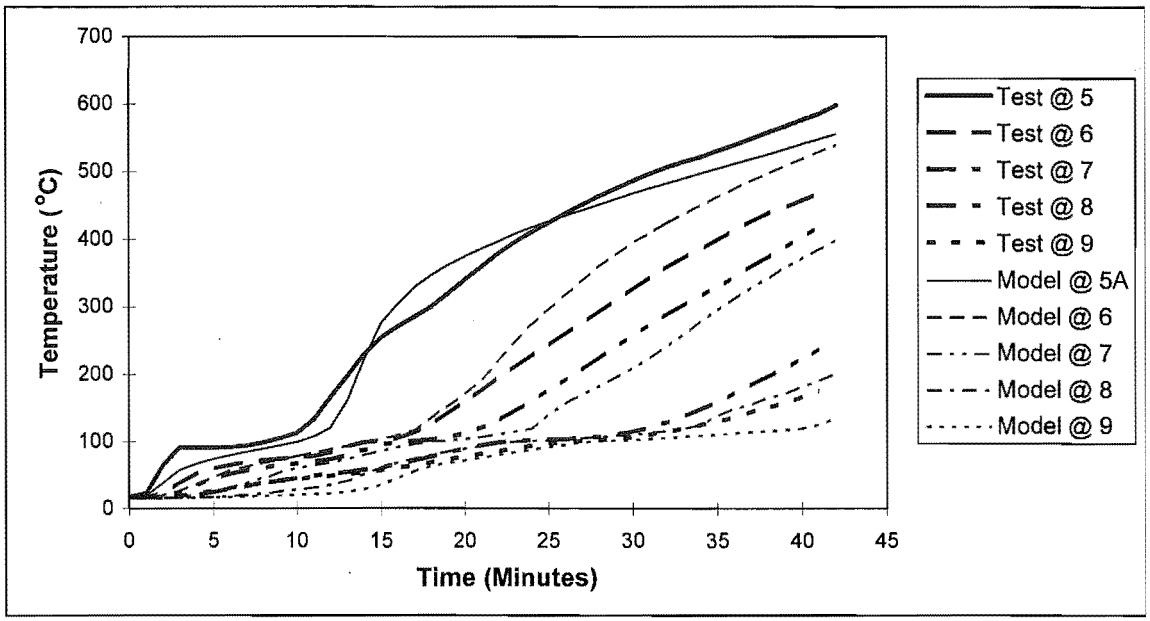

Figure 4.7 Test FR1582A Comparison with Model

The agreement at positions 5, 6 and 7 is not as good as for wall FR1582B. The model values are low at positions 8 and 9. Figure 4.8 shows that the comparison is better for the positions closer to the fire side, 10 and 11. It is very good for positions 12 and 13 (Figure 4.2).

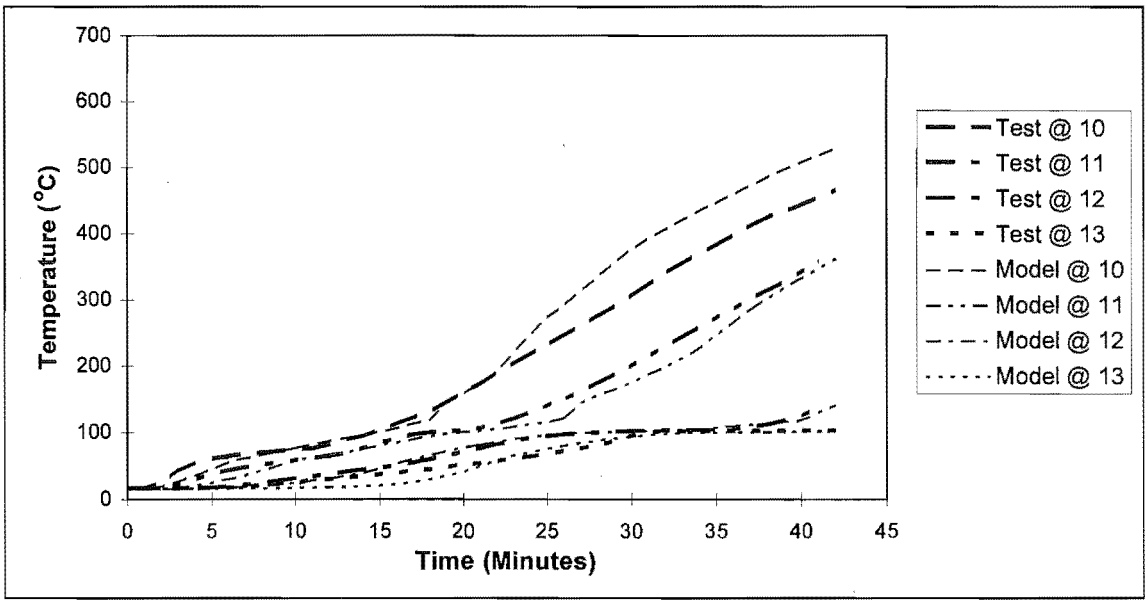

Figure 4.8 Test FR1582A Comparison with Model

4.3.3 FR1611

Wall FR1611 has a FRR of 60 minutes (Winstones 1992). It is made up of 69*45 mm studs at 600 mm centres, and a layer of 12.5 mm Fyreline Gibraltar Board on each side.

4.3.3.1 Temperature Comparison Through the Wall

Figure 4.9 above refers to positions 2, 3 and 4 in Figure 4.1 and is for heat flow through the cavity.

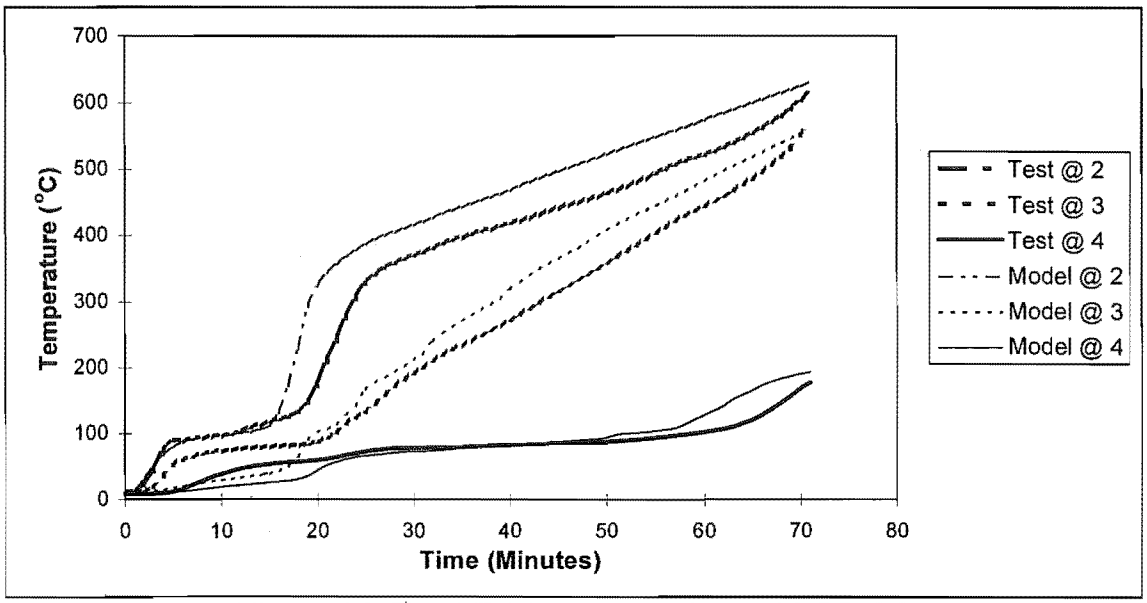

Figure 4.9 Test FR1611 Comparison with Model

The comparison is poorer than for the previous two walls. The model overpredicts the temperatures.

4.3.3.2 Temperature Comparison in the Stud

Figure 4.10 shows the comparison at positions 5 to 9 (Figure 4.2).

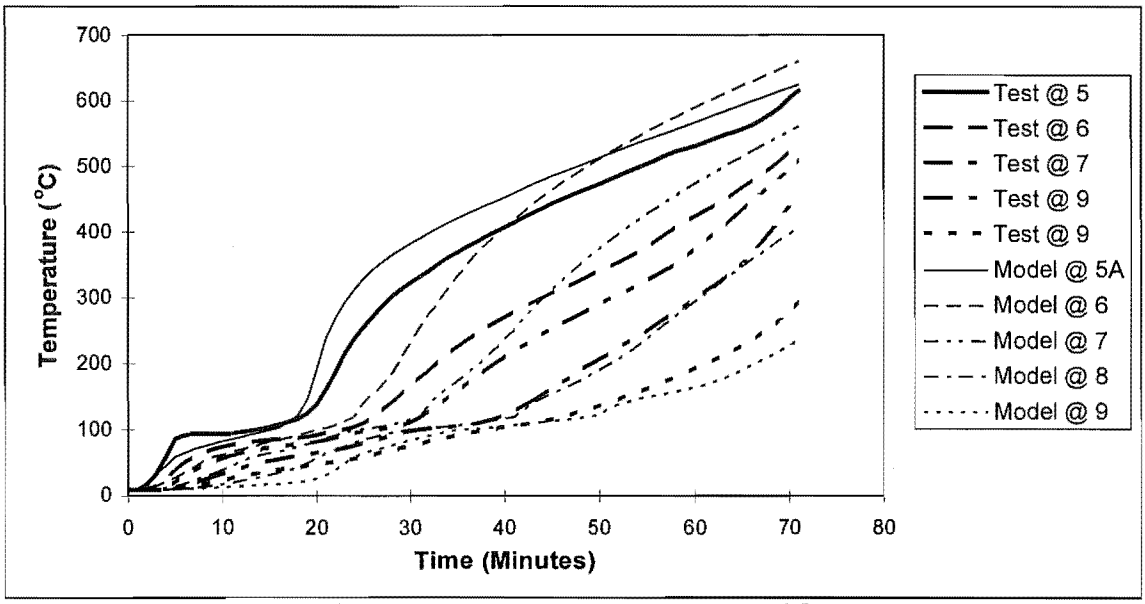

Figure 4.10 Test FR1611 Comparison with Model

Again the comparison is poorer than for the previous two walls. The model at positions 5, 6 and 7 shows significantly higher temperatures than for walls FR1582A and

FR1582B. The comparison is good at position 8 and the model temperatures are slightly low at position 9.

Figure 4.11 refers to temperatures on the centreline of the stud, positions 10 to 13 inclusive in Figure 4.2.

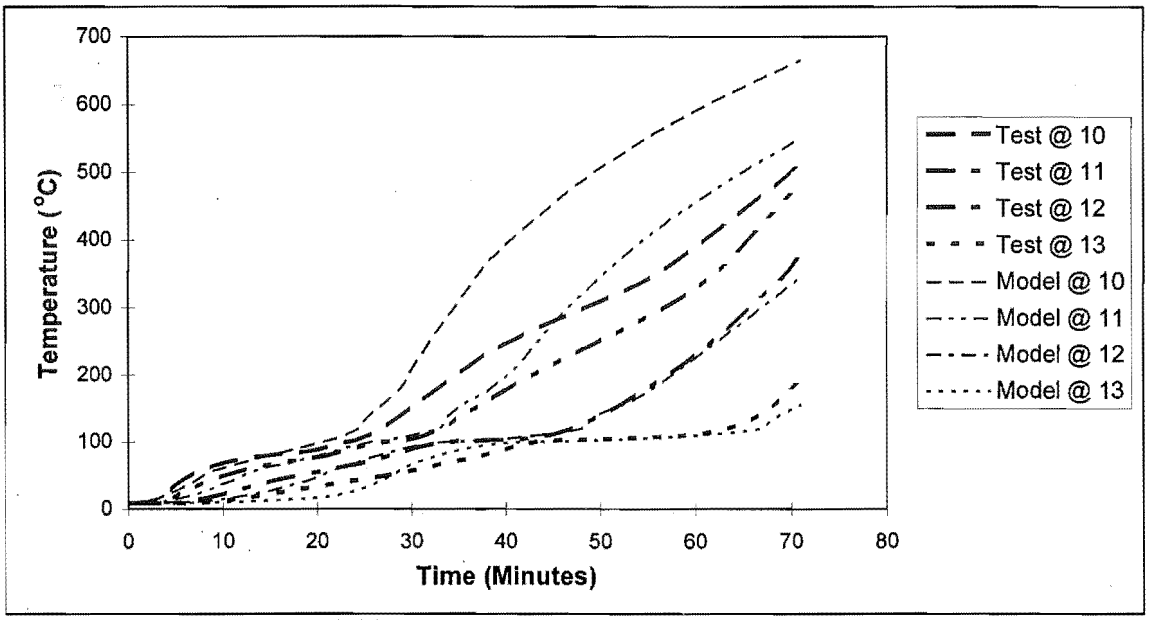

Figure 4.11 Test FR1611 Comparison with Model

Again the model temperatures are significantly higher for the positions closer to the fire side, 10 and 11, especially after 40 minutes. The correlation is good for positions 12 and 13.

4.3.3.3 Discussion of Comparison

In terms of the heat transfer through the wall, FR1611 behaved better in the test than the model would predict. This is also the case in the stud, for the positions closer to the fire. (positions 5,6,7,10 and 11). Good comparison was achieved further into the stud (positions 8,9,12 and 13).

This may be a repeatability problem. As this wall configuration has a FRR of 60 minutes and the test went for 69 minutes before failure, it could be assumed that this wall was an above average example. The gypsum plasterboard linings are often optimised to give an FRR to the nearest 30 minutes by varying material properties such as density. The aim of the board design is to achieve a the time to failure only a few minutes over that required, hence a larger variation between the time to failure and the rating may imply an above average test result.

The other possibility is that the gypsum had a higher than normal moisture content. This additional moisture would be "free", that is not chemically bound to the crystal structure of the plasterboard. The plateau in temperature at position 2 is longer than that for the model. This plateau at 100°C is due to the energy lost in evaporating water. This test was carried out in mid winter (July) and the initial temperature of 7.6°C is lower than that for the other tests (15-17°C). The lower ambient temperatures may have resulted in slower drying of the board and hence a higher moisture content. Some of this additional moisture would be driven into the stud, increasing the effective conductivity of the timber. This would compensate for the increase in specific heat of the gypsum plasterboard. This combination of effects leads to minimal change in the temperatures deep within the stud, so the comparison at positions 8, 9, 12 and 13 remains close.

4.3.4 FR1777

The fourth and last wall assembly used for calibration is a wall made up of 90*35 mm studs at 600 mm centres, and one layer of 16 mm Fyreline Gibraltar Board on each side (FR1777). This wall has a FRR of 90 minutes (Winstones 1992). The comparison between test and model results for this wall are shown in Figures 4.12 and 4.13.

4.3.4.1 Temperature Comparison Through the Wall

Figure 4.12 refers to positions 2, 3 and 4 in Figure 4.1 and is for heat flow through the cavity.

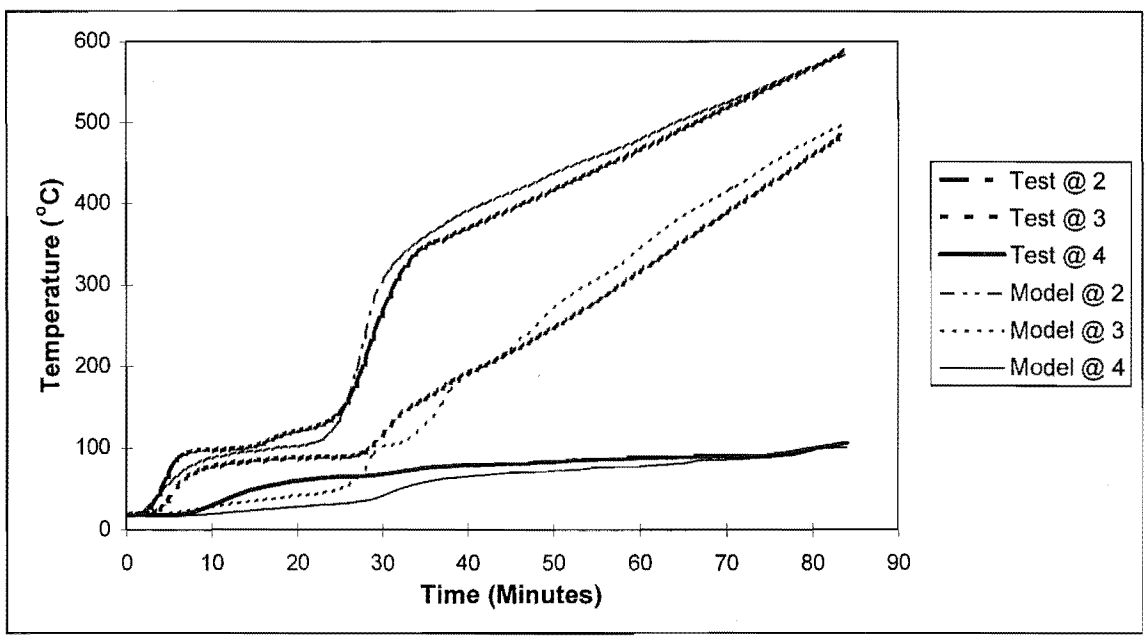

Figure 4.12 Test FR1777 Comparison with Model

The comparison is similar to that for FR1582A, but is better than the other two walls. The discrepancies are the same as previously, and for the same reasons of moisture movement and ablation not being modelled.

4.3.4.2 Temperature Comparison in the Stud

Figure 4.13 shows the comparison at positions 15, 10, 11, 12 and 14. (Figure 4.2).

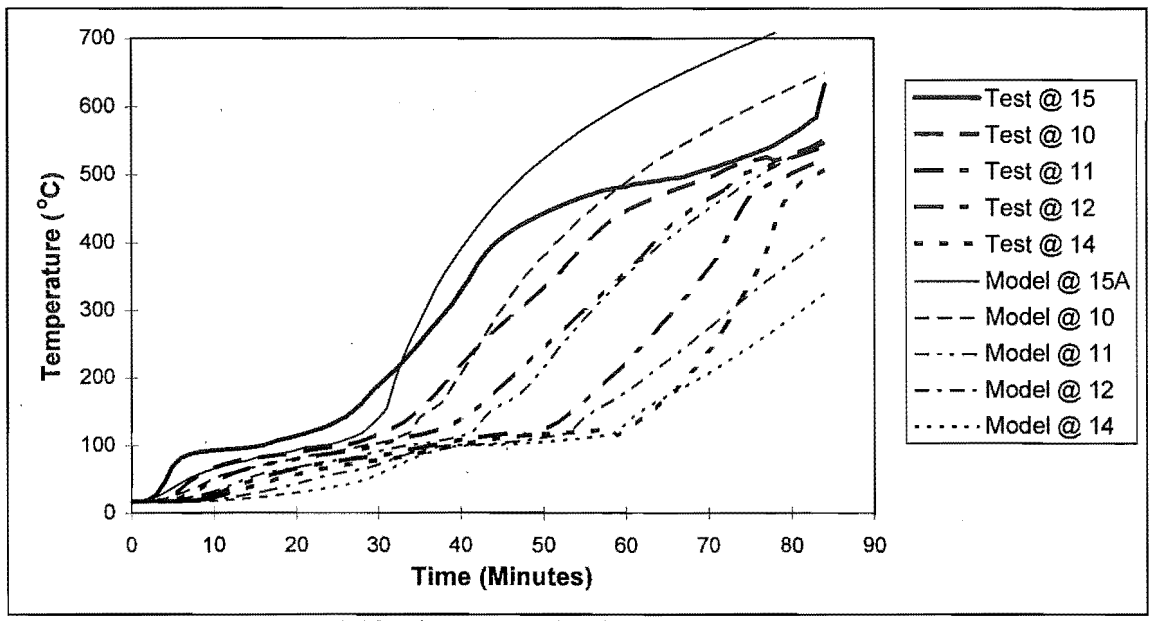

Figure 4.13 Test FR1777 Comparison with Model

The agreement at positions 15 is poor. It is reasonable at the other positions up until about 60 minutes.

4.3.4.3 Discussion of Comparison

After 60 minutes the temperatures in the stud rise rapidly. It is possible that the stud had ignited and burnt rapidly through. This is unusual as the spontaneous ignition temperature is about 600°C for wood, but is lower for prolonged exposure. Flames may have passed through a gap in the lining enabling piloted ignition to occur at a much lower temperature. The low temperatures at position 15 and 10 may simply be due to variation in the wood. Wood, being a natural material is highly variable, both between pieces and within pieces. This specimen failed prematurely due to a loss of integrity at 84 minutes. The other three tests failed due to the insulation criterion. The model does not hold after an integrity failure because the geometry of the system then changes. This may explain the differences between the comparisons for this test and the other three tests mentioned is Section 4.3.

4.4 Validation with Test Series FR1515

A series of three load-bearing tests were carried out by BRANZ in 1991. They are FR1515A, FR1515B and FR1515C. They are all made up of 90*45 mm studs at 600 mm centres lined with 14.5 mm Fyrestop Gibraltar Board. The stud loads are 16, 8 and 10 kN per stud respectively. As their thermal performance should be identical, the average values for temperatures were used for comparison purposes. Disc thermocouples were located in positions 2 and 4 (Figure 3.1) and positions 9 to 13 inclusive (Figure 3.41). The density of 14.5 mm Fyrestop board is 661 kg/m^3.

This wall has a FRR of 60 minutes (Winstones 1992). The comparison between test and model results for this wall are shown in Figures 4.14 to 4.16.

4.4.1 Temperature Comparison Through the Wall

Figure 4.14 refers to positions 2 and 4 in Figure 4.1.

The comparison is reasonable except the plateau at 100°C is shorter in the model results and there is some discrepancy towards the end of the test at position 4.

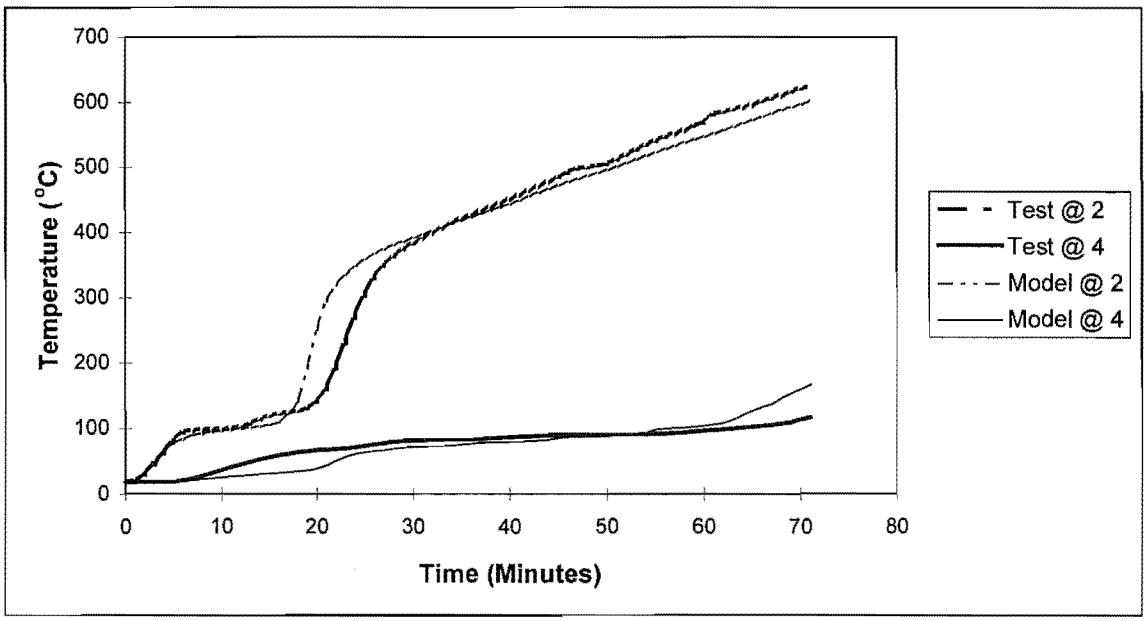

Figure 4.14 Test FR1515 Comparison with Model

4.4.2 Temperature Comparison in the Stud

Figure 4.15 shows the comparison at positions 5 to 9 (Figure 4.2).

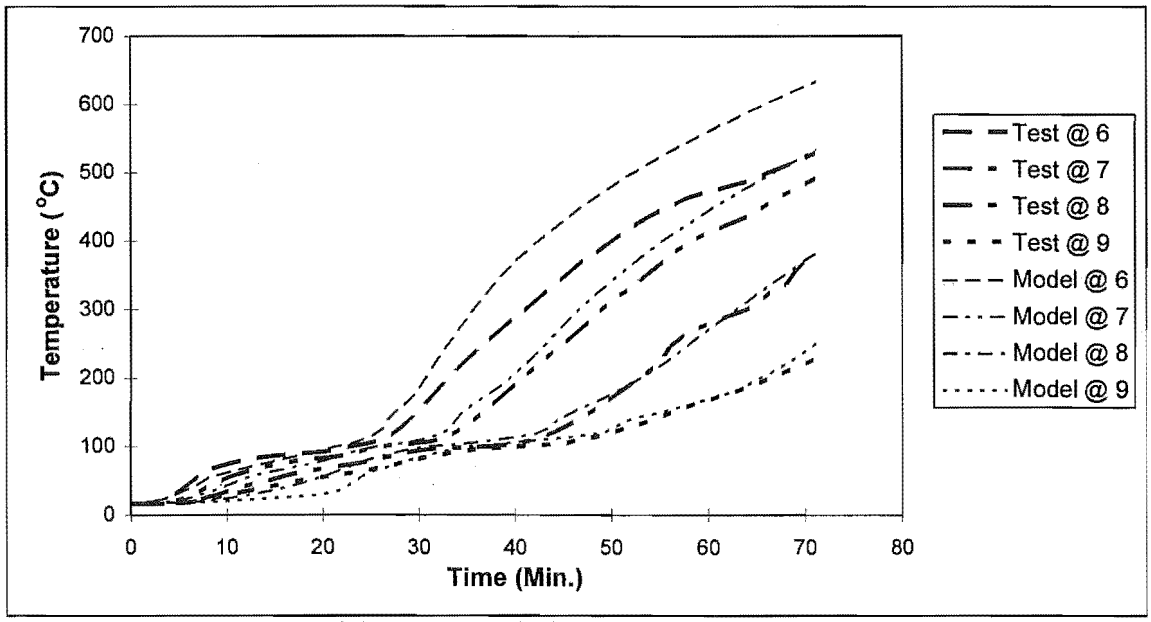

Figure 4.15 Test FR1515 Comparison with Model

The model overpredicts temperatures at positions 6 and 7. This is consistent with other tests. Agreement at positions 8 and 9 is very good.

Figure 4.16 refers to temperatures on the centreline of the stud, positions 10 to 13 inclusive in Figure 4.2.

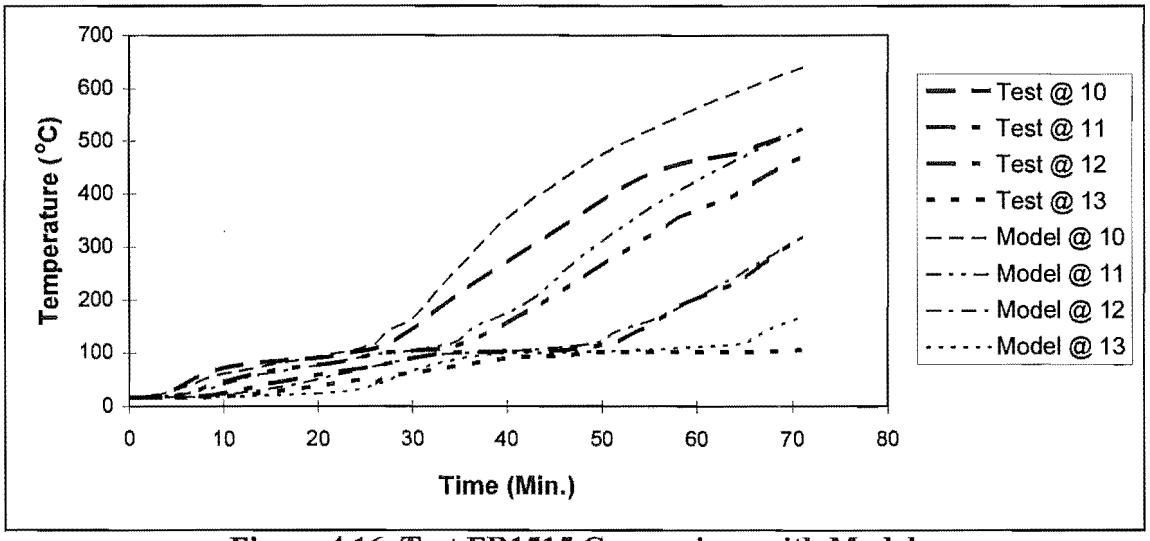

Figure 4.16 Test FR1515 Comparison with Model

The model overpredicts temperatures at positions 10 and 11 and 13. This is also consistent with other tests. Agreement at position 12 is very good.

Overall, the model predicted the temperature profiles quite well for this test. The model was run without any previous knowledge of the test data.

4.5 Calibration of the Pilot Furnace

Section 3.9.1 describes how the characteristics of furnaces may affect results. Some available test data was from tests using the pilot furnace at BRANZ. This furnace is approximately 1 by 2 metres and 1 metre deep. The furnace used for the other tests is 3 by 4 metres by about 1 metre deep. The geometry is significantly different and size effects are apparent. The severity of exposure will be less in the pilot furnace (Section 3.9.1). The two pilot tests FP1583A and FP1583B are identical in all other respects to walls FP1582A and FP1582B respectively. By manipulating the models for these walls, it was possible to determine appropriate values for the heat transfer coefficients, for the furnace side of the wall. All other parameters were not altered.

4.5.1 FP1583B

The comparison between test and model results for wall FP1583B are shown below.

4.5.1.1 Temperature Comparison Through the Wall

Figure 4.17 refers to positions 2, 3 and 4 in Figure 4.1.

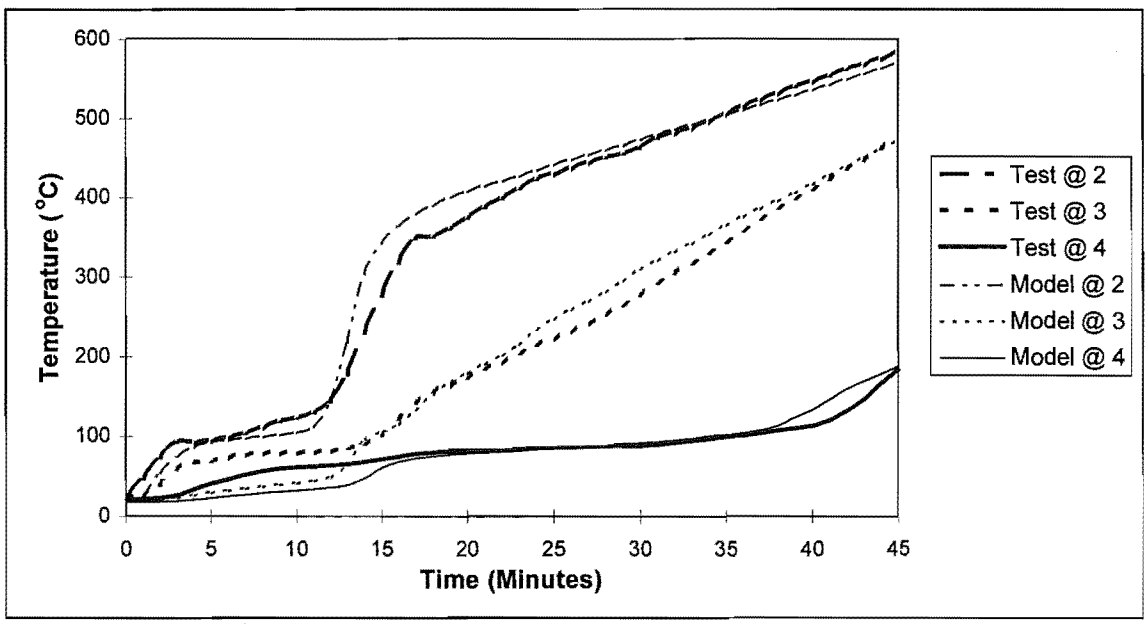

Figure 4.17 Test FP1583B Comparison with Model

The comparison is very good at all the positions, that is positions 2, 3 and 4.

4.5.1.2 Temperature Comparison in the Stud

Figures 4.18 and 4.19 shows the comparison at positions 5 to 13 (Figure 4.2).

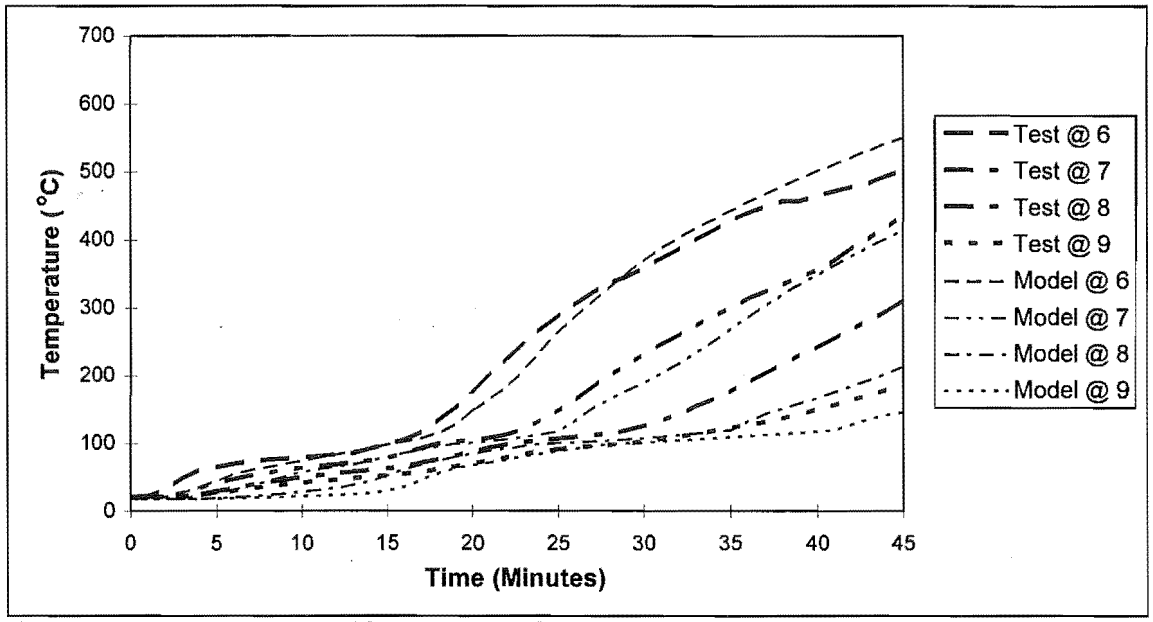

Figure 4.18 Test FP1583B Comparison with Model

Figure 4.18 shows a good comparison at positions 6 and 7. The model underpredicts temperatures at positions 8 and 9.

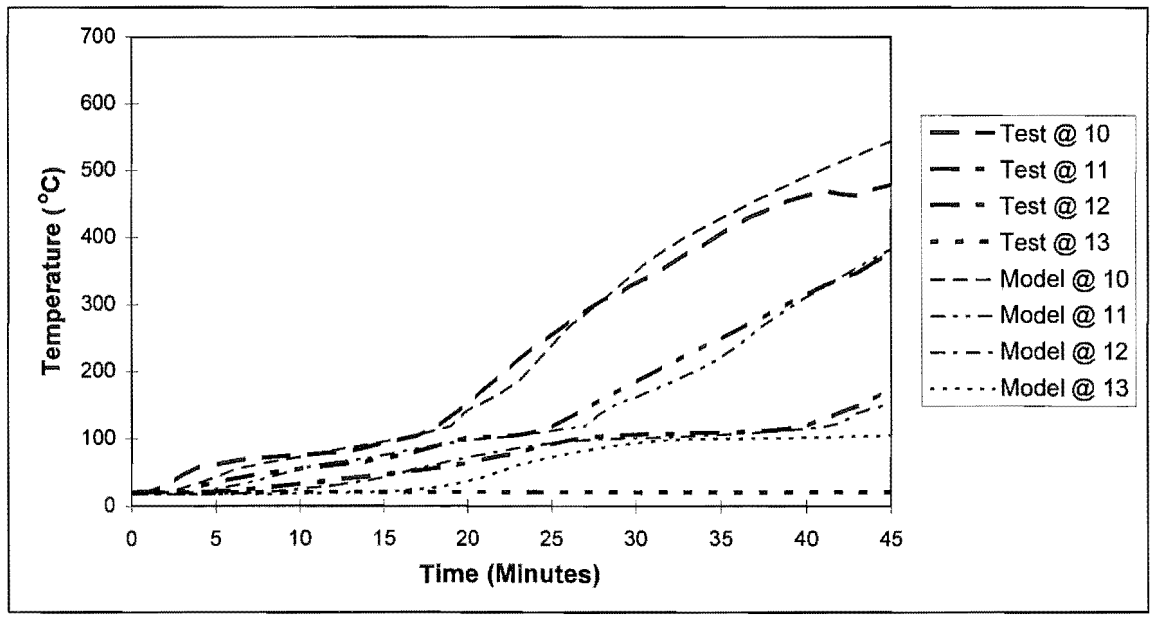

Figure 4.19 Test FP1583B Comparison with Model

The comparison is very good for all positions in Figure 4.19, except position 13. The test data is anomalous at this point. It appears the thermocouple at this position was not working, and only the initial temperature is recorded throughout the test. Overall the model predicts the temperatures well.

4.5.1.3 Heat Transfer Coefficients for Test FP1583B

The correlation for FP1583B was achieved by reducing the effective emissivity from 0.8 to 0.5 and the convection coefficient β from 1.0 to 0.8.

4.5.2 FP1583A

Test FP1583A was more difficult to model because the furnace had been driven too hard at the start of the test. The actual temperature was initially much higher than the ISO-834 curve, but was then decreased before dropping down to the ISO curve and gradually increasing again. The actual furnace temperatures were used to model this wall, rather than the ISO time temperature curve that was used in the models of previous tests.

4.5.2.1 Temperature Comparisons Through the Wall

The comparison between test and model results for this wall are shown in Figures 4.20 to 4.22. Figure 4.20 refers to positions 2 and 4 in Figure 4.1. The comparison is poor at position 2. Initially this may be because the furnace is small, with a large bounding area to volume ratio. The walls of the furnace will heat up very slowly compared with the gas temperature. As most of the radiation incident on the specimen is from the furnace walls, the incident radiation will be lower than the net value for the emissivity of the furnace would suggest, as both the temperature of the furnace walls is significantly lower than that of the gas. The dip occurs in the model and test temperature curves.

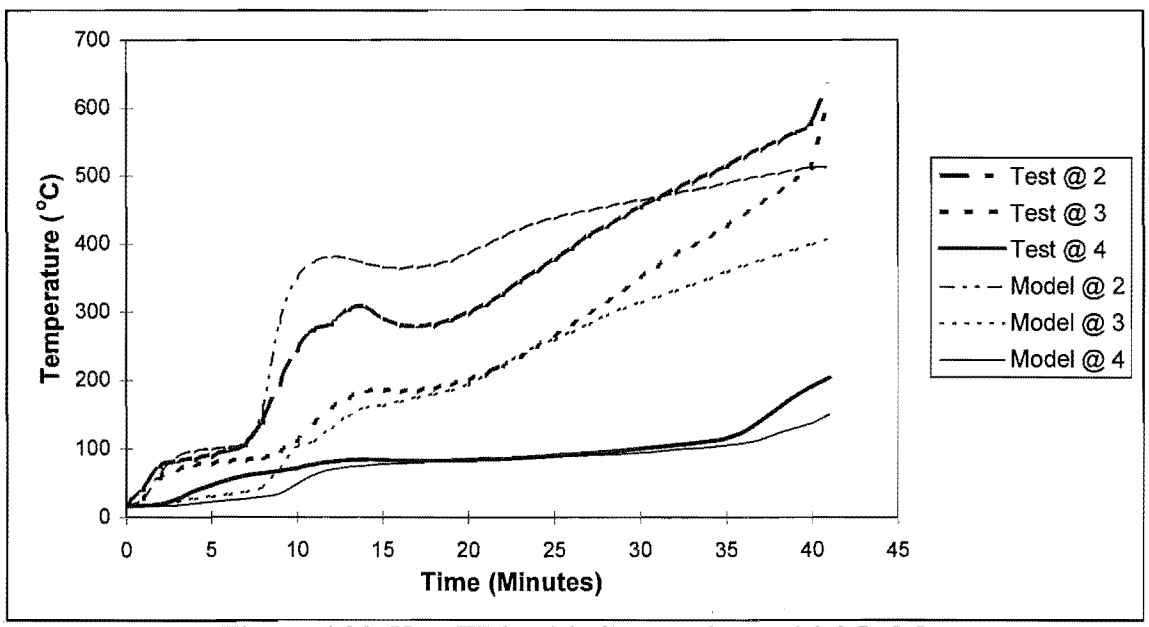

Figure 4.20 Test FP1583A Comparison with Model

The comparison at position 3 and 4 is good until the later stages of the test. The model underpredicts the temperatures at the end of the test throughout the wall. It is possible that in the test, cracks opened up in the lining allowing furnace gases to enter the cavity, increasing the temperatures throughout the assembly. These gases would also ignite the stud. This will obviously raise the temperature within the stud. This problem is a common occurrence towards the end of tests, but is more common in load-bearing tests.

4.5.2.2 Temperature Comparison in the Stud

Figure 4.21 shows the comparison at positions 5 to 9 (Figure 4.2).

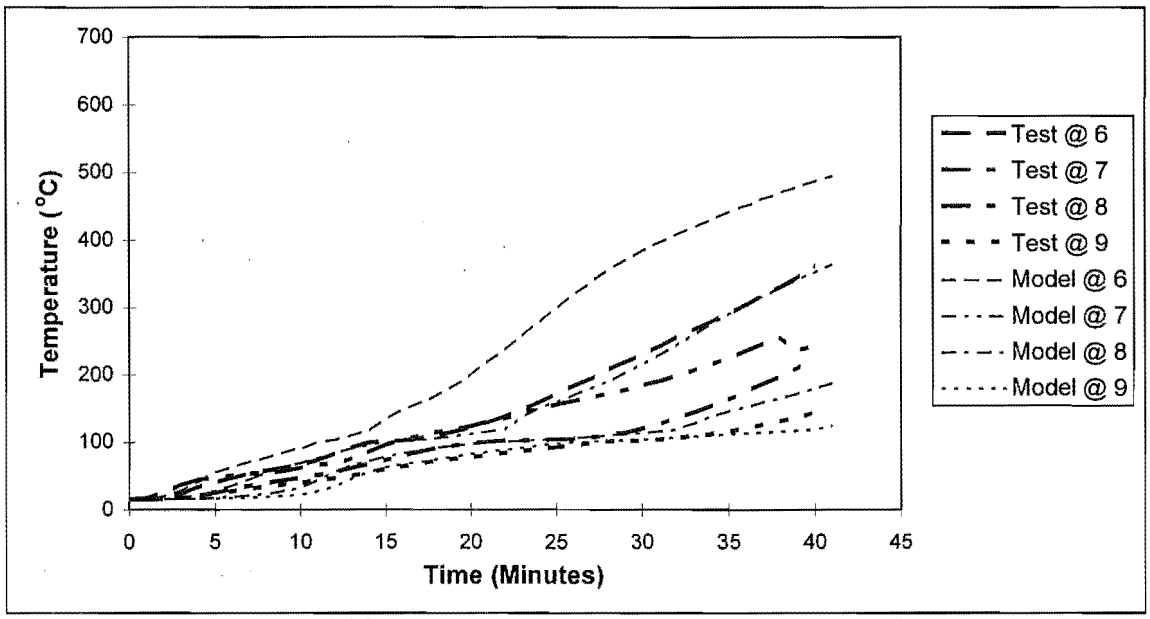

Figure 4.21 Test FP1583A Comparison with Model

The model severely overpredicts temperatures at positions 6 and 7. This is probably due to the fact that the stud is burning. However the model underpredicts to a lesser degree the temperatures at positions 8 and 9.

Figure 4.22 refers to temperatures on the centreline of the stud, positions 10 to 13 inclusive in Figure 4.2.

The model overpredicts temperatures at position 10. Agreement at position 11,12 and 13 is very good. This is consistent with positions 6 to 9. Overall the model predicts temperatures reasonably accurately within the stud, despite the problems with the predictions within the cavity on the unexposed face and close to the outside of the stud.

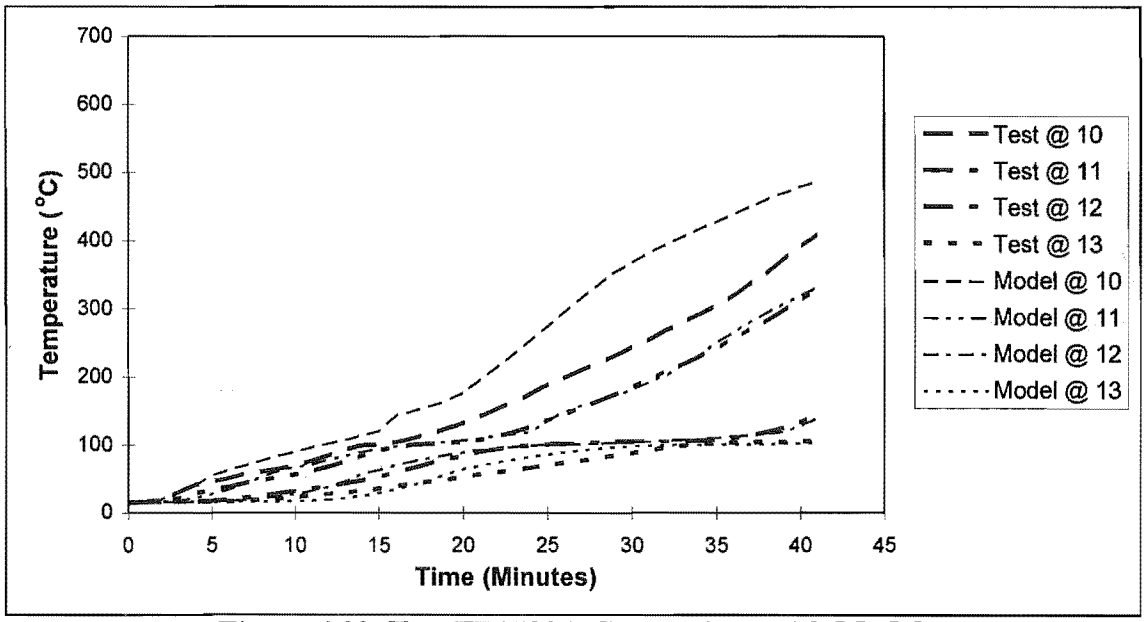

Figure 4.22 Test FP1583A Comparison with Model

4.5.3 Heat Transfer Coefficients for the Pilot Furnace

The assumption of emissivity being equal to 0.5 and the convective coefficient being 0.8 appears to be justified for the pilot furnace.

4.6 Non Standard Furnace Tests

In July of 1994, BRANZ undertook two tests in the pilot furnace using non standard time temperature curves. The time-temperature curves were provided by the author. Two curves were developed using COMPF-2, a compartment fire computer model described in Chapter 2. The first is a fuel bed controlled crib fire, with a high ventilation factor. The high ventilation results in a slow rate of temperature build up. The heat release rate decreases at a rate proportional to the square root of the mass remaining. At about 54 minutes the heat release rate is too low to maintain the temperature reached, and the temperature steadily decreases.

4.6.1 FP1972 Time-Temperature Curve

The time temperature curve is shown in Figure 4.23.

The dashed curve was that specified, and the solid line, that achieved in the test. It can be seen that some difficulty was experienced in following a non standard curve.

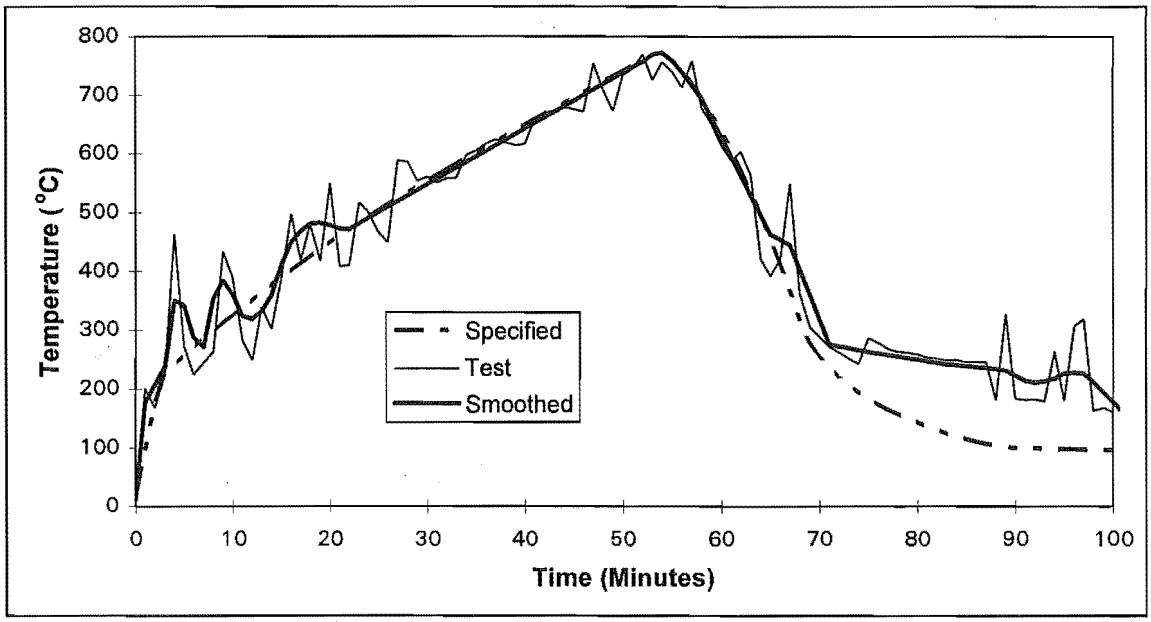

Figure 4.23 Time Temperature Curves for FP1972

4.6.2 FP1970 Time-Temperature Curve

On the other hand, FP1970 is intended to simulate a ventilation controlled hydrocarbon pool fire. The initial rate of temperature increase is very fast, and the maximum temperature is very high as shown in Figure 4.24:-

The fire is of very short duration. It was anticipated that the lining would remain in place on the furnace side and a structural failure would occur, so some information could be gained about the behaviour of the wall during the cooling phase. The lining fell off and an integrity failure occurred before a structural failure could occur.

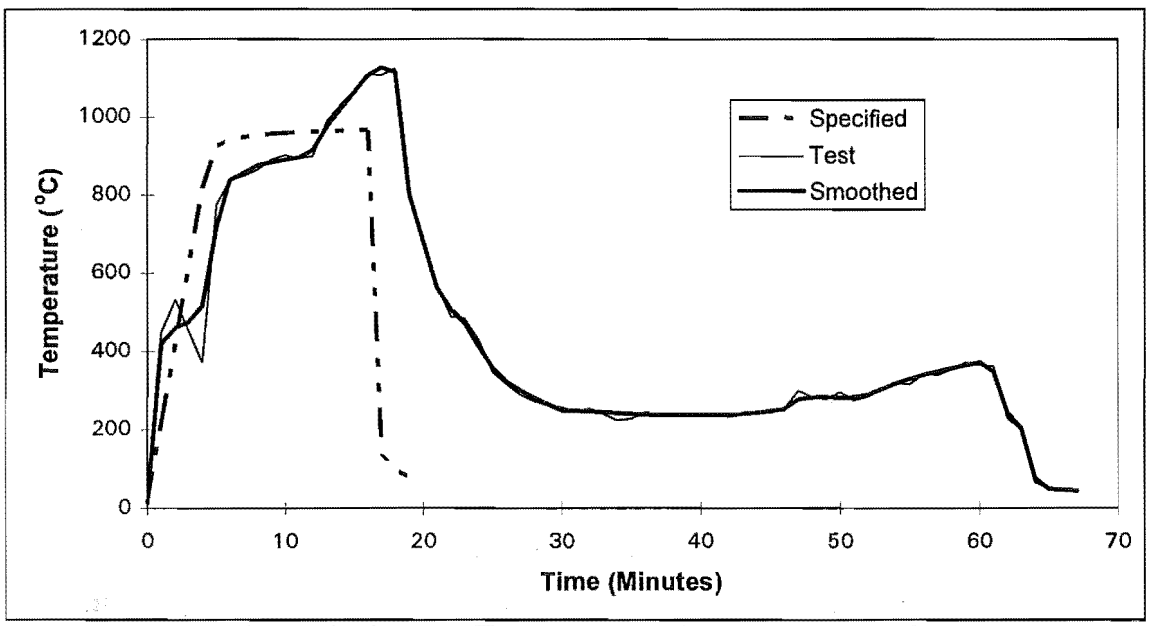

Figure 4.24 Time Temperature Curves for FP1970

4.6.3 Method of Comparison for Both Tests

The results were predicted before the tests were carried out. Agreement was adequate for the slower fire, but not for the hydrocarbon pool fire. This is because the test curve varied significantly from the specified curve. The models were re-run using the actual furnace time-temperature curve. These curves were smoothed, in order to reduce the number of time-temperature pairs, (TASEF allows a maximum of 50 pairs), and to avoid numerical instabilities in the model caused by abrupt temperature changes.

4.6.4 Pilot Furnace Test FP1972

The temperature profiles in test FP1972, with a time-temperature curve for a fuel surface controlled fire, are predicted well by the model. The comparisons shown below in Figures 4.25 to 4.27, are those produced using the smoothed furnace temperature history as input.

4.6.4.1 Temperature Comparison Through the Wall

Figure 4.25 shows the temperature comparison through the wall

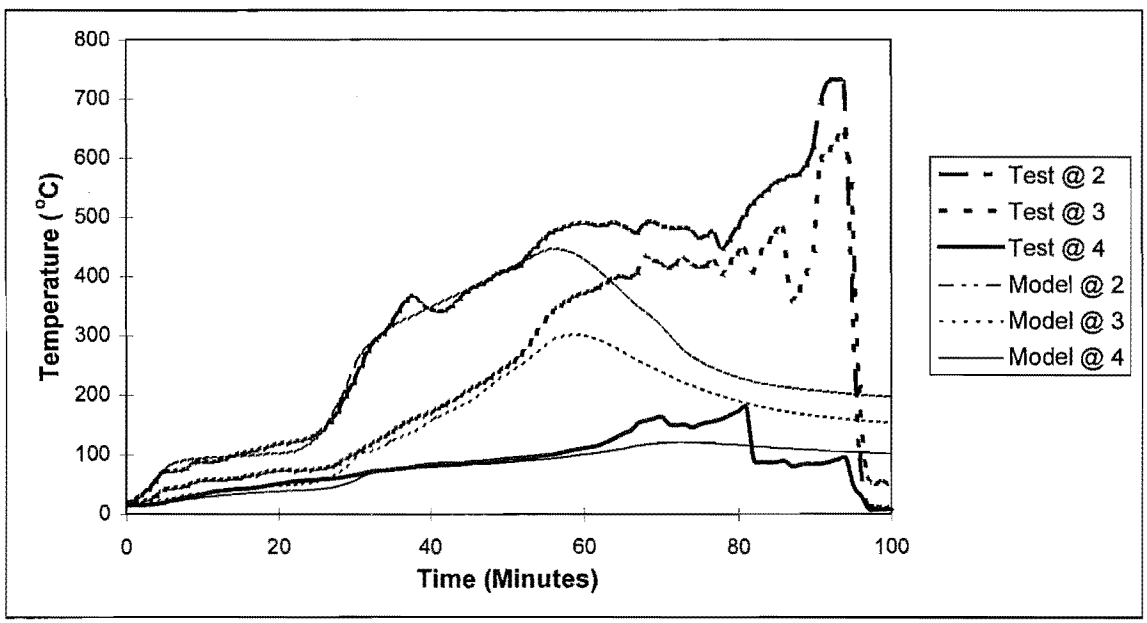

Figure 4.25 Test FP1972 Comparison with Model

The correlation is excellent up until 50 minutes at positions 2 and 3 and for 60 minutes at position 4. In the tests at about 50 minutes a gap opened up between the lining sheets. Furnace gases were then able to enter the cavity and the stud ignited, at which point the model becomes invalid. TASEF does not model internal heat generation

satisfactorily. The same problem is apparent for the temperature profile within the studs (Figures 4.26 and 4.27).

4.6.4.2 Temperature Comparison in the Stud

The temperature comparison at positions 6 to 8 within the stud is shown in Figure 4.26.

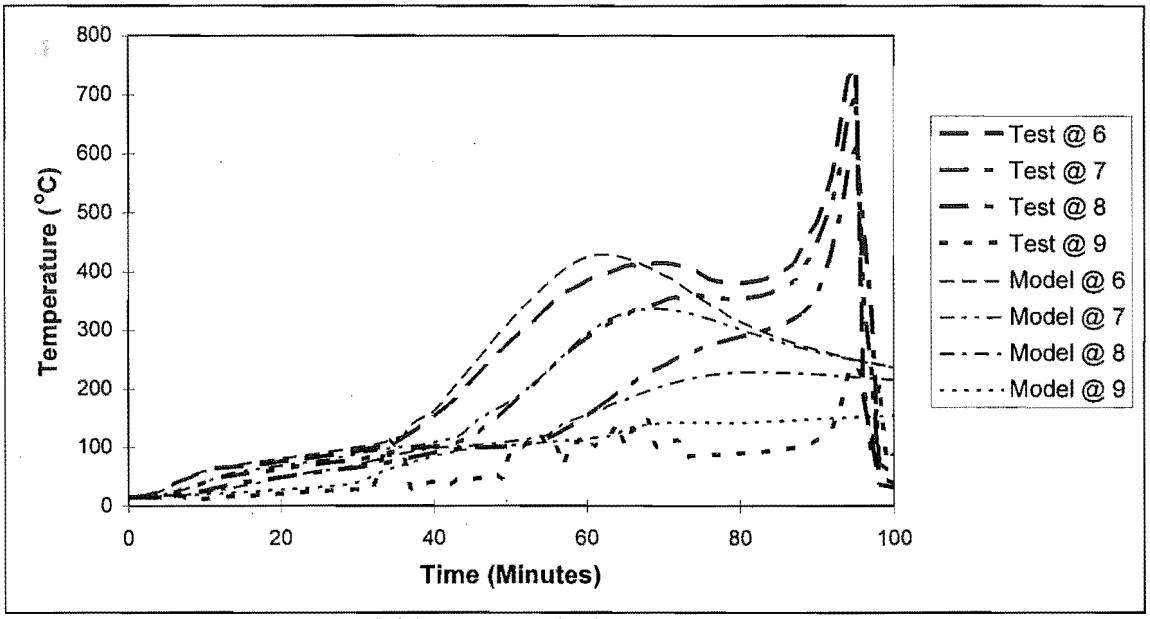

Figure 4.26 Test FP1972 Comparison with Model

At positions 6 to 9 the model predicts the temperature profile well for about 70 minutes. The thermocouple at position 9 appears to be "dropping out", and giving a reading below the actual temperature for some of the test.

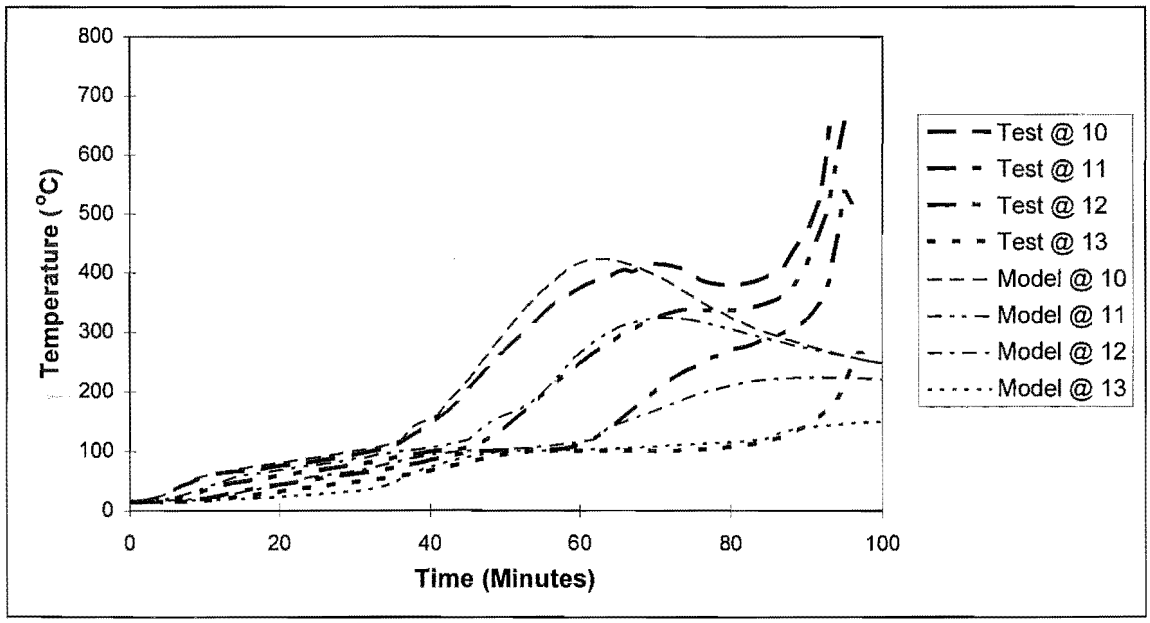

Figure 4.27 Test FP1972 Comparison with Model

At the centreline of the stud (Figure 4.27), the model is valid for about 70 minutes at positions 10 to 11 and for 90 minutes at position 13.

This is a very good result, because the temperature at position 13 has the largest effect on the overall thermal degradation of the stud as a whole.

4.6.5 Pilot Furnace Test FP1970

The model is not as good at predicting the response of a wall to the hydrocarbon pool fire time-temperature curve, test FR1970. This is not surprising as the time-temperature curve is of short duration with high rates of temperature change. It is far easier to model heat transfer in situations that are closer to steady state.

4.6.5.1 Temperature Comparison Through the Wall

The temperature profile through the wall predicted by the model is on the conservative side, as shown in Figure 4.28.

At positions 2 and 3 the model is conservative, by about three minutes. It is roughly equivalent at position 4 for the first 27 minutes. The peak in temperature reached at position 4 is not shown by the model.

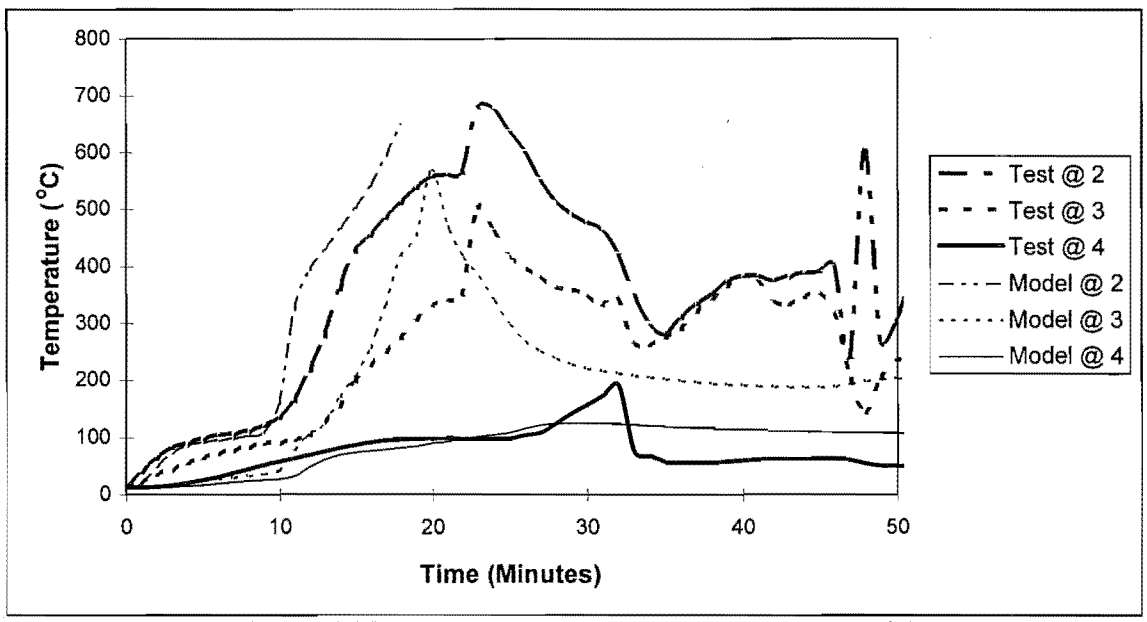

Figure 4.28 Test FP1970 Comparison with Model

During the test, the furnace temperature reached 1020°C, at about 19 minutes. This temperature was 160°C higher than was specified. At this time, the lining on the exposed side of the wall fell off. This was modelled by restarting the TASEF model after 19 minutes with the lining removed and a specified temperature profile, identical to that at 19 minutes in the first run. Since the lining is removed, position 2 is in a

"fictitious" region, and returns a nil temperature. Hence the temperature curve for position 2 stops at 19 minutes. Despite this modification of the model, it is inaccurate after about 25 minutes. This is due to ignition of the stud as in test FR1972.

4.6.5.2 Temperature Comparison in the Stud

The temperature profile at the centreline of the stud is shown in Figure 4.30.

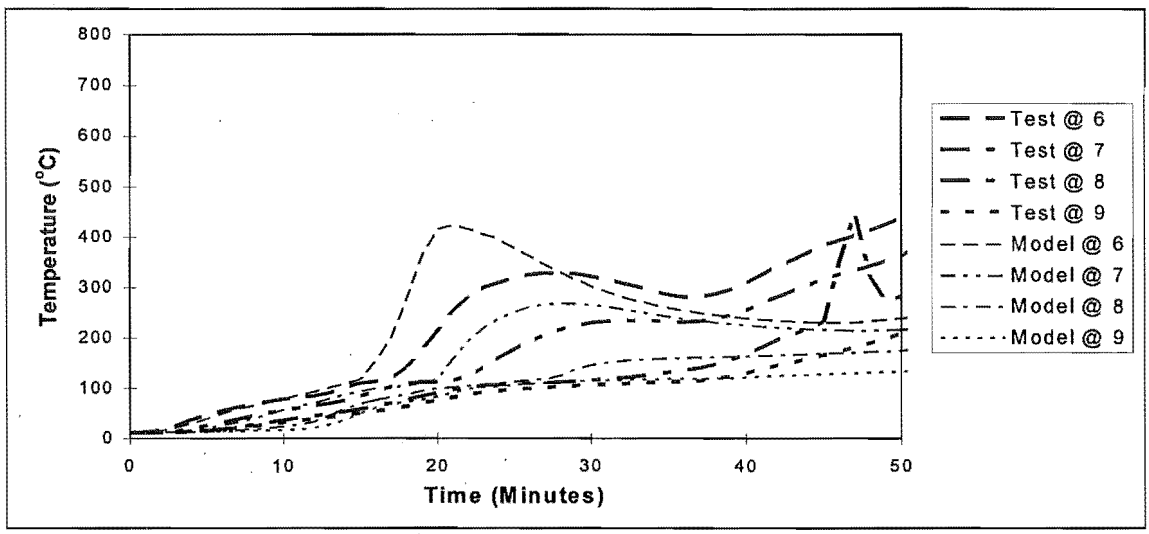

Figure 4.29 Test FP1970 Comparison with Model

The temperature is overpredicted at positions 6, 7 and at position 8 after 30 minutes and at position 9 is good for 40 minutes. The temperature profile at the centreline of the stud is shown in Figure 4.30.

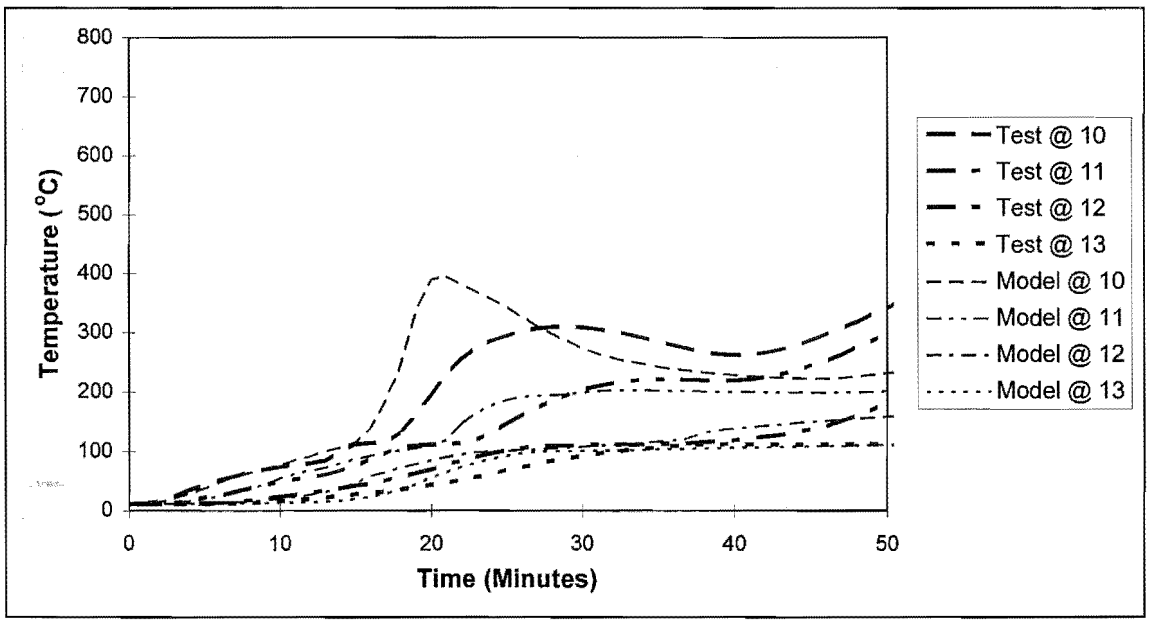

Figure 4.30 Test FP1970 Comparison with Model

The temperature is also overpredicted at position 10 and is good at position 9 for 30 minutes. It is good for 50 minutes at positions 12 and 13. This is consistent with the prediction for positions 6 to 9. Overall the model is conservative for test FR1970.

4.6.6 Heat Flux Measurements in Non-Standard Tests

Both test FP1970 and FP1972 were instrumented with a Gardon type heat flux metre. This meter measures the total incident heat flux, both radiation and convective heat flux. The values recorded are compared with values calculated from the temperature of the furnace and the heat transfer equation,(equation 3.2), and shown below in Figures 4.31 and 4.32. The heat transfer coefficients used are those given in Table 3.4 for the fire side of the wall., that is an emissivity of 0.8, a convection coefficient of 1.0 and a convection power of 1.33.

The measured values show large fluctuations as shown in Figure 4.31. This is due to the local variation of temperature and fluid flow within the furnace.

The differences between the measured and calculated values are attributable to the fact that the gas temperature is measured and not the furnace wall temperatures. As much of the radiation is from the walls of the furnace, calculating the radiation from the furnace gas temperature results in problems. These are more apparent in test FP1970, the short, sharp fire. Initially the furnace walls are at a much lower temperature than the gas, hence the measured heat flux is lower than that calculated on the basis of the furnace gas temperatures (Figure 4.32).

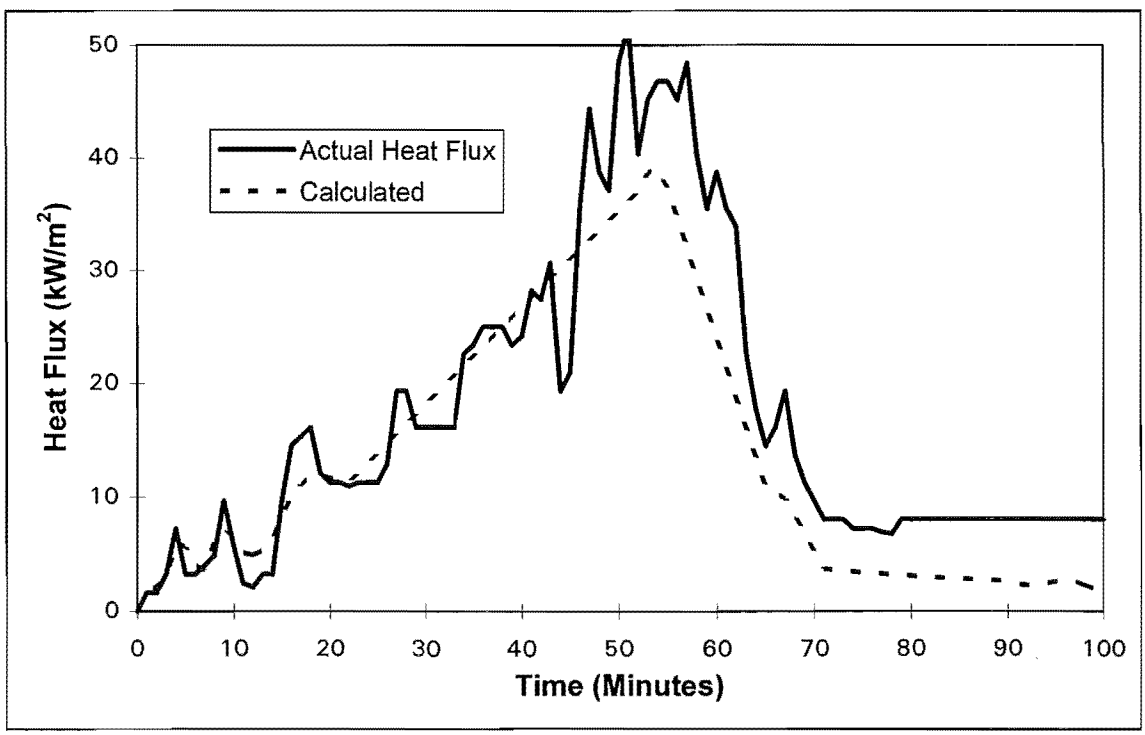

Figure 4.31 Heat Flux To Wall, Test FP1972

As the wall temperature catches up the radiation is underpredicted as shown in Figure 4.32. This problem is far less significant in a fire with a slow temperature build-up (Figure 4.31). The time-temperature curves are shown in Figures 4.23 and 4.24.

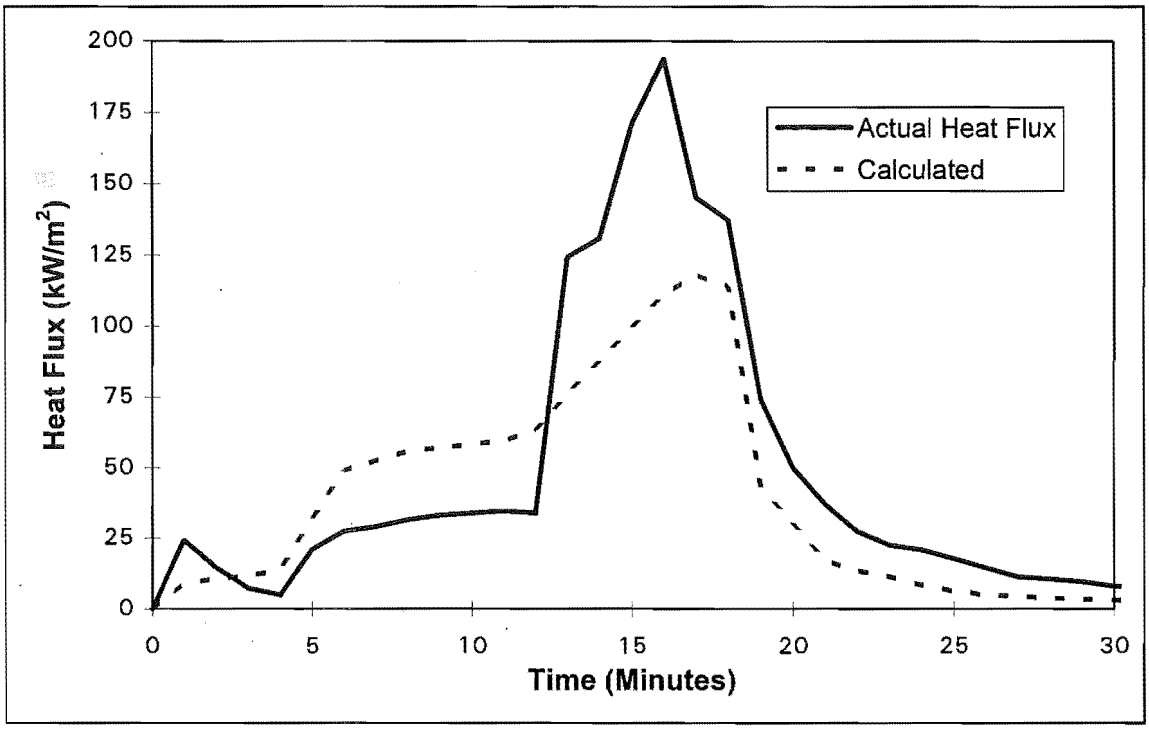

Figure 4.32 Heat Flux To Wall, Tests FP1970

A linear regression was carried out on the ratio of the measured heat flux and the heat flux calculated using the furnace gas temperatures and an emissivity of 1.0. This resulted in an effective gas emissivity of 0.60 for test FP1972 and 0.63 for test FP1970. Assuming the heat flux meter has an emissivity of about 1.0 and gypsum plasterboard an emissivity of 0.9, the effective emissivity can be calculated using Equation 3.13. This gives values of 0.56 and 0.59 respectively for FP1972 and FP1970. It is higher for test FP1970, because the temperature of the thermocouples will lag behind that of the gas temperature to a greater extent in a short high temperature fire. These values compare well with the value used of 0.5.

4.7 Results

Two important parameters are the time to insulation failure and the time to onset of charring in the stud. These are defined, respectively, as the time that the temperature in position 1 in Figure 4.1 increases by 140°C and the time at which 290°C is reached at

position 5 in Figure 4.1. Comparisons of these for test results and model predictions are shown in Table 4.2.

The time to failure due to the insulation criteria is underpredicted in three cases and overpredicted in two. The worst overprediction is 4%.

Test Number	Insulation		Charring	
	Test	Model	Test	Model
FR1582B	42.1	39.6	17.1	15.5
FR1582A	39.2	40.1	22.6	15.5
FR1611	68.1	62.7	27.2	22.9
FR1777	NR*	NR*	37.7	34.6
FR1515	NR*	NR*	NI*	NR*
FP1583B	43.8	41.9	17.8	16.9
FP1583A	37.8	41.7	11.7	12.0
FP1970	76.4	NR*	NI*	38.3
FP1972	29.7	NR*	NI*	12.7
*NR not reached			*NI not instrumented	

Table 4.2 Model Predictions and Test Results for Insulation and Charring Criteria

The time to failure due to the charring criteria is underpredicted in all cases. The worst value is 30% out, but in terms of time it is only 7.1 minutes.

4.8 Conclusions

Overall, the model appears to predict the temperature profiles in tests well, although it is conservative for fast, hot fires. It is desirable to make the theoretical results conservative.

The values of various properties have been manipulated to some extent in the calibration of the model. The resulting values may not be absolutely correct, but are valid for the model, since the model has some limitations, such as the inability to model mass transfer, the movement of moisture and pyrolysis products through the wall materials and across the void.

Chapter 5 Thermal Time Equivalence for Walls

This Chapter describes how the compartment fire model COMPF-2 (Babrauskas 1979), described in Chapter 2 was used to develop time-temperature curves for a range of ventilation factors and fuel loads. The wall model developed in Chapter 3 was then subjected to the time-temperature curves developed using COMPF-2. The maximum temperature values for the insulation and charring criteria were recorded and an equivalent time deduced from the furnace tests results. The results were then compared with those found using the CIB formula described in the introduction, Chapter 1.

The procedure for combining the compartment fire model and the finite element wall model is discussed. Input parameters are described and sensitivity studies are carried out on parameters that are not easily determined and may have a significant effect on the results. The effect of varying these parameters is shown by comparing time equivalence values, in order to compare the severity of the fire in terms of its impact on structural members rather than less significant results such as temperatures in the compartment. Finally, the overall results are discussed and conclusions drawn.

5.1 Failure Criteria

Initially the failure of the specimen was determined by using the following two temperature based criteria:-

(i) The time to failure of the wall due to the insulation criterion, that is, the time at which the temperature at the unexposed side of the wall (position 4 in Figure 5.1) undergoes an increase of 140°C.

(ii) The time to "structural failure" defined as the time to onset of char in the timber framing (position 5 in Figure 5.1), assumed to occur at a temperature of 290°C.

The first of these is unlikely to be the cause of failure in a load-bearing wall and the second is somewhat conservative. However it will be followed up by a more rigorous study of structural capacity.

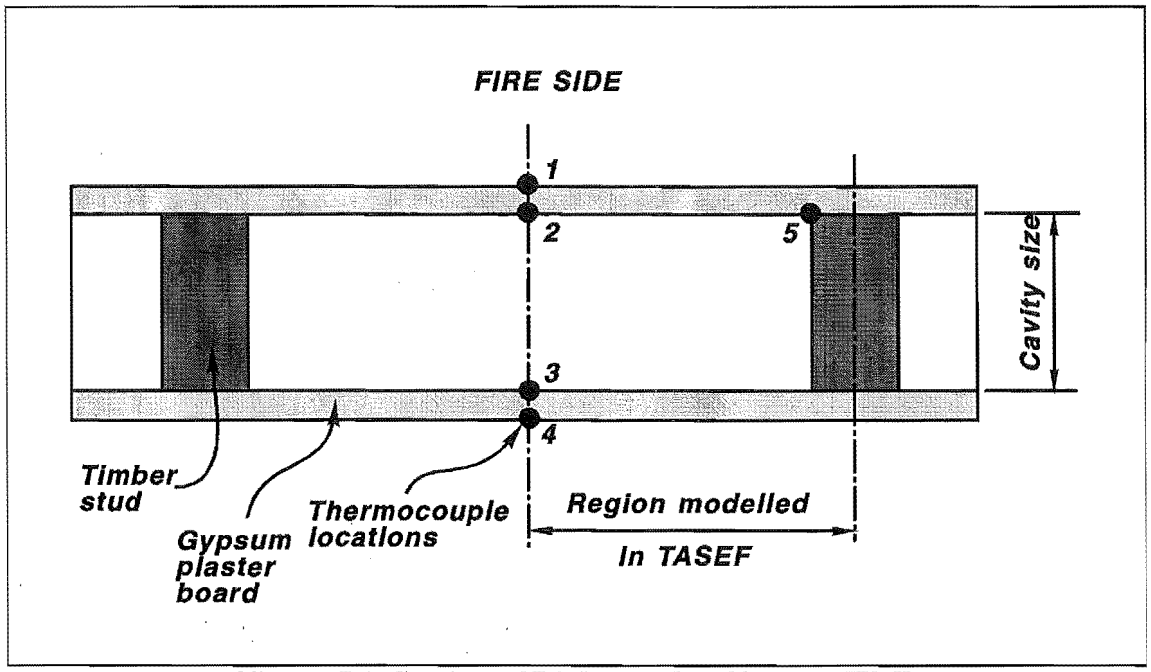

Figure 5.1 Section of Light Timber Framed Wall

5.2 Computer Calculation of Time Equivalents

The calculated time equivalence is found by subjecting the finite element wall model described in Chapter 3 to a compartment fire time-temperature curve derived using COMPF-2 (or in some cases the Swedish time-temperature curves). COMPF-2 is described in Chapter 2 and the parameters used in this study are described in Section 5.3.1.

For each pair of ventilation factor and fuel load, the maximum temperature is found at the two locations in the wall assembly defining the charring and insulation criteria, described in Section 5.1.

The time at which these temperatures are reached in the same two locations, during an ISO-834 test is then found. These two times are defined as the calculated time equivalent. In some cases the maximum temperature reached in the wall model when exposed to a compartment fire is higher than the maximum temperature reached during the test. In that case the data point is omitted from subsequent analysis.

When comparisons are made between data sets generated by changing one variable then data points that occur for an opening, fuel load pair in only one series are deemed to be invalid. This is to avoid errors being introduced by fuel load and opening factor size effects in the comparison.

The comparison between the calculated time equivalent and the time equivalent found using the CIB formula (Thomas 1986), is reported graphically for both criteria. Generally when sensitivity studies are carried out only one wall size, the wall with 12.5 mm gypsum plasterboard linings and a 69 mm thick cavity are reported. The exception is the comparison with the Swedish time-temperature curves for reasons that will be described in Section 5.6.3.

5.3 Assumptions and Values Chosen for Variables

The program, COMPF-2 was used to derive the compartment fire temperatures. Heat transfer through the walls was modelled using TASEF (Sterner and Wickstrom 1990).

5.3.1 COMPF-2

COMPF-2 is described in Section 2.5. The exact variables used to give the time-temperature curves for the determination of the time equivalence of light timber framed walls are specified below:-

(i) A range of opening factors were used. The opening factor is defined in Section 2.3.1.2. This opening factor, V, is given by:-

$$V = A_w H_v^{1/2} / A_t \tag{5.1}$$

where:- A_W is the window area (m^2)

H_v is the height of the window (m)

A_t is the total bounding surface area of the compartment, including the window area (m^2)

The range of values is given in Table 5.1. The ventilation factor is that used in the CIB formula. The CIB formula is from Thomas (1986), and the BIA formula is from the

New Zealand Building code (NZBIA 1992). Details of both these formulae are described in Section 1.2.1. For some window sizes, the window is too big to fit into one wall. In this case there would be two windows or a combination of doors and windows.

WINDOW			Opening Factor	Ventilation Factor	Ventilation Factor
Height	Width	Area	(Eqn 7)	CIB (Eqn 1.2)	BIA (Eqn 1.3)
(m)	(m)	(m^2)	($m^{1/2}$)	($m^{-1/4}$)	(Dimensionless)
1.0	2.75	2.75	0.025	1.437	1.547
1.5	3.00	4.50	0.050	1.015	1.023
2.0	3.00	6.00	0.077	0.818	0.836
2.0	4.00	8.00	0.103	0.709	N/A
2.0	5.00	10.00	0.129	0.634	N/A
2.0	6.00	12.00	0.154	0.579	N/A

Table 5.1 Ventilation Parameters

(ii) A range of fuel loads, in terms of energy per square metre will be used, hence the calorific value chosen for the wood or wood equivalent becomes irrelevant. The values used are; 100, 200, 300, 400, 500, 600, 800 and 1200 MJ/m^2 of floor area.

(iii) The compartment size chosen is typical for buildings likely to be constructed from light timber framing and is shown in Figure 5.2.

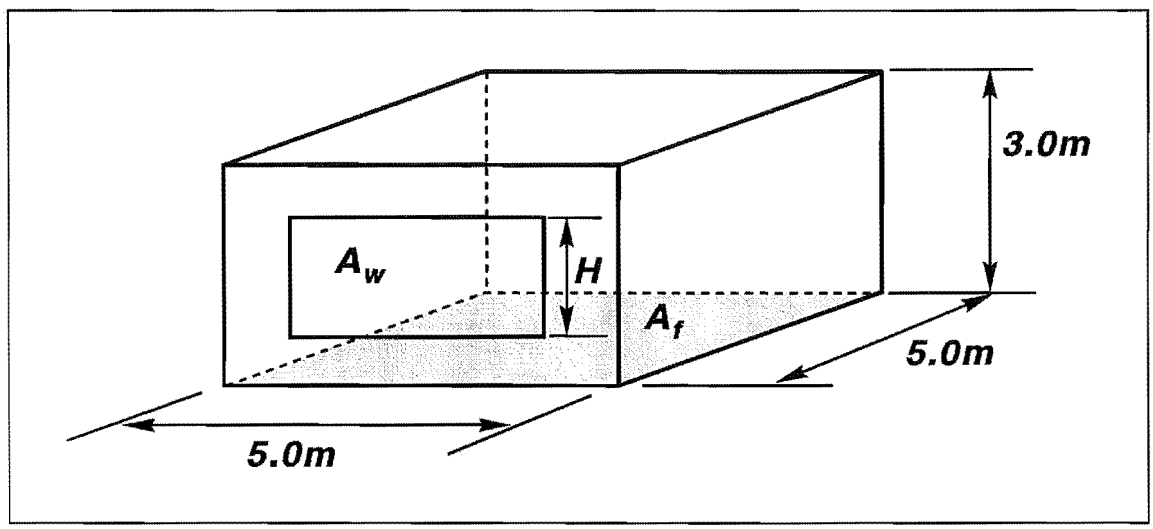

Figure 5.2 Layout of Compartment

The total floor area is 25 m^2 and the total bounding surface area is 110 m^2.

The size of the compartment is assumed not to affect the time equivalent.

(iv) Percentage pyrolysates burned will be 70%.

(v) The fire will be ventilation controlled throughout. This is achieved by using the pessimising option over the pyrolysis rate.

(vi) The initial rate of temperature increase within the compartment is 100°C per minute. This is to allow for the fact that COMPF-2 starts with a heat balance and an initial compartment temperature that is significantly higher than ambient.

(vii) COMPF-2 output time-temperature curves stop when the compartment temperature drops below 80°C. The curve is then modified as follows: it drops to 20°C in 30 minutes and remains at 20°C for 90 minutes in order to ensure that the maximum temperature is reached on the ambient side.

5.3.2 TASEF

The calculated time equivalence for a wall assembly is based on the maximum temperature found in critical locations in the wall assembly, obtained using TASEF. The time-temperature curves defined above in Section 5.2.1 were used as input time-temperature curves in the TASEF analysis.

Four different wall assemblies are used, with different combinations of stud size and lining thicknesses. The wall assemblies are for the four used for correlation of the wall model in Chapter 4 and are described in Table 5.2.

Furnace Test Number	Lining Thickness (mm)	Cavity Width (mm)
FR1582A	9.5	69
FR1582B	9.5	90
FR1611	12.5	69
FR1777	16	90

Table 5.2 Parameters of Walls Used

The combinations of four wall layouts, six ventilation factors and eight fuel loads give a total of 192 simulations. There are less than 192 data points in the results because some temperature values are higher than those reached in the furnace tests as described in Section 5.2.

5.3.3 Time-Temperature Curves

Figure 5.3 shows three families of curves produced for the three opening factors, 0.05, 0.103 and 0.154, three fire loads, 400, 800 and 1200 MJ/m^2 and for the wall with a 9.5 mm lining and 90 mm cavity. The legend shows the opening factor and fuel load

respectively. The ISO-834 standard fire test curve is also shown in Figure 5.3, giving temperatures considerably lower than the COMPF-2 output.

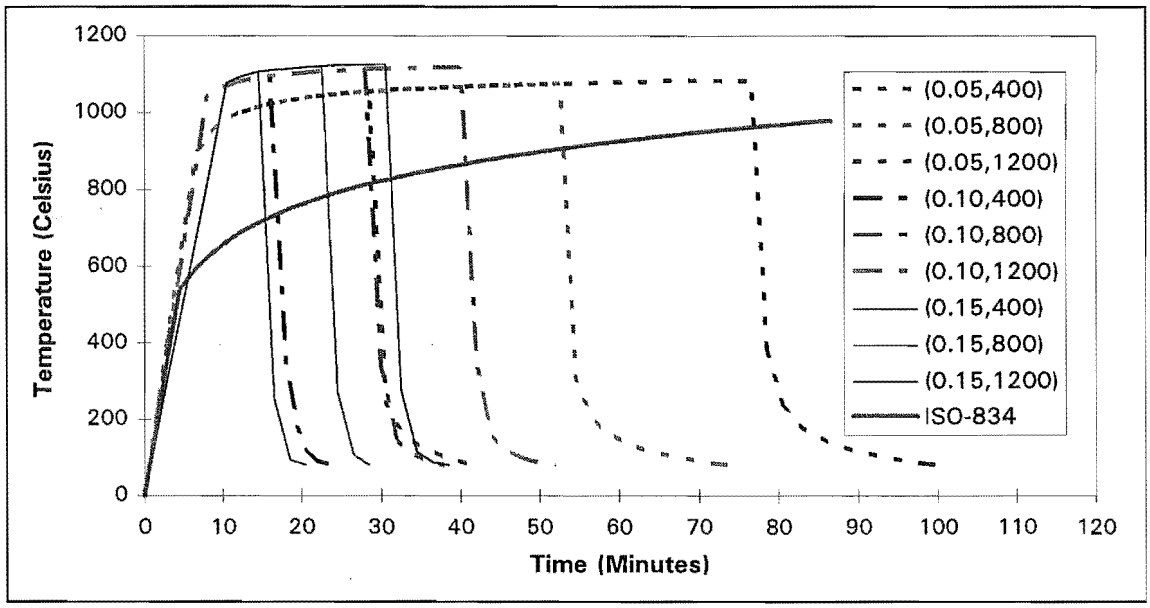

Figure 5.3 Families of Time-Temperature Curves

5.3.4 Heat Transfer Coefficients

The heat transfer coefficients were altered from those used for the furnace model at the fire side of the wall, for both radiative and convective heat transfer. This is to allow for the differences in the thermal environment between a furnace and a compartment fire. The values used must be the same in COMPF-2 and TASEF. The program COMPF-2 was modified to allow for this.

5.3.4.1 Radiation

Three sets of runs were carried out on the 12.5 mm wall using emissivity values of 0.8, 0.9 and 1.0 on the fire side of the wall. Figures 5.4 and 5.5 show the effect that varying the wall emissivity has on the equivalent time of exposure for the charring and insulation criteria respectively.

The symbols are data points for each series and the straight lines are linear regressions of the results. The regression values are calculated only using valid points as described in Section 5.2.

The value for emissivity has no significant effect on either the temperatures or the time equivalent. Changing the value for emissivity has two compensating effects, if the value is increased then:-

(i) More heat is lost to the walls, so the compartment temperature is lower.

(ii) The proportion of heat from the heat balance entering the walls is higher.

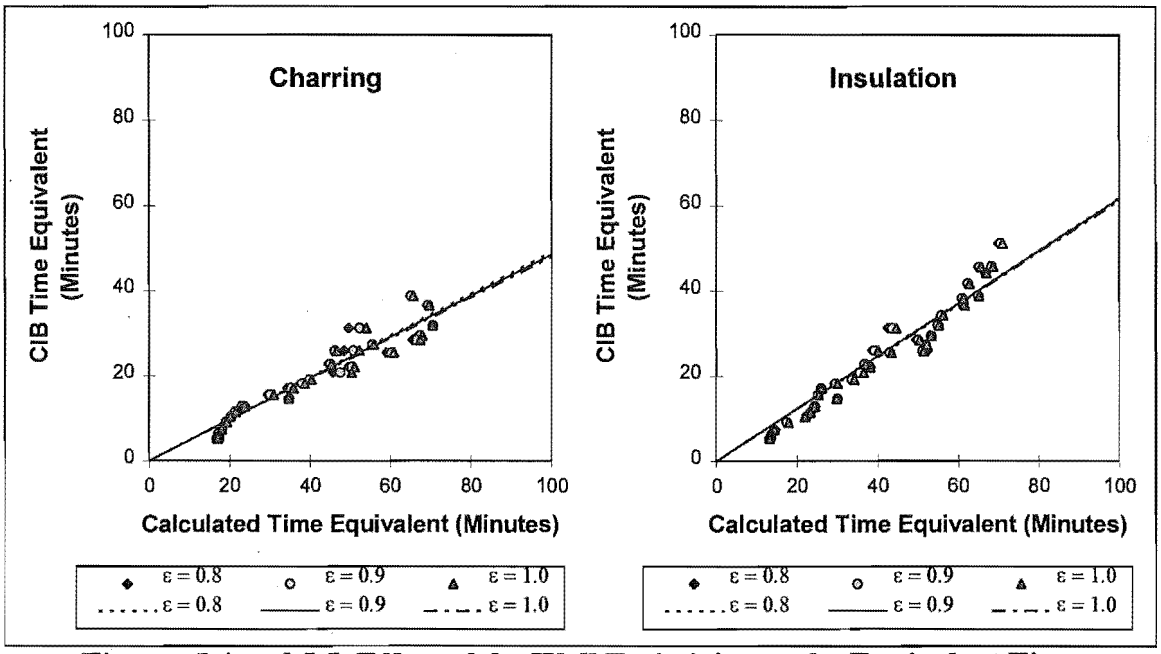

Figures 5.4 and 5.5 Effect of the Wall Emissivity on the Equivalent Time

The overall result of these two effects is for no significant change to occur for small differences in the value of emissivity used.

Drysdale (1985) states that for thick luminous flames from hydrocarbon fuels it is common to assume black body behaviour, that is, an emissivity of 1.0, hence for the compartment gases it is assumed to be 1.0. Combining this value with a wall emissivity of 0.9 gives an effective value of 0.9. This is higher than the value of 0.8 used to correlate the wall model undergoing furnace exposure (Chapter 4) because of the differing emission characteristics of the furnace and a compartment fire.

5.3.4.2 Convection

Three sets of runs were carried out on the 12.5 mm wall using values for the heat transfer coefficient β (see Equation 3.2) of 2.0, 5.0 and 10.0 on the fire side of the wall. All other parameters remained the same.

Figures 5.6 and 5.7 show the effect of varying the convection coefficient has on the equivalent time of exposure for the charring and insulation criteria respectively.

The symbols are data points for each series and the straight lines are linear regressions of the results. The regression values are calculated only using valid points as described in Section 5.2.

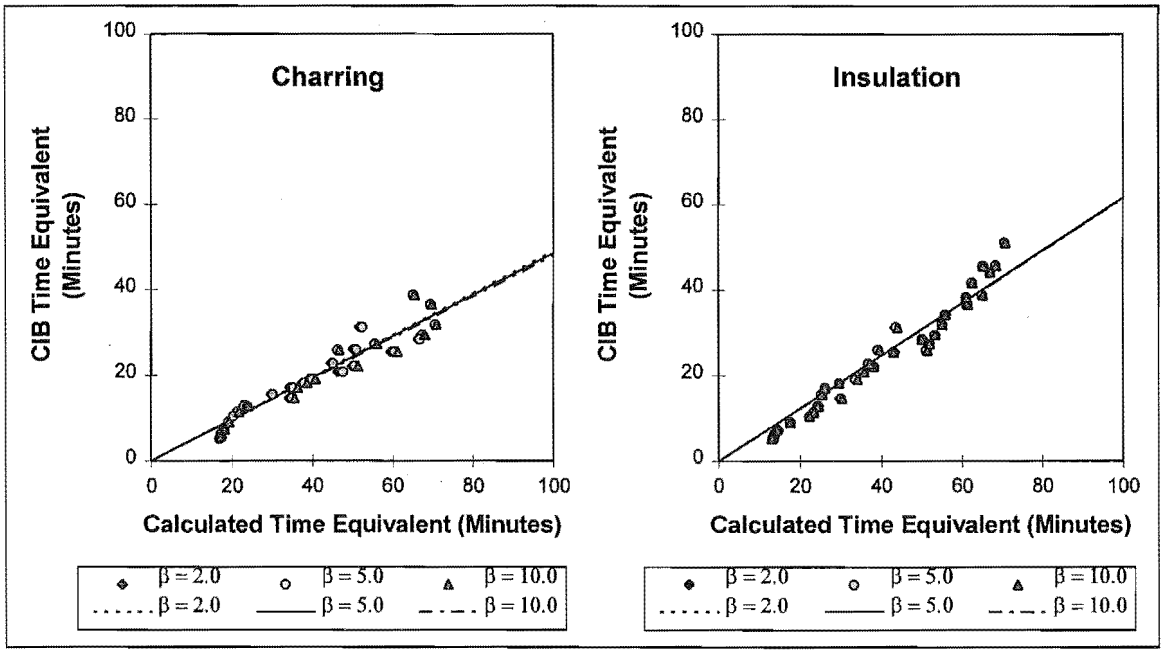

Figures 5.6 and 5.7 Effect of the Convection Coefficient on the Equivalent Time

The value for the convection coefficient has no significant effect on either the temperatures or the time equivalent because the temperature difference between the gas and the exposed wall surface is small. Most of the heat flux is due to radiation as it is in a furnace. (see Section 3.4). Changing the value of the convective coefficient has two compensatory effects, similar to those described in Section 5.3.1.1 above, for changing the value used for emissivity.

The convection coefficient, β, used is also higher (5.0 compared with 1.0), than that used to calibrate the wall model for furnace exposure (Chapter 4) as the air flow in a burning compartment is not as well defined as in a furnace and is more turbulent.

5.4 Matching Variables in the Sub-Models

The time-temperature curves found above for the four different wall assemblies were input into the finite element, TASEF based, model of the wall assemblies. Some parameters must be identical for both models and some parameters must be adjusted in COMPF-2 to allow for differences in the way that the walls are modelled.

The heat transfer through the walls must be equivalent in the two models. This is achieved by using the same heat transfer coefficients and emissivity values for calculating the heat transfer at the boundaries. The same can not be done for the heat transfer through the wall, excluding the boundaries, because TASEF is a two

dimensional finite element model of the wall and COMPF-2 uses a one dimensional homogeneous model of the wall in order to calculate the heat flow into the walls in the compartment heat balance. Hence effective conductivity and enthalpy must be used in COMPF-2 in order to simplistically model a more complex mode of heat transfer in the wall.

The properties of the timber framed cavity wall had to be modified to mimic those of an equivalent solid wall. The two properties that need to be altered are enthalpy and conductivity.

5.4.1 Enthalpy

Enthalpy is the integral over temperature of the product of specific heat and density and is input as such to COMPF-2. The density term was altered in a relatively simple way, considering the walls modelled are symmetrical. By altering the density term to be a weighted average of density over the thickness of the wall, the enthalpy as a function of temperature for the entire wall remains the same as for the lining with a finite enthalpy and assuming zero enthalpy for the air in the cavity.

5.4.2 Conductivity

The conductivity also had to be altered, but this is more complex due to the highly non-linear variation in heat transfer, by radiation and convection with respect to temperature.

5.4.2.1 Methods of Calculating Effective Conductivity

Several ways of calculating the effective value for the overall conductivity were considered. They are:-

(i) Multiplying the conductivity by the ratio of the total wall thickness over the lining thickness (of both sides) and assuming the conductivity does not increase over 300°C.

(ii) Multiplying the conductivity by the ratio of the cavity width over the lining thickness (of both sides) and assuming the conductivity does not increase over 300°C.

(iii) Multiplying the conductivity by the ratio of the total wall thickness over the lining thickness (of both sides) for all conductivity values.

(iv) Multiplying the conductivity by the ratio of the cavity width over the lining thickness (of both sides) for all conductivity values.

The differences between these methods is shown in Figure 5.8 for a wall with 9.5mm linings on each side and a 69mm wide cavity. The basic conductivity is that defined in Chapter 4 for gypsum plasterboard and the roman numerals refer to (i) to (iv) above.

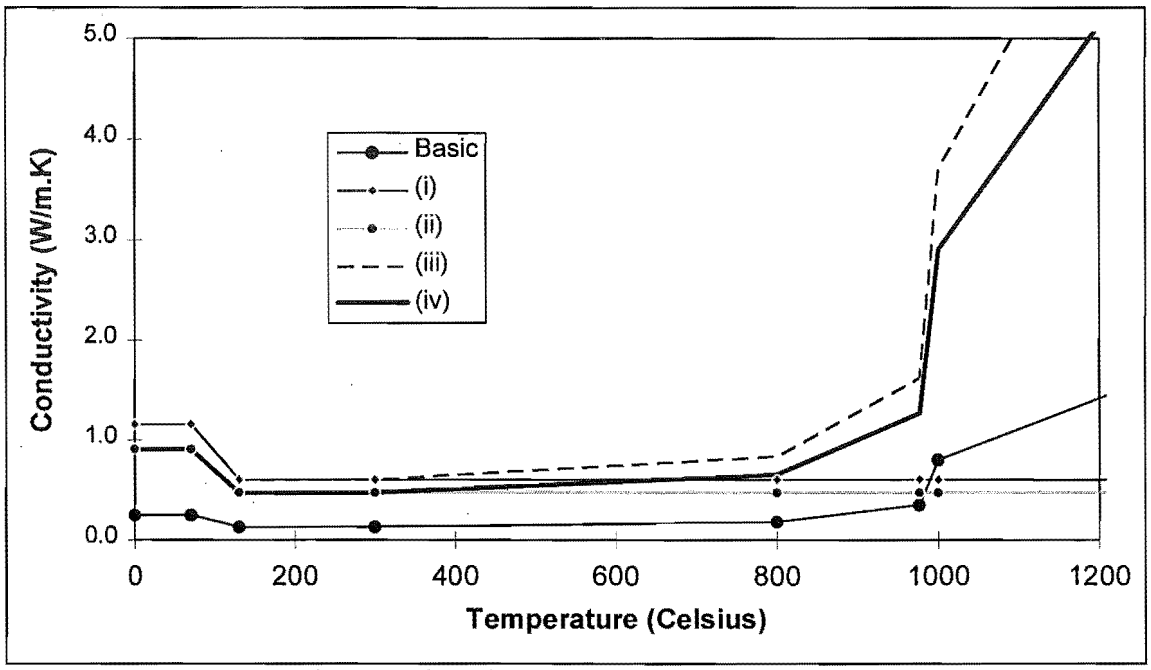

Figure 5.8 Effective Conductivity of Entire Wall Section

5.4.2.2 Comparison of Methods

Comparisons were made of the temperatures on the fire side and ambient side of the wall calculated using both COMPF-2 and TASEF. Method (i) resulted in a reasonable comparison whereas method (ii) resulted in the temperature on the ambient side calculated using TASEF being much higher than that calculated using COMPF-2. The comparison using method (iii) resulted in the temperature on the ambient side calculated using TASEF being much lower than that calculated using COMPF-2, while method (iv) resulted in a slightly better comparison than method (ii).

Method (iv) is preferable over method (ii), because the effective conductivity will increase at a rate that is higher than a linear relation to the temperature would predict; since the level of radiation flux across the cavity is dependent on the fourth power of temperature. In method (ii), however the effective conductivity remains constant over 300°C, despite the increase in conductivity of gypsum plasterboard over 300°C.

Method (iii) is an upper limit on the effective conductivity as it implies there is no resistance to heat flow across the cavity. The values calculated using method (iv) are

slightly lower than those calculated using method (iii), but apart from that fact, there is no theoretical justification for using this method of calculating the effective conductivity. The sensitivity of the results to these various methods was 10% on the slope of the charring time equivalent (CIB versus calculated) and 11% for insulation. The method chosen, (ii), is in the middle of this range.

5.4.3 Effect on Wall Boundary Temperatures

The temperatures found using COMPF-2 and TASEF on both the exposed and unexposed side of the walls were compared for three combinations of the opening factor and fuel load, for the four wall layouts mentioned previously. The three combinations are shown in the first three rows of Table 5.3 and are for a long cool fire, an average fire and a short hot fire.

Figure Number	Lining Thickness (mm)	Cavity Width (mm)	Opening Factor ($m^{1/2}$)	Fuel Load (kJ/m^2)
5.14	9.5	90	0.025	400
5.15	9.5	90	0.103	800
5.16	9.5	90	0.154	600
5.17	12.5	69	0.103	800

Table 5.3 Parameters for Walls and Fires Used in Figures 5.9 to 5.12

Figures 5.9 to 5.12 are for four selected combinations of walls and fires. Their parameters are shown in Table 5.2.

This was a representative range of the 192 runs that were carried out. In general, the other two sizes of walls, 9.5 mm linings with a 69 mm thick cavity and the 16 mm linings with a 90 mm cavity had a better comparison. The comparison was better for longer fires. This is expected, because time-dependent models tend to become more accurate as the problem tends more towards steady state.

Overall the comparison was good, apart from the initial growth phase and tends slightly towards the conservative side as the temperatures on the ambient side are more often than not higher using the TASEF model. This means that COMPF-2 slightly underpredicts the heat lost through the wall, resulting in a higher value for the compartment temperature as less heat is lost through the walls.

The COMPF-2 runs stop when the compartment temperature decreases below 80°C, hence the two COMPF-2 temperature plots cease before the two TASEF plots in the Figures 5.9-5.12.

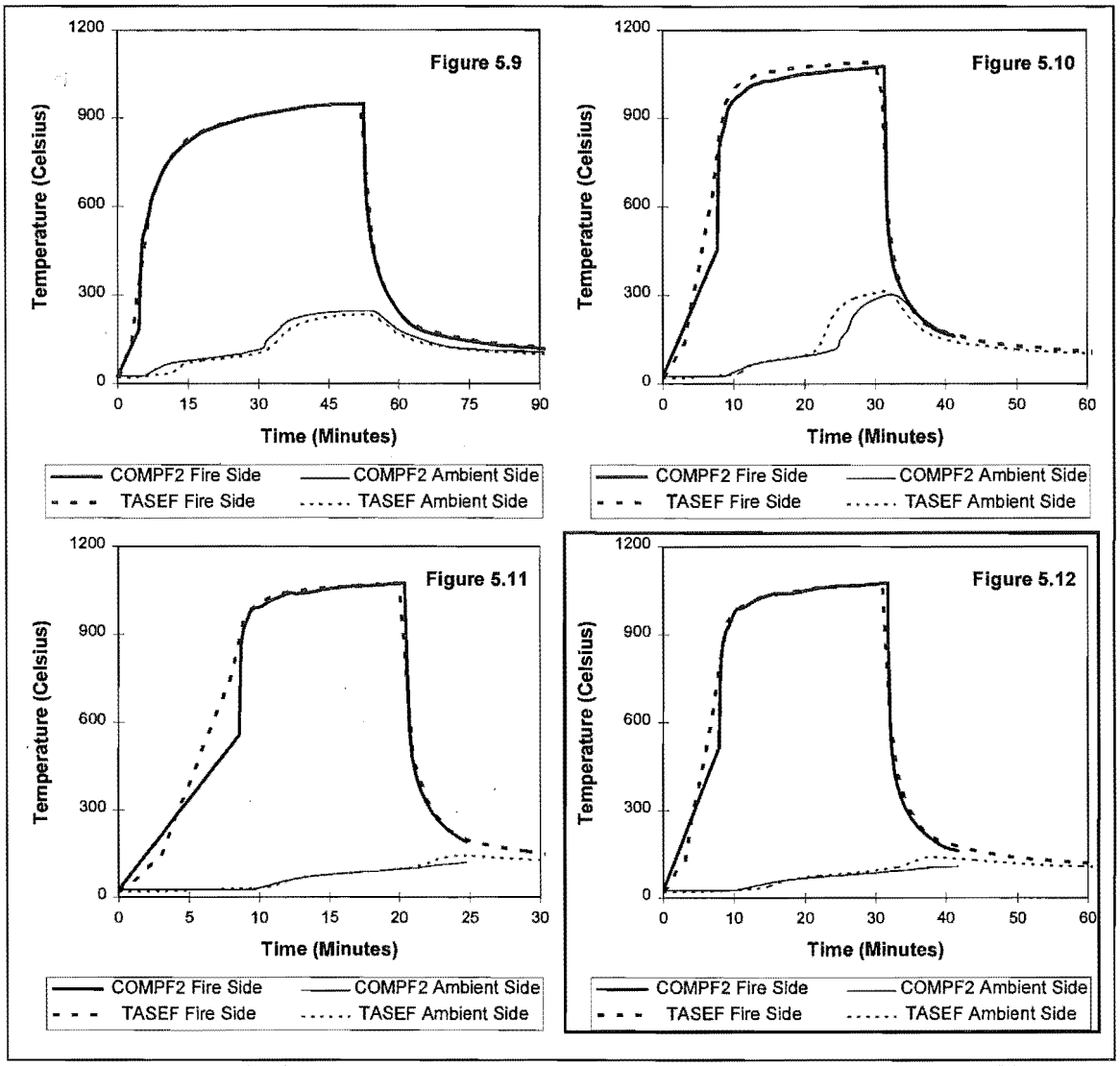

Figures 5.9 to 5.12 Comparison of Wall Boundary Temperatures Using COMPF-2 and TASEF

5.5 Overall Results

The maximum temperature values for the insulation and charring criteria were recorded and an equivalent time deduced from the furnace tests results. Values for time equivalents were calculated using Equation 1.1, with $C = 0.09$, the recommended value for lightweight linings (see Section 1.2.2). Not all points were valid as some time equivalents were outside the duration of the fire tests as described in Section 5.2.

5.5.1 Charring Criterion

The relationship between the CIB time equivalent derived using Equation 1.3 and the calculated time equivalent, for charring, is shown in Figure 5.13.

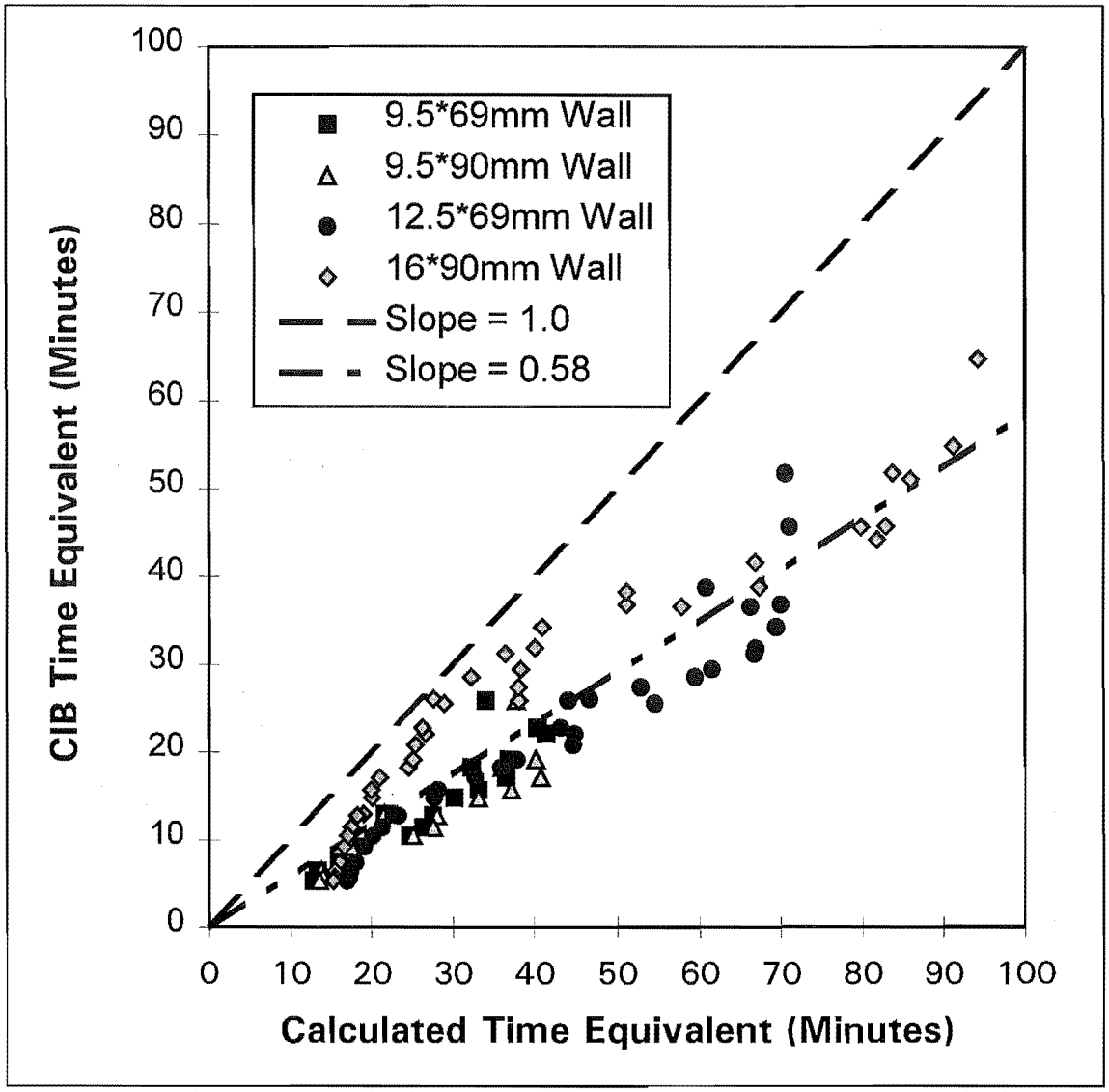

Figure 5.13 CIB Time Equivalent vs. Computer Prediction of Time Equivalent for Charring Criterion

The symbols are data points for the four different wall layouts used (Table 5.2). The walls with the thicker linings performed better, since their calculated time equivalent was shorter relative to the CIB time equivalent, than for the thinner walls. The lower line represents a linear regression of the results. The upper solid line represents a one to one relationship. Overall the calculated time equivalent is 58% of that calculated using the CIB formula, which therefore underpredicts the time equivalent by 71% of the calculated value. The correlation coefficient for the regression is 0.88.

If, however the BIA formula is used (Equation 1.3), with a value of $C = 0.08$, then the slope of the linear regression through a plot of BIA time equivalence versus calculated time equivalence is 57% with a correlation coefficient of 0.85.

5.5.2 Insulation Criterion

Figure 5.14 plots the CIB versus the calculated time equivalent for insulation.

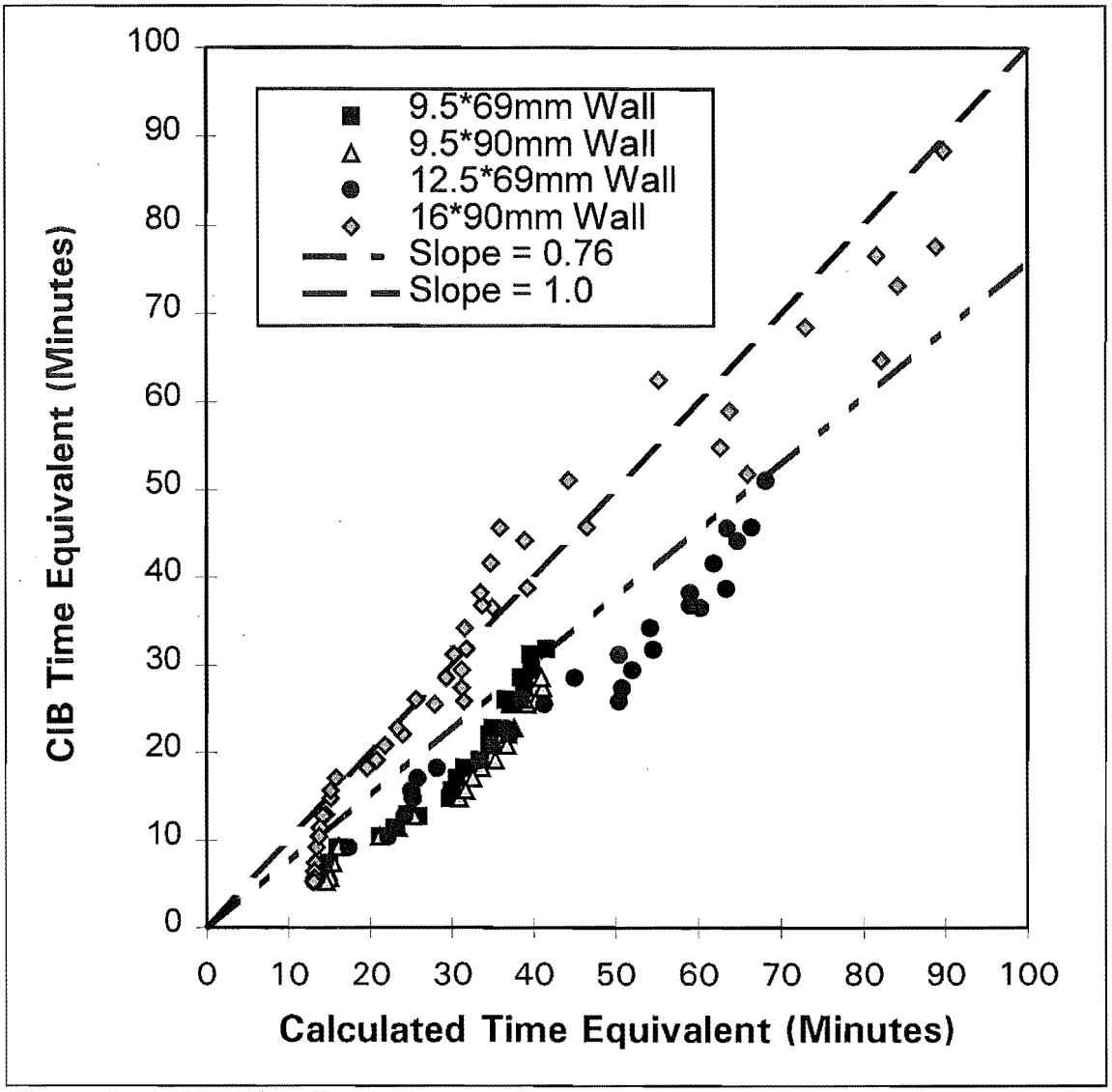

Figure 5.14 CIB Time Equivalent vs. Computer Prediction of Time Equivalent for Insulation Criterion

As was the case for the charring criterion, the walls with the thicker linings performed better, since their calculated time equivalent was shorter relative to the CIB time equivalent. The lower line represents a linear regression of the results. The upper line represents a one to one relationship. Overall the calculated time equivalent is 76% of that calculated using the CIB formula, which therefore underpredicts the time equivalent by 32% of the calculated value. The correlation coefficient for the regression is 0.82.

If the BIA formula is used (Equation 1.4), with a value of C = 0.08, then the slope of the linear regression through a plot of BIA time equivalence versus calculated time equivalence is 74% with a correlation coefficient of 0.78.

5.5.3 Summary

The correlation between the two methods is good, with a linear dependence. The CIB Equation (1.1) predicts the trend of the results, but consistently underestimates the values.

The dependence between time equivalent and total fuel load appears to be slightly less than linear, as the BIA and Eurocode formulae would suggest. In the formulae it would be more appropriate to use the fuel load raised to a power of about 0.9, rather than 1.0.

The scatter in the data appears to be less than that of the data used to correlate the original time equivalent formula (Law 1977). The scatter in Law's data is partly due to experimental error and repeatability problems. These do not occur with computer models.

As the term C in Equation (1.1) is poorly defined, it may be appropriate to alter this value in order to produce the appropriate equations for the two criteria given here. The correlation for the insulation criterion is the better of the two.

5.6 Sensitivity Study

The most critical parameters in the compartment fire sub-model were varied in order to determine their effect on the overall results.

The three parameters are:-

(i) The fraction of fuel burnt within the compartment (Section 5.6.1).

(ii) The shape of the decay phase of the fire, shown by it's effect on the latter part of the time-temperature curves (Section 5.6.2).

(iii) The effect of using the Swedish time-temperature curves rather than COMPF-2 output (Section 5.6.3 and 5.6.4).

5.6.1 Fraction of Fuel Burnt

The most critical parameter in COMPF-2 is input as "BPF", and represents the percentage of pyrolysis gases that burn inside the compartment. It can be thought of as

the percentage of heat available in the fuel that is released within the compartment. It is always less than 1.0 as the mixing within the compartment is not perfect. It also allows for the fact that with charring fuels, not all of the fuel is pyrolised. COMPF-2 (Babrauskas 1979), recommends a value between 0.7 and 0.9. Values from other sources range from 0.55 to 1.00. The range 0.7 to 0.9 is more reasonable. It is lower for ventilation controlled fires than for fuel bed controlled fires. Three sets of computer runs were carried out on one wall layout with one layer of 12.5 mm gypsum plasterboard and 69*45 mm studs, using values of BPF of 0.7, 0.8 and 0.9.

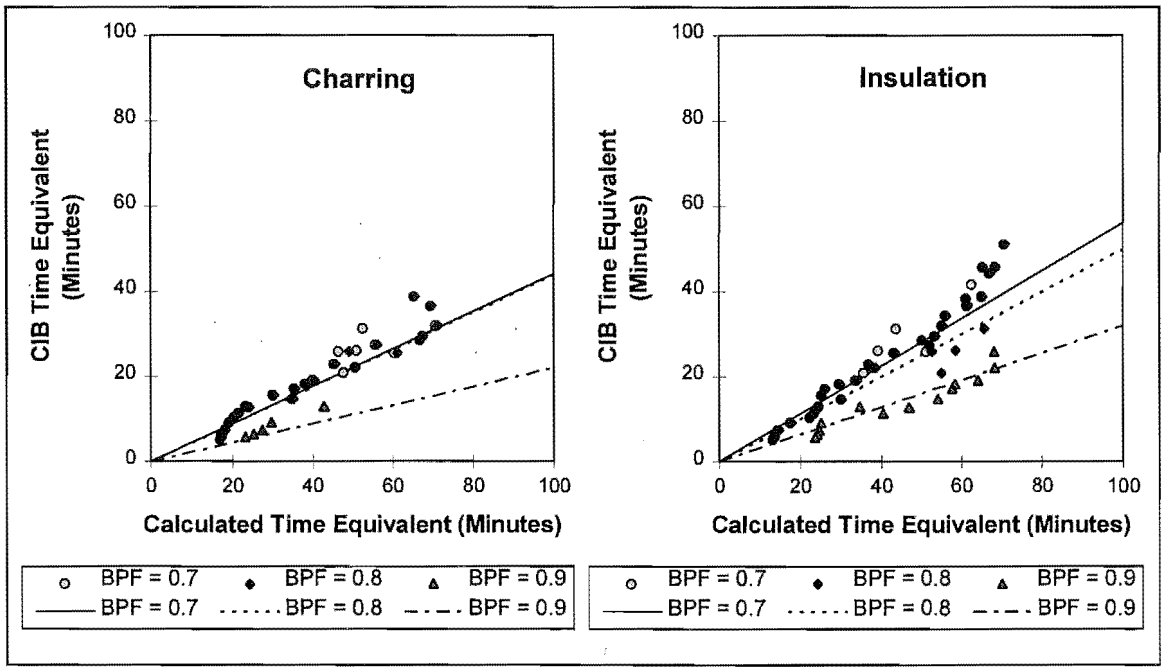

Figures 5.15 and 5.16 Effect of the Percentage of Pyrolysates Burnt on the Equivalent Time

Figures 5.15 and 5.16 show the effect that varying the percentage of pyrolysates burnt has on the equivalent time of exposure for the charring and insulation criteria respectively. Data points are shown by symbols, the lines are linear regressions of the data points in each set. For both criteria a change from 0.7 to 0.8 has little effect, but changing to a value of 0.9 the calculated time equivalent is about twice that for a BPF of 0.7

The effect is very significant for longer fires, and reasonably significant for shorter fires.

In this study, pessimised pyrolysis is assumed, hence the fires are highly ventilation controlled. In a ventilation controlled regime it is appropriate to use a lower value of BPF and inasmuch as there is little variation between the results when using 0.7 or 0.8, a value of 0.7 is employed.

5.6.2 The Decay Phase

The other parameter that may have a significant effect on the results is the shape and length of the decay phase of the fire. Three alternative decay phases were investigated:-

(i) Pessimised pyrolysis is assumed. This has been used so far in this work. With a pessimised pyrolysis rate, the burning rate is constant until all fuel is burnt, then the temperatures drop quickly as the only heat is from the cooling of the walls.

(ii) The burning rate is at the constant ventilation controlled burning rate until two thirds of the fuel is consumed. The burning rate is then assumed to decrease at a rate inversely proportional to the time remaining squared for a time equivalent to twice the duration of the ventilation controlled phase. The time-temperature curve is then calculated using COMPF-2 and the prescribed heat release rate curve described. This type of decay phase is hereinafter referred to as a "t^2" decay phase and a fire incorporating such a decay phase as a t^2 fire.

(iii) The burning rate is at the constant ventilation controlled burning rate until two thirds of the fuel is consumed. The burning rate is then assumed to decrease at a linear time-dependent rate for a time equivalent to the duration of the ventilation controlled phase. The time-temperature curve is again calculated using COMPF-2 and the prescribed heat release rate curve.

5.6.2.1 Effect on the Time-Temperature Curve

Figure 5.17 shows the effects of the above changes on the time-temperature curve.

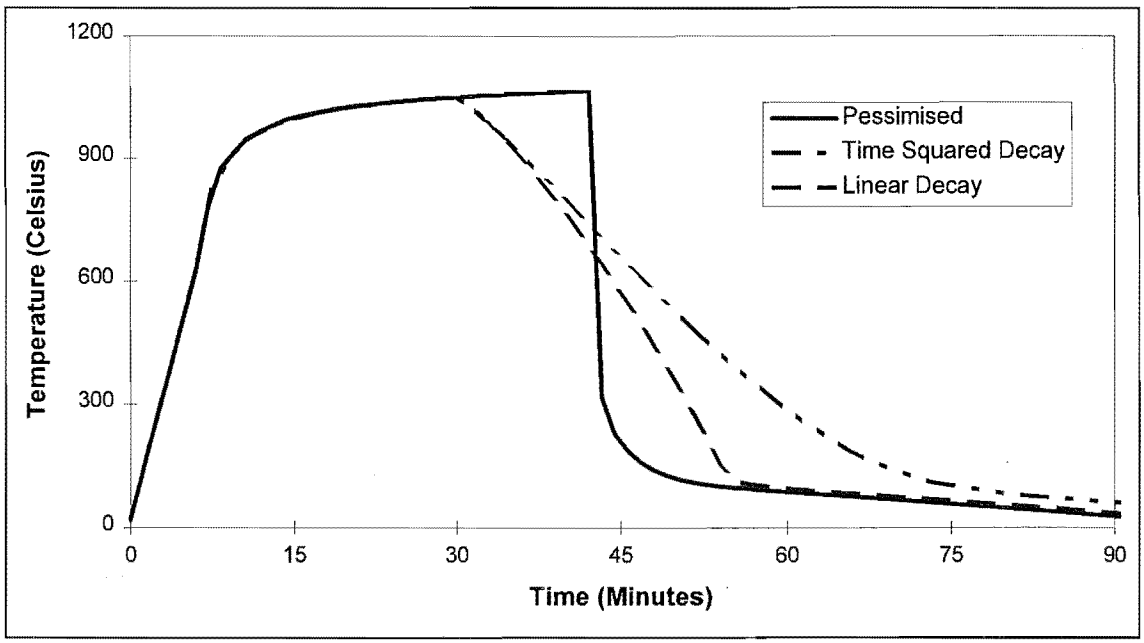

Figure 5.17 Effect of the Shape of the Decay Phase on Temperatures

The first option results is that used previously and the second and third option only result in changing the shape of the curve after two thirds of the fuel has been burnt. The shapes of the curves for a fire with a duration of about forty-five minutes when the burning rate is ventilation controlled, that is pyrolysis is pessimised, throughout the first thirty minutes as shown in Figure 5.17.

Magnusson and Thelandersson (1970) showed the effects of varying the shape and length of the decay phase on the temperature of a steel column. The growth and fully developed period of the fire was the same and only the decay phase varied. The range of decay phases used varied from an instantaneous drop in temperature to 10°C per minute as shown in Figure 5.18.

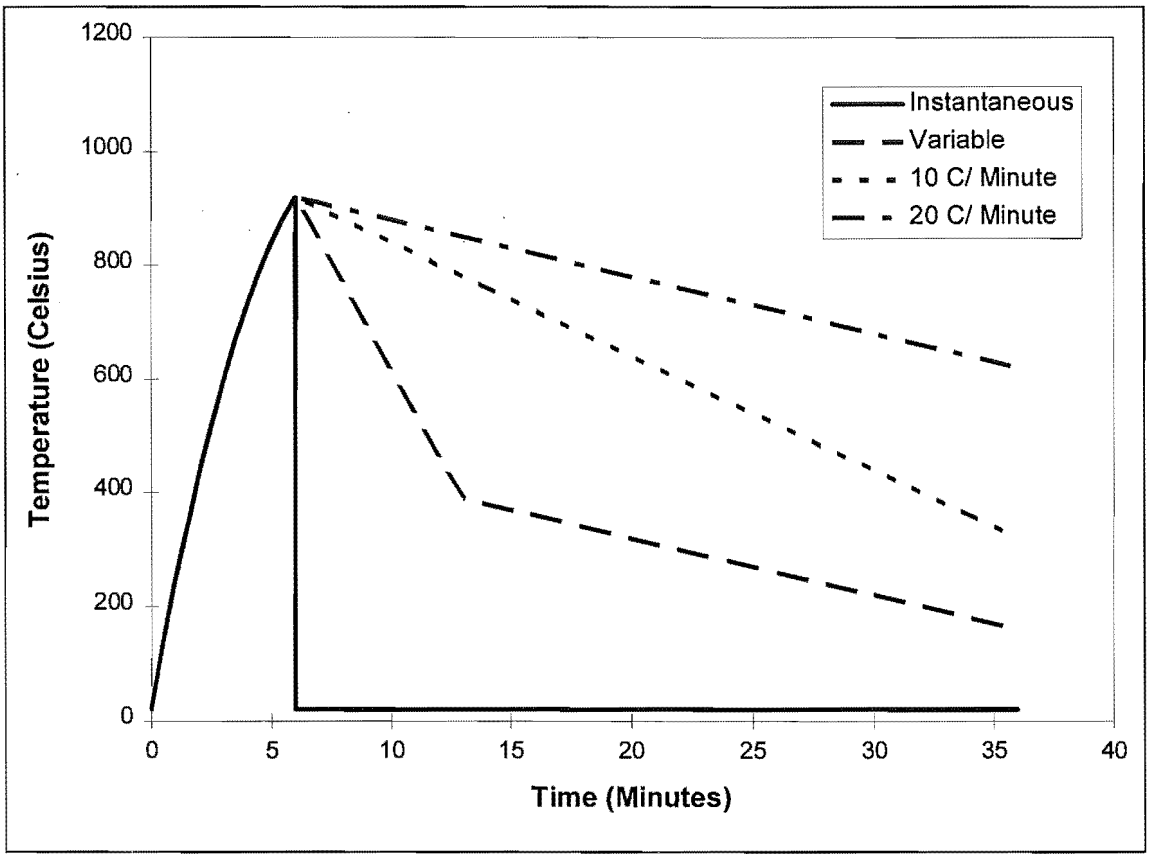

Figure 5.18 Decay Phases used by Magnusson and Thelandersson (from Magnusson and Thelandersson 1970)

However as the rest of the time-temperature curve has the same shape, the total fuel energy required to produce a fire that drops from 900°C at a time of five minutes to ambient temperature ninety minutes later is much greater than the energy required to produce a five minute fire with an instantaneous temperature drop at that point. In this study, the heat release rate curve is varied and temperatures calculated using a heat balance. In each of the three cases shown in Figure 5.17, the total amount of energy released is the same.

5.6.2.2 Effect on the Time Equivalence

The effect that these changes have on the thermal response of the structure is far more important than the effect on the time-temperature curve.

The effect on the charring and insulation criterion is shown in Figures 5.19 and 5.20 respectively.

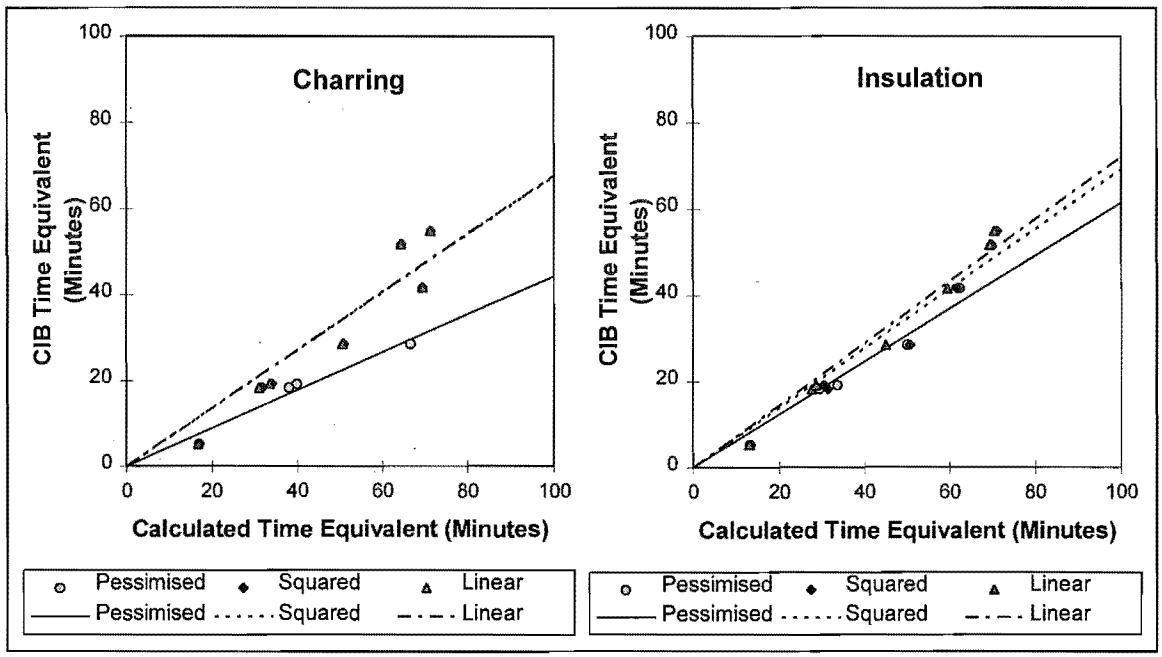

Figure 5.19 and 5.20 Effect of Varying the Heat Release Rate During the Decay Phase on the Time Equivalence

The three series of points in Figures 5.19 and 5.20 refer to the original values for the time-temperature curve calculated assuming pessimised pyrolysis, an inverse time squared decay phase and a linear decay phase respectively. The straight lines are linear regressions of the respective data series.

For the charring criterion, assuming a inverse time squared decay phase results in calculated time equivalents that are 52% lower than those assuming pessimised pyrolysis, and 53% lower if a linear decay phase is assumed. The difference between using an inverse time squared and a linear decay phase is insignificant (1.0%).

For the insulation criterion, assuming an inverse time squared decay phase results in calculated time equivalents that are 13% lower than those assuming pessimised pyrolysis, and 17% lower if a linear decay phase is assumed. The difference between using an inverse time squared and a linear decay phase is then 4.0%.

Using time-temperature curves that have been developed using COMPF-2 and assuming pessimised pyrolysis is conservative for both charring and insulation criteria, but is more conservative for the charring criterion.

5.6.3 Shortcomings in the COMPF-2 Time-Temperature Output

In Section 5.3.1, two assumptions regarding the initial and final temperature curves during a fire were described. They are:-

The initial rate of temperature increase within the compartment was 100°C per minute.

The time-temperature curves drops from 80°C to 20°C in 30 minutes.

The effect of the first assumption was checked by assuming an instantaneous temperature increase at the start of the fire. The effect of the second assumption was checked by assuming an instantaneous temperature from 80°C at the end of the COMPF-2 run to 20°C in one minute. Having an instantaneous initial temperature rise reduced the calculated time equivalents by 6.5% for the insulation criterion and 12% for the charring criterion, but having a very rapid drop in temperature at the end had no effect.

5.6.4 The Swedish Time-Temperature Curves

Tabulated values from the Swedish time-temperature curves were used as input to the wall model and time equivalents found. The tabulated values were for a type G compartment (Magnusson and Thelandersson 1970), that is, one with 80% of the bounding surfaces composed of two 13mm gypsum plasterboard panels on each side of a 100 mm cavity, supported by steel studs. There are four layers of plasterboard in total. The other 20% of the bounding surfaces is concrete.

5.6.4.1 Ventilation and Fuel Load Parameters of Curves Used

It was not possible to use the same values for fuel load and ventilation factors in this comparison as was used in the other comparisons. This is because of the problems with interpolating the Swedish time-temperature curves to obtain curves for intermediate values of the fuel load and the opening factor.

Magnusson and Thelandersson (1970) suggest that interpolation could be used for intermediate values, but this results in the decay phase starting earlier than the amount of fuel load would dictate. For example, the time-temperature curve calculated by interpolating the two adjoining curves is significantly different from the values calculated by Magnusson and Thelandersson as shown in Figure 5.21.

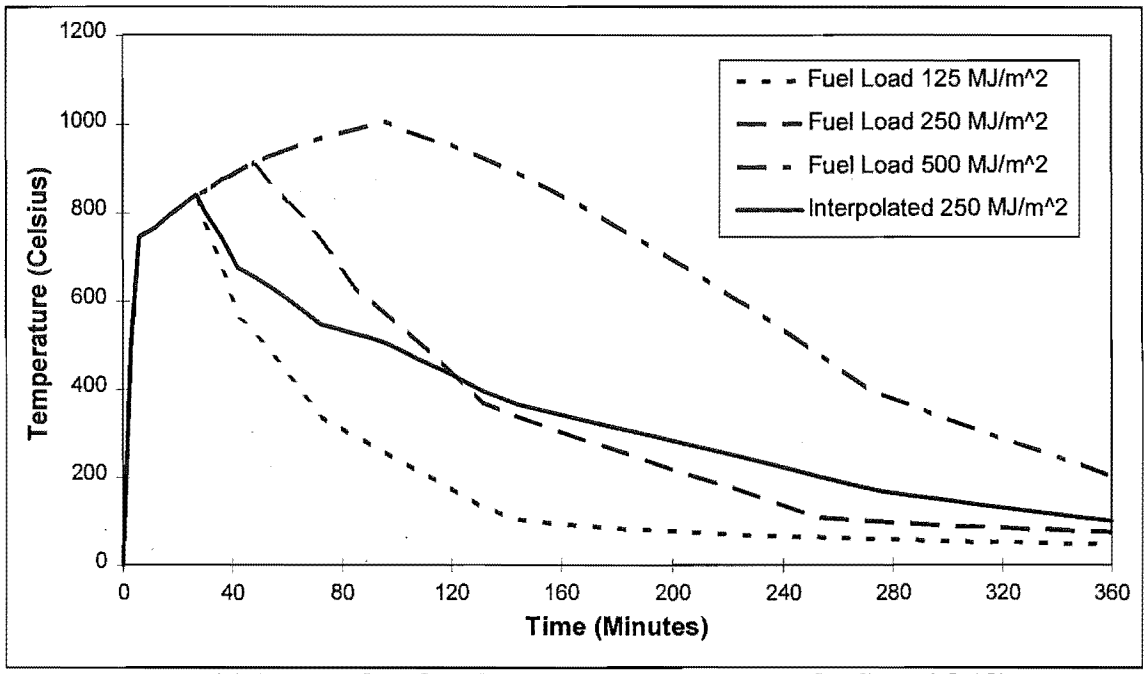

Figure 5.21 Interpolated and Calculated Values for the Swedish Time-Temperature Curves

In Figure 5.21 a curve for a fuel load of 250 MJ/m^2 is shown , which is calculated by linear interpolation of the curves for fuel loads of 125 MJ/m^2 and 500 MJ/m^2 along with the curve for a fuel load of 250 MJ/m^2 given by Magnusson and Thelandersson. The interpolated curve is less severe than the calculated curve because of the shorter length of time at close to maximum temperatures. This is not compensated for by the region after 120 minutes where the interpolated values are higher than the calculated values because little heat is transferred by radiation at these low temperatures, since radiation is proportional to the fourth power of the temperature.

Table 5.4 shows the mix of ventilation factors and fuel loads used for the comparison. There were 12 combinations used for each of the four wall layouts, resulting in a total of 48 simulations for the comparison.

WINDOW			Opening Factor	Ventilation Factor	Fuel Loads			
Height	Width	Area		Old CIB (Eqn 1.3)	per Unit Floor Area			
(m)	(m)	(m^2)	(m$^{1/2}$)	(m$^{-1/4}$)	(MJ/m^2)			
1.00	2.20	2.20	0.020	1.607	55.2	166	828	1100
1.69	3.00	5.08	0.060	0.928	166	331	828	1657
2.22	4.00	8.87	0.120	0.656	331	662	994	1657

Table 5.4 Ventilation and Fuel Load Parameters for Comparison with the Swedish Curves

5.6.4.2 Results from Comparison

Using the Swedish time-temperature curves as input into the TASEF wall model resulted in a calculated time equivalent that is less than that derived using a curve developed using COMPF-2, assuming pessimised pyrolysis. This occurs for both the charring and insulation criteria.

5.6.4.3 Charring Criterion

Figure 5.22 shows the effect of using the Swedish curves on the time equivalent for the charring criterion.

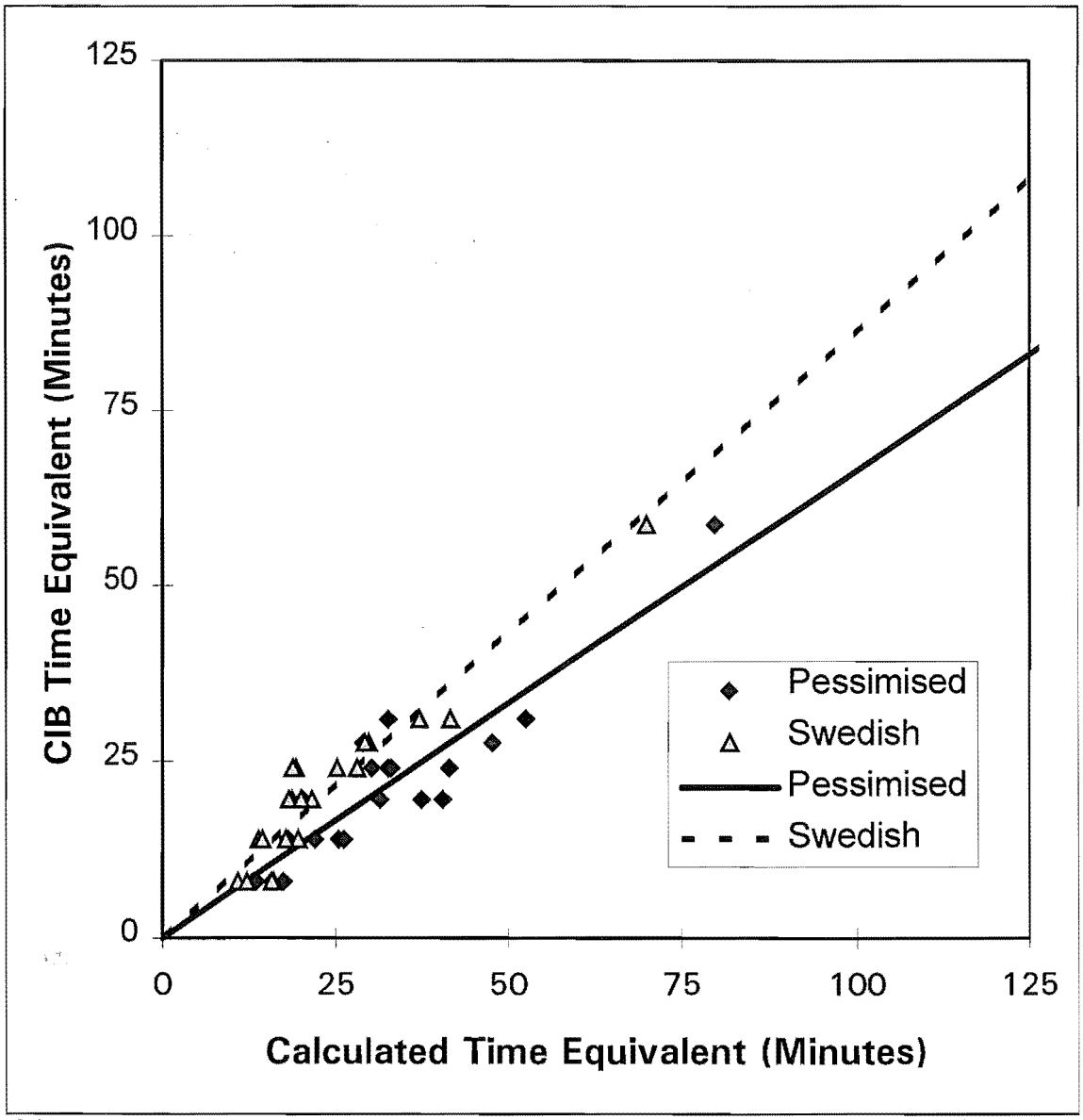

Figure 5.22 Effect of Using Swedish Time-Temperature Curves on The Charring Time Equivalence

The symbols are data points and the straight lines are linear regressions of the data points. The regression is only for valid data points that are present in both series (see

Section 5.2). The calculated time equivalent is in most cases lower when using the Swedish curves, hence the walls perform better. However for long CIB time equivalence values, the values for calculated time equivalence are much lower than when using the COMPF-2 output.

The regression line for the Swedish values is considerably higher (30%) than that for the COMPF-2 results.

5.6.4.4 Insulation Criterion

Figure 5.23 shows the effect that using the Swedish curves as input has on insulation.

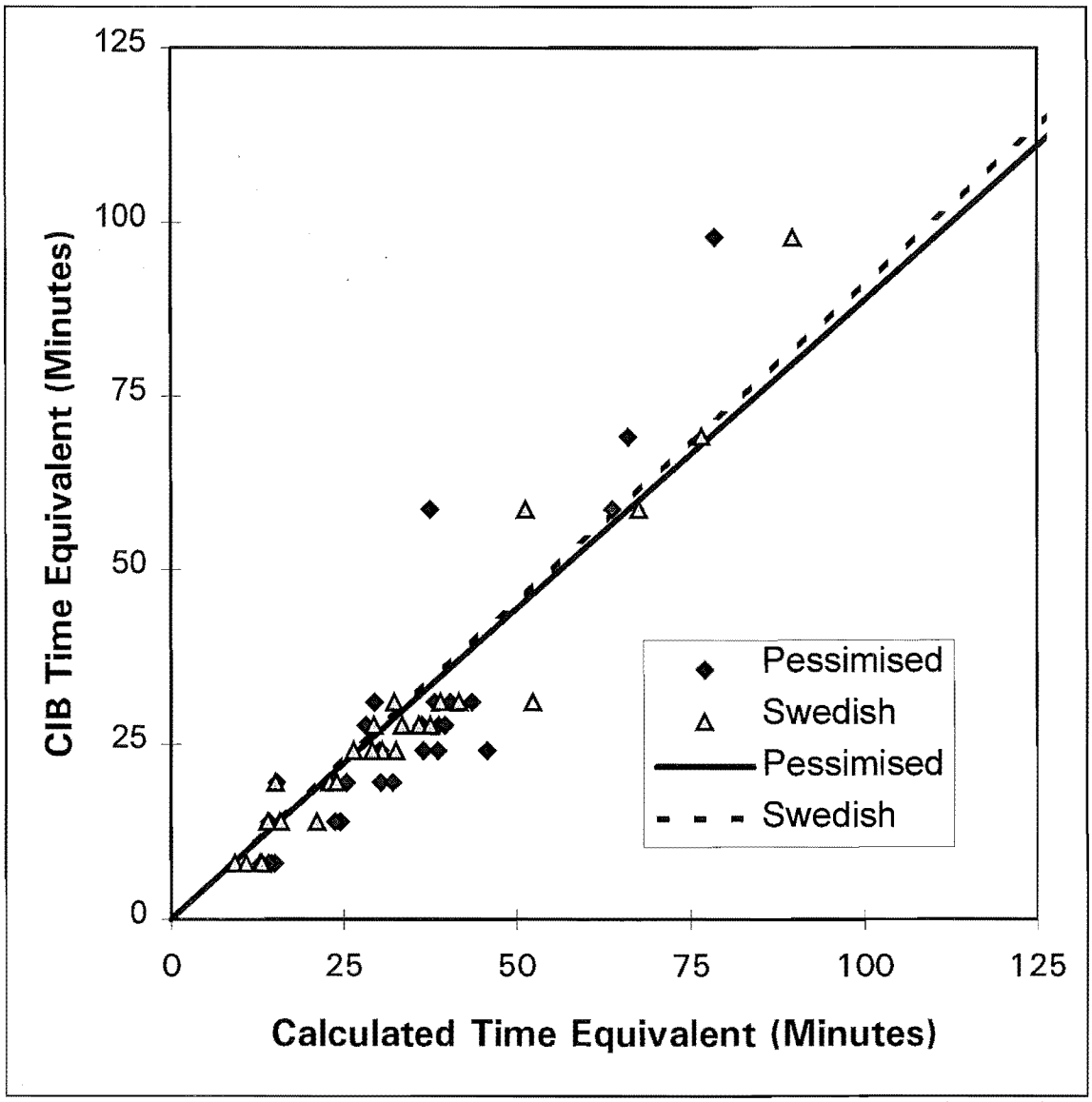

Figure 5.23 Effect of Using Swedish Time-Temperature Curves on The Insulation Time Equivalence

Once again the symbols are data points on the straight lines are linear regressions of the data points. The regression is only for valid data points that are present in both series (see Section 5.2).

The calculated time equivalent is in most cases slightly lower when using the Swedish curves, hence the walls perform marginally better. However for long CIB time equivalence values, the values for calculated time equivalence are much lower than when using the COMPF-2 output. If the values found using the Swedish curves as input corresponding to valid data points are only used then the regression for the Swedish values is slightly more (1%) than that for the COMPF-2 results.

5.6.5 Discussion of the Effect of the Swedish Curves

For the insulation criterion, a linear regression of all the data points found using the Swedish curves results in a one to one correlation with the time equivalents predicted using the CIB formula. This is not surprising it is similar to the situation for which the CIB formula is designed for. The CIB formula was originally developed by Law (1977), and modified by a CIB working party (Thomas 1986), to predict the severity of a compartment fire on a protected steel section. Such a section is shown in Figure 5.24.

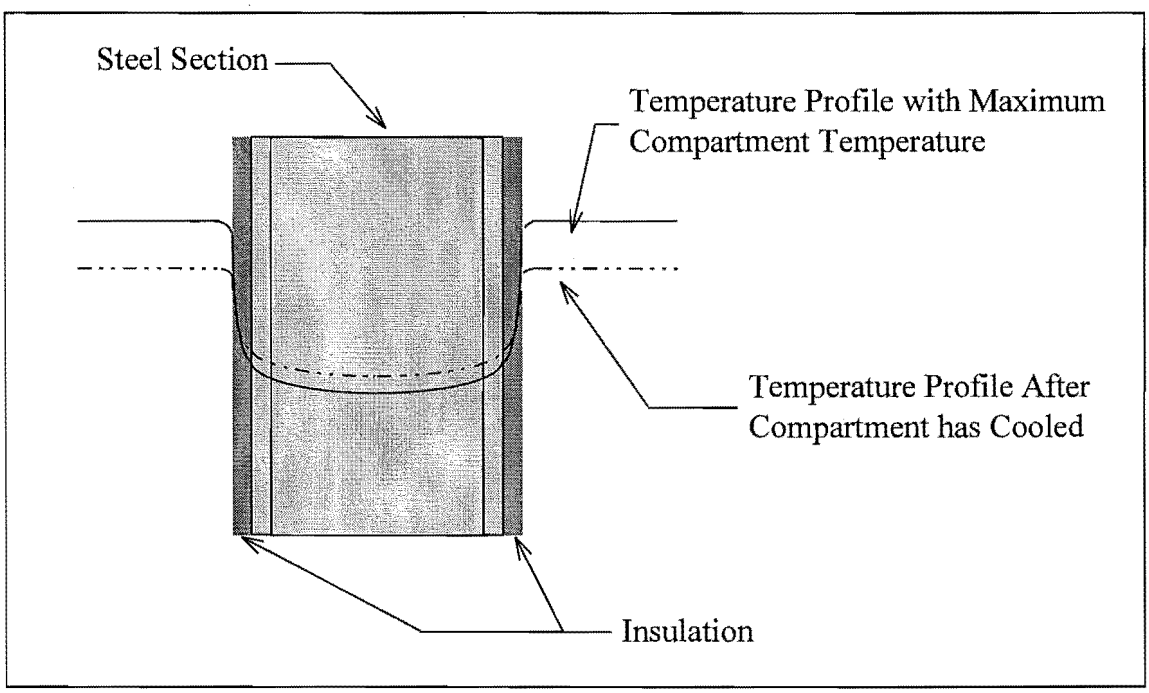

Figure 5.24 Temperature Profile Through Steel Section Exposed to Fire

The CIB formula was devised using values from experiments that were very similar or in some cases the same as those used to develop the Swedish curves. The situation is similar because the point at which the charring first occurs is protected by an insulating membrane (Figure 5.22), similar to the way in which a steel section is protected by an insulating layer of low conductivity. For the insulation criterion the situation is completely different as can be seen in Figures 5.25, so it would be unlikely that the CIB formula would match exactly.

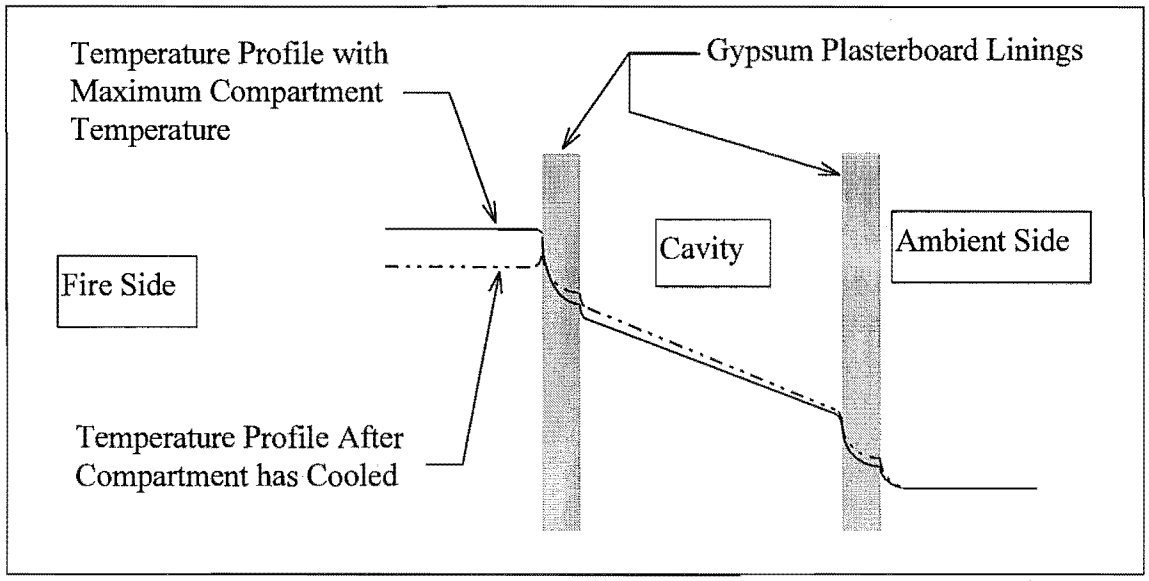

Figure 5.25 Temperature Profile Through Cavity Wall Exposed to Fire

The steel section is of very high conductivity and has a very small variation in temperature across it (Figure 5.24). It is surrounded by a layer of insulation with a very high temperature gradient. When the compartment starts to cool, heat continues to flow into the steel section due to this high thermal gradient.

On the other hand in a cavity wall there is no "heat sink" of high conductivity steel to carry away heat and hence the temperature gradient is much smaller. When the compartment temperatures start to decrease, most of the heat in the lining is released back into the compartment, although a small amount will continue further into the wall (Figure 5.25). These differences account for the fact that the temperature in steel sections continue to increase significantly after the maximum fire temperature is reached, but the temperature increases only slightly in cavity walls. This means that a long decay phase has a more severe effect on steel than on cavity walls.

5.7 Conclusions

5.7.1 Time Equivalence

The CIB time equivalent formula underestimates the equivalent fire severity of light timber framed walls, when considering thermal behaviour compared with predictions made using the computer models in this study. The relationship appears to be highly linear with correlation coefficients of 0.88 and 0.82 for charring and insulation respectively.

The CIB formula could be modified by using a constant with two different values for the insulation and charring criteria, to give a better prediction of wall behaviour.

The BIA formula is not as good as the CIB formula because the relationship between values calculated using it and the calculated time equivalent is not as linear as it is using the CIB formula. The correlation coefficient is lower for both the charring and insulation criteria.

The dependence between time equivalent and total fuel load appears to be slightly less than linear.

5.7.2 Other Conclusions

The two dimensional finite element wall model developed using TASEF, consisting of two distinct materials and a cavity can be modelled as a simplistic one dimensional homogeneous wall in order to solve the heat balance in COMPF-2.

The percentage of pyrolysates that is burnt within the compartment is significant.

The values used for the emissivity and convection coefficient are not critical, provided that they are within reasonable limits.

Assuming pessimised pyrolysis (that is ventilation control throughout) the fire is highly conservative, compared with both similar time-temperature curves with different decay phases. Assuming pessimised pyrolysis (that is ventilation control throughout) the fire is highly conservative compared to using the Swedish time-temperature curves.

5.7.3 Further Work

It would be desirable to produce standard time-temperature curves or standard parameters to model such curves. A curve that is derived assuming that two thirds of the fuel is burnt at a ventilation controlled rate, and then at a decreasing rate inversely proportional to the time squared would be a reasonable choice.

A multi-variable regression of all the data points generated could be carried out in order to produce a more accurate time equivalent formula.

The charring criterion is a first approximation of the structural performance of a wall. The calculated structural capacity is of far more significance. Determination of the calculated time equivalence for the structural capacity of light timber framed walls will be described subsequently.

Chapter 6 House Fire Results and Comparison with Models

6.1 Description of the Test

In October 1995, a derelict house was donated to the Fire Engineering program at the University of Canterbury, with the intention that it be burnt down. The author utilised one room in the house to model a compartment fire in gypsum plasterboard lined room. The fuel load was composed of wood pallets. An external window approximately 1.8 m square was filled with a standard half hour light timber framed wall. Temperatures were recorded within the room, through the test wall and within dummy studs in the test wall.

6.1.1 Compartment Set-up and Instrumentation

The test compartment was 3.9 m by 3.8 m and 3.12 m high. In order to prevent premature fire spread the ceiling was lined with two layers of 9.5 mm "Fyreline" gypsum plasterboard. The walls were lined with one layer of 9.5 mm "Fyreline" gypsum plasterboard. The plasterboard was screw fixed to the ceiling and walls. The joints were not stopped but covered with strips of plasterboard. The floor was covered with one layer of 9.5 mm "Fyreline" gypsum plasterboard, in order to cover the holes in the floor. The test wall was 1.9 m wide and 1.8 m

Figure 6.1 The Test Compartment

high and constructed from kiln dried 90*45 mm pinus radiata framing timber. It was lined with one layer of 9.5 mm "Fyreline" gypsum plasterboard on each side. The base of the test wall was 800 mm above the floor.

6.1.2 Compartment Instrumentation

The compartment was instrumented with two sets of thermocouples. There was a tree of bead thermocouples located at the centre of the room, with thermocouples at 300, 600, 900, 1500, 2100 and 2700 mm from the ceiling of the room. The thermocouple 900 mm from the ceiling did not give a reading throughout the fire. In addition there was a vertical row of sheath thermocouples at 300 mm centres alongside the test wall. The thermocouples 200, 800, 1400 and 2000 mm from the ceiling were 4 mm sheath thermocouples. There were 1.5 mm sheath thermocouples at 500, 1100, 1700, 2300, 2600 and 2900 mm from the ceiling.

6.1.3 Wall Instrumentation

There were three sets of five disc thermocouples located through the wall in positions 2 to 5 as shown in Figure 6.2. An additional thermocouple was located in the cavity, halfway between positions 2 and 3. This is identical to the setup used for ISO-834 furnace tests at BRANZ (Collier 1992).

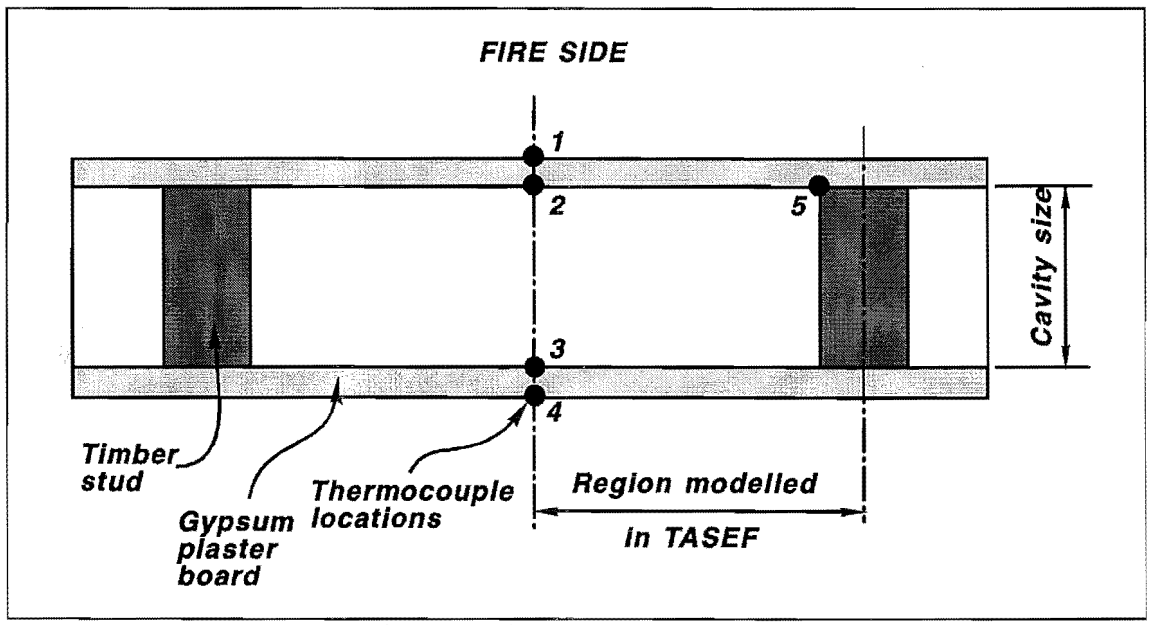

Figure 6.2 Location of Disc Thermocouples

In addition four sheath thermocouples were inserted into the centreline of two dummy studs as shown in Figure 6.3.

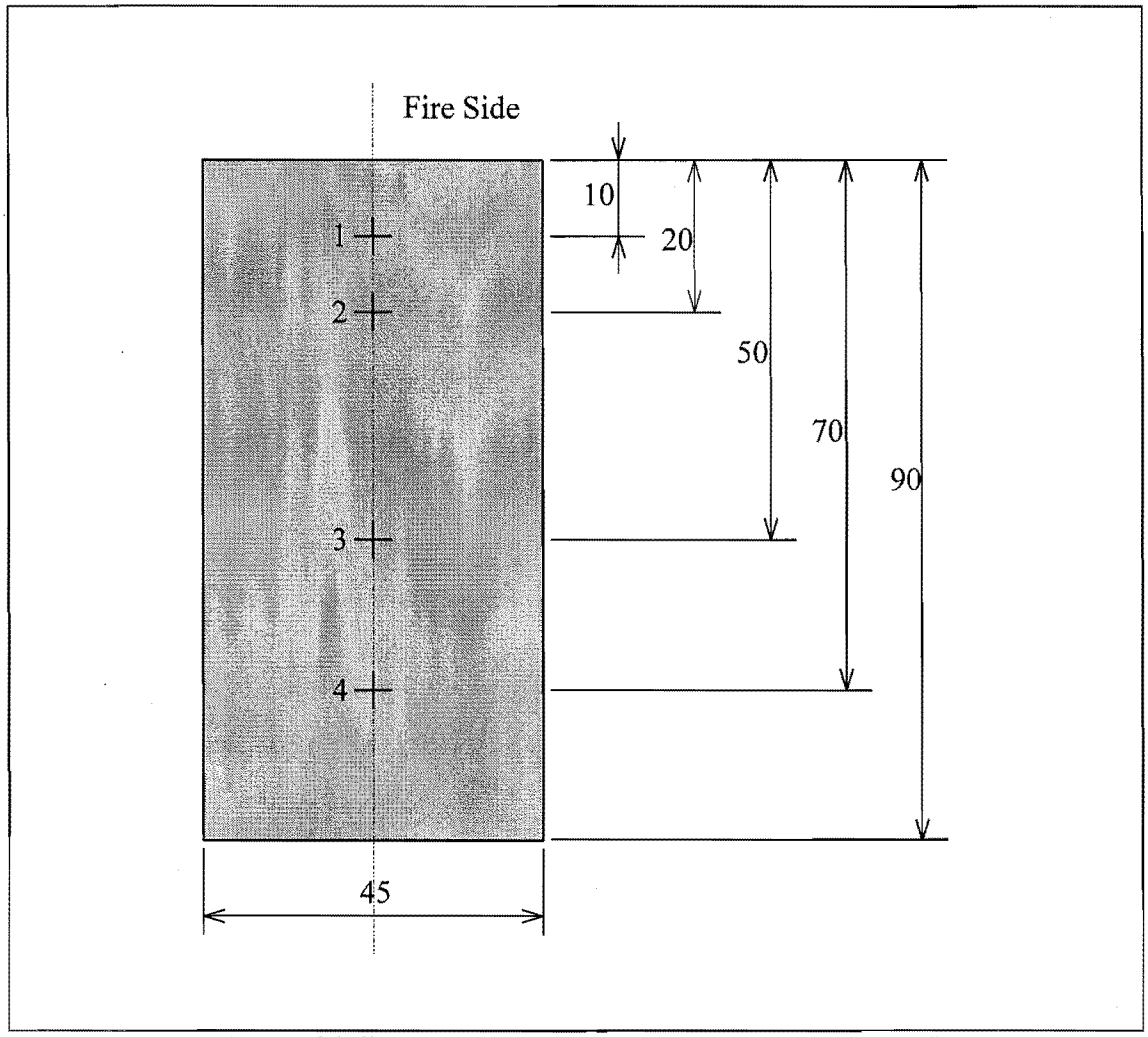

Figure 6.3 Layout of Thermocouples in Dummy Stud

6.1.4 Fuel Load

The fuel load was composed of four 1.5 metre high stacks of timber pallets on a square grid 0.5 metres apart. The timber was 400 kg of pinus radiata at a moisture content of 20%, giving a fuel load of 400 MJ/m^2 of floor area. The stacks are shown in Figure 6.1

6.2 Behaviour of Test Fire

The data logger was started and run for 10 minutes to stabilise data collection.

At 10 minutes the four cribs were lit using newspaper soaked in methylated spirits. After 11 minutes the flames were half way up the stacks (~0.75 m high). After 14 minutes all four cribs went out.

At 15 minutes the fire was restarted using foam rubber squabs approximately 400 mm square in the base of the stacks.

Two minutes after ignition the flames had hit the ceiling and the plume reached the walls

Flashover occurred about 30 seconds later.

After 22 minutes from ignition the first layer of the ceiling fell down.

After 24 minutes from ignition the fire appeared to reduce in intensity. This may have been due to the fuel burning out, but was more likely be due to the fire penetrating the walls and altering the ventilation characteristics.

25 minutes after ignition the flames were through the exterior walls of the compartment.

30 minutes after flashover the test wall was still intact apart from flames that issued from a hole cut into the exterior lining in order to attach the thermocouples.

Figure 6.4 and 6.5 Compartment 90 Seconds and Five Minutes after Ignition

A series of photographs, Figures 6.4, 6.5 and 6.6 show the test compartment and the test wall during the fire. Figure 6.4 shows the compartment 90 seconds after flashover, Figure 6.5 shows the compartment about 5 minutes after flashover. Figure 6.6 shows the test wall about 12 minutes after flashover.

Figure 6.6 Test Wall 12 Minutes after Flashover

6.3 Comparison of Compartment Temperatures with the Model

The comparison between the predicted temperatures and those recorded at the centre of the room and at the side of the room are shown in Figure 6.7.

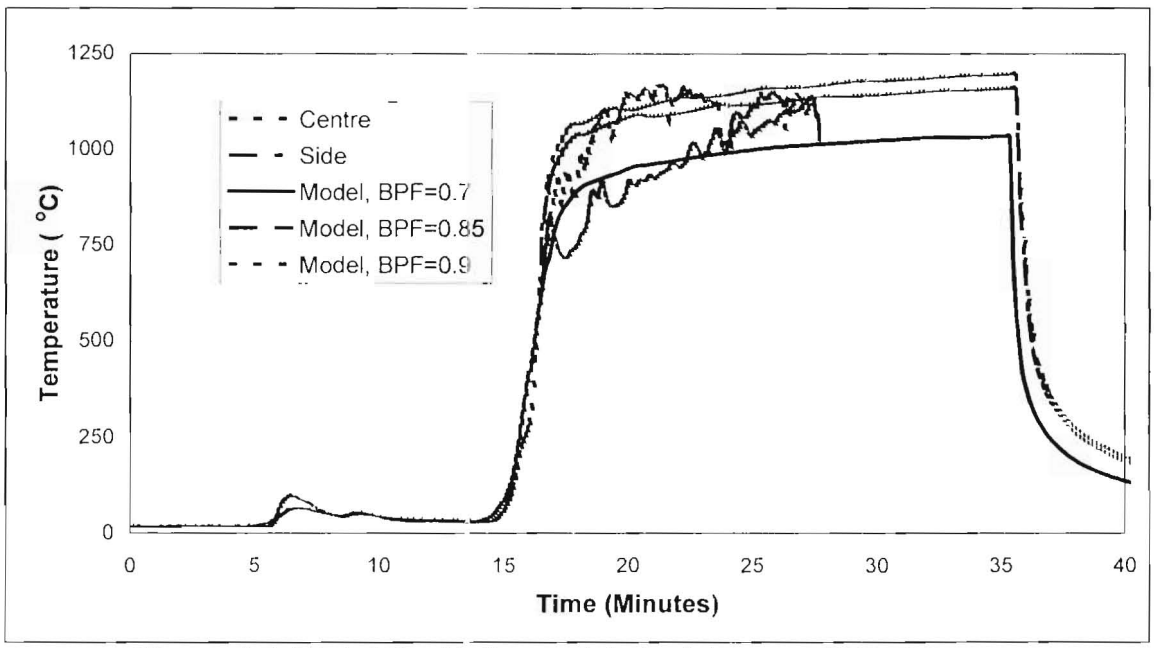

Figure 6.7 Model Prediction and Actual Average Temperatures

The temperatures within the room were predicted using COMPF-2 (Babrauskas 1979) assuming ventilation control, for the geometry of the room, the size and shape of the

window, and the compartment boundaries. A time delay of 1.5 minutes was subtracted from the graphs of the four millimetre thermocouples to allow the larger thermocouple lag compared with the 1 mm thermocouples. The temperatures were then averaged over the height of the room.

In previous work (Chapter 5) the fraction of burnt pyrolysates (BPF) used was 0.7. This parameter is a measure of the combustion efficiency and represents the proportion of energy in the fuel that is released within the compartment. The BPF typically varies from about 0.7 for highly ventilation controlled fires to over 0.9 for fires burning in the open, that is, fully fuel bed controlled fires. In the compartment, the fuel consisted of pallets, made up sticks of 12 mm and 35 mm width. The fuel bed controlled pyrolysis rate for these sticks was 2.4 and 0.6 kg/s respectively at the start of the fire. The rate reduces as the fire continues. The fuel-bed controlled burning rate is similar to the ventilation controlled burning rate of 0.35 kg/s. The fire is therefore only slightly ventilation controlled, the air supply is not highly limited, so the combustion efficiency is higher than 0.7. A value of 0.85 gives a good correlation with the temperatures at the centre of the room.

It is not possible to determine when the fuel burnt out within the room as the fire spread to adjacent compartments and temperature measurements were halted before the fuel in the compartment burnt out.

6.4 Variation of Temperatures within the Compartment

Models of post-flashover fires assume an even temperature throughout the compartment. It can be seen in Figure 6.7 that the thermocouple array at the side of the room recorded substantially lower temperatures (approximately 250°C lower) than the tree in the middle. Some of this may be attributed to thermocouple lag and shaft losses (Babrauskas and Williamson 1978b) as the array at the side of the room consists of sheath thermocouples and the central array is composed of bead thermocouples with a far smaller thermal mass. The thermocouples at the side of the room may "see" less of the compartment because of their proximity to the wall. These factors do not explain

such a large difference. The difference is considered to be mostly due to the loss of energy to the wall as it initially heats up, resulting in a decrease in temperature from the centre of the room to the sides. As the heat flow through the wall approaches steady state the temperature across the room becomes more constant as is shown in Figure 6.7.

6.5 Comparisons with Wall Heat Transfer Models

The temperature history measured within the compartment was used as input to a two-dimensional finite element model of the wall, and the temperatures through the wall assembly and within the stud were compared with measured temperatures. The thermal model was developed using TASEF (Sterner and Wickstrom 1990) and is described in Chapters 3 and 4.

6.5.1 Through the Wall

The temperatures were measured with disc thermocouples through the wall in locations 2, 3, 4 and 5 in Figure 6.2. The temperatures through the wall were predicted before the test using the predicted time-temperature curve as input. The comparison between this and the actual temperatures is not reported due to the significant difference between the predicted and measured temperatures within the compartment. Figure 6.8 shows the comparison between predicted and measured temperatures.

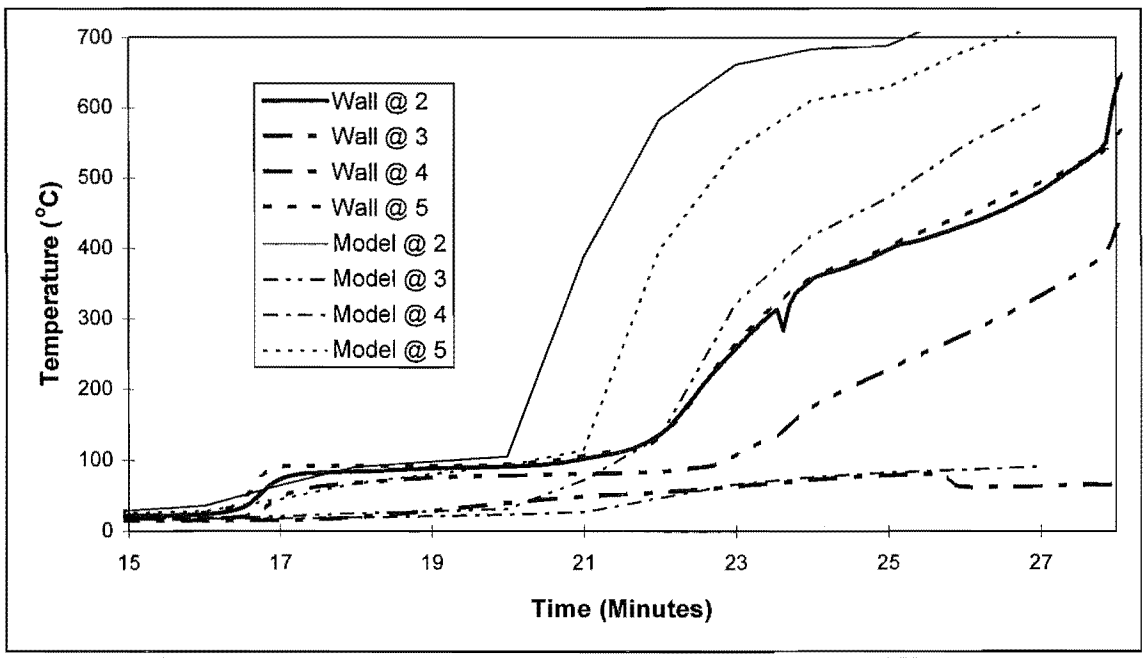

Figure 6.8 Temperature Profile Through Wall Using Central Temperatures

The compartment temperatures used to produce the results shown in Figure 6.8 are those through the wall when the temperatures measured at the centre of the room are used as input to the finite element model of the wall.

The comparison at points 2, 3 and 5 is poor with the predicted temperature being much higher than that recorded. The comparison at point 4, on the ambient side of the wall is good. An emissivity of 0.9 and a convection coefficient of 5.0 was used. The convection power is 1.33. (see Section 3.9.3). A sensitivity analysis was performed, varying the value of the emissivity from 0.7 to 1.0, with little effect on the temperatures.

Figure 6.9 shows the same relationship when the temperatures at the side of the room is used.

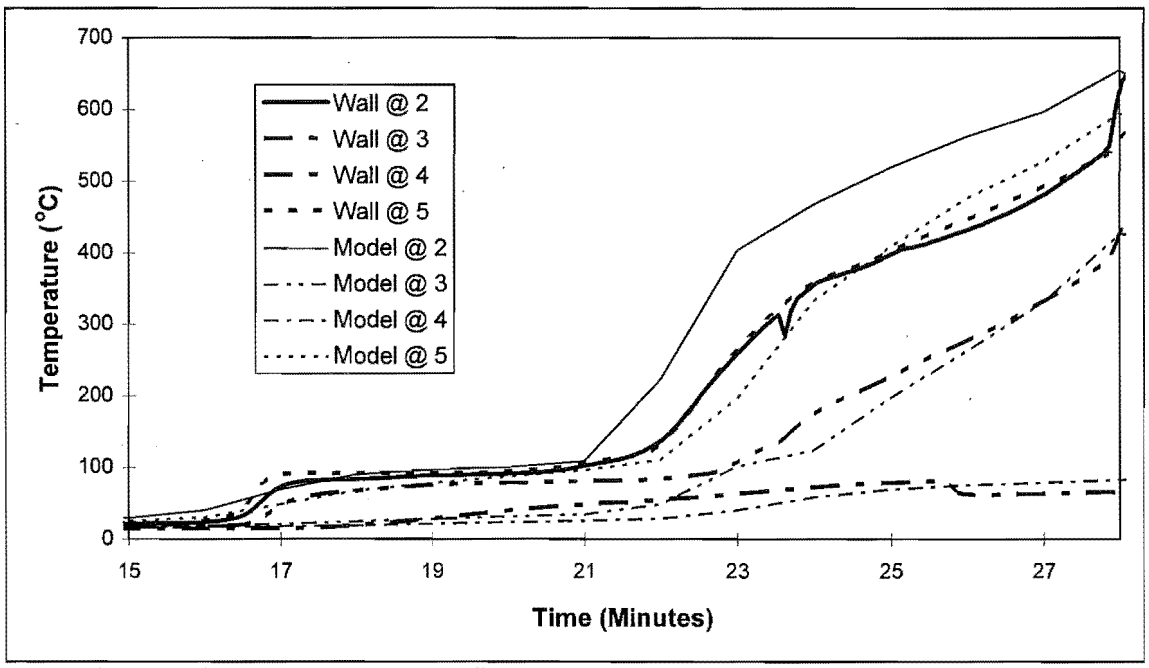

Figure 6.9 Temperature Profile Through Wall Using Side Temperatures

The comparison is better at point 2 and good at points 3 and 5. It is slightly worse at point 4.

Figure 6.10 shows the comparison when an average of the temperatures at the side and centre of the room is used. The comparison is better than that for the central temperatures but worse than for using those at the side.

Overall using the temperatures at the side of the room adjacent to the test wall gives the best prediction of temperatures through the wall. The temperature plot used is far more significant than varying the emissivity or convection coefficients.

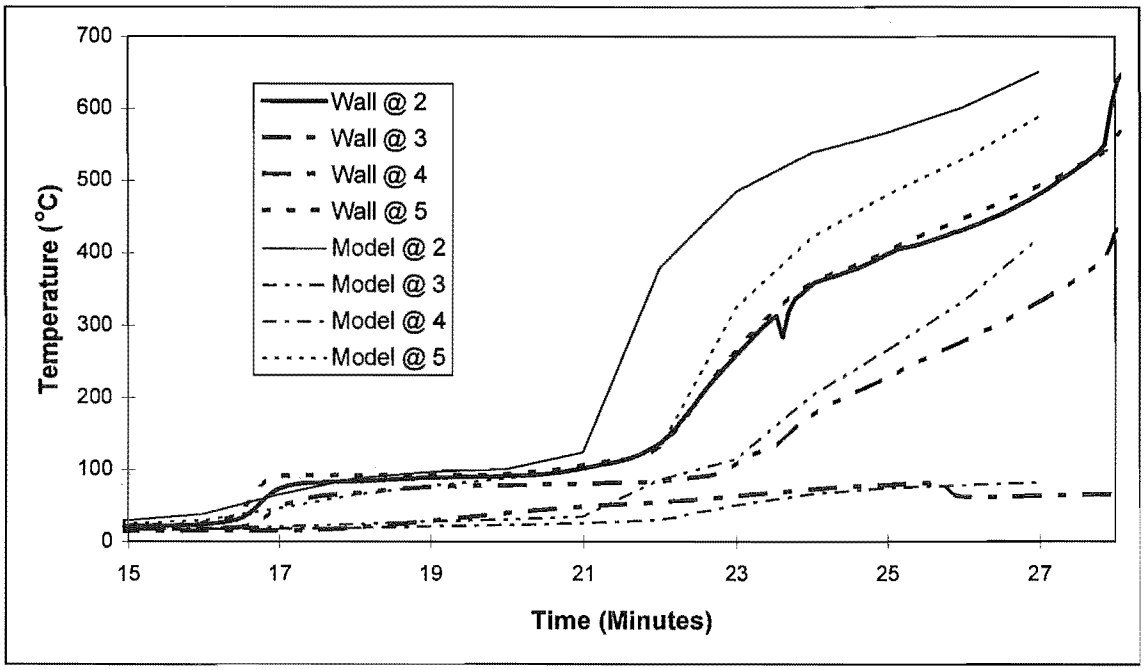

Figure 6.10 Temperature Profile Through Wall Using Average Temperatures

6.5.2 Within the Stud

The temperatures were measured with sheath thermocouples through the wall in locations 1, 2, 3, and 4 in Figure 6.3. Figure 6.11 shows the comparison between predicted and measured temperatures through the stud when the temperatures measured at the centre of the room are used as input to the finite element model of the wall.

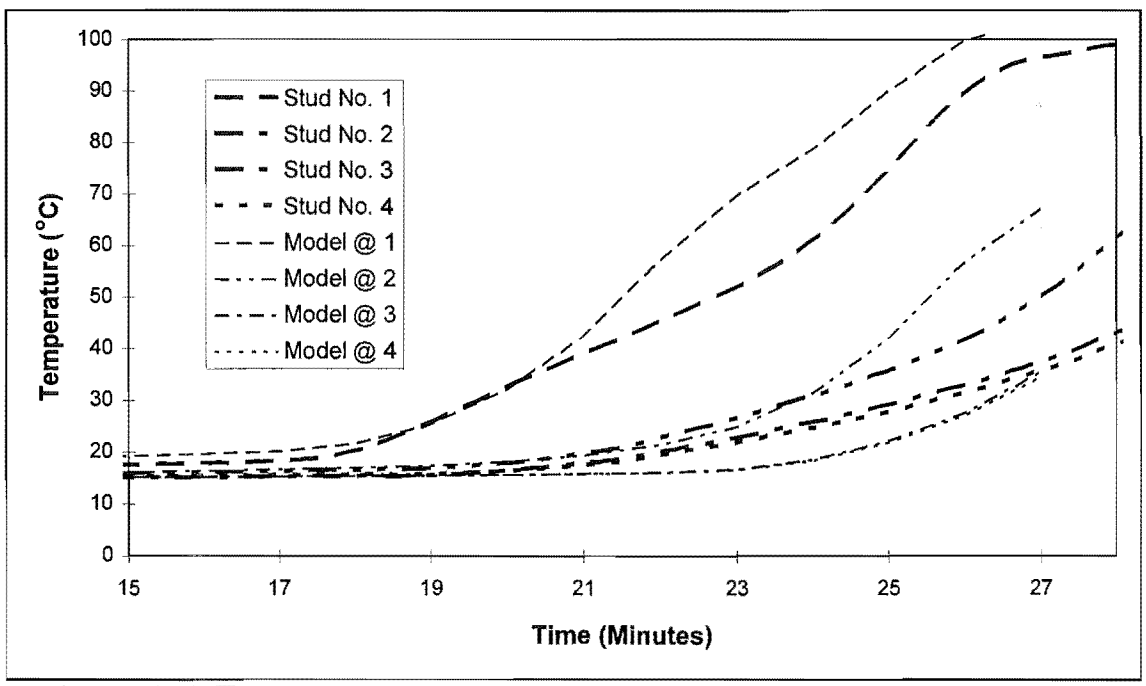

Figure 6.11 Temperature Profile Through Stud Using Central Temperatures

Overall the comparison is reasonable, being high at points 1 and 2 and low at points 3 and 4. The scale is much larger than Figures 6.8, 6.9 and 6.10 so the differences seem

larger in comparison. The actual difference between the measured and predicted temperatures is less than 15°C at most.

Figure 6.12 shows a similar comparison, but the temperatures at the side of the room are used as input to the wall model. The comparison is good at points 1 and 2 but poor at points 3 and 4. Points 3 and 4 are more significant in determining the strength of the stud.

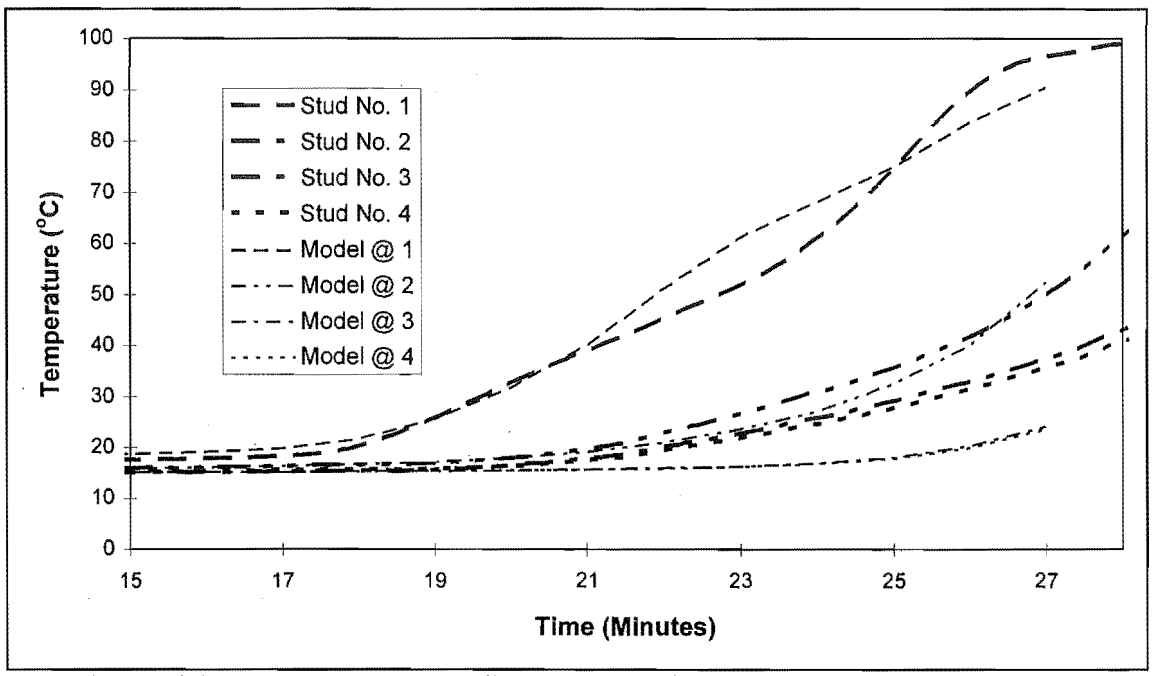

Figure 6.12 Temperature Profile Through Stud Using Side Temperatures

The temperature profiles through the stud when an average of the centre and side temperatures is used is shown in Figure 6.13.

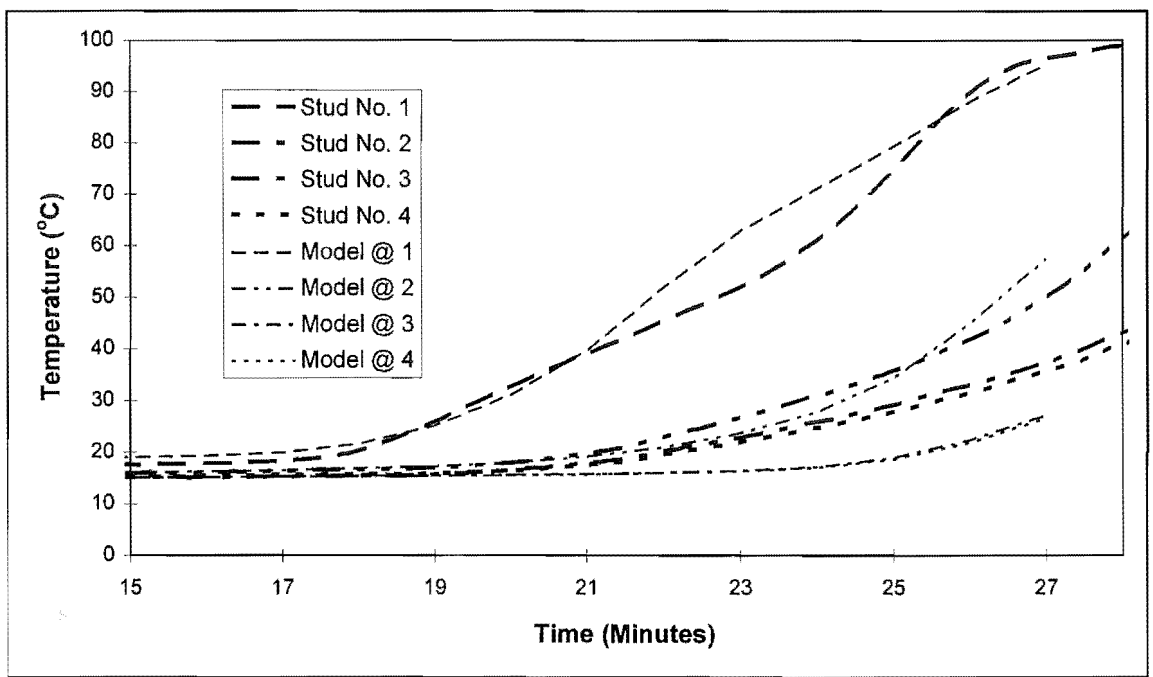

Figure 6.13 Temperature Profile Through Stud Using Average Temperatures

Again the comparison is good at points 1 and 2 and the predicted temperatures are low at points 3 and 4. There is little difference between using the side and average temperatures. Overall use of the temperature plot at the side of the room gives the best result for temperatures within the stud.

6.5.3 Summary

Using the temperatures recorded at the side of the results in the best overall prediction of the temperature through both the stud and the wall. This may be because the convection coefficient is dependent on the temperatures adjacent to the wall and with the sootiness of the smoke from incomplete burning of the timber, the wall will not "see" much of the radiation from the centre of the room due to absorption by smoke particles.

6.6 Conclusions

This experiment has raised several issues for the use of COMPF-2 and other single zone models to predict time-temperature curves:-

COMPF-2 and the assumptions made in this study appear to underpredict both the peak and average temperatures within the compartment, for this particular test.

The value of "BPF", the percentage of energy in the fuel released in the compartment has a significant effect on compartment temperatures and is the most critical value that must be assumed.

The emissivity or convection coefficient between the fire and the wall has little effect on temperatures in the wall.

The temperatures are not constant throughout the compartment, especially at early stages of a fast growing fire that reaches flashover very rapidly.

The test also had some scientific drawbacks:-

The impact of the test fire on the test wall is unknown because temperature readings were terminated before the maximum temperatures were reached, so the comparison of the severity between the predicted fire and the actual fire can not be made.

The prediction of temperatures through the test wall seems adequate, given that this was only one test and assuming some experimental error. This test is one of very few full scale test carried out on a large-scale light timber framed compartment that the author knows of. Other tests have generally involved the use of concrete compartments as the substrate for light timber framed walls, hence the characteristics of the compartment boundaries are different.

Mass loss rates and mass flows through the opening were not recorded.

Despite the lack of several fundamental measurements in the test, it has provided information that will be useful in devising future tests in lightweight compartments. It is highly desirable that more full scale tests should be carried out in compartments that are representative of real compartments in buildings that utilise lightweight construction, rather than the atypical concrete bunker often used in fire tests.

Chapter 7 Time Equivalence for Concrete and Steel Structures

7.1 Introduction

In the earlier part of the work with timber walls, it was found that the time equivalence formula for walls with only vertical openings (Thomas 1986) and the latest version (NZBIA 1992) underestimate the time to failure for timber walls. The formula are described below. It was also found that the dependence of the time equivalence on the fuel load is somewhat less linear than both versions of the formula would predict.

Recent tests in the United Kingdom (Kirby et al 1994) showed that for larger compartments the Eurocode formula was unconservative, underestimating the measured time equivalent by up to 82% in one test and was unconservative by a significant factor in the other eight tests they performed. They recommend modifying the formula to give longer time equivalents by increasing the value of the compartment lining parameter (Equation 7.1). The concept of time equivalence was developed originally by Law (1977) as an academic exercise. The author of this dissertation does not believe that it was intended to be used in design.

The alteration of the Eurocode formula to incorporate horizontal vents is apparently not supported by any published and refereed paper.

As a consequence of these factors it was decided to review the time equivalence for a selection of steel and concrete structural elements using computer modelling. This process is described in Section 7.2.

7.1.1 The Time Equivalence Formulae

The two formulae referred to in this Chapter are the CIB formula described in Thomas (1986) and the BIA formula, derived for use in the Eurocode (1993) and with modified

coefficients used in the New Zealand Building Code (NZBIA 1992). They are described in Section 1.1.

7.2 Methodology

This study used two computer models, to calculate the time equivalents of steel concrete and timber structures and compares the values found with the values calculated using the Eurocode and CIB formulas.

(i) A finite element model of steel, concrete and timber assemblies was developed using the TASEF program. This model was validated using test data.

(ii) A set of characteristic time-temperature curves for compartment fires were developed using the computer program COMPF-2, a post-flashover compartment fire model, allowing for the different thermal behaviour of the compartment boundaries.

(iii) The finite element model of the walls developed in step (i) were subjected to the time-temperature curves developed in step (ii).

(iv) The temperatures within the assembly found in step (iii) were compared with the temperatures from step (i) to obtain the equivalent time of exposure for each time-temperature curve.

(v) The equivalent time of fire exposure from step (iv) was compared with the BIA time equivalence formula.

7.3 Compartment Model Set-Up

The compartment fire was modelled using COMPF-2, a public domain single layer post-flashover compartment model. It is described in Chapter 2. Babrauskas (1979) outlines the coding for the program and the basis for the program is described by Babrauskas and Williamson (1978a, 1979). It uses a heat balance to calculate temperatures within a compartment. The pyrolysis rate is determined by four different sub-routines, allowing for crib fires, hydrocarbon pool fires, fuel bed controlled fires for objects of 2, 4 or 6 surfaces or by "pessimisation". Pessimisation results in adjusting a parameter to give

the worst possible result at that time given the other parameters. For example pessimising over the pyrolysis rate, results in the highest possible pyrolysis rate given the other parameters, so the pyrolysis rate is limited by the ventilation and the fire is ventilation controlled. Pessimising over the pyrolysis rate as done for this study will result in higher compartment temperatures, but the fire duration will be shorter. This may or may not be conservative.

7.3.1 Variables use in the COMPF-2 Compartment Model

COMPF-2 is described in Section 2.5. The exact variables used to give the time-temperature curves for the determination of the time equivalence of steel and concrete structural elements are the same as for the light timber framed walls, described in Section 5.3.1 and summarised below:-

(i) A range of opening factors (Equation 5.1) was used as shown Table 7.2.

WINDOW			Opening Factor	Ventilation Factor	Ventilation Factor
Height (m)	Width (m)	Area (m^2)	(Eqn 7) ($m^{1/2}$)	CIB (Eqn 1.2) ($m^{-1/4}$)	BIA (Eqn 1.3) (Dimensionless)
1.0	2.75	2.75	0.025	1.437	1.547
1.5	3.00	4.50	0.050	1.015	1.023
2.0	3.00	6.00	0.077	0.818	0.836
2.0	4.00	8.00	0.103	0.709	N/A
2.0	5.00	10.00	0.129	0.634	N/A
2.0	6.00	12.00	0.154	0.579	N/A

Table 7.2 Ventilation Parameters

(ii) The compartment size chosen is shown in Figure 7.1.

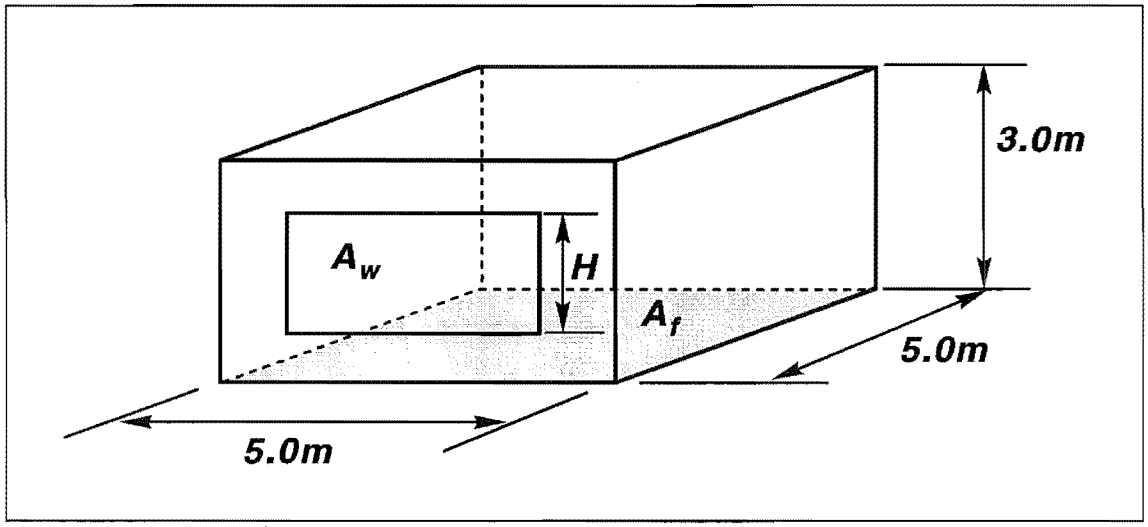

Figure 7.1 The Compartment used in the Model

The total floor area is 25 m^2 and the total bounding surface area is 110 m^2.

(iii) A range of fuel loads were used, with values of: 100, 200, 300, 400, 500, 600, 800 and 1200 MJ/m^2 of floor area.

(iv) Percentage pyrolysates burnt within the compartment will be 70%

(v) The fire will be ventilation controlled throughout. This was achieved by using the pessimising option over the pyrolysis rate.

(vi) The initial rate of temperature increase within the compartment was $100^{o}C$ per minute.

(vii) After the COMPF-2 time-temperature output stops, when the compartment temperature drops below $80^{o}C$; the temperature drops to $20^{o}C$ in 30 minutes and remains at $20^{o}C$ for 90 minutes.

7.4 Model Set-Up

The structures are modelled using the two-dimensional finite element heat transfer package, TASEF (Sterner and Wickstrom 1990). The failure criterion was defined as when the temperature of the hottest part of the steel section or the steel reinforcing reaches a critical temperature of $500^{o}C$.

There were two concrete structural elements modelled, one typical wall and one typical floor. Two steel elements were modelled, a steel I-beam supporting a 100 mm floor slab and a structural steel column. Both were protected with 16 mm Fyreline gypsum plasterboard. In addition four layouts of light timber framed walls protected with gypsum plasterboard were modelled earlier. Each assembly was subjected to a time-temperature curve, developed as described above.

7.4.1 Concrete Structures

The concrete structures are modelled as being in a compartment with concrete bounding surfaces. The thickness of the boundary is an average of the wall and ceiling thickness, weighted over the respective area of each. The density of the concrete is 2400 kg/m^3. The thermal properties of the concrete and steel used are the default values for enthalpy and conductivity used in the TASEF program. The heat transfer coefficients at the boundaries are shown in Table 7.3. The determination of appropriate values for the heat transfer coefficients was described in Chapter 3.

Position	ε	β	γ
Fire Side	0.9	5.0	1.33
Ambient Side	0.6	2.2	1.33

Table 7.3 Heat Transfer Coefficients for Concrete Structural Elements

7.4.1.1 Concrete Floor

The concrete floor was a 150 mm deep slab with 20 mm reinforcing bar at 300 mm centres.

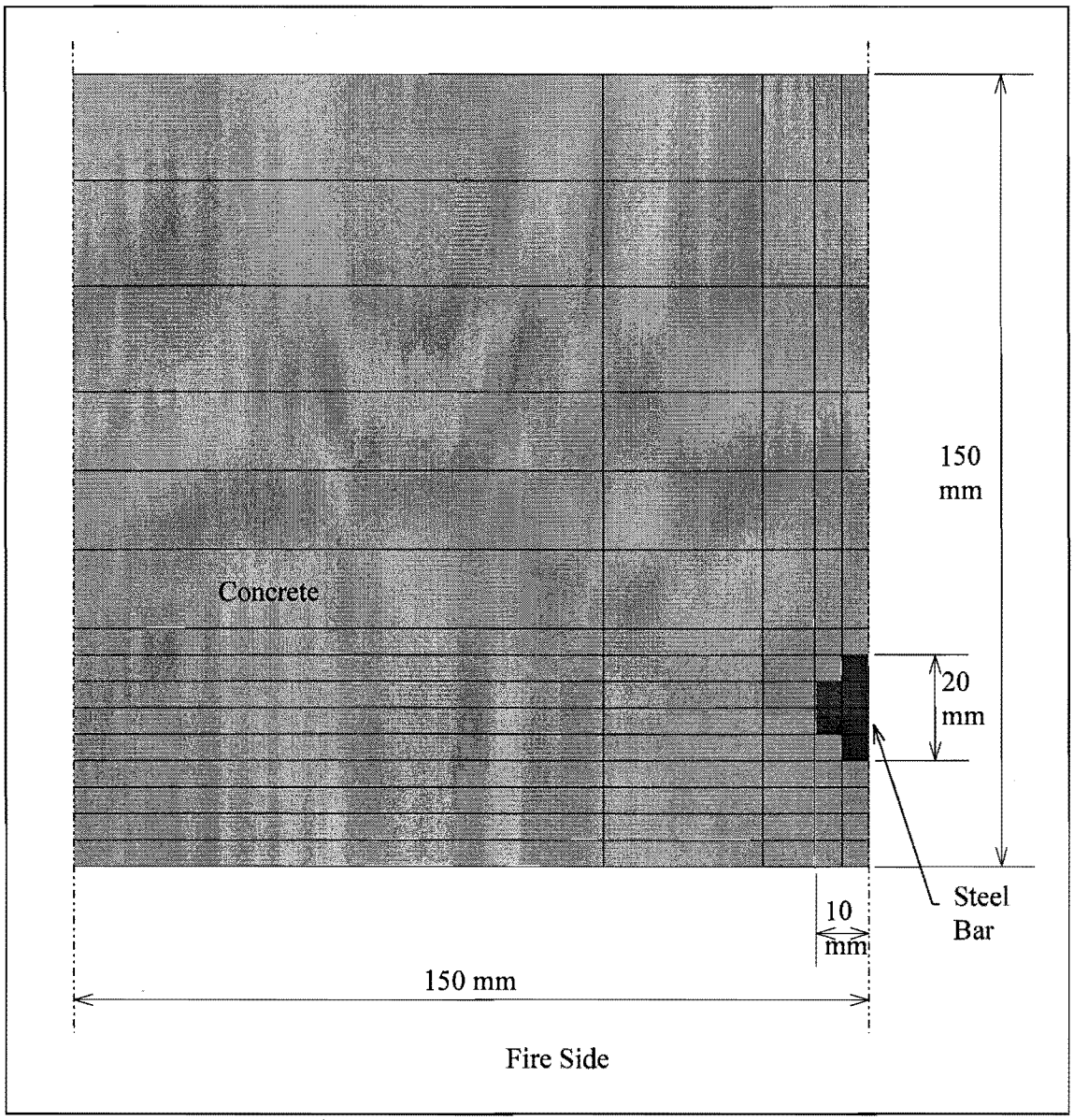

Figure 7.2 Layout of Concrete Floor

The bar has 20 mm of cover, as required in the New Zealand concrete code, NZS3101:1995 (SANZ 1995) for internal slabs. This is a reasonably common set-up for a suspended slab in New Zealand. The size of the reinforcing bar was not critical as it does not affect the temperatures of the bar significantly. The layout of the finite

element grid is shown in Figure 7.2. Symmetry was used to reduce the size of the model.

7.4.1.2 Concrete Wall

The concrete wall modelled is typical of tilt-slab construction often used in New Zealand for separation between multi-unit warehouse buildings and for low-rise apartment developments. These are typically 90 mm to 150 mm thick walls with reinforcing centrally located. In this case the reinforcing was a 20 mm reinforcing bar in a 100 mm thick wall giving 40 mm cover to each side. The layout is shown in Figure 7.3.

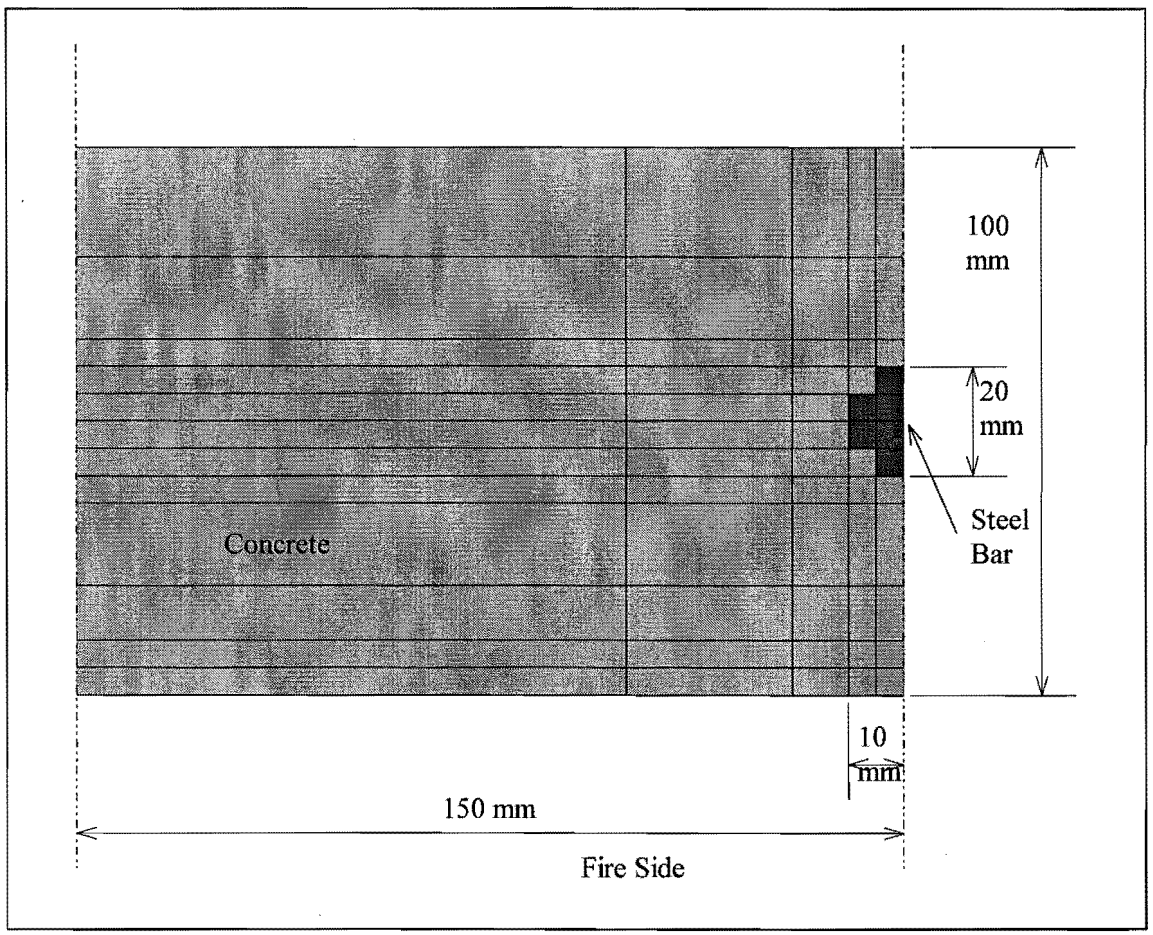

Figure 7.3 Layout of Concrete Wall

7.4.2 Steel Structures

The steel structures are modelled as being in a concrete walled compartment identical to that used for the concrete structural elements. The thermal properties of the steel used are the default values for enthalpy and conductivity used in the TASEF program. The values used for gypsum plasterboard are defined in Chapter 3. The heat transfer coefficients at the boundaries are shown in Table 7.4.

Position	ε	β	γ
Fire Side	0.9	5.0	1.33
Within the Void	0.8	1.0	1.33
Ambient Side	0.6	2.2	1.33

Table 7.4 Heat Transfer Coefficients for Steel Structural Elements

The value of emissivity used within the void was higher than that used for the light timber framed walls described in Chapter 3, because steel has a higher emissivity than wood.

7.4.2.1 Steel I-Column

The steel column modelled was a 250UC section, protected by a layer of 16 mm gypsum plasterboard. The column was isolated in the middle of the compartment and hence was exposed to fire on four sides. Symmetry was used to reduce the size of the finite element model and hence only one quarter of the column was modelled.

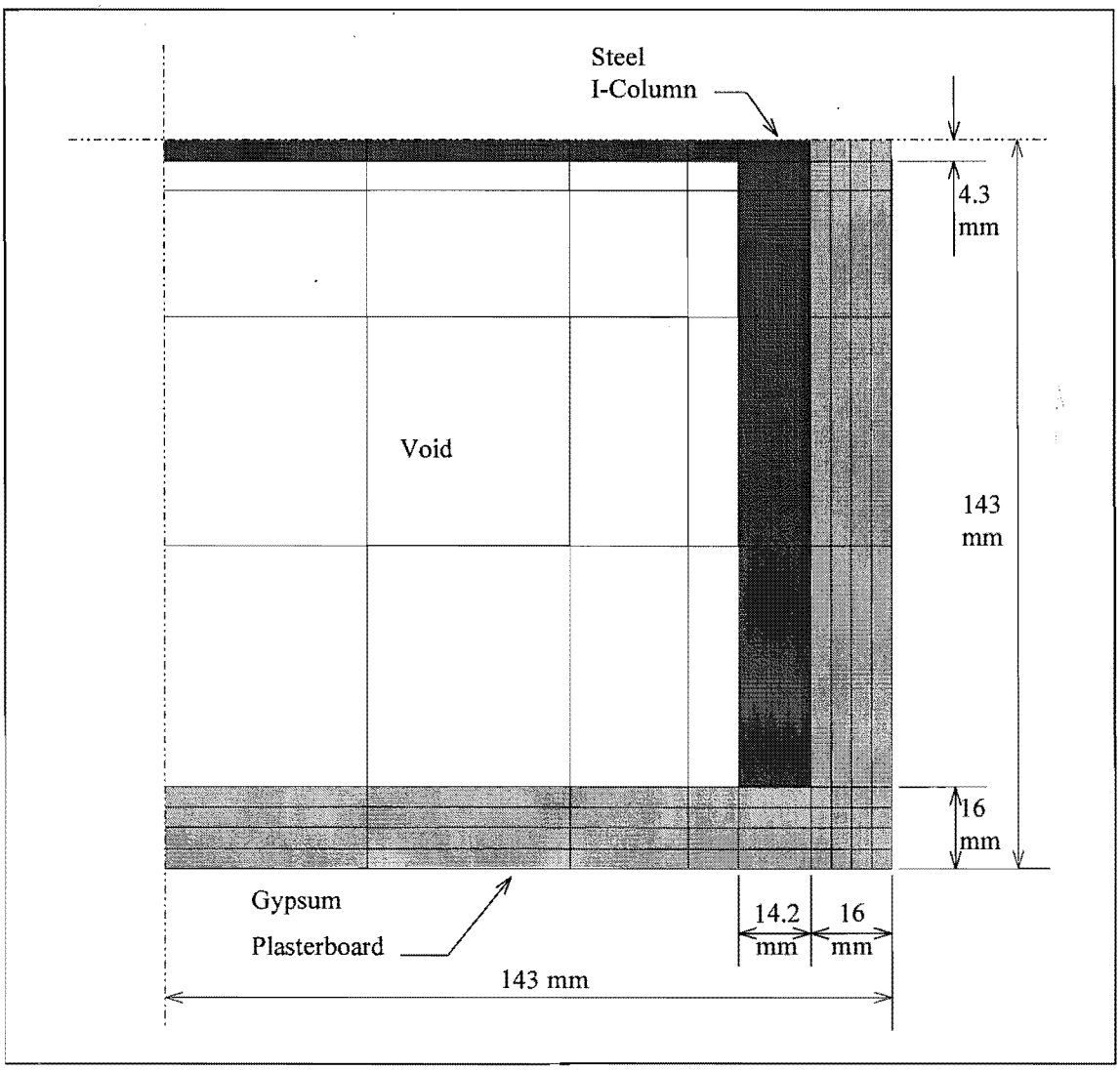

Figure 7.5 Layout of the Structural Steel Column

7.4.2.2 Steel I-Beam

The steel beam was a 360UB57 as shown in Figure 7.4.

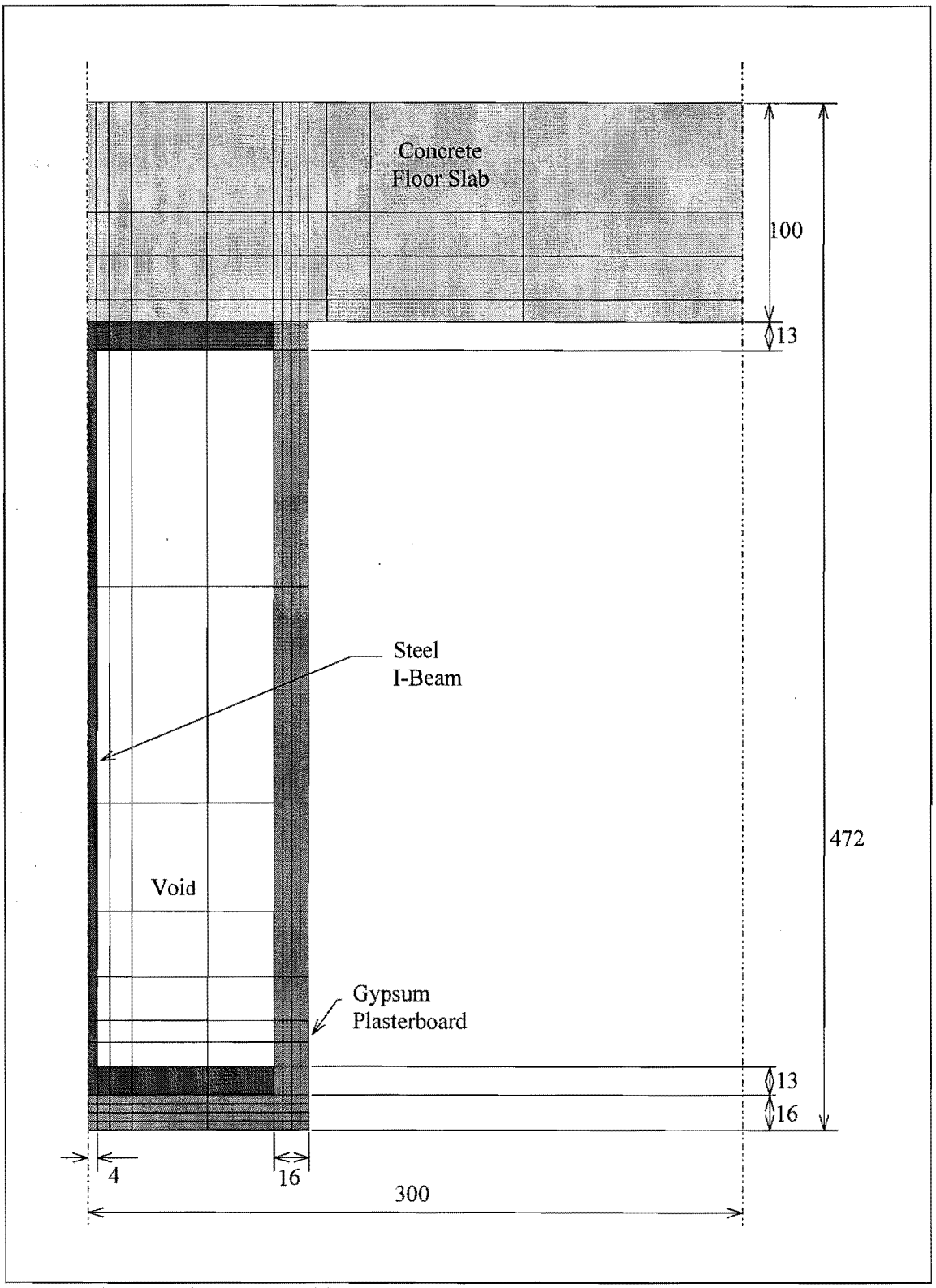

Figure 7.4 Layout of Structural Steel Beam and Concrete Floor Slab

The beam supports a 100mm concrete slab and was protected by a layer of 16 mm gypsum plasterboard.

7.5 Results

When using the time equivalent formulae a value for the parameter **c** (Equation 1.3) must be chosen. This parameter accounts for the thermal behaviour of the compartment boundaries. It was therefore different for concrete and gypsum plasterboard lined walls. The value used for the steel and concrete structural members was that for a concrete lined compartment. A value of 0.07 was used for the CIB formula and 0.055 for the BIA formula. these values were originally found by fitting a curve to various compartment fire test results.

7.5.1 Concrete Walls and Floors

The time equivalent value found using the CIB formula is plotted against the time equivalent calculated using the modelling process described earlier in this Chapter and is shown in Figure 7.7.

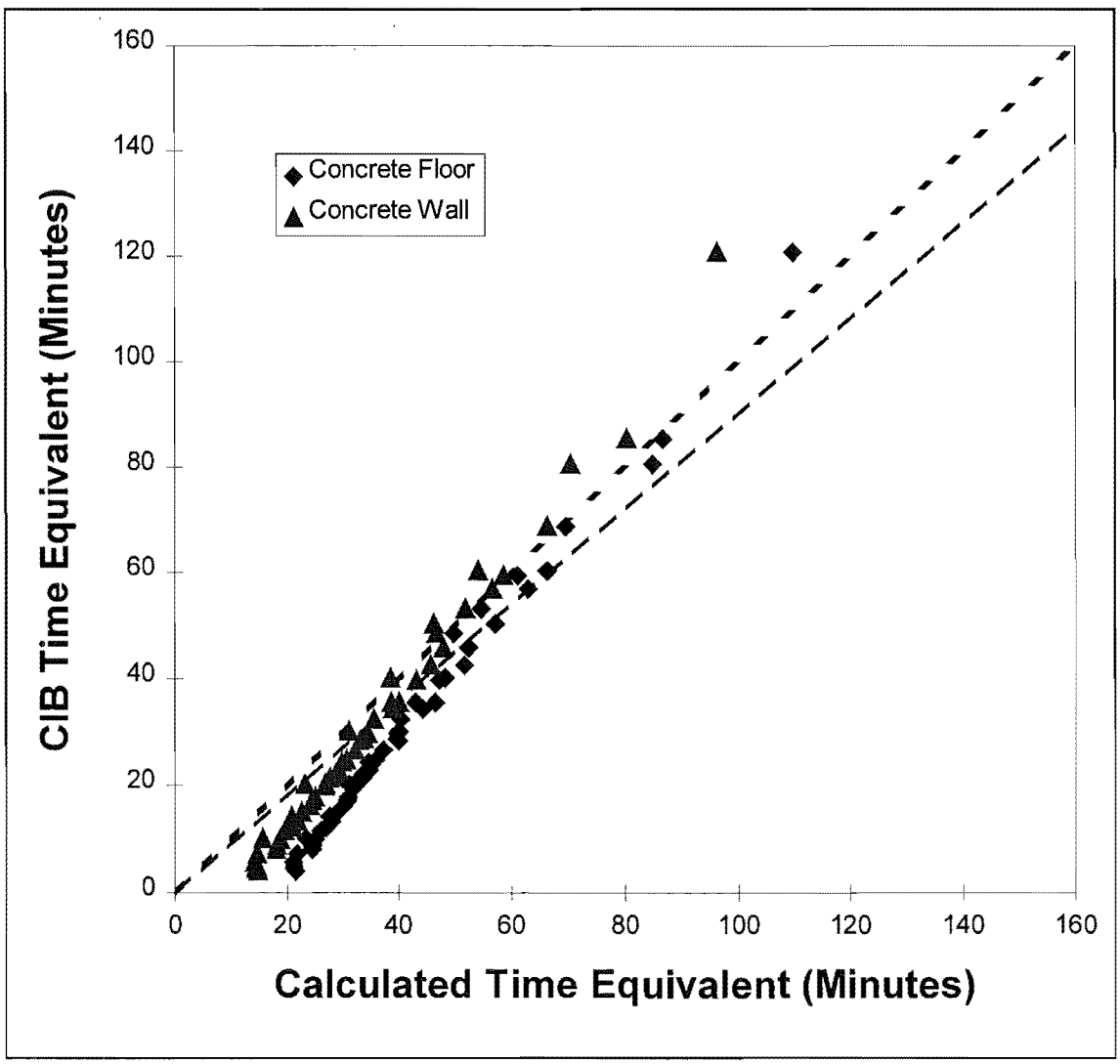

Figure 7.7 Comparison for Concrete Structural Elements

The dotted line shows a 1:1 relationship and the lower dashed line is a regression through the results. The slope of the regression is 0.90 on average. The 95 percentile slope was 0.96 and the 5 percentile was 0.84, with a correlation coefficient (R^2) of 0.87. On average the CIB formula overestimates the time to failure by 11%.

7.5.1.1 Comparison Using the BIA Formula

For the concrete lined compartment the regression of the comparison gives a slope of 0.80 on average. The 5 percentile was 0.75, with a correlation coefficient (R^2) of 0.80. On average the BIA formula overestimates the time to failure by 25%.

7.5.2 Steel Columns and Beams

Figure 7.8 shows the data points found using the model and the average regression line.

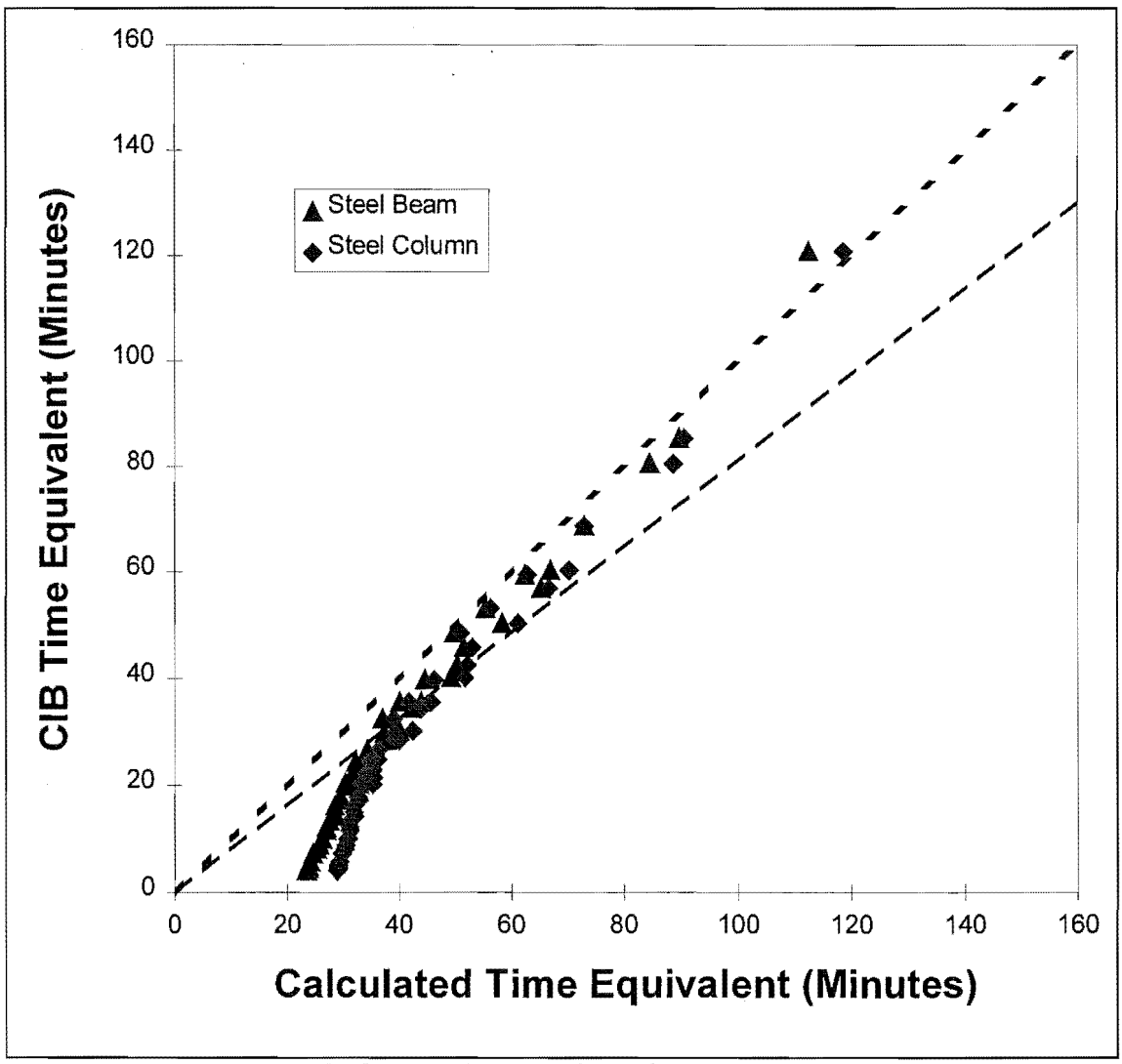

Figure 7.8 Comparison for Steel Structural Elements

For the steel structural elements the slope of the regression is 0.81 on average. The 95 percentile slope was 0.86 and the 5 percentile was 0.77, with a correlation coefficient (R^2) of 0.83. On average the CIB formula overestimates the time to failure by 16%. Both column and beam have a fire resistance rating (FRR) of one hour, hence the points around this region are of more interest. The poor agreement at low values of time equivalent may not occur if an assembly with a lower FRR is modelled, however a minimum FRR is desirable to allow for effects of local heating in fire plumes and ceiling jets. The fire severity would be higher in a compartment with light weight boundaries.

7.5.2.1 Comparison Using the BIA Formula

For the steel structural elements the regression of the comparison gives a slope of 0.70 on average. The 95 percentile slope was 0.77 and the 5 percentile was 0.66, with a correlation coefficient (R^2) of 0.87. On average the BIA formula overestimates the time to failure by 43%.

7.5.3 Effect of the Assumptions about the Time-Temperature Curve

It was assumed that the initial rate of temperature rise was 100°C per minute in the compartment and it takes 30 minutes for the compartment temperature to drop from about 80°C to 20°C, after the COMPF-2 output finishes. These assumptions are described in Section 7.3.1 and are due to limitations in COMPF-2. The effect of these assumptions were checked by removing the growth phase and the decay phase in turn and comparing the results with those found using both assumptions. The results from this analysis are tabulated in Table 7.5. This decay phase should not be confused with the changes made to the heat release rate towards the end of the fire in the next Section.

Structural Type	Desription	Average	95 percentile	5th percentile
Concrete	Normal	0.90	0.94	0.86
Concrete	No Growth Phase	0.93	0.97	0.90
Concrete	No Decay Phase	0.90	0.94	0.86
Steel	Normal	0.81	0.86	0.77
Steel	No Growth Phase	0.83	0.88	0.79
Steel	No Decay Phase	0.81	0.86	0.77
Average	Normal	0.85	0.82	0.88
Average	No Growth Phase	0.88	0.85	0.91
Average	No Decay Phase	0.85	0.82	0.88

Table 7.5 Effect of Time-Temperature Assumptions

Ignoring the assumption about the decay phase has little effect, merely an increase of 0.2-0.3% in the slope. Adding an initial rate of temperature rise to the time-temperature curve results in an decrease of about 3% in the slope. This was not significant given the accuracy of the method.

7.5.4 Effect of the Shape of the Decay Phase

The compartment post-flashover fire model as used in this study COMPF-2 does not allow for a decay phase. Since the pyrolysis rate was pessimised, it was at its ventilation controlled maximum until the fuel runs out. Real compartments contain a variety of fuel objects. These objects have differing fuel bed controlled burning rates. Many items and materials have such high fuel bed controlled burning rates that they will burn in a ventilation controlled manner. Some items will burn more slowly, resulting in a decrease in the heat release rate towards the end of the fire. Magnusson and Thelandersson (1970) looked at this problem. They altered the temperatures within the decay phase in order to produce different shaped decay phases. The decay phases they used are shown in Figure 7.10.

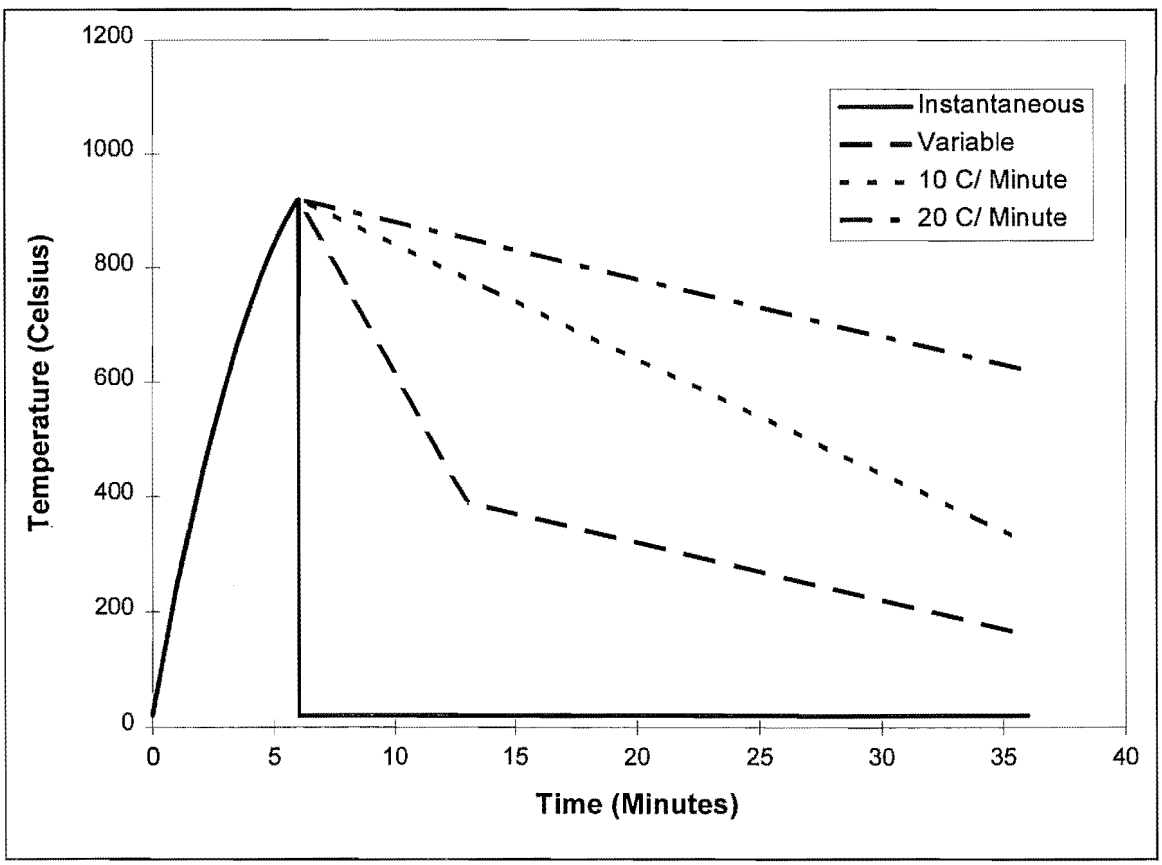

Figure 7.10 Decay Phases used by Magnusson and Thelandersson (from Magnusson and Thelandersson 1970)

It is not possible to get such long decay phases as shown here, if the fuel has burnt. If the temperature is to be maintained at such high levels then some burning must still be taking place. There is simply not enough energy within the heated boundary slabs to give such slow rates of cooling within the room. These decay phases therefore imply a different fuel load for each different shaped decay phase.

A better way of comparing decay phases is to reduce the pyrolysis rate and use a heat balance to calculate the resulting temperatures. This was done in this study by modifying COMPF-2. The pyrolysis rate was assumed to be constant until two thirds of the fuel was consumed. After this point two different decay phases were considered. A linear decrease in the pyrolysis rate, with a decay time double that required for the remaining fuel to burn at the ventilation controlled rate. An inverse time squared decrease in the pyrolysis rate was also used with a decay time treble that required for the remaining fuel to burn at the ventilation controlled rate. The temperature histories resulting from the COMPF-2 analysis of the three different pyrolysis rates are shown in Figure 7.11.

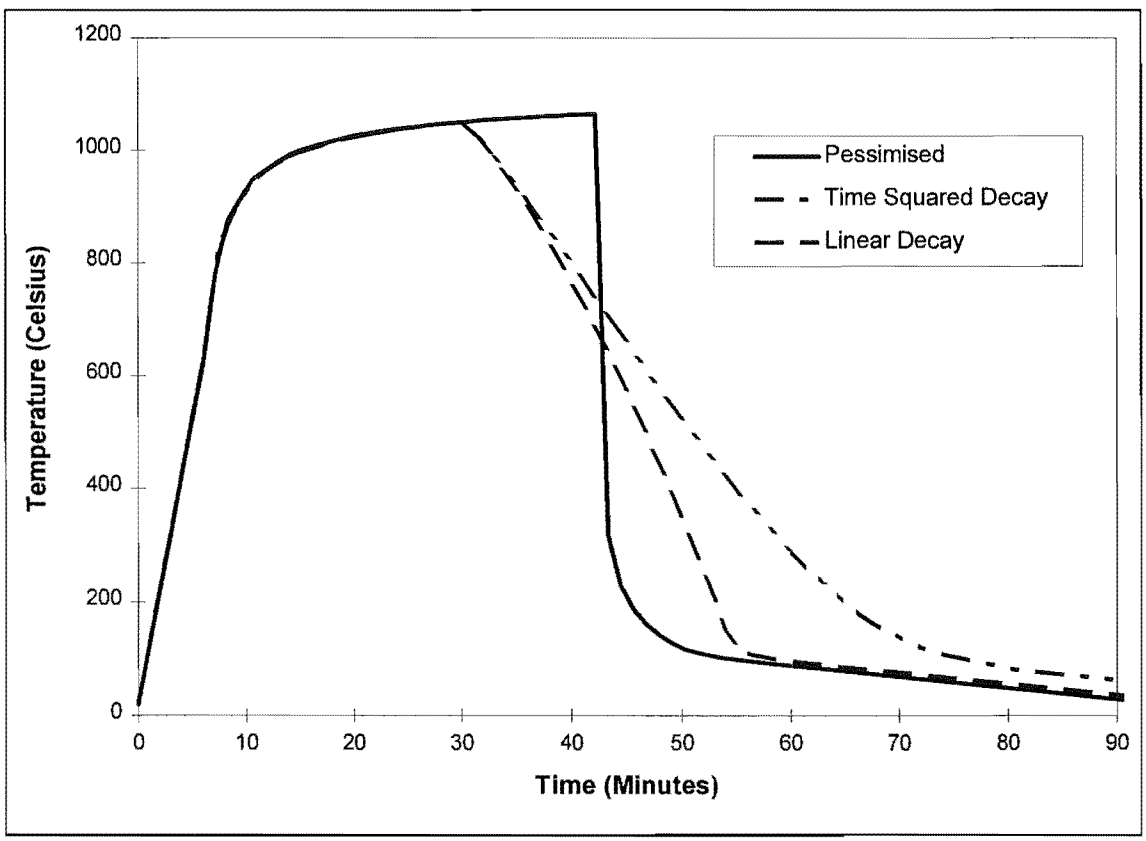

Figure 7.11 Shape of Decay Phases

Ideally the ratio of the fraction of pyrolysates burnt within the compartment to those released should be increased from 0.7 at the start of the decay phase to about 0.85 at the end of the decay phase. This is because the fire is no longer ventilation controlled in the

decay phase. Earlier work (Chapter 5) showed that varying this ratio over the length of a fire did have a significant effect on the comparison with the formula, especially for longer fires, however it will not be significant for a short period at the end of the decay phase. A value of 0.7 was used in Chapter 5.

The effect of the shape of the decay phase is summarised separately for steel and concrete structural elements.

7.5.4.1 Concrete and Steel

Table 7.6 summarises the effect of the shape of the decay phase on the time equivalent. The shape of the decay phase has little effect on concrete structures. The linear decay phase reduces the slope of the regression by less than 1% and the t^2 decay phase increases it by less than 1%. This was not the case for steel structural elements. The linear decay phase reduces the slope by about 12% and the t^2 decay phase by about 11%.

Structural Type	Desription	Average	95 percentile	5th percentile
Concrete	Normal	0.90	0.94	0.86
Concrete	Linear Decay	0.89	0.94	0.85
Concrete	t^2 Decay	0.91	0.95	0.86
Steel	Normal	0.81	0.86	0.77
Steel	Linear Decay	0.71	0.74	0.68
Steel	t^2 Decay	0.72	0.76	0.69
Average	Normal	0.85	0.88	0.82
Average	Linear Decay	0.78	0.81	0.75
Average	t^2 Decay	0.78	0.82	0.76

Table 7.6 Effect of The Shape of the Decay Phase on Steel and Concrete

The shape of the decay phase has a more significant effect on steel structural elements. This is because the temperature gradient through the insulation around a piece of steel has a high temperature gradient and the large mass of steel is a heat sink due to the high conductivity of the steel. Concrete has a high temperature gradient close to the surface, but this decays quickly further away from the surface. Hence most of the heat is lost back to the compartment after the compartment temperature starts to drop.

7.5.4.2 Decay Phase Recommended

The t^2 decay phase is recommended. The linear decay phase is less severe, but is more realistic given that the distribution of fuel is likely to be biased towards faster burning objects.

7.6 Conclusions

The time equivalent formulae used at present have been shown to be highly unconservative compared to this study and should be modified by increasing the coefficient **c** and by applying a safety factor. The scope of application of the formula should be severely restricted. It was originally designed for steel structural elements with light insulation and there is little or no research to back its extension to other materials. The performance of steel would have been found to be worse in a compartment with light-weight boundaries.

In most cases a more rigorous analysis should be performed.

Chapter 8 Calibration of the Structural Model with Bending Tests

The next stage in the development of the complete model, is the development of a structural model. Temperature dependent stress-strain relationships were developed using test data supplied by König (1991) as the basis for a finite element structural model.

8.1 Description of König's Tests

König tested timber beams in pure bending in a small furnace (Figure 8.1).

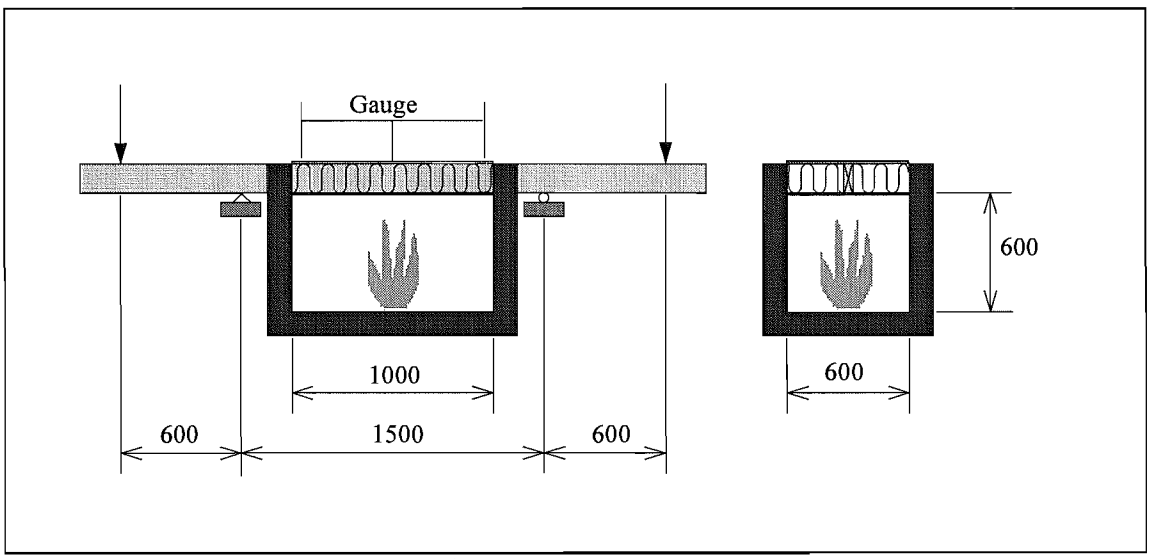

Figure 8.1 Layout for König's Tests

The beams are clad in gypsum plasterboard that is slit in the direction across the beam in order to avoid composite action in bending. Most of the tests were carried out with no lining on the fire side, however for one series, series 2, the beam was clad with plasterboard on the fire side. The cavity is filled with rock wool. This is normal practice for exterior walls in Sweden.

The vertical mid-span deflection was measured by König during his tests over a horizontal gauge length of 900 mm and the horizontal deflection was measured over this length as well. These two values enable the position of the neutral axis to be calculated.

Reference tests were also carried out to determine the capacity of the beams under cold conditions. The fire tests were carried out for various values of the load ratio. The load ratio is the applied load as a ratio of the predicted ultimate strength under cold conditions. Tests were carried out on three sizes of stud, some with the fire exposed side of the stud in compression (Figure 8.1) and others with reverse loading, with the fire side in tension. The first case is more important to a study of walls as the fire exposed side is normally in compression. This is because the exposed side shrinks as the moisture evaporates, causing the stud to bend away from the fire. König supplied data from the tests outline in Table 8.1.

Test Series Number	Width (mm)	Depth (mm)	No. Tests	Stress State on Exposed Side	Further description
S1	45	145	12	Compression	
S1a	45	145	13	Compression	Increasing of load
S2	45	145	9	Compression	Lining on exposed side
S3	45	145	15	Tension	
S3a	45	145	13	Tension	Increasing of load
S4	45	95	12	Compression	
S5	45	95	15	Tension	
S6	45	195	12	Compression	
S7	45	195	12	Tension	
P	45	145	2	-	No external load
T	45	145	2	-	No external load

Table 8.1 Summary of König's Tests

Data was supplied from 117 individual tests. The results from series 1a and series 3a do not vary significantly than those for series 1 and 3 respectively.

8.2 Material Properties for the Structural Model

For this model the properties that are required are the strength and stiffness of timber in compression and tension parallel to the grain. These properties are dependent on the moisture content, temperature and time.

8.2.1 Data on Mechanical Properties

In a piece of timber heated by fire, the temperature varies with time as the temperature of the fire changes and the heat penetrates more deeply into the wood. Both strength and stiffness are reduced by increasing temperature, but more so in compression than tension.

Gerhards (1982), gives a summary of available information on the effect of moisture content and temperature on mechanical properties. There is a great deal of variability and no tests were done on timber with high moisture content and high temperature. No tests are known to the author on the quantification of the effects of steam on timber.

Glos and Henrici (1991) carried out tests on Norwegian spruce (picea abies) at 20°C, 100°C and 150°C. They reported the modulus of elasticity, the modulus of rupture, density and moisture content at each temperature. The specimens tested at high temperature had low moisture contents of 10% or less. They conclude that "the effect on the strength properties of structural timber of common sizes and quality is less pronounced than reported in previous research papers". They also state that "the effect of temperature on the elastomechanical properties of the wood appear to be stronger with higher moisture content than with lower moisture content". The low moisture content at high temperatures in their tests highlights the difficulties of testing wood at high moisture content and high temperature.

The moisture content also changes with temperature and time. As a piece of wood is heated, the moisture is evaporated, some of this moisture is lost, but most is driven further into the wood. This moisture then condenses, increasing the moisture content at that point, often up to 30% moisture content. A moisture content of 30% is at or about the fibre saturation point for many species of timber. Increasing moisture content (up to the fibre saturation point) decreases wood strength and stiffness. At the fibre saturation point therefore, the strength and stiffness of wood is a minimum as a function of moisture content.

Steam affects wood significantly; it greatly reduces the stiffness of wood in compression, and possibly the strength as well. This phenomenon is used by woodworkers to bend wood while exposing it to steam. It was used by König (1991) and Young and Clancey (1996) to explain some of the observations they made of their

tests. These observations and the significance of them will be described later. This loss of stiffness due to the presence of steam can be thought of as creep as it is time-dependent.

In theory it is not difficult to measure the strength of a piece of timber at high temperature and high moisture content, but in practice it is difficult to ensure that the timber is at the same moisture content and temperature throughout. Assumptions have to be made about the temperature. Thermocouples can not be inserted in a piece of timber without affecting the timber's strength or thermal properties. Moisture content is more difficult to maintain or measure than temperature. Measuring or maintaining the concentration of steam is even more difficult. Even if these problems were overcome, the effects of these transient parameters over a small area and a small period of time in a stud within a wall are likely to be significantly different to those in a small test specimen, with constant parameters over the cross-section and over time. The combination of these effects may be more or less severe than simple addition or multiplication of the effects would suggest.

Size effects are also significant. Timber is a non-homogeneous material. It is assumed to contain random defects that determine the strength of the material. In a larger area there is more likelihood of a defect than in a smaller area. In a stud in bending, only the extreme fibre is at the maximum tension stress and only a small part of the compression side at the maximum compression strength. The moisture content and temperature vary throughout the stud, hence the parts of the cross-section that are highly stressed are very small compared to those in axial tension or compression test specimens. Size effects are more significant in materials that exhibit brittle behaviour. Wood is brittle in tension and ductile in compression.

8.2.2 Method for Developing Model

Given the problems described above in accurately determining strength and stiffness as a function of temperature and moisture content in this study, the properties are determined by taking reasonable starting values and modifying them within reasonable limits in order to give a good correlation with König's tests.

The test data included time to failure for different load ratios, deflections as a function of time, and the neutral axis depth, (calculated from the vertical deflection and the

horizontal deflection of the top of the beam) as a function of time. The model was calibrated on all this data.

Five series of tests were used to calibrate and check the model. Series 1 and 3 were used to calibrate the model initially. Series 2 test specimens were protected by a layer of gypsum plasterboard on the exposed face, hence the temperature distribution is different. Series 2 was initially used to check the model, but the model was altered slightly after these results were compared. Series 1, 2 and 3 were for 145*45 mm beams. Series 4 and 5, with 95*45 mm beams, were then used to check the model, using the same parameters for both the thermal and structural model.

8.2.3 Strength and Stiffness

Mechanical properties referred to are the properties parallel to grain.

8.2.3.1 Strength and Stiffness at Ambient Temperatures

Initially the strength and stiffness in tension and compression and the stiffness must be determined at ambient temperatures. König carried out reference tests to determine the modulus of rupture of the specimens. A 145*45 mm stud has an average modulus of rupture of 56 MPa and a modulus of elasticity of 12.8 GPa. These are both higher than that reported by Glos and Henrici (1991), of 45.0 MPa and 11.5 GPa respectively. The ultimate strength for clear wood is greater in tension than compression (Bodig and Jayne 1982, Section 7.3.2). König used relatively defect free specimens in his tests (pers. com. König), hence it can be assumed that for the tests the ultimate tension strength is greater than ultimate compression strength. As the maximum tensile stress is an extreme fibre stress in bending, then size effects are not as significant as is the case when an in-grade specimen is subjected to pure axial tension. Compressive strength is little affected by defects and wood tends to be ductile in compression, hence size effects are less important in compression (Buchanan 1990).

The ratio of the axial compressive strength to the modulus of rupture for small clear specimens of some similar species (spruce, pine and fir) is about 0.5 to 0.6. In the model a value of 33 MPa was used for yield compressive stress, giving a ratio of 33/56 = 0.59. Once the yield compressive stress and the Modulus of rupture is known the

ultimate tensile strength can be calculated, by assuming that wood has a flat yield plateau and by equating the size of the compression and tension stress blocks at failure. This gives a value of 65 MPa for ultimate tensile strength. These values are consistent with observations König made of the reference tests, where yielding in compression was observed before failure in tension. This would not be the case if the ultimate tensile strength was less than the Modulus of rupture and the compressive yield stress greater.

A value of 12 GPa was used for the Modulus of elasticity at ambient temperatures and a value for Poisson's ratio of 0.045. As the specimens were unconfined, the Poisson's ratio does not affect the results.

The stress-strain relationship in compression is assumed to be bilinear. The second part is horizontal, that is the stress is constant after yield. It should actually be reducing with strain (Buchanan 1990), however this will not significantly affect the results and reduces the number of variables in the model.

8.2.3.1 Tensile Strength at Higher Temperatures

Gerhards (1982) shows a reduction in tension strength to 70% of ambient at 275°C and 50% at 290°C. These results are from two different researchers. One (Schaffer) predicts a slow decrease until about 200°C, and a rapid decay after that, whereas the other (Knudson) predicts a linear decay throughout the temperature range. Both of these results were for wood at 0% moisture content. The actual moisture content will vary from 0% at high temperatures to 30% in the band where steam has recondensed as the moisture is driven through the wood. Gerhards shows a decrease in strength of between 15 and 25% as the moisture content increases from 12 to 25%. On the hot sides of the stud, the moisture content will be about 12% until 100°C and reducing to 0% by 120-150°C as the stud dries out. Further into the stud the moisture content will be higher than 12% in the region that is between about 70°C and 100°C, due to moisture that recondenses. These moisture effects are difficult to quantify and the drying out of the timber compensates for the loss of strength due to temperature increases. It is therefore assumed that up to 100°C, the strength is the same as at ambient temperatures.

8.2.3.2 Compressive Strength at Higher Temperatures

The reduction in yield compressive strength as a function of temperature is between 75 and 90% of ambient at 300°C. As a function of moisture content it reduces by 35-70% as the moisture content increases from 12 to 30%. Where steam is present the stiffness

and/or strength is low, hence this material does not carry significant load. Steam will be present when temperatures are above about 80°C and up to 120°C. It is therefore assumed that wood has no significant strength over about 80°C.

8.2.3.3 Stiffness at Higher Temperatures

The reduction in the modulus of elasticity is about 20-30% at 180°C and between 35 and 80% at 250°C (Gerhards 1982). As a function of moisture content it reduces by 15-20% as the moisture content increases from 12% to 28%. For bending tests, the modulus of elasticity found would be an average effective value, including the loss of stiffness in compression due to the effects of steam. Effective stiffness is defined as the stiffness that includes time-dependent effects such as a loss in stiffness in compression due to the presence of steam. The effective stiffness may therefore be different in compression and tension, which is not the case for "true" stiffness.

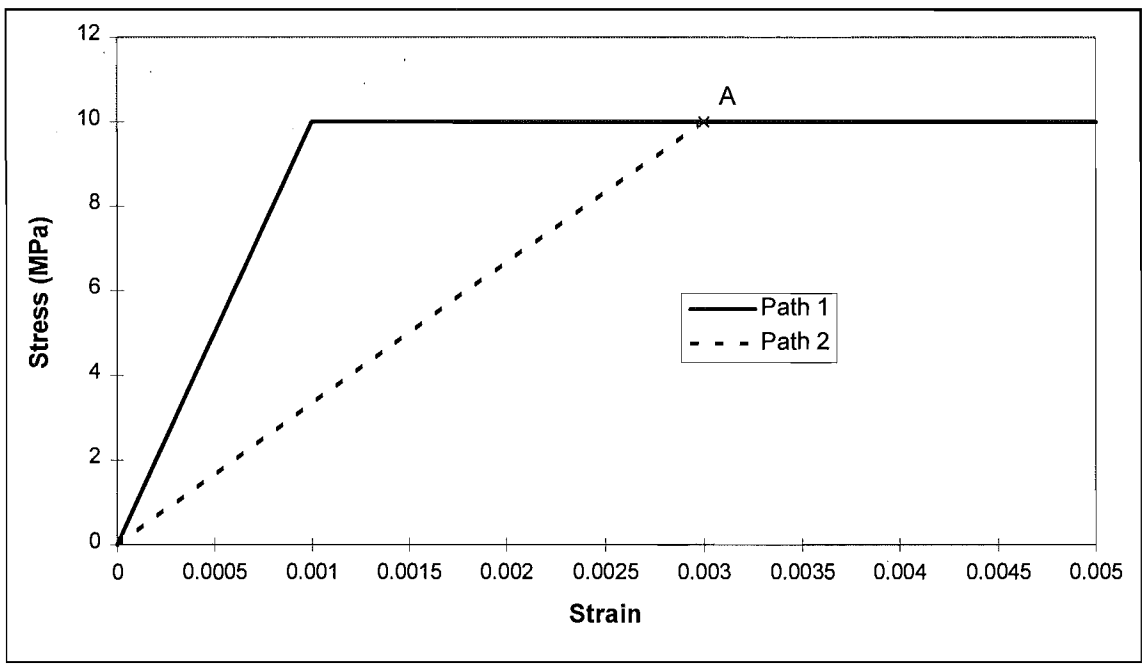

Figure 8.2 Stress-Strain States

Stiffness and strength must be considered together in this model, as a low effective stiffness implies low capacity of part of the material since adjacent parts have a higher stiffness. Since the model is not time-dependent, the stress-strain state that is reached is more important than the path by which this state was reached. For example in Figure 8.2, the state at point A is of far more significance than whether it was reached via path 1 or path 2.

Calibration of the model allowing for the effect of steam was achieved using the values for stiffness as shown in Table 8.2.

Tension		Compression			
Temperature	Percentage of Ambient Value	Temperature	Percentage of Ambient Value	Temperature	Percentage of Ambient Value
20	100	20	100	100	40
300	60	60	60	300	4

Table 8.2 Reduction in Modulus of elasticity (Stiffness) with Temperature

With an initial value of 12800 MPa found from König's reference test the values used are shown graphically in Figure 8.3.

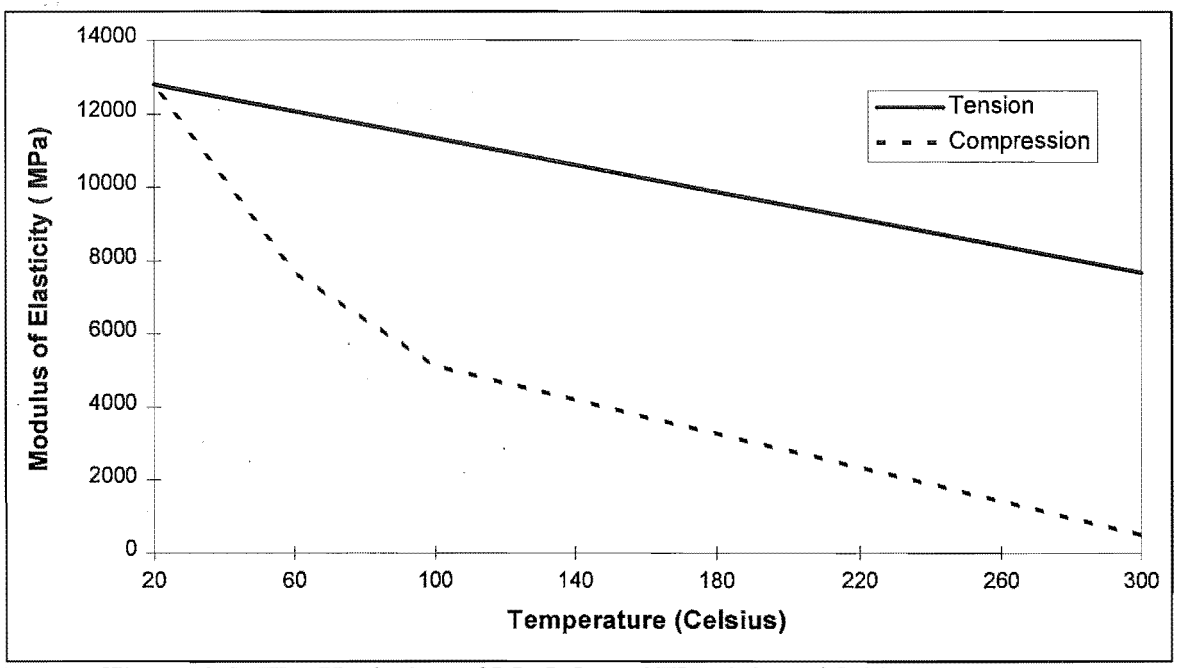

Figure 8.3 The Variation of Modulus of Elasticity with Temperature

The reduction of the modulus of elasticity with temperature is somewhat greater than that found by Glos and Henrici (1991). This can be attributed to the effects of very high moisture contents at high temperature as the moisture front is driven through the wood.

8.3 Thermal Model

The thermal model described in Chapters 3 and 4, had to be modified for these tests. The geometry of the assembly for most of König's tests is shown in Figure 8.4.

The studs are bigger and the cavity is filled with rock wool in König's test. In all of König's tests, except for series 2, there is no lining on the fire side of the assembly.

In series 1, 2 and 3 the studs are 145*45 mm. This is the size shown in Figure 8.4. Since the thermal and structural models are completely uncoupled there is no difference in the thermal model for series 1, with the fire side in compression and series 3 with the fire side of the stud in tension.

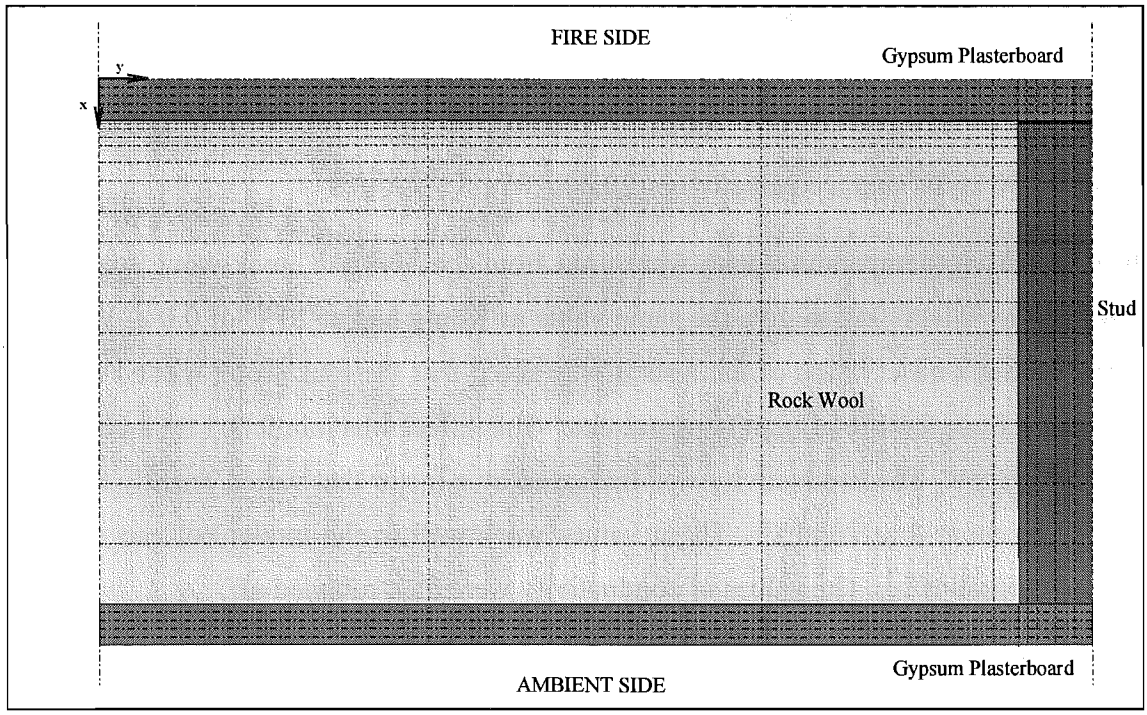

Figure 8.4 Layout of Grid for the Thermal Model

8.3.1 Thermal Properties of the Materials

A thermal model is required for these tests in order to provide a temperature distribution for input into the structural model. The thermal model must result in a good prediction of temperature in König's tests. The process of choosing values for the thermal properties of the rock wool in the beam tests is not as rigorous as for the materials in the wall model described in Chapter 3. Figure 8.5 shows the conductivity of the rock wool as a function of temperature.

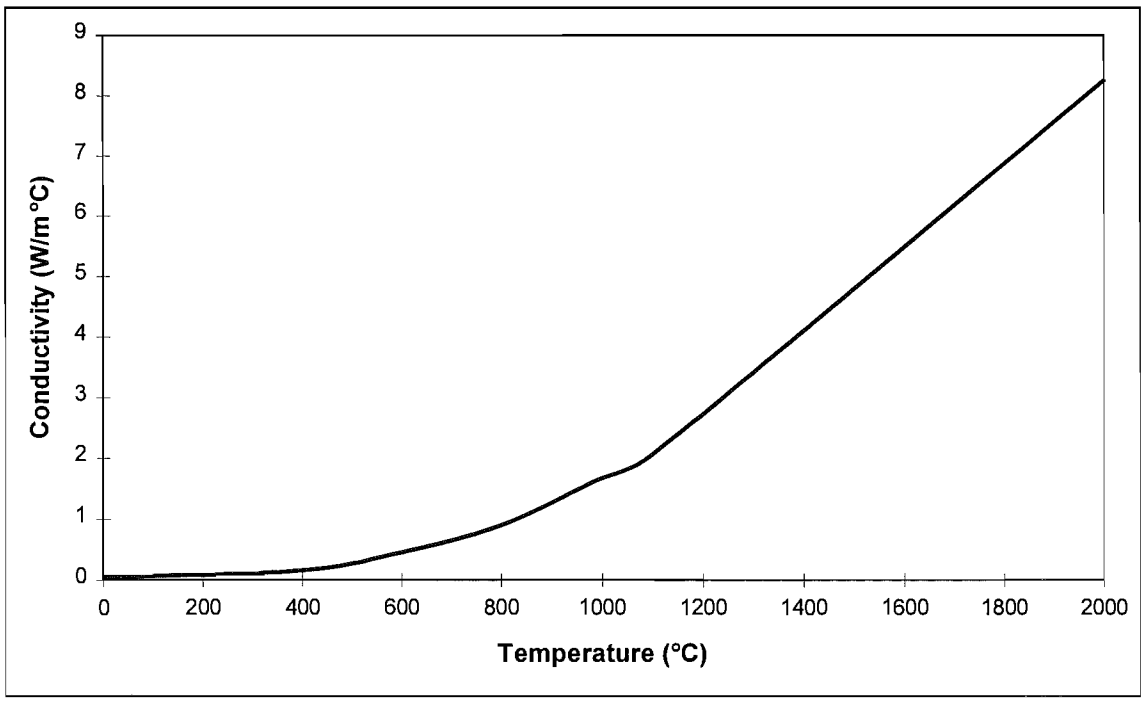

Figure 8.5 Conductivity of Rock Wool as a Function of Temperature

The values of conductivity and specific heat of rock wool are taken from the TASEF manual (Sterner and Wickstrom 1990) which has standard properties for rock wool of 50 kg/m^3 and 140 kg/m^3. König and Noren (1991) state that they used rock wool with a density of 30 kg/m^3 and a conductivity of 0.040 W/mK.

The conductivity-temperature pairs were used from the 50 kg/m^3 rock wool, but were multiplied by 0.04/0.042 to give the same value as König had at 20°C of 0.040 W/mK. During König's observation of the tests it was noted that the rock wool, melted and/or drew away from the fire at high temperatures. This effect was mimicked by increasing the conductivity. The conductivity was increased by a factor that varied linearly from 1 at 20°C to about 8 at 2000°C. These values work well in the model but can not be justified theoretically. The values of conductivity were then rounded off.

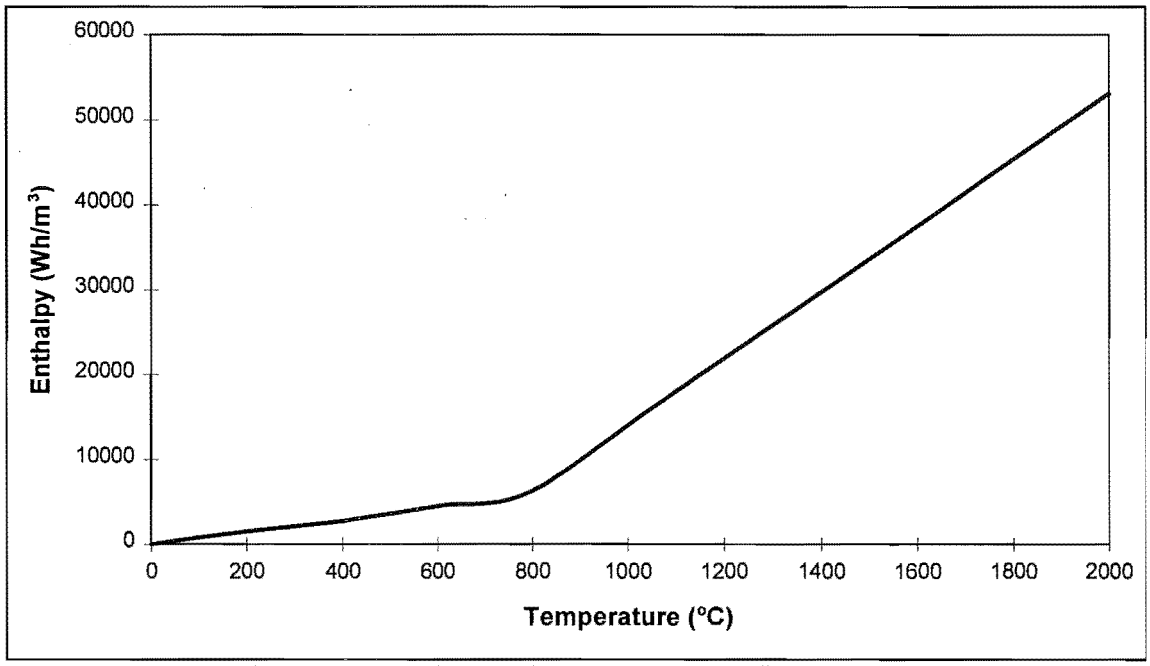

Figure 8.6 Variation of Enthalpy of Rock Wool with Temperature

TASEF utilises a specific volume enthalpy rather than separate inputs for specific heat and density. Specific volume enthalpy is the cumulative, piecewise product of specific heat, density and change in temperature. It is calculated piecewise because specific heat and/or density may vary with temperature. The standard specific volume enthalpy for 50 kg/m^3 rock wool is used, but multiplied by 0.6 as the density at 30 kg/m^3 is 60% of the standard material. The resulting specific volume enthalpy is shown in Figure 8.6.

8.3.2 Comparison of the Thermal Model with Tests

In König's tests there were thermocouples placed in the centreline of the beam as shown in Figure 8.7.

In series 1 and 3 there is no lining on the fire side of the beam, hence the region that is used to model the contact resistance between the lining and the stud (Section 3.10) is replaced by a region having the same properties as the rest of the timber.

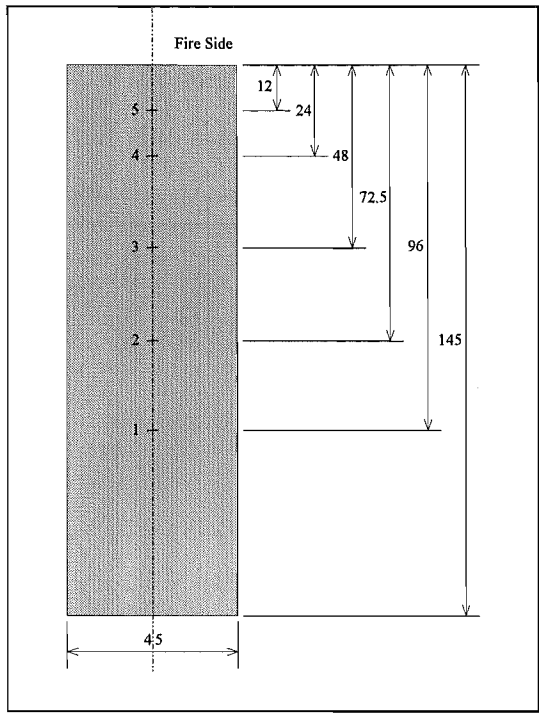

Figure 8.7 Location of Thermocouples in König's Tests

There were two sets of these thermocouples in each beam tested, however there were only eight channels were available for logging data, so locations 2-5 were used in short duration tests and locations 1-4 were used in longer duration tests. The finite element grid was modified slightly from the wall tests so that nodes were located at the points shown above in order to compare temperatures with the test results. The finite element grid used to input temperatures into the structural model are slightly different from that used to give the temperatures used to compare with temperatures from tests. The temperature distributions from these two model geometries are very similar.

8.3.2.1 Series 1 and 3 Tests

Figure 8.8 and 8.9 show temperature comparisons for two tests and the model at positions 1 to 4. The positions referred to are shown in Figure 8.7.

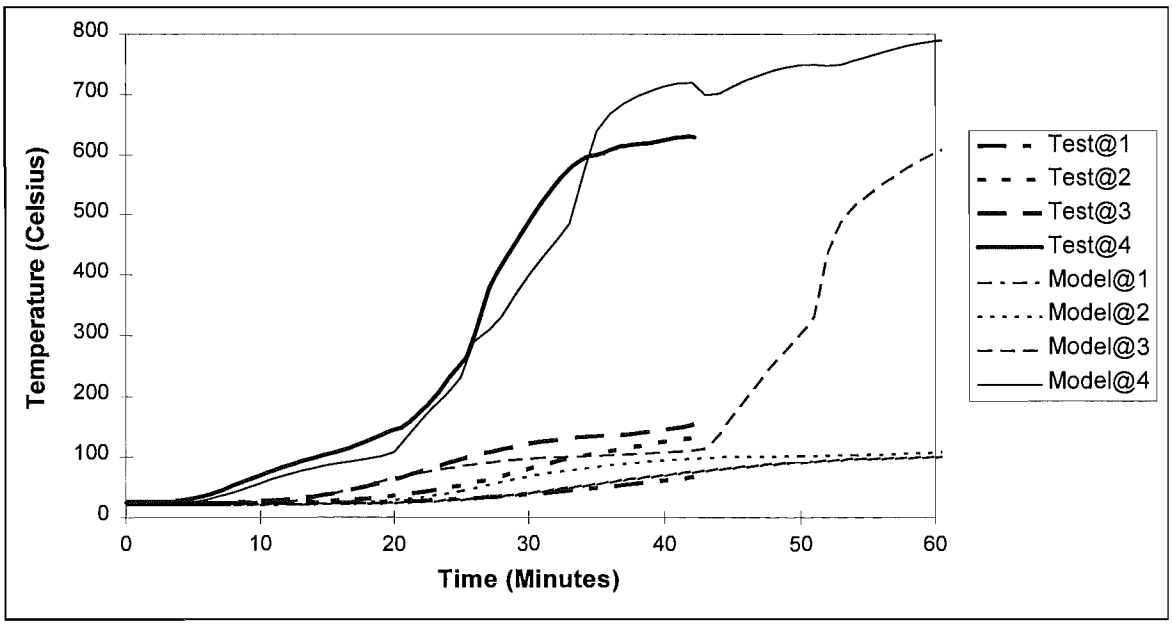

Figure 8.8 Comparisons of Temperatures for Test 204, Series 1

For both tests the temperature comparison is good at location 1, 96 mm into the stud and at location 4, 24 mm into the stud. The comparison at the other two points is good up until 20 to 30 minutes, but is only fair after that.

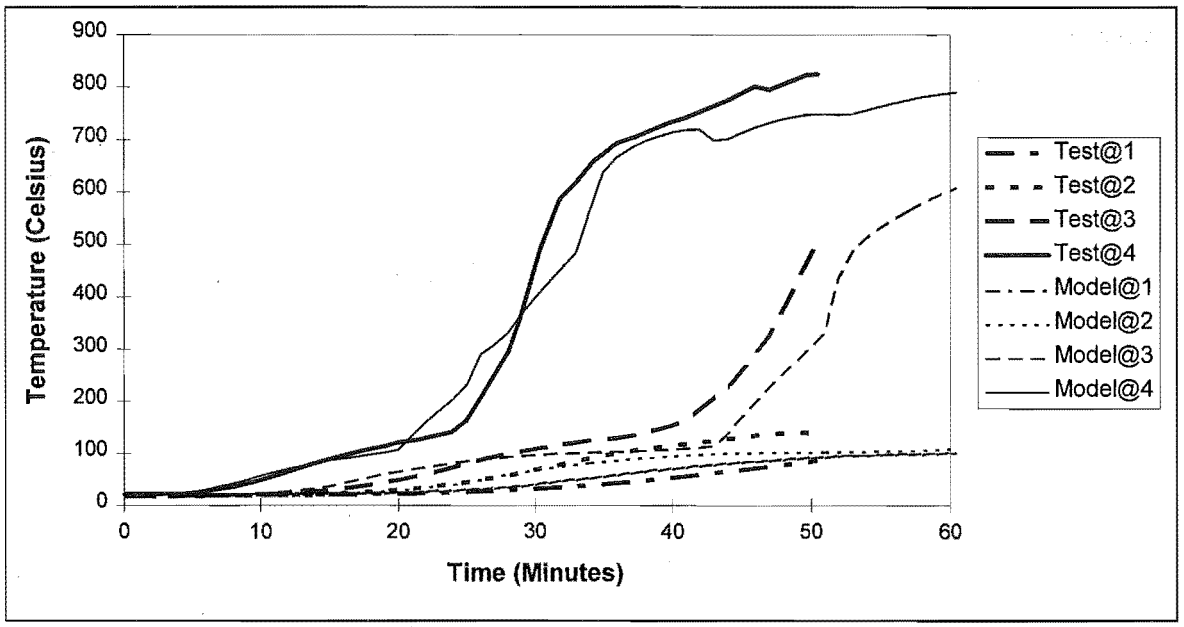

Figure 8.9 Comparisons of Temperatures for Test 222, Series 3

The comparison at positions 2-5 are shown in Figure 8.10 for a shorter duration test.

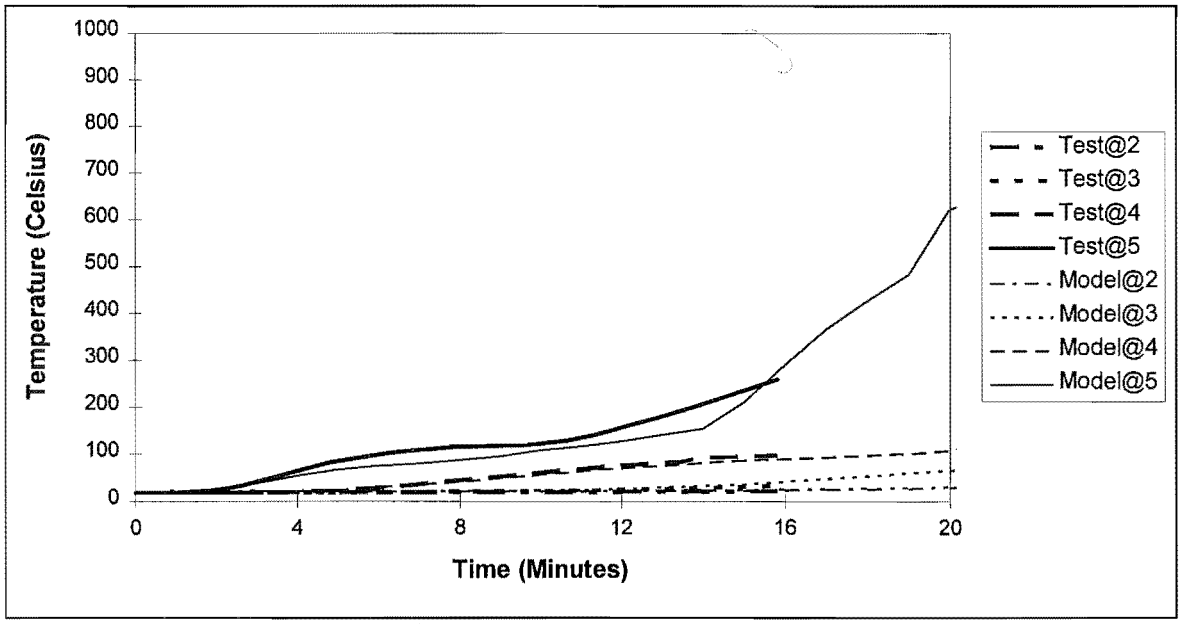

Figure 8.10 Comparisons of Temperatures for Test 209, Series 3

The comparison is good for the duration (15.8 minutes) of this test.

8.3.2.2 Series 2 Tests

In series 2, there was a lining on the fire side and the properties used in the thermal model are identical to those described in Chapter 3 except for the rock wool. The

properties of the rock wool are as used for modelling series 1 and 3 tests and described in Section 8.3.1. Figure 8.10 shows the comparison between test 209 and the model at locations 1-4.

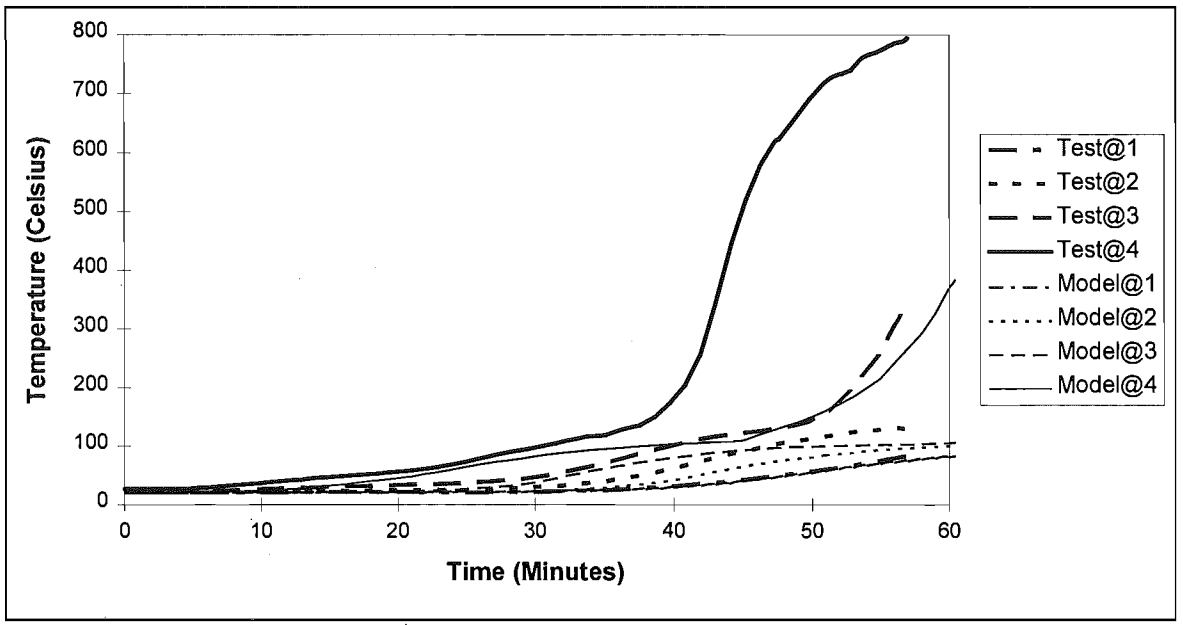

Figure 8.11 Comparisons of Temperatures for Test 209, Series 2

The comparison is reasonable for the first 40 minutes, and is only good at position 1 after that. However after 40 minutes significant charring will have occurred and the neutral axis will have shifted so far, that only the temperatures further than point 1 from the exposed face are significant. The comparison at positions 2-5 in another test is shown in Figure 8.12.

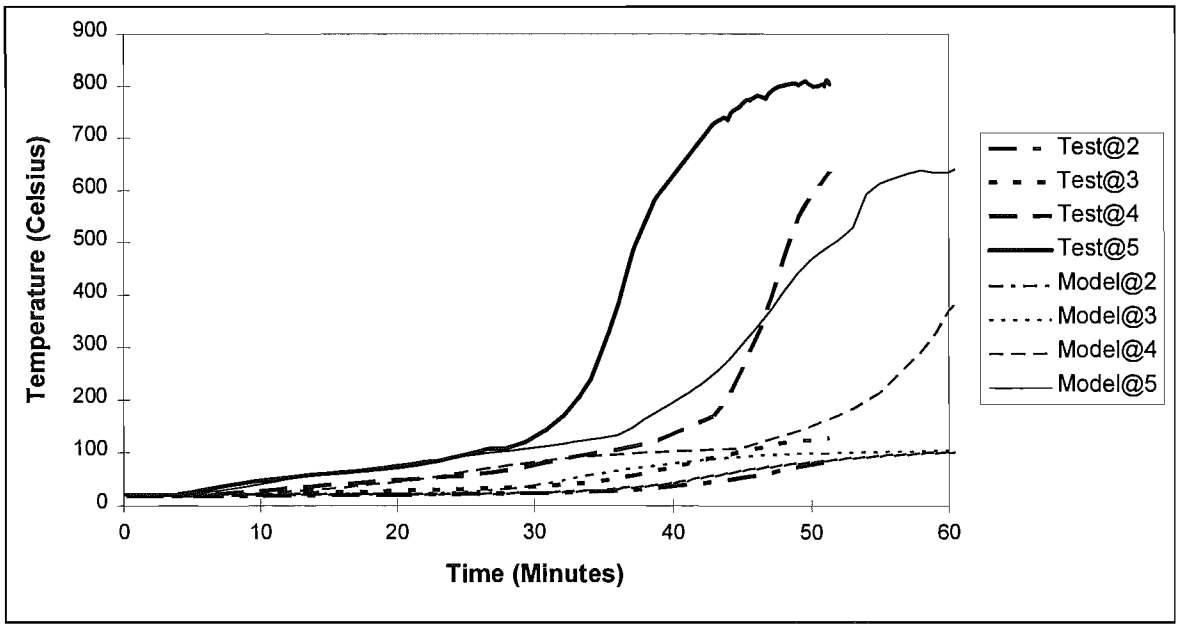

Figure 8.12 Comparisons of Temperatures for Test 205, Series 2

For this test the comparison at points 4 and 5 is good for only 30 minutes, but remaining good at position 2 and 3 for the duration of the test.

8.2.2.3 Summary of Comparisons Between the Thermal Model and Tests

Overall the comparison between measured and predicted temperatures is good for the series 1 and 3 and series 2 tests. The comparison is reasonably good at all points for up to 30 to 40 minutes. After this the model is only good for location 1 and possibly location 2. Locations 1 and 2 are 96 and 72.5 mm away from the exposed face of the stud and the temperatures at these locations are more significant after 30 or 40 minutes. After this time the hot portion of the stud is so hot it can no longer carry any significant stress, so it is not necessary for the temperature in this portion of the stud to be predicted accurately after about 30 minutes.

8.4 Structural Model

König's tests were modelled using ABAQUS (Hibbitt et al 1994) a general purpose finite element program, with time-dependent temperature fields developed using TASEF and input into the ABAQUS structural model. The structural model uses the stress-strain modules in ABAQUS. Symmetry was used to reduce the size of the model. It was assumed that lateral buckling of the compression edge of the beam does not occur, hence the beam is symmetrical over its breadth and only half the width of the beam is used. The beam is assumed to be restrained in direction across the beam and in rotation about the length and the depth of the beam by the cladding. The loading and restraint points are as shown in Figure 8.1, but as symmetry is used the model is 1350 mm long with the load at x=0, a support at x=700 mm and a restraint with all six degrees of freedom restrained at x=1350 mm. There are nodes at 50 mm intervals along the beam, hence the elements are 50 mm long. There are two elements across the beam (y direction) and half the thickness of the beam is used so the elements are 45/2/2 = 11.25 mm wide. There are 8 elements down the beam (z direction), which are 145/8 = 18.125 mm deep. The elements used are C3D8 three-dimensional solid stress-strain elements. These elements are strain governed, that is, the interpolation is carried out on the strain values and the stress calculated from the strain values using the stress-strain curve. The analysis is a static elasto-plastic routine which terminates when

deformations become excessive. The end of the model run occurs when lateral deflections start increasing at a very rapid rate, indicating an imminent failure.

A subroutine was written to input the time dependent temperature of the nodes in the fire-exposed middle portion of the beam. This subroutine is part of the ABAQUS input file and is compiled using an f77 Fortran compiler. ABAQUS then links the user subroutine to the ABAQUS main control routine along with any other subroutines that are used by the options specified in the input file.

The temperature profile is two-dimensional. Failure always occurred in the element set where the temperature changed abruptly from ambient in one cross-section to time-dependent in the next. This is due to sudden changes in the effective cross-section of the member at this point. As the beam is in pure bending with a constant bending moment, this is not significant. It is reasonable to assume that the temperature drop occurs over the length of one element, or 50 mm as the conductivity of wood is low. It is not practical to carry out a full three-dimensional heat transfer analysis of the system.

A drawback of ABAQUS is that the available material models all assume symmetric properties in compression and tension. For timber however, the yield strength in compression is lower than the ultimate tensile strength. Compression behaviour is elasto-plastic whereas the tension failure is brittle. This is overcome by using a different material in tension and compression. This means that the location of the neutral axis depth at failure must be checked to ensure that only tension material is on the tension side and compression material on the compression side. If the neutral axis is within an element, which is usually the case, then the strains, must be within or close to the elastic range in tension and compression, otherwise the part of the element that should be in the plastic range in compression may actually have failed in tension or vice versa. In compression, yielding is modelled by stipulating a yield stress. The failure strain is defined as 50 times the strain at first yield. In tension the strength reduces to near zero after the "failure" stress is reached This approach to the tensile strength does not affect the results, because when the low strength elements were removed from the model the results did not vary significantly.

8.5 Correlation with Bending Test Data

The model was calibrated at five points for each series. One point was at cold conditions, and four points were at various load ratios. The other parameter is the time to failure for that load ratio. The load ratios used were therefore 1.0, 0.7, 0.5, 0.3 and 0.1.

The data supplied by König included the midspan deflection over a 900 mm gauge length and the horizontal deflection of the unexposed side of the stud, also over 900 mm. From these two measurements, the neutral axis depth was calculated and supplied by König. The finite element model was used to vary the temperature dependent stress-strain relationships until a good comparison was achieved between the model and all of the test results listed above, for several different tests.

8.5.1 Series 1

Series 1 tests are for a 145*45 mm joist, loaded as shown in Figure 8.1. The compression side of the joist is exposed to the fire and there is no lining on the exposed side of the beam.

8.5.1.1 Time to Failure

Figure 8.13 shows the time to failure for the system as a function of the load ratio for the test results and the results from the model.

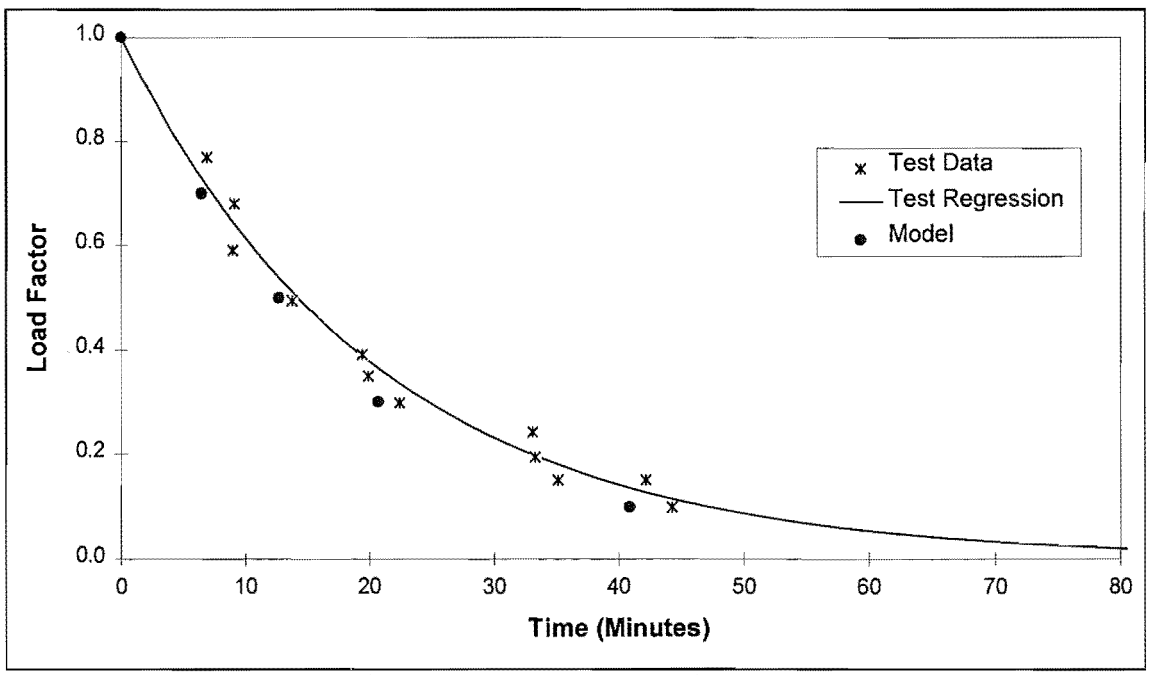

Figure 8.13 Comparison of Times to Failure for Series 1

An exponential regression curve was fitted through the test points by König. There is some scatter as one would expect with any series of tests involving timber, due to the variability of the material. An exponential decay or an inversed squared function is logical for the relationship because as the heat moves further into the wood, then the depth of the section that can carry load reduces. The moment capacity varies with the depth squared, hence an inverse squared function or the similarly shaped exponential function is appropriate. The model slightly underpredicts the time to failure, by about 10% at each data point. A data point is obtained at a load ratio of 1.0 with a time to failure of zero minutes, because this load ratio implies the failure load under cold conditions.

8.5.1.2 Vertical Deflections

A comparison of the mid-span deflections is shown in Figure 8.14.

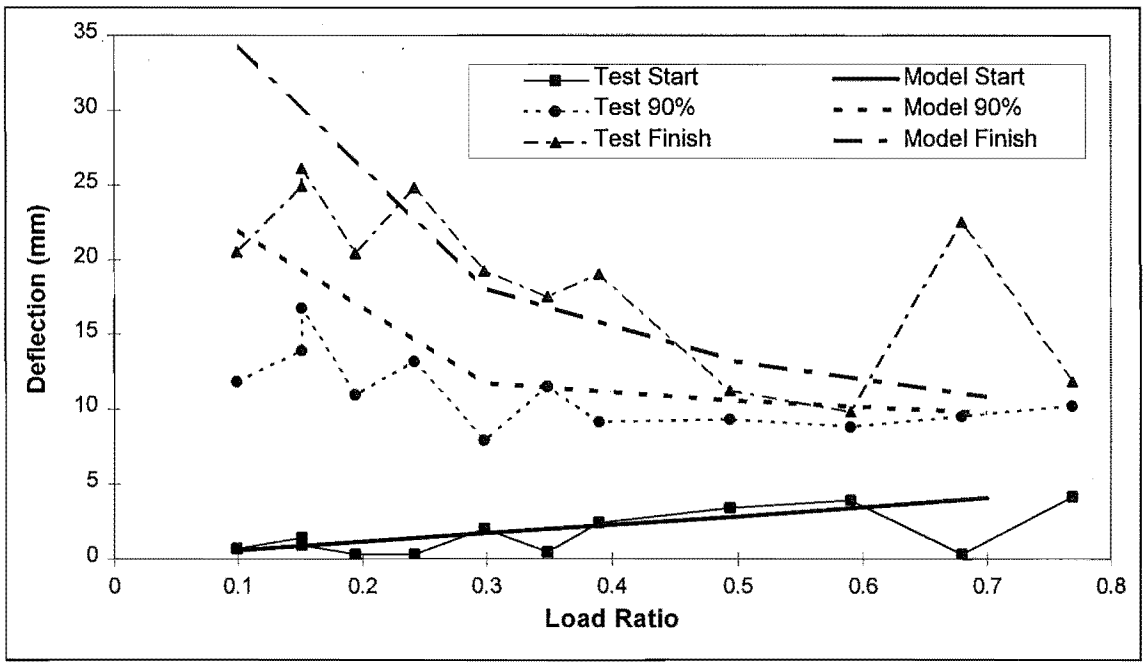

Figure 8.14 Comparison of Vertical Deflections for Series 1

The deflection curves shown are for the test specimens at the start and finish of the test and when the test is 90% complete in terms of time to failure. There is a large degree of scatter in the results due to the variability of timber. The deflections given by the computer model are also shown at the start and finish of the test and at 90% of the time to failure of the model. The time at 90% test time and 90% model do not have the same value. They are a fraction of the relevant time to failure.

The values at 90% of the time to failure are shown, because the criteria for the final deflection reading in a test is not well defined. At the end of a test the deflections are

increasing at a very rapid rate as the beam fails, hence the recorded deflection may be more a function of when the measuring apparatus could no longer record the deflection rather than any defined end of test.

At the start of the test the comparison is very good, when some allowance is made for scatter. At the end of the test the scatter is much larger, due to the problems of recording deflections described in the previous paragraph. At 90% of failure time the model overpredicts the deflection, especially at low levels of load ratio.

8.5.1.3 Neutral Axis Depth

The comparison of the neutral axis depth is shown in Figure 8.15. The depth is measured from the top of the beam.

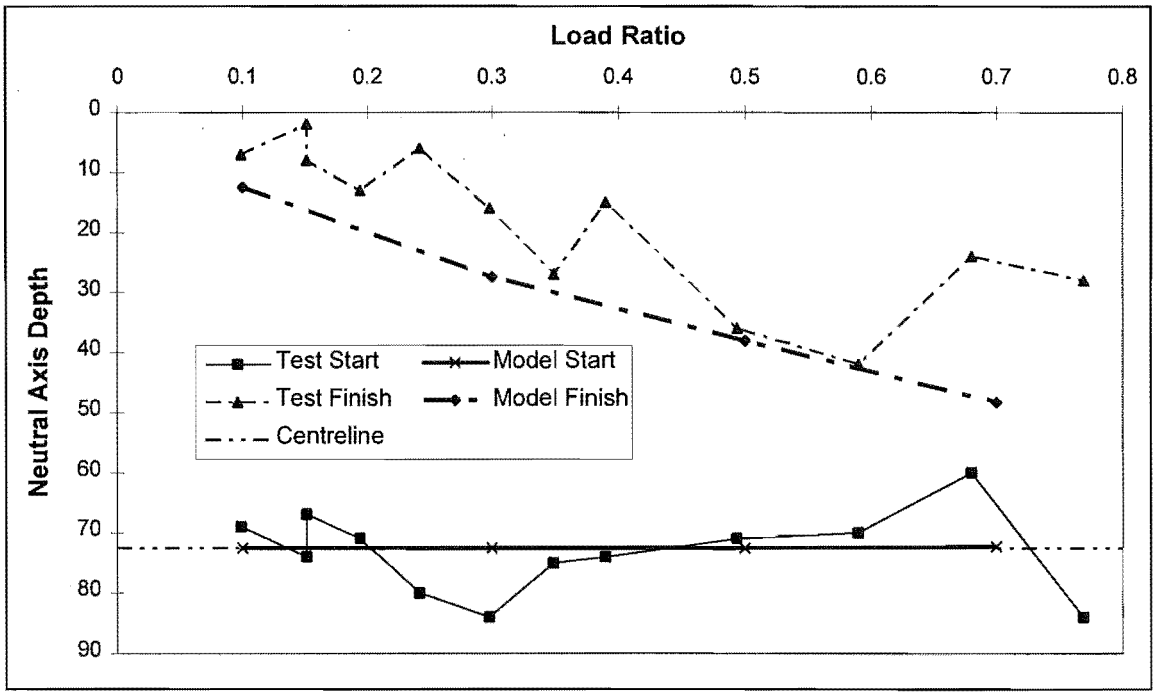

Figure 8.15 Comparison of Neutral Axis Depth for Series 1

The neutral axis depth in the tests is calculated from the horizontal deflection over a 900 mm gauge length and the vertical deflection over the same length. This calculation is less accurate than a direct measurement such as deflection but produces some worthwhile information. In the model it is found by interpolation from the strain values for the elements down the beam and averaged for the four sections across the beam.

The comparison of the neutral axis depth at the start of the test is good, when allowance is made for scatter. The model consistently underestimates the neutral axis depth at the end of the tests. This may be due to problems in defining the deflection at the end of the

test as described previously or could be because strength or stiffness of the wood in compression has been overestimated.

8.5.2 Series 3

Series 3 tests are also for a 145*45mm stud, loaded as shown in Figure 8.1, however in this series the tension side of the beam is exposed to the fire. There is no lining on the exposed side of the beam (as for series 1).

8.5.2.1 Time to Failure

The comparison of the times to failure for this series is shown in Figure 8.16.

There is more scatter in the test data than in series 1, probably because of the greater effect that defects in the wood have on tension strength than they have on compressive strength. The model compares very well with the test regression, except at low load ratios.

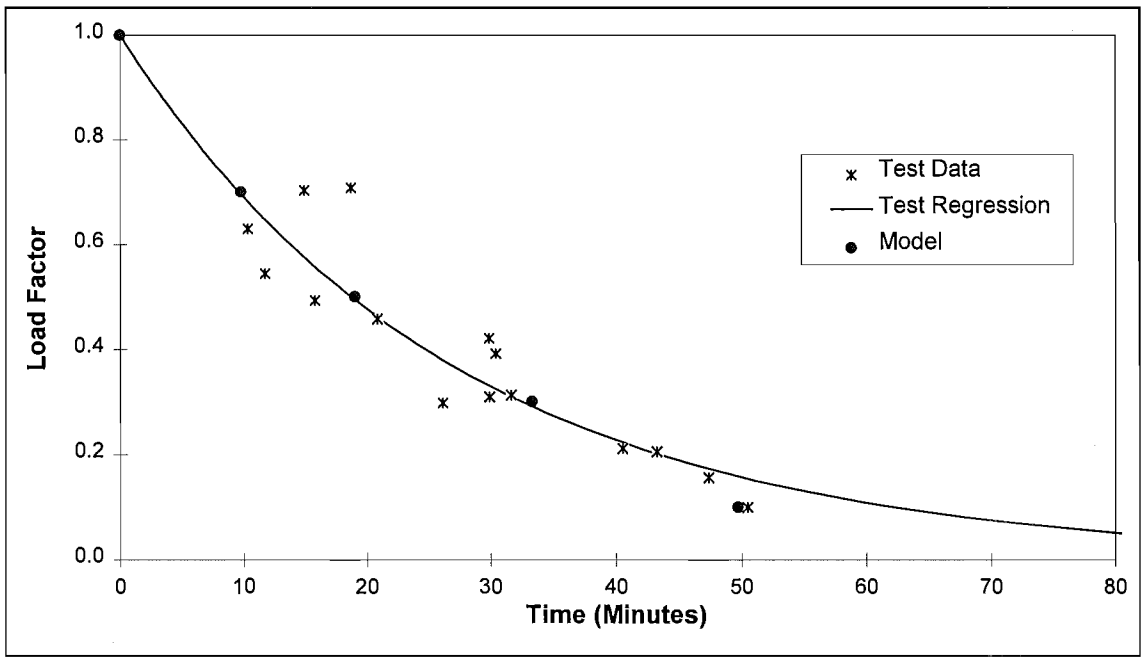

Figure 8.16 Comparison of Times to Failure for Series 3

8.5.2.2 Vertical Deflections

The comparison between the starting deflection in the model and the tests is very good as shown in Figure 8.17.

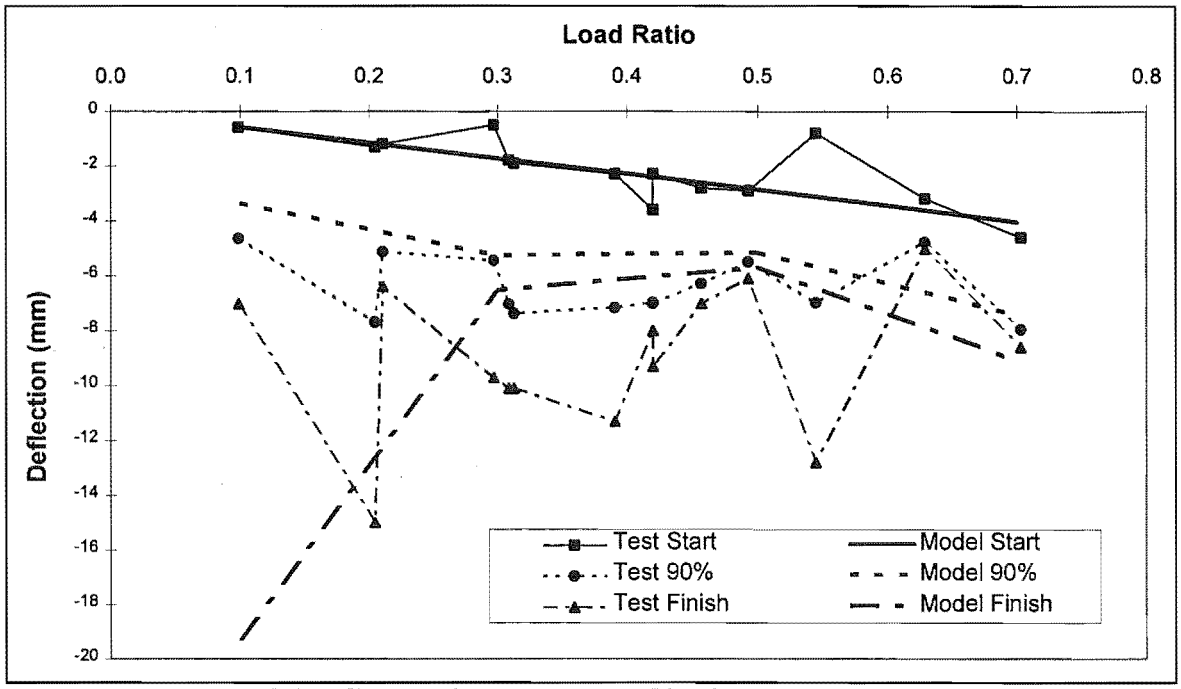

Figure 8.17 Comparison of Vertical Deflections for Series 3

The comparison at 90% is reasonable, however at the end of the test the test results appear to be highly variable, so it is difficult to make conclusions about the comparison.

8.5.2.3 Neutral Axis Depth

In the series 3 tests, the comparison between the starting neutral axis depth in the model and the tests is very good as shown in Figure 8.18.

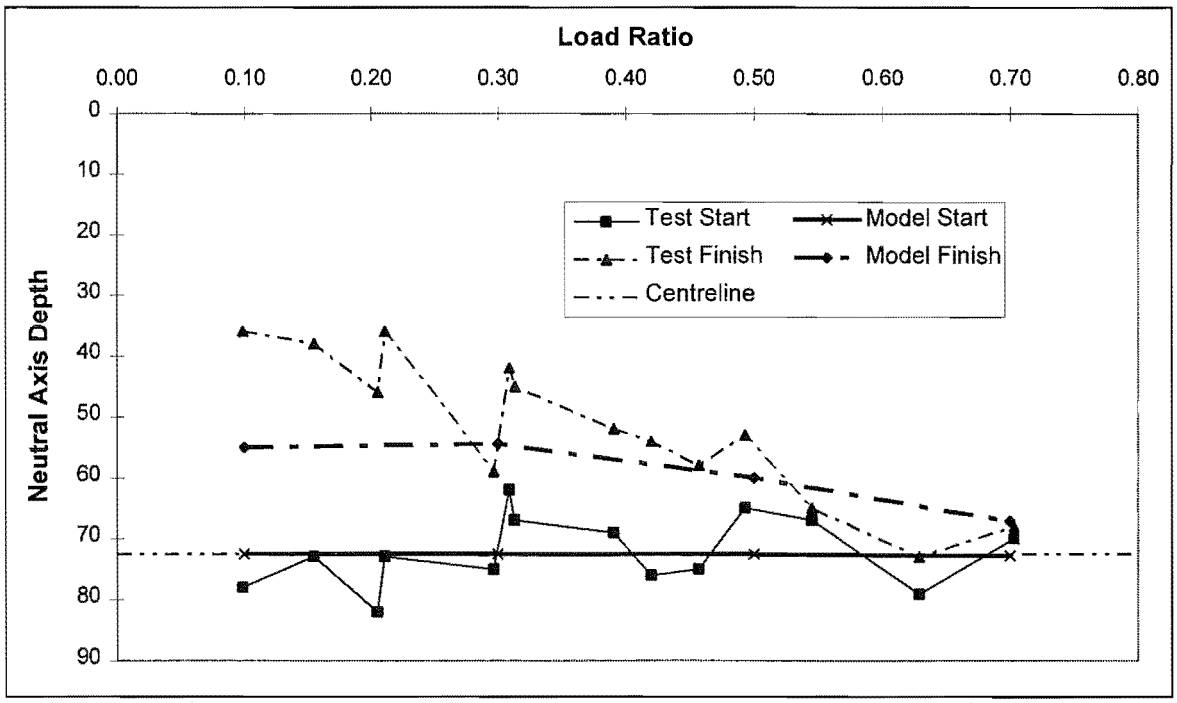

Figure 8.18 Comparison of Neutral Axis Depth for Series 3

The comparison at the end of the test is reasonable, except at low levels of load ratio. As the time to failure comparison is not very good for low load ratios, this is not surprising.

8.5.3 Series 2

The series 2 tests are identical to the series 1 tests, except that a 12.5 mm gypsum plasterboard lining is attached to the exposed edge of the beam The compression side of the beam is exposed to the fire. This series provides a useful check on the strength values used in the model for series 1 and 3 because although the structural model is identical to that used in series 1, the temperature profile is different because of the gypsum plasterboard lining. Series 2 is very significant because the walls that will be modelled later are similar, being lined on the fire-exposed side.

8.5.3.1 Time to Failure

The test regression curve in Figure 8.19 has the same coefficient as that used for series 1, but is offset by about 15 minutes. This is to allow for the time delay before the exposed side of the stud starts to heat up appreciably, as the heat penetrates the lining on the fire exposed side of the assembly.

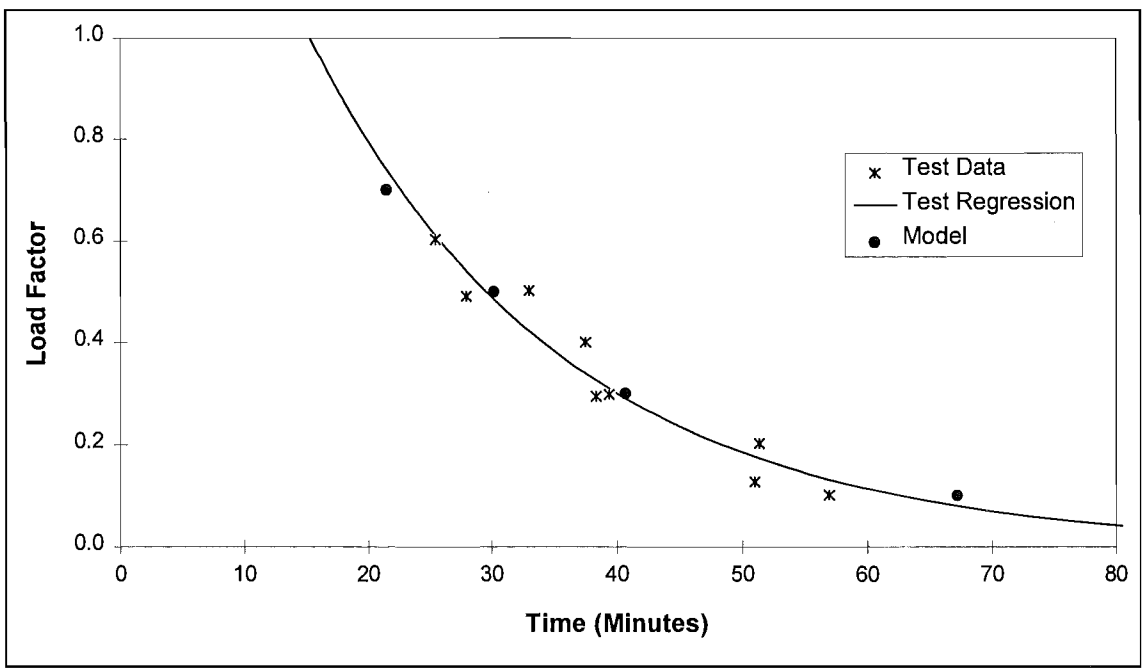

Figure 8.19 Comparison of Times to Failure for Series 2

There is some scatter in the test data. Overall the model predicts the time to failure well, but there is a hint that it is on a different shaped curve, with it underpredicting the time for high load ratios and overestimating it for low load ratios.

8.5.3.2 Vertical Deflections

At the start of the series 2 tests, the model prediction of the deflection is excellent apart from one point at a load ratio of about 0.5, as shown in Figure 8.20. As the deflection for this test does not appear to change during the test it can be reasonably assumed that there was a problem with the test procedure. The deflection value may not have been measured or there may have been other problems. This point can therefore be ignored. The model consistently overestimates the deflection at 90% of time after allowance has been made for scatter in the test results. It also overestimates the deflection at the end after allowance has been made for scatter in the test results, but the scatter is so great that it is hard to compare the trend in the results. It can be seen in both the model and test results that there is some sort of trend towards higher deflections at the end of the test for lower load ratios.

The results shown in Figure 8.20 for the model do not vary significantly from the deflection results for the model for series 1, shown in Figure 8.15. This would be expected because at failure the temperature distributions are similar. The differences are more significant for the test results, but this may be due to variability in the timber.

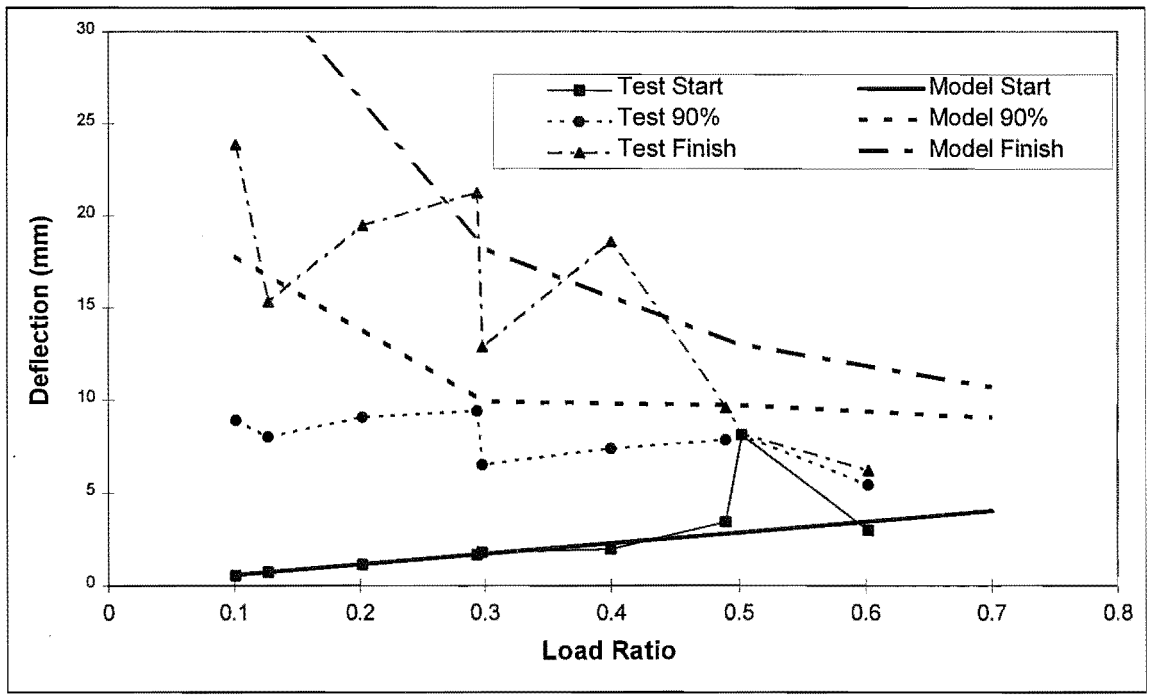

Figure 8.20 Comparison of Vertical Deflections for Series 2

8.5.3.3 Neutral Axis Depth

The shift in neutral axis depth for series 2 is shown in Figure 8.21. The comparison is very good at the start of the tests, again with allowance for scatter, and good at the end.

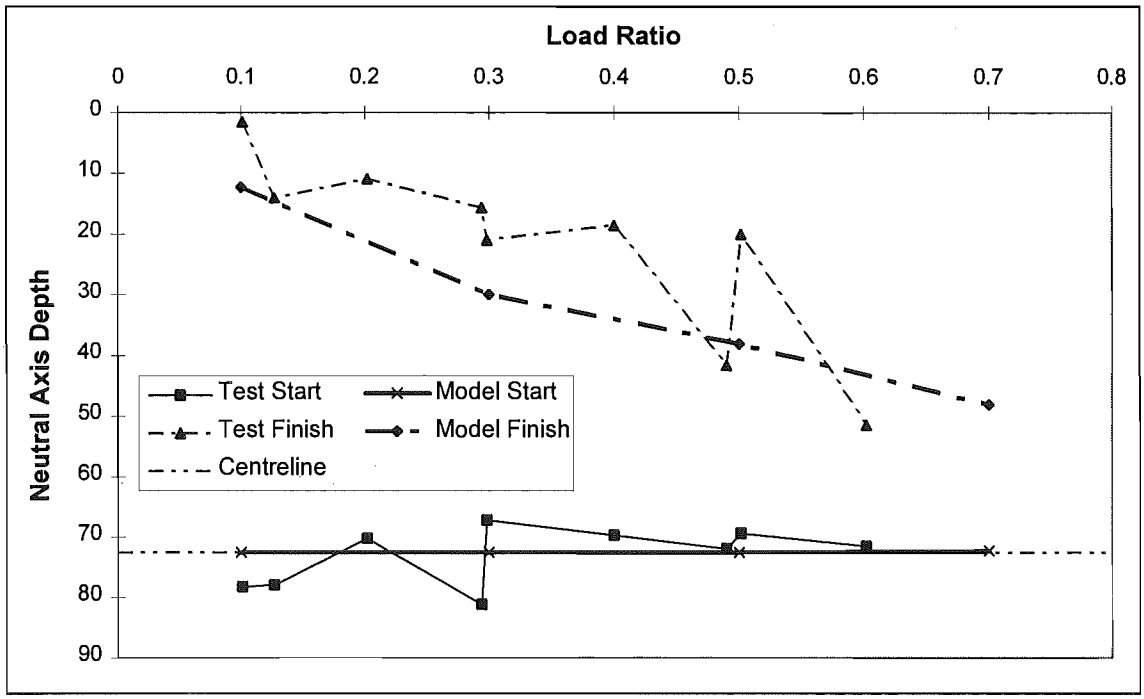

Figure 8.21 Comparison of Neutral Axis Depth for Series 2

8.6 Results from Initial Analysis

The final values for the strength of the timber are shown in Figure 8.22. The values used at lower temperatures are derived as described in Sections 8.2.3.1 and 8.2.3.2. It is assumed that wood has no strength at 300°C and the shape of the curves between 80°C and 300°C gives the best correlation with the test data.

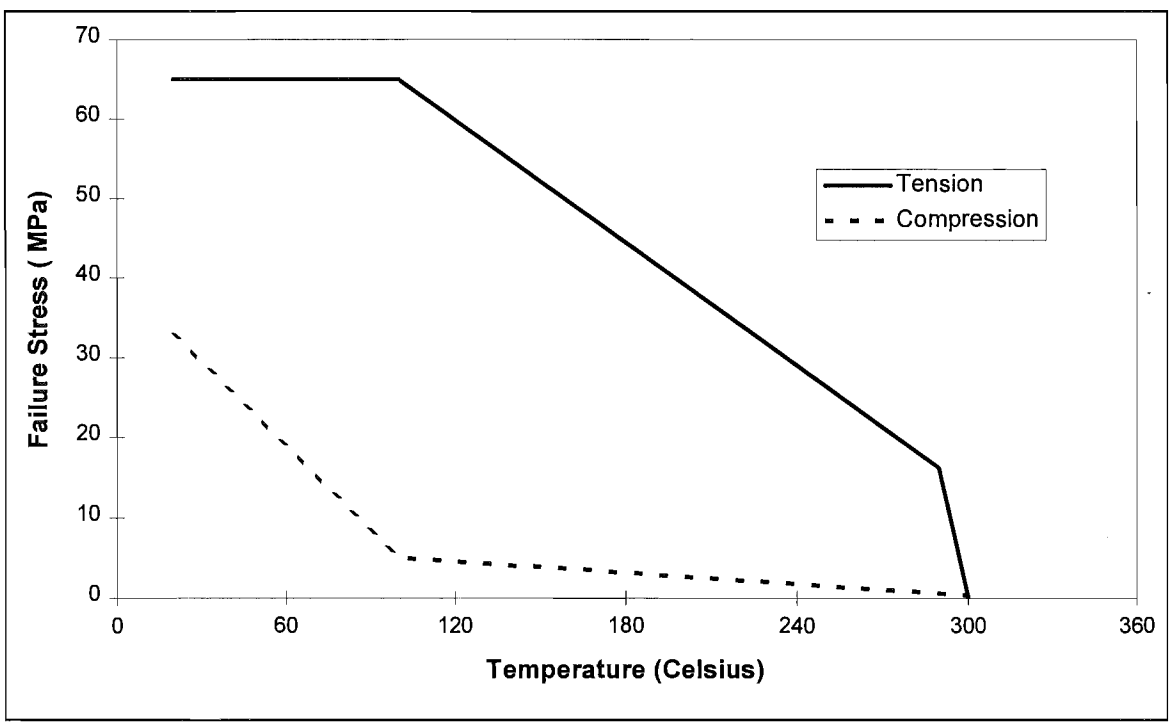

Figure 8.22 Temperature Dependency of Failure Stress

The graphs in the preceding 3 Sections were the results from a series of computer runs using basically the same data. They were the last in a large number of runs, that produced good results.

These simulations were a trial and error process to find "effective" temperature dependent values for the compressive and tensile strength of timber. The models shown graphically above used the stiffness values as shown in Figure 8.3.

The values of strength and stiffness used produce good comparisons with test data. The values for strength and stiffness in compression are lower and decay more rapidly with temperature than those in tension. This is in order to match the larger deflections and larger shift in neutral axis depth, when the compression side of the beam is exposed to fire. It also allows for the shorter time to failure when the compression side is exposed to fire.

The reduction of the strength in tension and compression is somewhat greater than that implied by Glos and Henrici's values for the modulus of rupture. This can be attributed to the effects of very high moisture contents at high temperature as the moisture front is driven through the wood.

8.7 Validation of Model Using Results from Later Tests

König also supplied results from tests on 95*45 mm beams (series 4 and 5) and 195*45 mm beams (series 6 and 7) in the same test set-up. The series 4 and 5 test results were used to validate the thermal and structural models for the beams described above.

8.7.1 Series 4

The series four tests consisted of 95*45 mm beams with no lining on the fire side and with the fire exposed side in compression. The comparison between the test and model for the time to failure is shown in Figure 8.23.

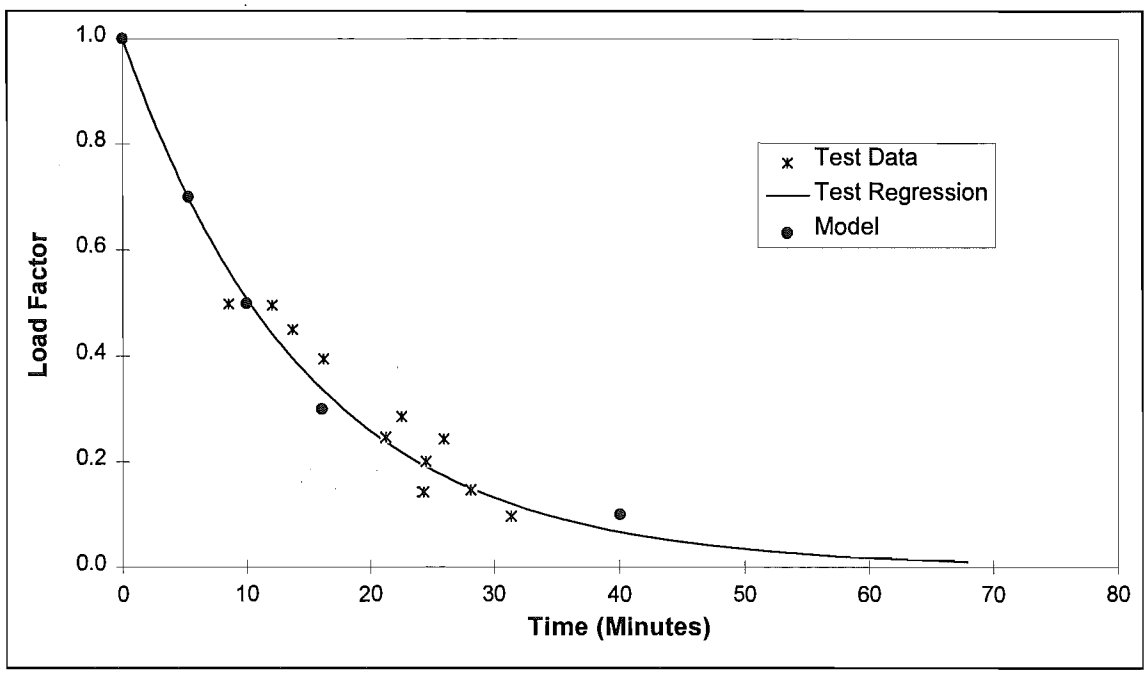

Figure 8.23 Comparison of Time to Failure for Series 4

The comparison is good, considering that this is a validation test.

8.7.2 Series 5

The series 5 tests were identical to the series 4 tests except the fire exposed side was in tension. The test data in Figure 8.24 show more scatter than series 4, as expected for tension tests versus compression tests.

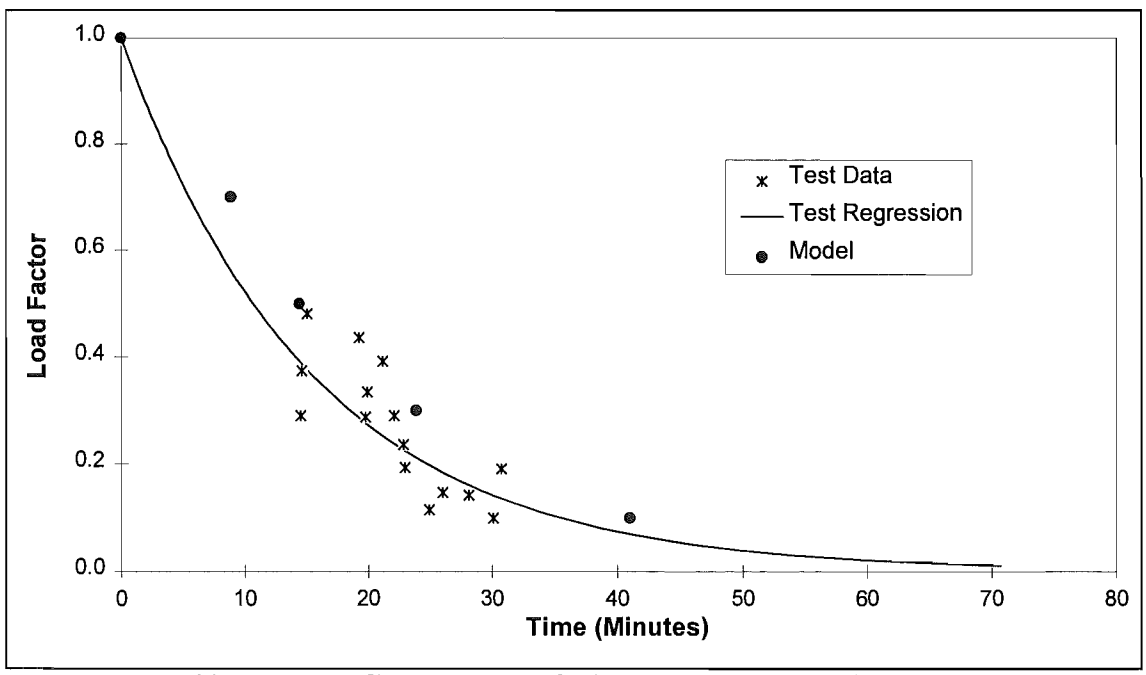

Figure 8.24 Comparison of Time to Failure for Series 5

The model consistently overestimates the time to failure.

8.8 Results

Figure 8.25 shows the final values used for yield strength and stiffness as a temperature dependent series of strength versus stiffness curves. The shape of these curves is a result of the values reported in section 8.2.3 and manipulated within the bounds described to give a good correlation with the substantial amount of test data available.

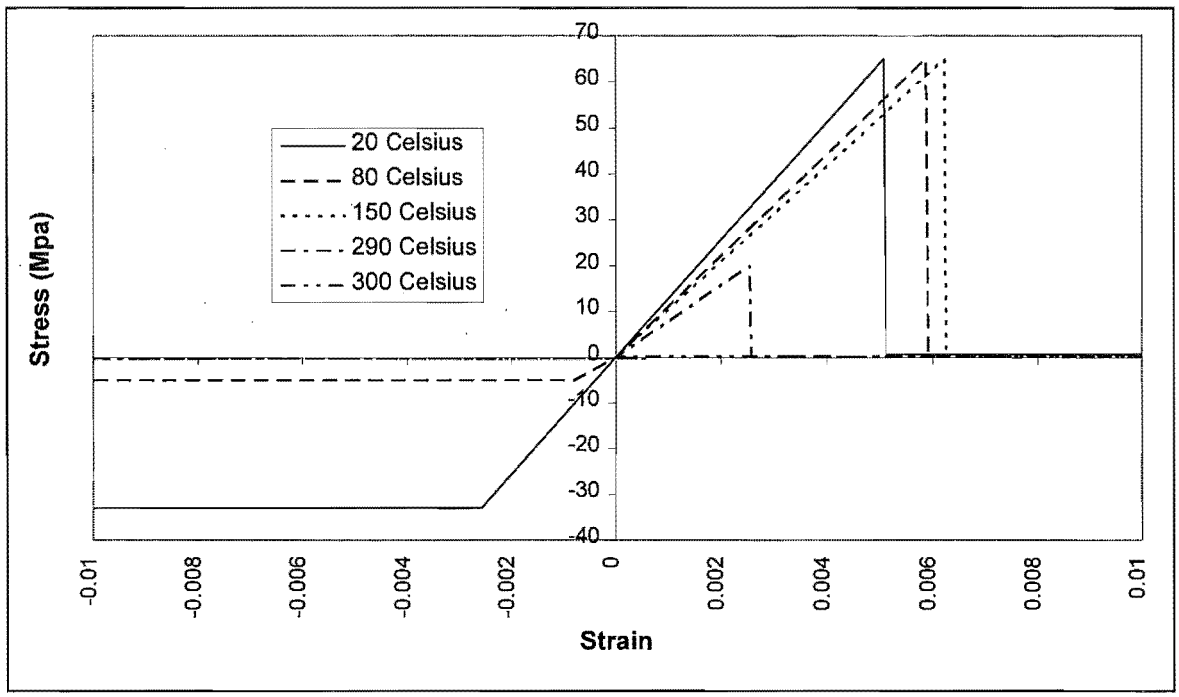

Figure 8.25 Temperature Dependent Stress-Strain Curves

The regressions of the test data in series 4 and 5 are very similar. This is also the case for series 6 and 7, the compression side exposed and tension side exposed series for 195*45 mm beams respectively. This means that the behaviour with the tension and compression sides exposed to fire is very similar. This was not the case for series 1 and 3. It can therefore be assumed that the time to failure is closer for the tension and compression cases than series 1 and 3 would predict.

8.9 Conclusions

The results for series 1, 3 and 4 show that the model is very good for beams with the fire exposed side in compression for a range of load ratio varying from 0.3 to 0.7 as is typical of most structures.

Given similar times to failure for the tension and compression cases for series 4 and 5 and series 6 and 7 respectively, the strength and stiffness in compression may be higher, and that in tension lower than used here.

The process of developing a model for König's beam tests has given an indication of effective temperature dependent stress and strain properties of timber. These properties take into account moisture and time dependent effects on wood properties. It is likely that these properties will need modification for use in a wall model.

The process has produced values for properties that work for the given situation. They are effective properties not measured properties. Given the lack of accuracy in the thermal model, the properties found here are adequate for the purpose, giving a consistent level of accuracy.

Chapter 9 Calibration of the Structural Wall Model

After the development of a structural model for beams in pure bending, it was necessary to extend this to walls. In walls the member is subject to axial loading and bending. The timber may exhibit different stress-strain behaviour to the timber used in the beam test because of the species difference. In the wall tests the timber used was radiata pine (pinus radiata) whereas for König's tests the material was Norwegian spruce (picea abies).

9.1 Description of the Wall Tests

The data from nine wall tests was supplied by the Building Research Association of New Zealand (BRANZ). Some data were supplied with the permission of Winstone Wallboards Ltd. Seven data sets were from tests using the full sized furnace (3.0 m high by 3.0 m specimen size), and two tests in the pilot furnace (2.22 m high by 1.03 m specimen size). The full sized specimen is shown in Figure 9.1. All the walls were symmetrical with one layer of gypsum plasterboard on each side. The gypsum plasterboard was nail fixed to the studs according to the manufacturer's specification (Winstones 1992). The top and bottom plates were bolted to the test frame and the loading platen respectively. The top and bottom plates were nailed to the studs with two nails as per the New Zealand code for non-specific timber design, NZS3604 (SANZ 1990).

The deflections were measured at nine points and the mid-height deflection was compared.

The wall is loaded by a platen at the bottom and restrained by a concrete panel at the top. Both the panel and the platen can be regarded as being rigid compared with the

timber top and bottom plates and hence the plates were not free to rotate. The studs at the extreme left and right hand side of the walls are cut short in order to prevent them from contributing to the strength of the wall.

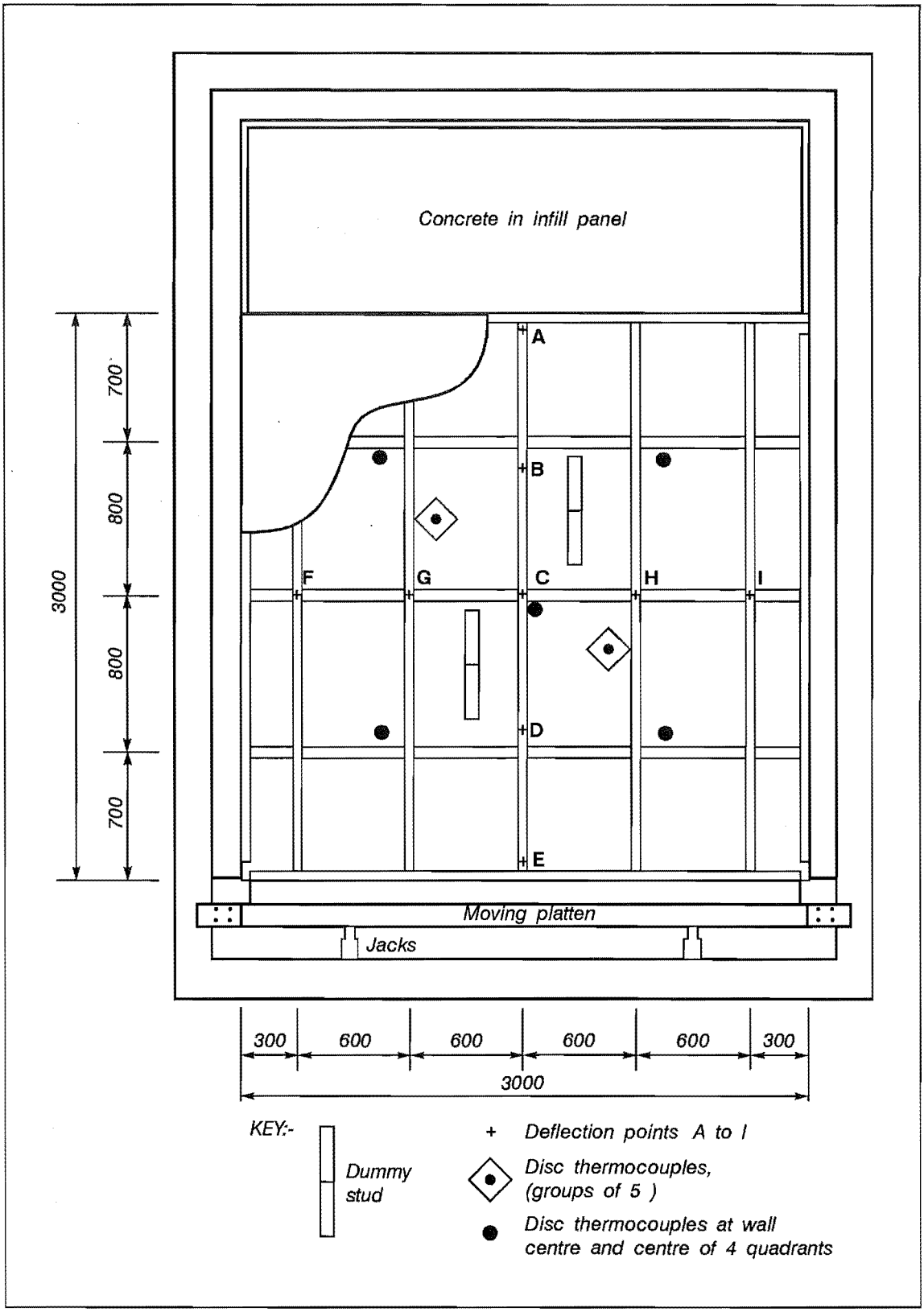

Figure 9.1 Full Size Furnace Test Specimen Layout

The pilot specimen is shown in Figure 9.2.

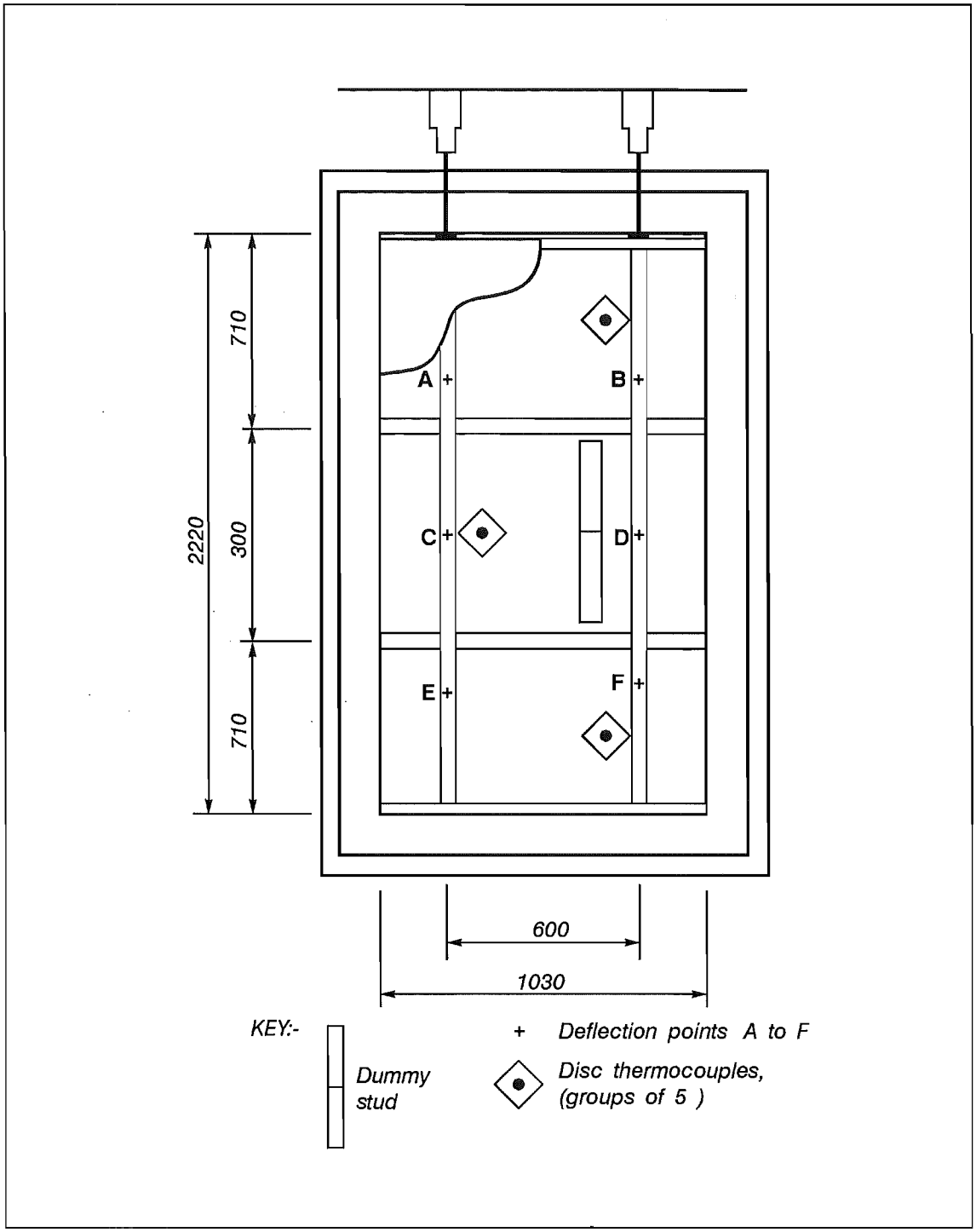

Figure 9.2 Pilot Test Specimen Layout

Unlike the full size test specimen the studs are loaded individually. The hydraulic jacks are connected so they have the same hydraulic pressure and hence exert the same force on each stud. The mid-height deflection at points C and D was averaged before comparison with the computer model.

A variety of lining thicknesses, stud sizes and loadings were tested as shown in Table 9.1.

Test Code	Furnace	Lining Thickness (mm)	Stud Depth (mm)	Stud Width (mm)	Wall Height (m)	Stud Load (kN)
FR1582A	Full	9.5	69	45	3	2.8
FR1582B	Full	9.5	90	45	3	8
FP1583A	Pilot	9.5	69	45	2.2	5
FP1583B	Pilot	9.5	90	45	2.2	13
FR1611	Full	12.5	69	45	3	2
FR1515A	Full	14.5	90	45	3	16
FR1515B	Full	14.5	90	45	3	8
FR1515C	Full	14.5	90	45	3	10
FR1777	Full	16	90	35	3	3

Table 9.1 Wall tests Used for Model Calibration

Structural failure of the walls was signified by a drop-off in load as the horizontal deflection of the stud at mid-span started to increase at a very rapid rate. At the same time the vertical deflection increased at such a high rate that the loading apparatus could not keep up and the applied load could no longer be carried. The rapid increase in deflection is due to the softening of the timber due to temperature and moisture effects, leading to large plastic deformations in the area of maximum compressive stress on the fire side of the stud. Tension failures of the timber on the ambient side were not observed. If the load had been left on a tension failure would eventually be expected on the ambient side of the stud.

As the test progresses the top of the studs rotate and the point of application of the load shifts away from the fire. This helps the wall to maintain its load-carrying capacity as it reduces the eccentricity of loading. This is described by König (1995).

9.2 Thermal Model

The thermal model for the walls is described in Chapters 3 and 4. It is a two-dimensional heat transfer model, and uses the TASEF (Sterner and Wickstrom 1990) heat transfer program running on a personal computer. The two-dimensional model is converted to a three dimensional model by assuming the temperature profile through the cross-section of the stud is constant along the length of the stud. The top and bottom plate are assumed to remain at the ambient temperature. The plates do not heat up as much as the studs, because they are protected on one side and are close to the sides of the furnace, where the thermal exposure is less severe. Calculating the temperature within the top and bottom plates would require a three-dimensional finite element heat

transfer model which would take in the order of weeks to run and hence is not practical. Any thermal degradation of the top and bottom plates is allowed for in the ambient mechanical properties assumed for the timber.

Although the thermal model compares well with the data from tests overall, it tends to underpredict the temperatures within the studs that are protected by thinner linings. Experimental error, repeatability problems and problems with the measurement of temperatures within the furnace (see Section 3.9.1) affect the results from the thermal model.

In order to prevent the structural model from being affected by shortcomings in the thermal model the temperature profiles within the studs were modified to give a better comparison with test data. These modified temperatures are only used in order to develop the structural model. This correction may be partly due to the moisture movement being ignored in the thermal model. This modification to the thermal model is only used for walls with thin linings.

The temperatures were multiplied by 1.2 to give a better correlation at failure for the walls lined with 9.5 mm and 12.5 mm plasterboard. This factor was found by comparing the temperature from the thermocouples in the stud at 50mm depth with the temperatures from the thermal model, at the quarter point and midline of the stud and the same depth. The average value of these ratios was found. In the walls with only 66mm or 69mm studs the ratios at both the 50mm and 20mm depths were averaged. It was used for the five walls with thin linings, (less than or equal to 12.5 mm), that is, FR1582A, FR1582B, FP1583A, FP1583B and FR1611.

In tests FR1515A, FR1515B and FR1515C, the stud temperatures from the thermal model were multiplied by a factor of 0.73. The low value of this factor is due to the use of timber with a very high oven-dry density of 490 kg/m^3. This equates to an air-dry density of 570 kg/m^3 at 12% moisture content. This is much higher than the typical air-dry density of pinus radiata of about 450 kg/m^3. When the thermal model was re-run with a density of 570 kg/m^3 and a temperature correction of 0.9, the structural failure times were similar to those given later in this Chapter. The walls in tests FR1515A, FR1515B and FR1515C appear to perform better thermally than any of the other walls tested, hence a modification factor of 0.9 is required. This performance is indicated by

the temperature on the ambient side of the wall being somewhat higher at the end of the test than the recorded temperature as shown in Figure 4.14.

9.3 Structural Model

The structural model was developed using ABAQUS (Hibbitt et al 1994) a general purpose finite element package. The finite element mesh for a stud cross-section is shown in Figure 9.3, and a part elevation through the wall is shown in Figure 9.4.

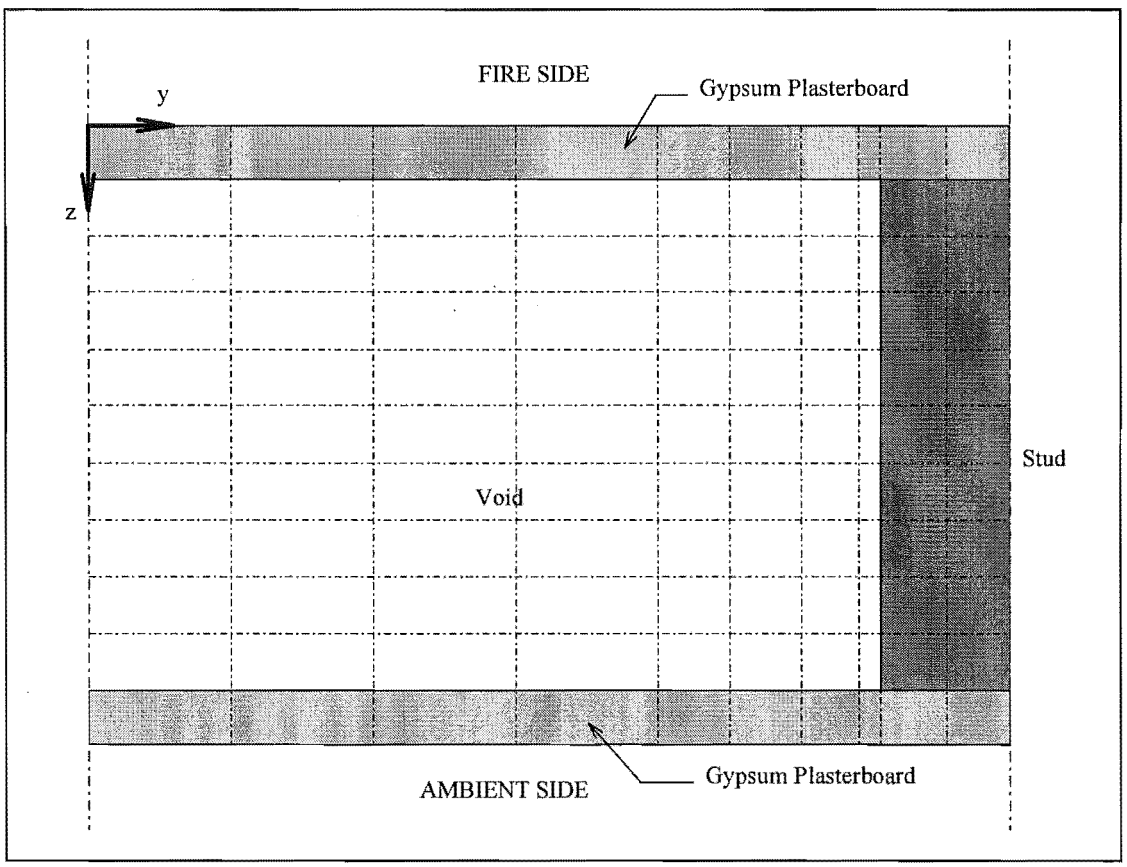

Figure 9.3 Horizontal Cross-Section Through the Stud

A single stud was modelled in order to substantially reduce the complexity of the model. Symmetry was used to further reduce the complexity of the model, hence half the height of the wall, and half the stud was modelled.

The top plate was modelled to half the distance to the next stud. There are two layers of elements in the top plate and the nodes are spaced at approximately 50 mm centres down the stud.

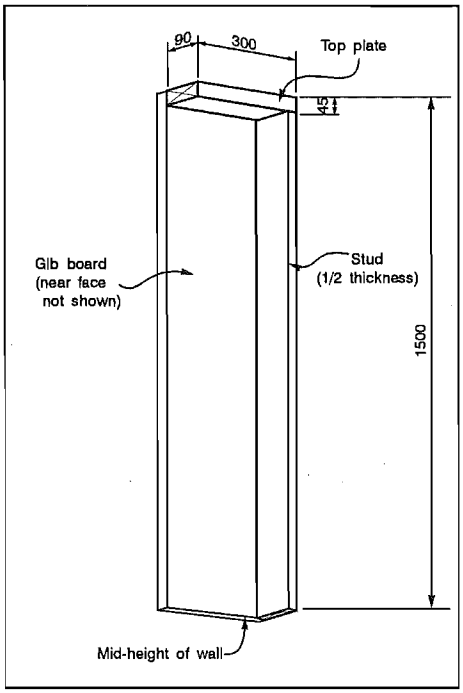

Figure 9.4 Cross-Section Through the Wall

The gypsum plasterboard was assumed not to contribute to the strength and stiffness of the wall, as it degrades at temperatures over 120°C. This is certainly true on the fire side, where the gypsum plasterboard reaches very high temperatures quite quickly. This assumption was checked by modelling the wall with gypsum plaster board on the ambient side. This resulted in an increase of between 2 and 5% in the time to failure and will be described further in Section 9.6.3.

9.3.1 Boundary Conditions and Loading

All the nodes on the top side of the plate were restrained to the same vertical deflection. The mid height cross-section of the stud is restrained by a symmetry boundary condition, that is it is fully restrained except lateral shrinkage and swelling can occur. The centreline of the stud is restrained by a symmetry boundary condition, in the direction across the thickness of the stud. The top plate is restrained in the direction across the thickness of the stud at the ends of the portion modelled and in the direction across the depth of the stud at the mid-depth of the wall.

The axial load was applied to the top side of the plate, over the area immediately above the stud. This is a simplification of the expected loading pattern. An average furnace pressure of 5 Pa is taken into account by a lateral load on the stud. The presence of this load does not affect the results.

9.4 Mechanical Properties

The mechanical properties required are the compressive strength and stiffness in the stud parallel to the grain and the strength and stiffness perpendicular to the grain in the plate at the top and bottom of the wall. These properties vary with temperature, time and moisture content.

The mechanical properties for the plate are adjusted to give average values, which remain constant over the temperature range throughout the test.

A summary of available data on mechanical properties of timber at high temperatures is given in Section 8.2.1. Given the problems discussed in Section 8.2.1 in accurately determining strength and stiffness as a function of temperature and moisture content in this study the properties are determined by taking reasonable starting values and modifying them within reasonable limits in order to give a good correlation with the wall tests.

9.4.1 Strength and Stiffness at Ambient Temperatures

The timber used in the wall tests was not tested to determine its strength or stiffness. The strength and stiffness had to be assumed from data from other sources.

9.4.1.1 Parallel to the Grain

Walford (1994), reported modulus of rupture values of 30.4 and 35.4 MPa for long and short specimens for in-grade testing of number one framing grade pinus radiata. These tests were on studs cut from a 25 year old stand of trees. In the fire tests the samples were selected visually, rejecting lengths with excessive curvature or knots. This selection process would result in a higher average strength for the specimens, hence an average modulus of rupture of 40 MPa was assumed. The relationship between the modulus of rupture and the ultimate compressive strength is assumed to be the same as for the Norwegian spruce used in König's tests. This gives a value for the ultimate compressive strength of 24.1 MPa, or approximately 60% of the value for the modulus of rupture. This is close to the value given in Table 6 of Walford (1994) of a compressive strength of 26.4 MPa for number 1 framing grade. Tsehaye and Buchanan (1996) tested juvenile pinus radiata and found a mean value of 26.1 MPa for compressive strength.

The material behaviour was assumed to be elasto-plastic in compression.

The modulus of elasticity used at ambient temperatures was 7200 MPa. This comes from Table 6 of Walford (1994) for Number 1 Framing grade pinus radiata.

As the specimens do not get to the stage that tension failure occurs on the ambient side, the tension strength is not required for modelling behaviour of walls.

9.4.1.2 Perpendicular to the Grain

The top and bottom plates are modelled as remaining at ambient temperature. For this reason the values used were half of the values assumed for ambient temperatures.

The compressive strength used was 4.8 MPa. The ratio of compressive strength perpendicular to the grain to compressive strength parallel to the grain for pinus radiata in the New Zealand Structures Standard (SANZ 1993). is approximately 40%. The compressive strength parallel to the grain was 24.1 MPa. The resulting value of 9.6 MPa was halved to give an average value over the range of temperatures within the top and bottom plate during the test of 4.8 MPa.

The ratio of the modulus of elasticity perpendicular to the grain to modulus of elasticity parallel to the grain for pinus radiata was assumed to be 1:20. The resulting value of 360 MPa was divided by four to give an assumed value over the range of temperatures within the top and bottom plate during the test of 90 MPa. This reduction also allows for the softening of the material due to the effects of steam. The low value allows for some rotation of the top of the stud, consistent with test results.

9.4.2 Mechanical Properties at Elevated Temperatures

Average values are used for strength and stiffness perpendicular to the grain as given in Section 9.4.1.2. Both strength and stiffness parallel to the grain reduce with increasing temperature.

The modulus of elasticity was assumed to remain constant until 60°C. It then drops to 30% of its original value by 120°C, remains constant until 295°C and then drops to effectively zero at 305°C. This is shown in Figure 9.5. The compressive strength is assumed to remain constant until 200°C is reached and then drops linearly to effectively zero at 300°C, as shown in Figure 9.6. The modulus of elasticity and the compressive strength are not reduced completely to zero because this causes numerical problems with the model. The effect of the elements at higher temperatures having a close to zero rather than zero strength and stiffness is negligible. The overall shape of the curves is that derived to give a good correlation with test results.

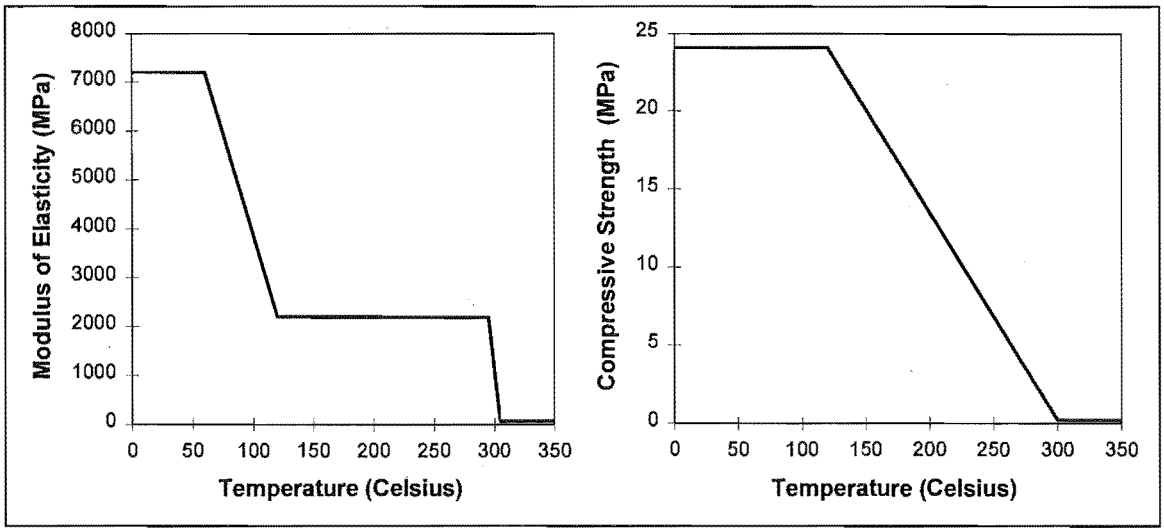

Figures 9.5 and 9.6 Modulus of Elasticity and Compressive Strength of Timber

9.4.3 Thermal Expansion and Shrinkage

During the initial part of the test, the walls tend to deflect towards the furnace, before moving away from it. This is due to longitudinal thermal expansion of the stud and the gypsum plasterboard. This effect is modelled by incorporating a total longitudinal thermal expansion of 0.175%, over the temperature range 0°C to 150°C, in the pair of elements in the stud closest to the furnace. This does not affect the behaviour of the wall later in the test.

Only a small part of the deflection may be attributed to longitudinal shrinkage in the timber as it is heated and dries out. Longitudinal shrinkage of the timber on drying is therefore ignored in the model.

9.5 The Behaviour of the Wall Model

The change in the point of application of the load, temperature, strain profile and stress profile along the centreline of the stud is shown in Figure 9.7. The point of application of the load shifts away from the furnace as the ends of the studs rotate due to the stud bending away from the furnace and vice-versa.

The temperature steadily increases on the fire exposed side of the stud throughout the test, reaching 600°C, after about 30 minutes. On the ambient side it reaches a maximum of 97°C just before failure.

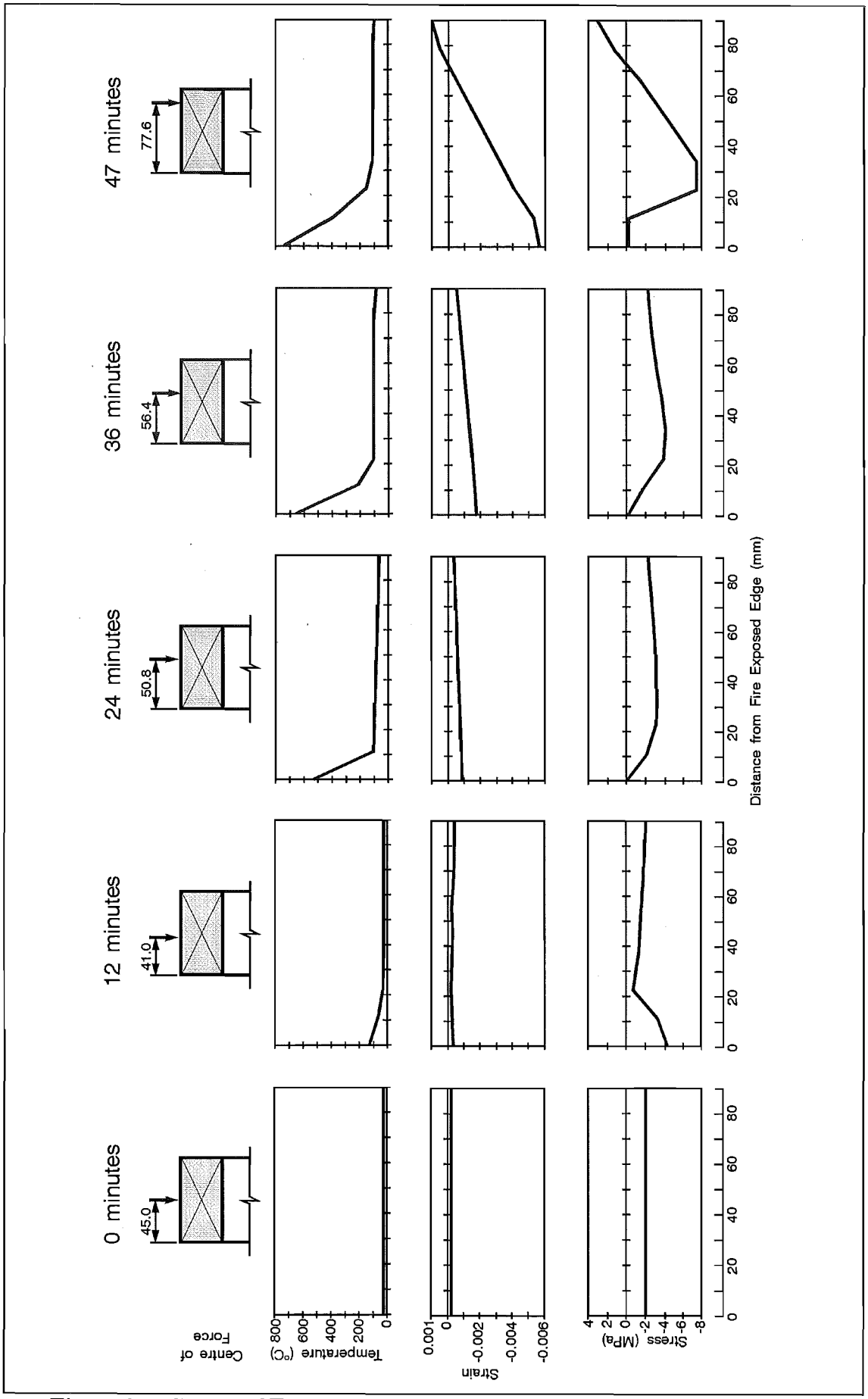

Figure 9.7 Centre of Force and Temperature, Strain and Stress Along the Centreline of the Stud

The horizontal deflection at mid-height and the centre of force at the top and bottom of the wall move towards the furnace initially and then away as the test progresses.

Both the stress and strain are constant across the section at the start of the run. At 12 minutes the strain profile varies little from that at zero minutes but most of the compressive stress is on the furnace side. This is due to the thermal expansion on the furnace side.

At 24 minutes, the curvature of the stud has reversed, starting to deflect away from the furnace. The strain profile shows more compressive strain on the fire side. The stress on the fire side is very low because of the loss of strength due to the high temperature. The centroid of the stress block is towards the fire side however, as this side is subjected to more compression as the stud bends away from the furnace. This process continues at 36 minutes.

At just before failure (47.1 minutes) the ambient side of the wall is in tension, however it is not outside the elastic range at its temperature of 97°C, so a tension strength does not need to be defined. The stress is close to zero for the first 12 mm depth. Once this point is reached the mid-height horizontal deflection starts to increase very rapidly and the model run ends.

Failure occurs after the movement in the point of application of the load exceeds the deflection resulting in a rapid increase in the bending moment induced by the P-Δ effect. The level of compressive stress on the fire side of the stud then increases rapidly to the point where the stud can no longer sustain the level of compressive stress on the fire side. The stud will progressively yield in compression across the stud away from the fire.

9.6 Comparison with Test Data

The structural model was compared to results from nine tests, consisting of combinations of two wall heights, four gypsum plasterboard thicknesses, two stud depths and two stud widths. The primary criterion for comparison was the time to failure, the secondary criterion being the mid-height deflection.

9.6.1 Failure Times

Table 9.2 describes the various tests and gives the time to structural failure in the test and for the model. In all cases except test FR1515A the difference is less than 10%. The average difference is -2.2%, that is, overall the model underpredicts the time to failure by 2.2%.

Test Code	Lining Thickness (mm)	Stud Depth (mm)	Stud Width (mm)	Wall Height (m)	Stud Load (kN)	Time to Failure	
						Test (minutes)	Model (minutes)
FR1582A	9.5	69	45	3	2.8	42	44.8
FR1582B	9.5	90	45	3	8	42	41.2
FP1583A	9.5	69	45	2.2	5	39	42.0
FP1583B	9.5	90	45	2.2	13	44	41.4
FR1611	12.5	69	45	3	2	69	66.6
FR1515A	14.5	90	45	3	16	46	38.5
FR1515B	14.5	90	45	3	8	70	69.6
FR1515C	14.5	90	45	3	10	60	60.6
FR1777	16	90	35	3	3	84	77.4

Table 9.2 Comparison of Test and Model Results

Test FR1515A was unusual in that the stud loading was very high. The wall did not exhibit the usual behaviour of deflecting towards the furnace initially and then away from the furnace as the test progressed. The wall continued to deflect towards the furnace, exposing the tension side of the stud to the fire. This is due to the high axial load. This uncharacteristic behaviour could not be modelled successfully with the simplifications used to model the boundary conditions. In the model, the compression side is exposed to the fire, this is a more severe case than when the tension side is exposed (see Chapter 8), resulting in a shorter time to failure in the model.

Some of the difference between the model and the test can be attributed to repeatability problems in the testing.

In test FP1583A the pilot furnace was overdriven and the temperature within the furnace varied considerably from the ISO-834 time-temperature curve. This was allowed for by using the actual furnace temperatures in the thermal model. When the temperatures fluctuate rapidly, the thermocouples tend to underpredict peaks in temperature due to thermocouple lag. This problem with furnace temperature measurement is described in Section 3.9.1. It is likely that the use of the measured furnace temperatures results in a more severe under-prediction of the thermal exposure than is normally the case in a furnace test.

9.6.2 Horizontal Deflection

Figure 9.8 shows the horizontal deflection for the studs at mid-height of the wall for test FR1582B. The three test curves are for the stud at the centreline of the wall (point C in Figure 9.1), the two studs next to the central stud (the average deflection of points G and H in Figure 9.1),and close to the quarter points and the two studs 300 mm from the edge of the test specimen (the average deflection of points F and I in Figure 9.1).

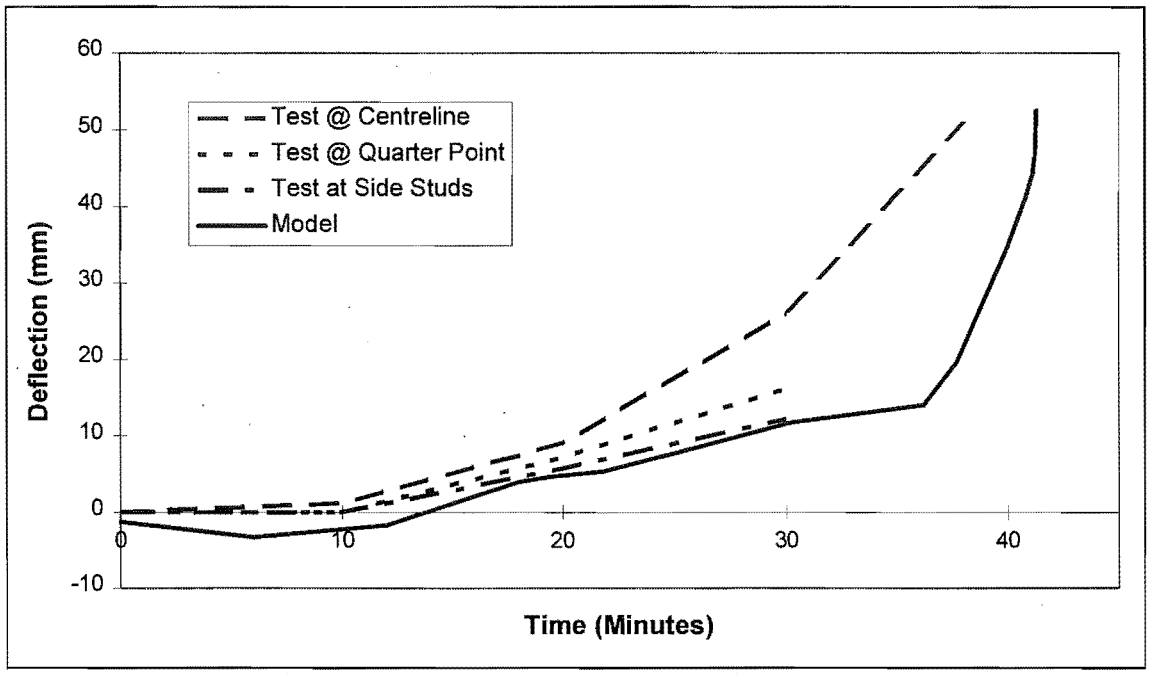

Figure 9.8 Comparison of Horizontal Deflections for Test FR1582B

The model underestimates the deflection throughout the test until at or about the failure time. The model shows an initial deflection towards the furnace, that reverses as the test progresses. This is observed in most wall tests.

Only one stud was modelled, so the deflection is an average for the wall and does not take into account load sharing effects. The studs closer to the centre of the wall char more quickly than the ones at the side of the wall, due to the thermal exposure being more severe in the centre of the wall. The differential charring rates were demonstrated by König (1995). This is because most of the radiation from the furnace comes from the walls of the furnace and the centre of the wall "sees" more furnace wall than the edges of the wall. The central studs are also less restrained by the lining on the ambient side in the first part of the test, some two-way action occurs but this is ignored in the model. The central studs start to deflect more quickly than the model predicts. Then the relatively rigid loading beam redistributes the load to the outer studs, slowing the deflection and preventing premature collapse of the studs with the most deflection. The

model used a higher stiffness to avoid premature failure when modelling a single stud and hence the deflections were underestimated by the model.

Incorporating longitudinal shrinkage at a reasonable level of 0.1% to 0.2% does not significantly increase the deflections.

In the pilot furnace test specimens there were only two studs at approximately the quarter points. Their thermal exposure was the same and because of symmetry they would be expected to deflect the same amount, since they were loaded individually, load shedding could not take place. There is a good comparison between the deflections for test FP1583A. The comparative deflections for pilot furnace test FP1583A are shown in Figure 9.9.

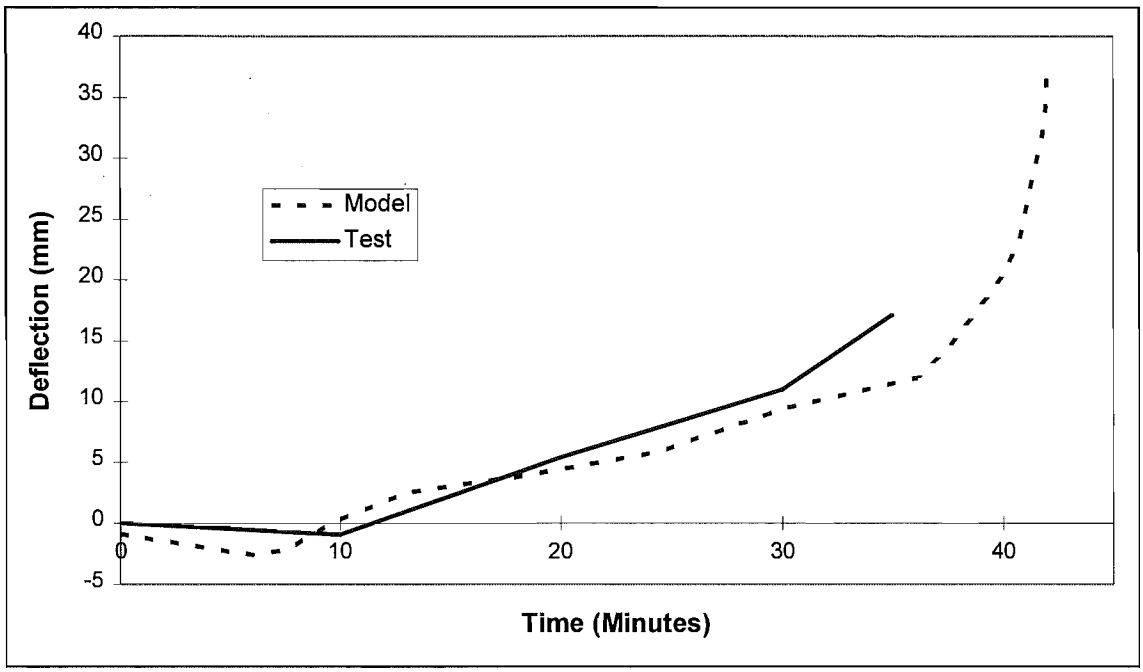

Figure 9.9 Comparison of Horizontal Deflections for Test FP1583A

In the other test in the pilot furnace (FP1583B) the model overpredicts the deflections. The pilot test gives a better validation of model performance because the studs were individually loaded in the pilot furnace. Compared with the two pilot tests the model overpredicts the deflection because it was validated on the full size tests. The difference between the deflection comparison in the two pilot tests is due to experimental error.

9.6.3 Effect of Composite Action with the Gypsum Plasterboard

The gypsum plasterboard lining may also carry a proportion of the load, however since gypsum plasterboard degrades rapidly at temperatures over 100°C and because the

lining is not rigidly fixed to the board the effect may be minimal. A computer model study of studs with the lining rigidly attached to the ambient side of the studs was made on three of the tests, (FR1582A, FR1582B and FR1777), mentioned above to determine if this effect significantly affected the results. The lining on the fire side of the studs is ignored as its load capacity is minimal, due to thermal degradation.

The gypsum plasterboard is subjected to compression throughout most of the test due to the overall shortening of the wall. Shortly before failure the gypsum plasterboard is in tension as the bending of the stud increases rapidly.

The modulus of elasticity and compressive strength of gypsum plasterboard at ambient temperatures is given by Stanish (1994) as 820 MPa and 6.4 MPa respectively. This is the average of his values for 9.5, 12.5,16 and 19 mm "Fyreline" boards. The assumed modulus of elasticity and compressive strength of gypsum plasterboard as a function of temperature are shown in Figures 9.10 and 9.11 respectively. They are assumed to be at the ambient value until 20°C and then drop linearly until 50°C is reached.

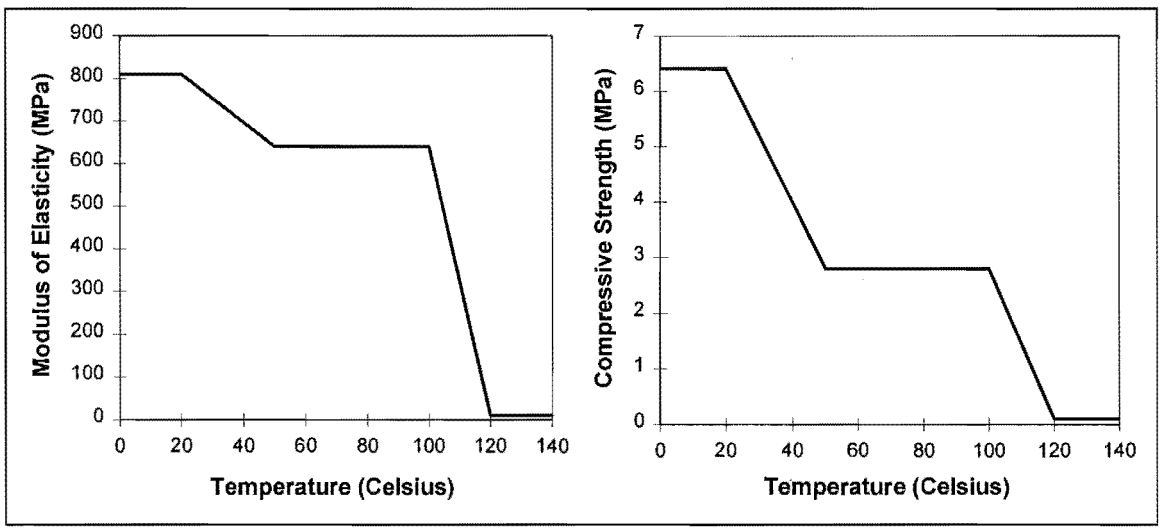

Figures 9.10 and 9.11 Modulus of Elasticity and Compressive Strength of Gypsum Plasterboard

The constant values between 50°C and 100°C of 640 MPa and 2.8 MPa respectively are those for 50°C from Fuller (1990). It is assumed that gypsum plasterboard has no effective strength or stiffness after calcination occurs at about 120°C. Fuller reports larger values in his tests for temperatures over 100°C. Fuller measured the air temperature, not the test specimen temperature. He heated the specimens for 13 minutes. In the first ten minutes the specimen was preheated without any load applied

and the time to failure was approximately 3 minutes after this. Despite the small size of the specimens, even with an exposure of 140°C, the average temperature in the specimen was just over 100°C, as calculated using a TASEF thermal analysis. The reason the temperature does not greatly exceed 100°C is due to the heat absorbed by the moisture in the gypsum plasterboard as calcification occurs between 100 and 120°C.

The tension strength in gypsum plasterboard is derived from the strength of the embedded glass fibres and the strength of the paper. When the test specimen is nearing failure the paper on the hot side of the board will be charred and will not contribute to the tension strength of the board. After calcification occurs the glass fibre will not be bonded to the gypsum and will hence contribute little tensile strength. The modulus of elasticity will be negligible after calcification occurs at 120°C.

The modulus of rupture at ambient temperature is 7.3 MPa with the paper attached and 2.0 MPa without the paper. The modulus of elasticity in bending at ambient temperature is 3000 MPa with the paper attached and 3900 MPa without the paper. The reduction on the modulus of elasticity when the paper is included is due to the increased thickness of the board when the modulus of elasticity is calculated. The paper does not significantly contribute to the stiffness in bending.

Given the data available, it is difficult to assume values for the strength and stiffness of gypsum plasterboard in tension. If the gypsum is assumed to have no tensile strength and stiffness, then these properties come from the paper and the glass fibre. Glass fibre has a very high tensile strength of 1500 MPa and a modulus of elasticity of 75 GPa. This high strength will not be developed, due to the bond between the glass fibres and the gypsum being unable to carry such high loads. Paper has a tensile strength of about 40 MPa. When this is divided by the ratio of paper thickness to overall thickness and averaged for 9.5, 12.5 and 16 mm boards it gives a value of 3.3 MPa. Without the paper the board has a modulus of rupture of 2.0 MPa. Since the ultimate compressive strength is higher than that, the bending specimens would have failed in tension at an extreme fibre stress of 2.0 MPa. The total tensile strength with paper then would be approximately 3.3 + 2.0 = 5.3 MPa. This is close enough to the compressive strength value of 6.4 MPa, so this value is also used in tension. The tensile stiffness of paper is about 10 GPa. Dividing this by the relative thickness of the paper and the plasterboard

gives a value of 800 MPa, similar to that used in compression, hence the same value is used in tension and compression.

The temperature dependence of the tensile properties are not known, however as the composite board degrades between 100°C and 120°C, the board will be unable to sustain tension loads after these temperatures have been reached. The temperature dependence of the properties is assumed to be the same as it was in compression.

Also because of the degradation of the gypsum plasterboard, the slip in the fasteners between the timber stud and the gypsum plasterboard would be such that little load would be transferred. The effect of the lining is summarised in Table 9.3.

Test Code	Lining Thickness (mm)	Stud Size (mm)	Stud Load (kN) (kN)	Time to Failure Test (minutes)	Model w/o Gib (minutes)	Model with Gib (minutes)	% Change
FR1582A	9.5	69*45	2.8	42	44.8	46.8	4.5
FR1582B	9.5	90*45	8	42	41.2	43.3	5.1
FR1777	16	90*35	3	84	77.4	79.2	2.3

Table 9.3 Effect of Incorporating Gypsum Plasterboard Lining in the Model

The addition of the gypsum plasterboard lining to the model is not very significant, increasing the estimated time to failure by 5% or less. The lining is not in fact rigidly attached to the stud, so the actual effect would be less, say 2-3%. It is assumed however that the gypsum plasterboard along with the dwangs prevents lateral buckling.

9.6.4 Significant Parameters

The strength of the stud in compression parallel to the grain at ambient temperatures has no effect on the time to failure. This is because the critical section, where the stress and strain is the highest, is on the hot side of the stud so the strength at higher temperatures governs the behaviour of the stud. The drop-off in strength with temperature is more significant. The most important factors are the stiffness parallel to the grain at high temperatures within the stud and the stiffness perpendicular to grain in the plates. The failure is governed by P-Δ effects and hence the stiffness parallel to the grain in the stud. If the stiffness perpendicular to grain in the plate is too high, then the stud exhibits double curvature and the point where the load is applied does not shift as the end of the stud rotates, which is not observed in the tests.

The load level significantly affects the results. For example when a load of 2.05 kN was applied to the stud in test FR1582A, the time to failure was 54 minutes, not 45 minutes when the correct load of 2.8 kN was used. The test series FR1515 (FR1515A, FR1515B and FR1515C), were identical except for the magnitude of the applied load. The time to failure varied from 46 to 70 minutes, with applied loads of 16, 10 and 8 kN per stud for tests FR1515A, B and C respectively.

9.6.5 Effect of the Element Size and Time Step Size

The model was re-run, halving the size of the elements in the cross-section in the stud and in all three dimensions in the top plate in the area directly above the stud. The element size was not halved along the length of the stud as the model would have been too large to run on the computer available. The stress and strain profiles along the stud only varied gradually along the length so further discretisation here would not affect the result.

This more detailed model of test FR1611 failed at 71.4 minutes compared with 66.6 minutes for the simpler model. The test time to failure was 69 minutes. The difference between the two models was therefore 7.2%, and is on the conservative side. The deflection plot for the more complex model was smoother than that from the simple model, but the deflections did not vary by a significant amount. A further check on the model by further reducing the element size was not possible. The model would have been too large for the resource limits on the computer available. It would be expected that a further halving of the element size would result in at most a 3% increase in the time to failure, resulting in a total (conservative) error of 10%.

The simple model was also run with initial time steps of 0.02 hours rather than 0.1 hours. The time to failure was the same (66.6 minutes) as the simple model and the deflections varied by less than 1%.

The wall used to test the convergence of the model had small studs and had one of the highest temperature gradients through the cross-section of the stud. For all of the other walls (except FR1582A and FP1582A), the temperature gradients were smaller and hence the error due to the large scale of the model would be smaller.

This model was used to calculate time equivalence and the same model is used for both the furnace test runs and the fire test runs so the errors due to the scale of the mesh would cancel to some extent.

9.6.6 Comparison with Clancy's Tests

Young and Clancey (1996) carried out fire resistance tests on 3.0 m high stud walls with pinned and fixed end conditions. In one test with pinned end conditions the gypsum plasterboard on the ambient side was fixed in such a way that it could not contribute to the load-bearing capacity of the stud. All the tests were on a 90*45 mm stud loaded at 8 kN per stud and lined with 16.0 mm gypsum plasterboard.

These tests were modelled using the process described in this Chapter and in Chapters 3 and 4. The density of the gypsum plasterboard was reduced to 600 kg/m^3 in order to allow for the apparently poorer thermal performance (based on temperatures in Clancey's tests and comparable tests in New Zealand) of the Australian gypsum plasterboard compared with the New Zealand product. This gave temperatures on the ambient side of the wall at about 30 minutes that were similar to those recorded in their tests. The end conditions were modelled as close as reasonably possible to the tests. The strength and stiffness values in the structural model were reduced by one sixth because Clancy used F5 grade pinus radiata whereas the New Zealand tests used to calibrate the model were number one framing grade, which is nominally equivalent to F6 grade. Table 9.4 shows a comparison of the test results with the model.

Test Description	Time to Failure in Test (minutes)	Time to Failure for Model (minutes)
Pin-Pin with Lining	34.5	36.2
Pin-Pin without Lining	28.0	31.0
Fixed-Fixed with Lining	58.0	65.4

Table 9.4 Comparison Between Clancy's Tests and the Model

The model results are within 12% of the test results, but more significantly the trends are the same, although the difference between the pin-pin wall with and without gypsum plasterboard is more in the tests than for the model. The effect of gypsum plasterboard is more significant when the end condition of the wall is pinned. This is because failure occurs earlier and the plasterboard has not degraded to the extent it does at the end of a test with "normal" end conditions.

9.7 Conclusions

The structural model as described in this Chapter predicts the time to failure of structural walls exposed to furnace tests, for a range of walls and loadings.

Composite action with the gypsum plasterboard increases the time to failure by less than 5%.

The model underpredicts the horizontal deflections in the wall until the time of failure.

The mechanical properties of pinus radiata at elevated temperatures derived in this Chapter differ from those derived to correlate the structural model with König's beam tests in Chapter 8. This can be attributed to the difference in properties between species.

Chapter 10 Structural Time Equivalence for Walls

10.1 Introduction

Once the structural model for timber walls has been developed and validated as described in Chapter 9, then a number of walls can be subjected to the temperature output from the thermal model (Chapters 3 and 4), run for differing compartment parameters using the compartment fire model (Chapter 2). From this, the structural time equivalent for various ventilation parameters and fuel loads can be deduced and compared with those calculated using the time equivalent formulae described in Chapter 1.

The CIB formula is used for the comparison because it is valid for the range of opening factors that are typical for light timber frame buildings. The relationship between the calculated and BIA time equivalent formula is also mentioned because it is specified in the New Zealand code (NZBIA 1992). Both formulae are described in Section 1.1.

10.2 Methodology

The overall methodology is described in the next five subsections.

10.2.1 Modelling Compartment Fires

The compartment fire model (COMPF-2) described in Chapter 2 was run for various fuel loads and opening factors. The parameters for the thermal properties of the boundaries were consistent with the wall being tested and a specified floor/ceiling, shown in Table 10.1.

Wall		Floor/Ceiling	
Stud Thickness (mm)	Lining Thickness (mm)	Joist Depth (mm)	Lining Thickness (mm)
90	9.5	240	12.5
70	12.5	190	12.5
90	16.0	290	16.0

Table 10.1 Framing and Lining thicknesses for the Compartments

The fuel loads used were 200, 400, 800 and 1200 MJ/m^2. The ventilation factors used are shown in Table 10.2.

WINDOW			Ventilation Factor CIB (Eqn 1.3)	Ventilation Factor BIA (Eqn 1.4)
Height (m)	Width (m)	Area (m^2)	($m^{-1/4}$)	(Dimensionless)
1.0	2.75	2.75	1.437	1.547
1.5	3.00	4.50	1.015	1.023
2.0	3.00	6.00	0.818	0.836
2.0	4.00	8.00	0.709	N/A
2.0	6.00	12.00	0.579	N/A

Table 10.2 Ventilation Parameters for the Compartments

The CIB formula used all five ventilation factors. Only the first three opening factors were valid for the BIA formula. The total number of runs per wall is now 20 for the comparison with the CIB formula, rather than 48, as was the case for the thermal analysis. This was because the structural model had a significantly longer run time than the thermal model. Only three walls were analysed using the structural model, to save time.

10.2.2 Modelling Temperatures Within the Stud

The thermal model of the walls described in Chapters 3 and 4, was subjected to the time-temperature curves derived using the compartment described in Section 10.2.1. From these data the nodal temperatures were extracted to provide a temperature input to the structural wall model. The modification factor for the temperatures described in Section 9.2 was not used here. This factor was used in order to prevent the calibration of the structural model being affected by errors in the temperature input. In a furnace test these errors could be found because temperature data were recorded within the stud during the test. It is not known whether they were appropriate in compartment fires as there are no data to ascertain their effect.

10.2.3 Modelling the Structural Response of the Wall

The structural model of the walls (Chapter 9) was run for each wall with temperature data from the thermal model described in Section 10.2.2. The load capacity was found, by a systematic trial and error process. Each run was time dependent and multiple runs for each combination of fuel load and ventilation factor had to be carried out to determine the failure load. The time dependence is because it is not possible to determine the worst temperature profile within the stud. The centreline of the stud is still getting hotter after the outside starts cooling, so the minimum load capacity of the stud occurs when the overall temperature profile gives the lowest temperature dependent strength of the stud as a whole. It is not possible to determine this time before the structural model is run. The load capacity was determined to the nearest 0.1 kN. The total run time was at least 15 minutes longer than the time at which the latest maximum temperature was reached in any part of the section, to the next 30 minutes. The capacity was deemed to be determined when the stud survived a certain load, but failed in the next load step when the load was incremented by 0.1 kN. The process by which the load is determined is shown graphically using data from the runs for one wall in Figure 10.1.

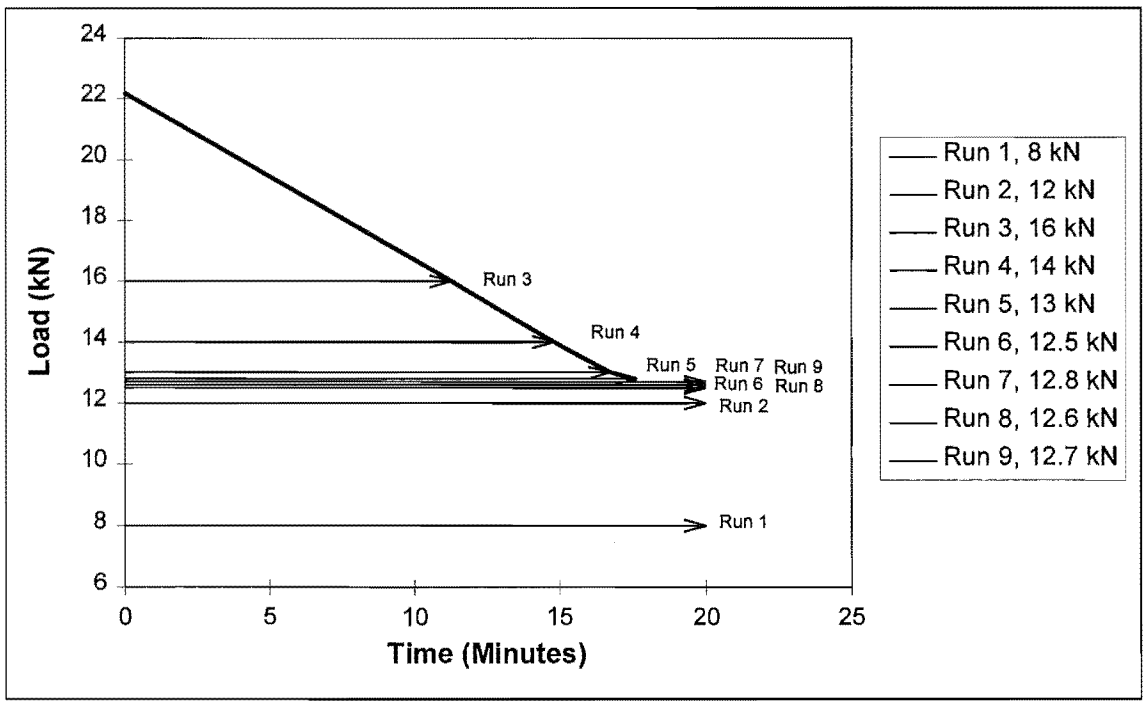

Figure 10.1 Determination of The Load Capacity

It is assumed that the strength and stiffness of the timber when cooling is not affected by previous high temperature excursions, that is, during the cooling phase the strength and stiffness is assumed to be the same as it was during the heating phase for any given

temperature. The effect of this assumption was checked by assigning to the stud the maximum nodal temperature reached at any time during the fire at each node and finding the load capacity. This was done for five combinations of ventilation factor and fuel load chosen at random. The effect of this was nil for two runs, reduced the capacity slightly for two runs and increased it slightly for one run. The overall effect was an average decrease in the load capacity by less than 5%.

The model would not be valid after the fire side lining has fallen off. This lining may fall off shortly after the time at which the test was halted due to structural failure, however, it was also assumed that the lining stayed intact and in place for the duration of the fire.

Table 10.3 shows the load capacity as a function of the fuel load and the opening factor for the 90*45 mm stud wall lined with 12.5 mm gypsum plasterboard.

Opening Factor ($m^{1/2}$)	Fuel Load (MJ/m^2)			
	200	**400**	**800**	**1200**
0.025	12.4	4.6	1.0	0.7
0.05	15.3	9.1	1.6	0.7
0.077	17.8	12.7	3.8	1.1
0.103	18.7	14.7	6.7	1.7
0.154	22.7	16.1	9.3	4.3

Table 10.3 Load Capacities for the 90*45 mm Stud Wall with 9.5 mm Lining (kN/Stud)

The load capacity reduces with the duration of the fire, that is, as the fuel load increases or the opening factor decreases. The trends in the load capacity for the other two wall layouts are very similar.

The failure mode is identical to that described in Chapter 9. The wall starts to deflect horizontally away from the fire and as the top of the stud rotates the point of application of the load also moves away from the fire. When the horizontal deflection becomes too large and the point of application of the load is so close to the edge of the stud that it can not move any further, the stud then fails in compression on the fire side, and the horizontal deflection increases almost instantaneously. The run terminates because the model can not cope with the extremely rapid deflections that immediately precede failure.

10.2.4 Characterising the Capacity - Time Curve for Furnace Exposure

Before a time equivalent could be calculated for the various compartment fire runs, the relationship between the load capacity and the time to failure must be characterised for the wall exposed to an ISO-834 test furnace. This was achieved by running the thermal model of the wall exposed to the ISO-834 time-temperature curve for a range of loads and the time to failure determined for each level of load. It was assumed that the lining stayed intact for the duration of the test. The load and time to failure are plotted in Figure 10.2.

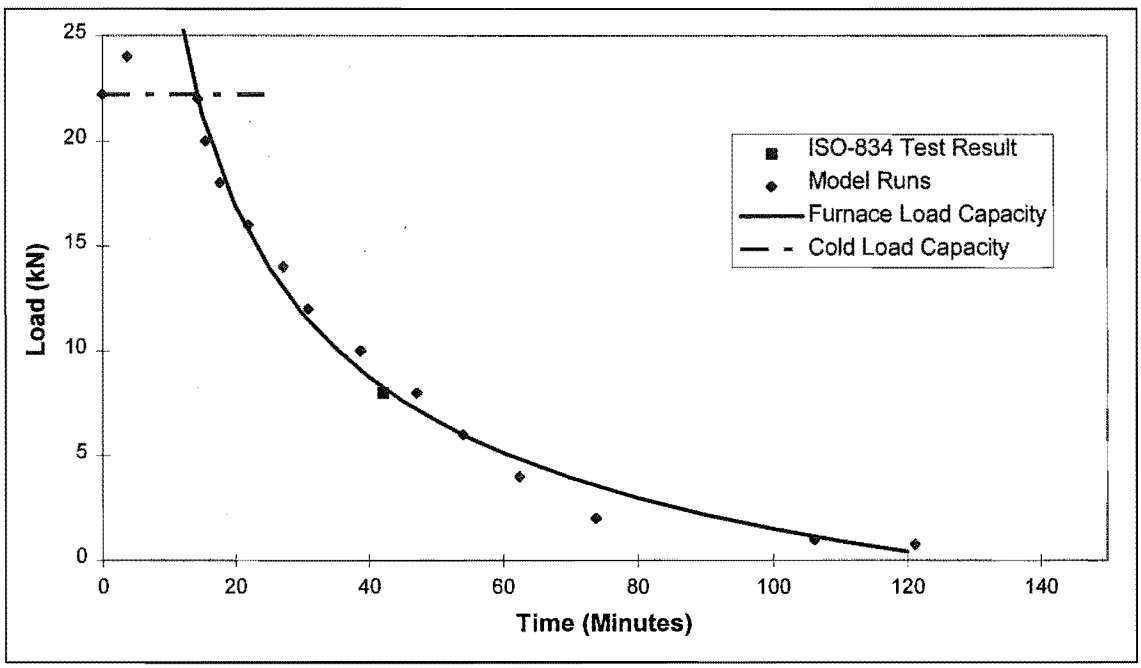

Figure 10.2 Time to failure for 90*45 mm Stud with 9.5mm Gypsum Plasterboard

A regression was used in order to calculate the time equivalent for the compartment fire runs. The same form of regression was used for each of the walls, as shown in Equation 10.1:-

$$t_e = \frac{a}{\sqrt{P}} + b \qquad (10.1)$$

where: t_e is the time equivalent (minutes)

P is the load (kN)

a, b are coefficients (dimensionless)

The point for the cold load capacity was omitted because the form of the regression does not allow it to pass through zero. The highest load that produced a result under fire conditions was also omitted from the regression because it is influenced by the cold load capacity of the wall.

The data points and regression for the other two walls are shown in Figures 10.3 and 10.4.

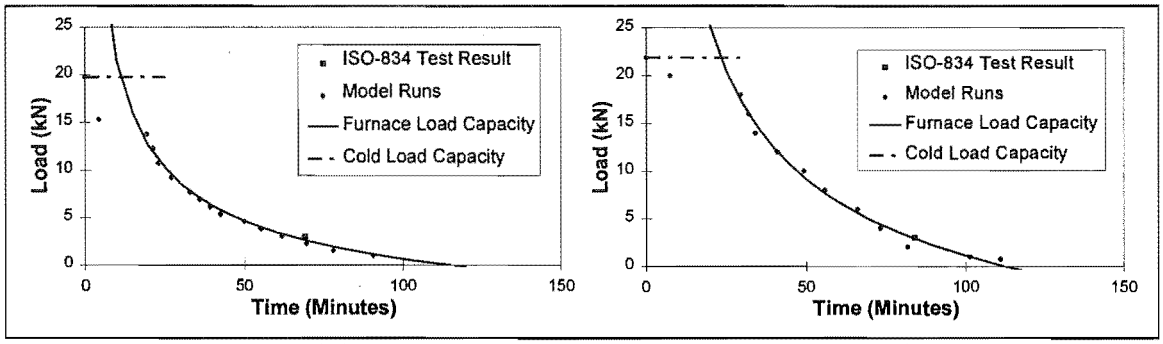

Figures 10.3 and 10.4 Time to Failure for 69*45mm Stud with 12.5mm Gypsum Plasterboard and 90*35mm Stud with 16mm Gypsum Plasterboard Respectively

The coefficients, ***a*** and ***b*** are different for the three walls, as shown in Table 10.4.

Stud Size (mm)	Lining Thickness (mm)	a ($kN^{1/2}$.min)	b (min)
90*45	9.5	124.5	-10.9
69*35	12.5	96.2	-9.0
90*35	16.0	193.5	-18.2

Table 10.4 Values for Coefficients a and b.

10.2.5 Calculating the Time Equivalent Values

The time equivalent values were then calculated for each combination of fuel load and ventilation by putting the load capacity found in Section 10.2.3 into the relevant formula from Section 10.2.4, giving a time in minutes. The definition of structural time equivalence is shown schematically in Figure 10.5.

The time equivalent is the time during an ISO-834 test which is equivalent to the maximum severity of a compartment fire, determined as being the point in time during the compartment fire at which the loadbearing capacity of a structural element is at a minimum (Section 1.3).

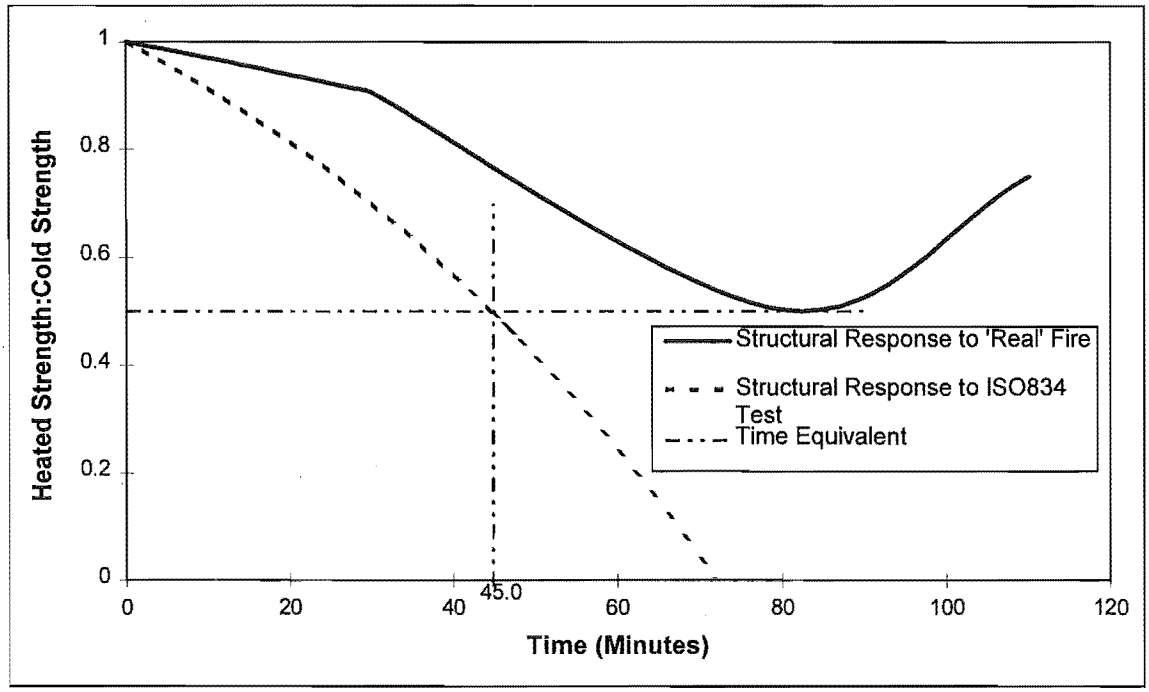

Figure 10.5 Definition of Structural Time Equivalence

Due to the fact that the modelled strength and stiffness of the timber as a function of temperature does not reach zero over 300°C, the section has a minimum load, below which the calculated load capacity can not go, regardless of the temperature profile (Section 9.4.2). This occurs at about 0.5 or 0.6 kN for the different stud sizes. To avoid this having an impact on the results these points were not included in the analysis. There was also one data point that had a load higher than the cold load and this was also omitted from the analysis.

The time equivalents for the wall with 90*45 mm studs and 9.5 mm gypsum plasterboard lining is shown as a function of the fuel load and ventilation factor in Table 10.5.

Opening Factor ($m^{1/2}$)	Fuel Load (MJ/m^2)			
	200	**400**	**800**	**1200**
0.025	28.5	64.2	108.7	N/A
0.05	22.5	38.6	98.5	N/A
0.077	18.8	27.7	71.3	106.9
0.103	17.6	23.6	49.8	97.0
0.154	N/A	21.2	37.8	66.7

Table 10.5 Calculated Time Equivalent Values for the 90*45 mm Stud Wall with 9.5 mm Lining (minutes)

The time equivalent reduces with the duration of the fire, that is, as the fuel load increases or the opening factor decreases. The trends for the other two wall layouts is very similar.

10.3 Results

The time equivalents found using the process described above were then plotted against the value calculated using the CIB formula and shown in Figure 10.6.

The comparison is good overall with the slope of the regression of 1.00 and a correlation coefficient, (R^2), of 0.72.

There is a significant difference between the comparison for the three different wall layouts. The slope for each layout is 0.95, 1.30 and 1.02 for the walls with 9.5, 12.5 and 16 mm lining respectively. This difference is due to the fact that different wall layouts respond differently to fires.

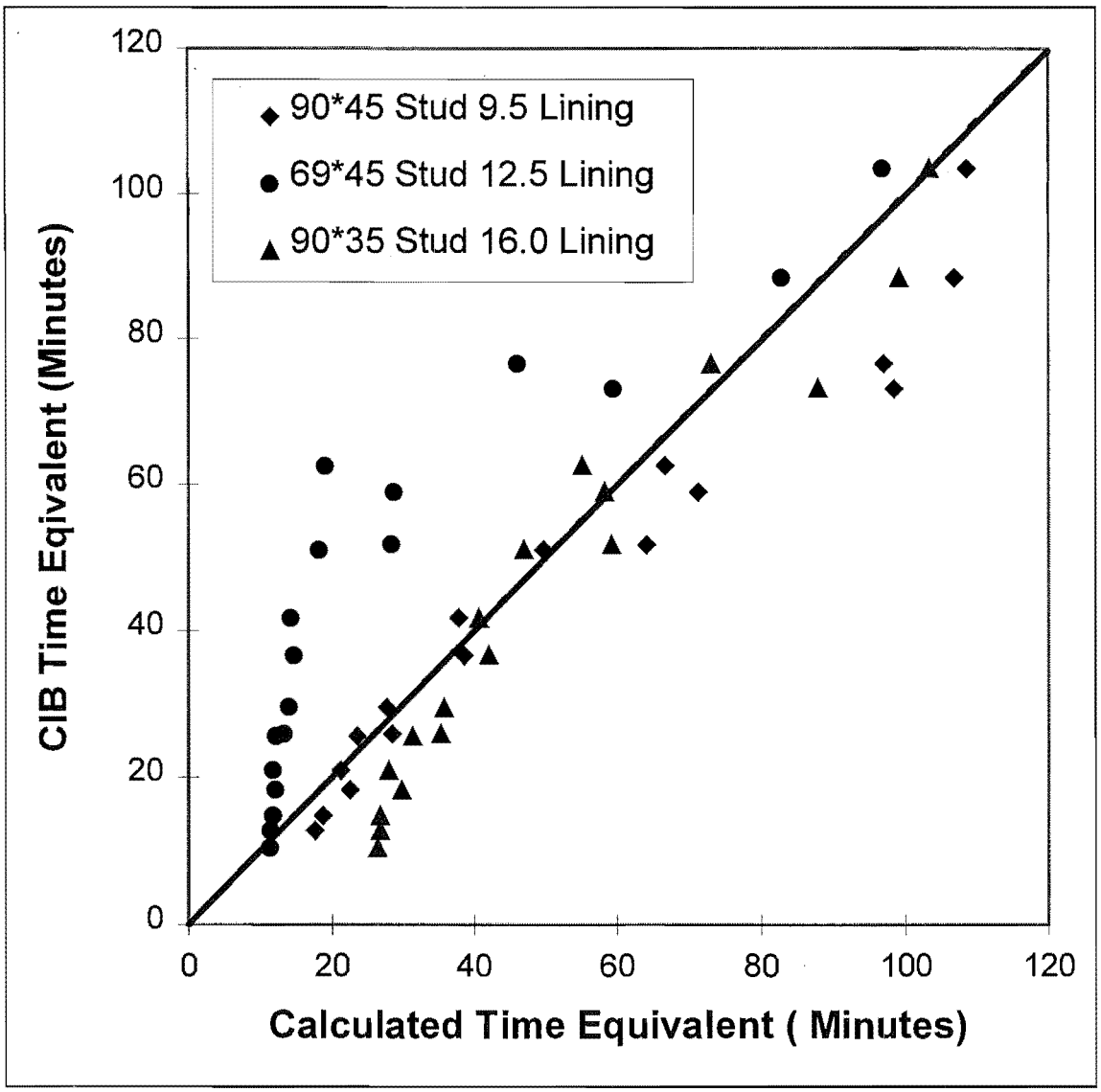

Figure 10.6 CIB Time Equivalent verses Calculated Time Equivalent for Structural Performance

10.3.1 Sensitivity Study

In Chapter 5, the time-temperature curve was modified in order to overcome the shortcomings of COMPF-2, which does not give a growth phase for the fire and terminates when the room temperature drops below 80°C (Section 5.3.1). The absence of a 100°C/minute growth phase resulted in a 12% increase in the slope of the regression for the charring criterion. It was decided to omit this growth phase in the structural analysis because it implies an increase in the total fuel load within the compartment above that specified (see also Section 5.6.2.1). The assumption that the compartment temperature takes 30 minutes to reach 20°C after the COMPF-2 output ends at about 80°C (Section 5.6.3) does not affect the results. The results of the sensitivity study (Section 5.6.1 and 5.6.2) for the charring criterion are used as this corresponds more closely with the structural criterion than the temperatures on the ambient side of the wall (insulation criterion).

Altering the emissivity or the convection coefficients also did not significantly affect the results, except for about 2% for the charring criterion (Section 5.3.4). A comparison using the Swedish time-temperature curves as input to the model was not done because the Swedish curves incorporate a number of assumptions that can not be justified, especially during the decay phase of the fire (Section 5.6.2.1).

The parameters that significantly affected the calculated time equivalents for the charring criterion are changing the value for the pyrolysates burnt within the compartment (BPF) from 0.7 to 0.9. This change resulted in the calculated time equivalence being halved (on average) for the charring criterion (Section 5.6.1). It was found in Section 5.6.1, that a change from 0.7 to 0.8 had little effect. The whole model was therefore run for one series of walls with a value for BPF of 0.9 rather than 0.7. The runs were carried out for one wall layout only, that is the wall with 90*45 mm studs lined with 9.5 mm gypsum plasterboard. Figure 10.7 shows the plot for that wall with a BPF of 0.7 and Figure 10.8 shows the plot with a BPF of 0.9 using the CIB formula for comparison purposes.

The slope of the regression has reduced significantly by 44%, and the correlation coefficient was good for both sets at a value of 0.94. This is similar to the reduction of 50% in the slope in the charring criterion, for a change in BPF of 0.7 to 0.9. The

number of points in the comparison was substantially reduced by the effect of the minimum load (Section 10.2.5), especially for a BPF of 0.9.

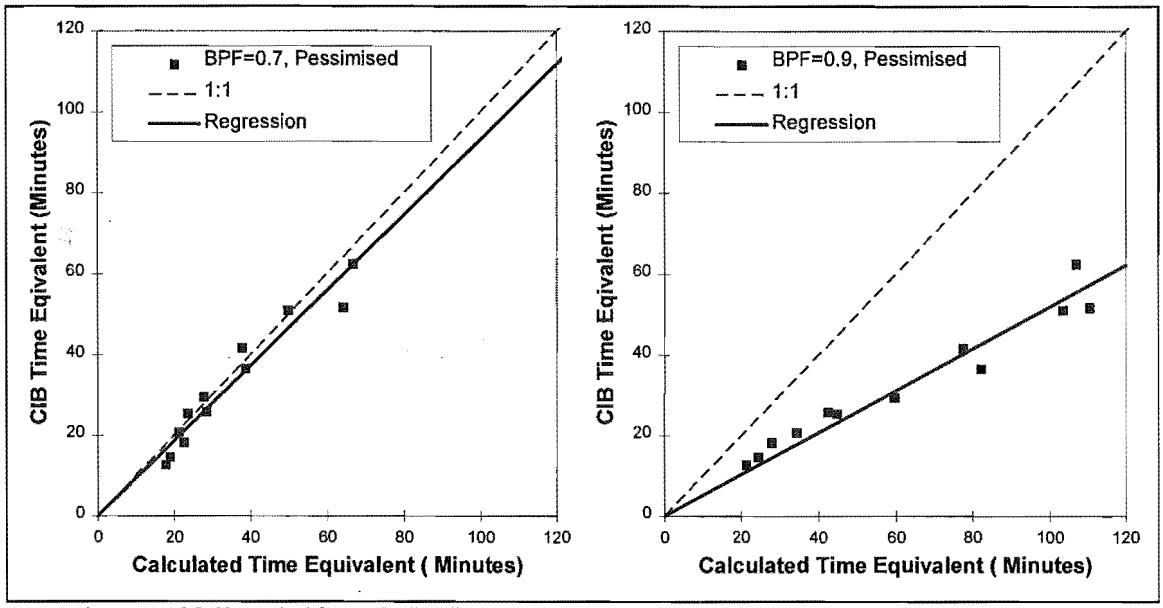

Figures 10.7 and 10.8 Calculated Time Equivalents for a BPF of 0.7 and 0.9 Respectively

Altering the shape of the decay phase increased the temperature based charring criterion results significantly, by 52% and 53% for the t^2 and linear decay phases respectively (see Section 5.6.2). For the structural analysis this effect was less marked for runs using a t^2 decay phase as shown in Figure 10.9 and 10.10.

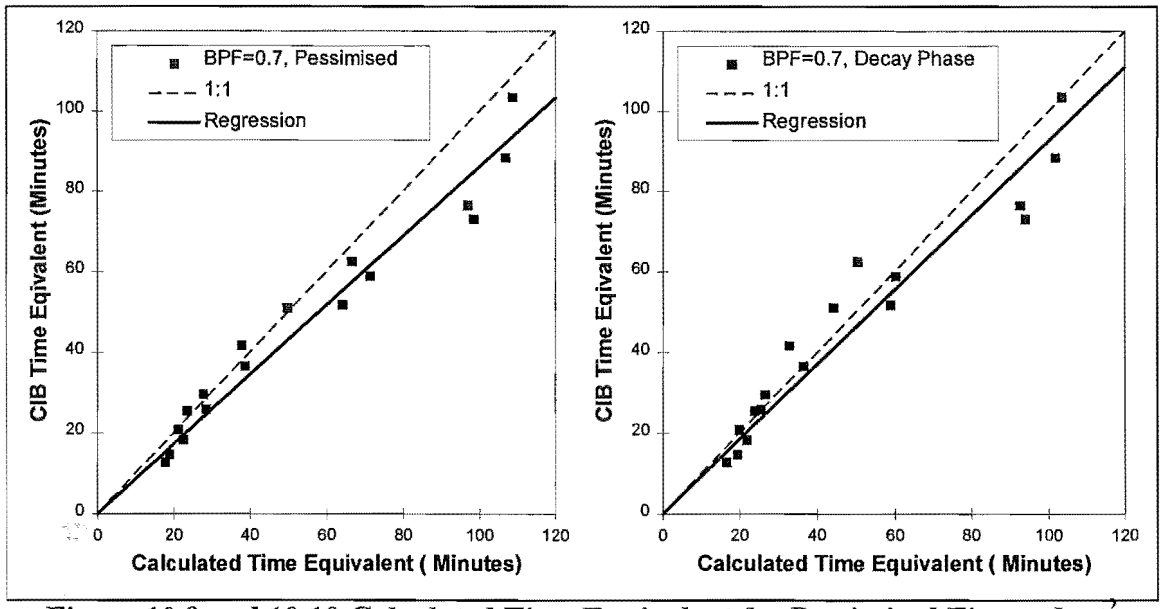

Figure 10.9 and 10.10 Calculated Time Equivalent for Pessimised Fire and a t^2 Decay Phase

The slope of the regression has increased by 8.8% and the correlation coefficient has also increased slightly. This increase is not large and would not normally warrant the additional complexity of using a decay phase rather than a fire that is pessimised throughout.

The t^2 decay phases used were produced by altering the shape of the heat release curve and using COMPF-2 to calculate the temperatures within the compartment. The total fuel load that was burnt during the course of the fire was the same for the three different shapes of the decay phase (see Section 5.6.2).

10.3.2 Validity of the Model at High Temperatures

After charring occurs in a large enough part of wood, it may not extinguish when the compartment fire goes out if there is enough oxygen in the cavity. This may cause localised failure in a timber structure after the fire has apparently gone out. This may or may not be a problem. It would not affect life safety, and is unlikely to allow fire spread to adjacent buildings. A localised failure is unlikely to lead to major structural collapse and given that it would occur between about 30 minutes and four hours after ignition, it could be assumed that the fire service response would prevent this occurrence.

To investigate this further, the regression shown in Figure 10.6 was re-calculated for the runs where the area of the charred cross-section (temperatures of greater than 300°C) does not exceed 100 mm^2. Another advantage of this reduction in the data set is that at temperatures below this, it is almost certain that the lining will be intact and so the thermal model will still be valid. This is then compared with the results from the charring criterion. The column in Table 10.6, labelled "<300°C" gives the values of slope and the correlation coefficient for these runs only.

CIB Formula	Structural		Charring
	All	<300°C	
Slope of Regression	1.00	0.86	0.65
Correlation Coefficient	0.72	0.55	0.88

Table 10.6 Values for the Regression Slope and R^2 for Complete and Reduced Data Sets

Omitting the runs in which charring is likely to continue results in a substantial reduction in the slope of the regression, from 1.00 to 0.86. The correlation coefficient is also substantially reduced from 0.72 to 0.55. A value of 0.55 is very poor and it is difficult to draw conclusions from the results. The slope is still higher than that given by the charring criterion (with no growth phase). The charring criterion is therefore a

conservative measure of structural failure by 24% when compared with the reduced (<300°C) data set for the structural criterion.

The sensitivity study described in Section 10.3.1, when analysed for these reduced data sets does not result in a change in the percentage difference between the base runs and those done with altered variables from the analysis of the full data set.

10.3.3 Results from The Comparison with the BIA Formula

Figure 10.11 is similar to Figure 10.6, but compares the BIA formula with the calculated time equivalents.

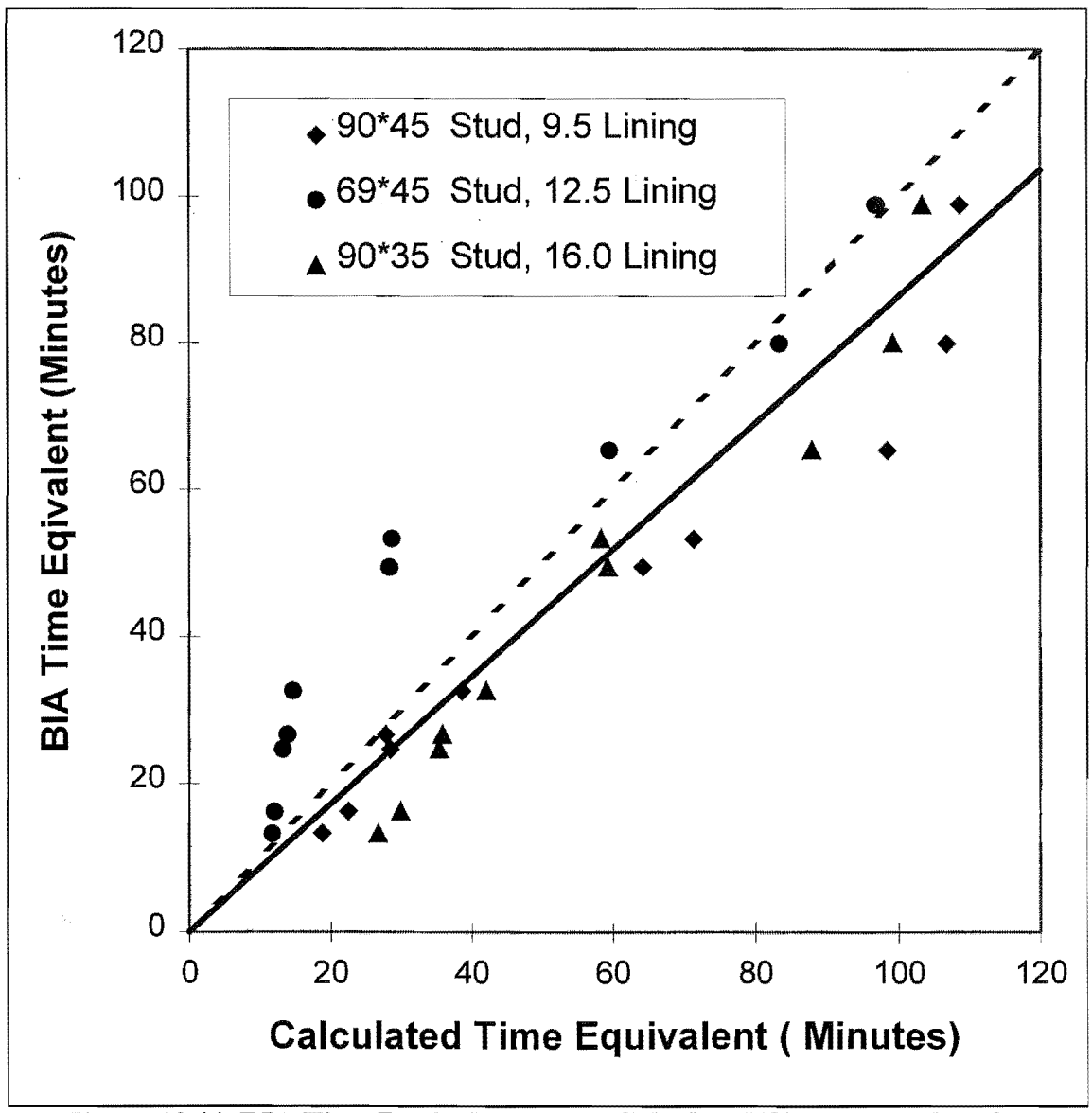

Figure 10.11 BIA Time Equivalent verses Calculated Time Equivalent for Structural Performance

The BIA formula is slightly conservative with a slope of the regression of 0.86. The correlation coefficient is 0.82.

There is a significant difference between the comparison for the three different wall layouts. The slope for each layout is 0.78, 1.10 and 0.92 for the walls with 9.5, 12.5 and 16 mm lining respectively. This difference is due to the fact that different wall layouts respond differently to fires.

10.3.3.1 Sensitivity Study for The BIA Formula

Two parameters were altered to check the sensitivity of the BIA time equivalent. They were the value for the percentage of pyrolysates burnt within the compartment (BPF) and the shape of the decay phase (Section 10.3.1). When these inputs were altered the percentage change in the slope of the regression was very similar to that found when using the CIB formula for the comparison.

10.3.3.2 Validity of the Model at High Temperatures

When data points are removed from the analysis because sufficient charring has occurred within the section to provide sustainable combustion after the compartment fire goes out, as shown in the "<300°C" column in Table 10.7, both the slope of the regression and the correlation coefficient is reduced.

BIA Formula	Structural		Charring
	All	<300°C	
Slope of Regression	0.86	0.75	0.64
Correlation Coefficient	0.82	0.56	0.88

Table 10.7 Values for the Regression Slope and R^2 for Complete and Reduced Data Sets

Omitting the runs in which charring is likely to continue results in a reduction in the slope of the regression, from 0.86 to 0.75. The correlation coefficient is also substantially reduced from about 0.82 to a very poor value of 0.56. The slope is still higher for both formula than that given by the charring criterion (with no growth phase). The charring criterion is therefore a conservative measure of structural failure by 15% when compared with the reduced (<300°C) data set for the structural criterion.

10.4 Conclusions

The agreement between both the CIB and the BIA formulae and the calculated time equivalents for the structural analysis of walls is reasonable with a fair value for the correlation coefficient of 0.72 and 0.82.

If the "<300°C" data sets are used the correlation coefficient is less than 0.6, which implies that there is too much scatter to justify using either the CIB or the BIA formulae. The lower values for the slope (0.86 and 0.75 for CIB and BIA respectively) found when charring was considered could be used when property protection is a consideration with a factor of safety to allow for the scatter of the results.

The effect of the shape of the decay phase and the proportion of pyrolysates burnt within the compartment is less severe on the structural time equivalence than it was for the temperature based criteria.

The temperature based charring criterion is a conservative method of estimating the structural performance.

The large degree of scatter and the variation between wall layouts indicates that the use of time equivalent formula is not an accurate method for predicting the structural response of light timber framed walls exposed to real fires.

Chapter 11 The Heat Transfer Model for Floors

11.1 Introduction

The floor sections modelled are typical in New Zealand timber construction. The joists are typically between 200*50 mm and 300*50 mm solid timber, with one or two layers of gypsum plasterboard on the underside of the ceiling. The flooring material is one layer of 20 mm particleboard. The only test results available were from one floor test with solid timber joists and three tests on "Twinaplate" floor joists. Twinaplate (Winstones 1989) joists are a proprietary product that consist of timber flanges and a corrugated steel web to form an I-Section.

The finite element floor model was developed and validated using the same procedure as described in Chapters 3 and 4 for the finite element wall model, using the program TASEF (Sterner and Wickstrom 1990).

11.2 Specific Heat, Enthalpy and Conductivity of the Materials

These properties were determined for wood and gypsum plasterboard as described in Sections 3.4 and 3.5. The thermal properties of wood and char are described in Sections 3.6 and 3.7. The particle board is assumed to have the same conductivity as the timber as described in Section 3.7, despite the difference in density. The specific heat is also assumed to be the same as timber, but since the density is higher, that is 600 kg/m^3 compared with 450 kg/m^3 for timber, the enthalpy of particleboard is taken as 33% higher than timber.

11.3 Heat Transfer Coefficients

The floors were modelled by assuming the above values for thermo-physical properties and modifying the heat transfer coefficients to give reasonable agreement for all four tests. The heat transfer coefficients were varied within a range that is deemed reasonable, considering values from the literature. The governing equation for heat transfer in TASEF at boundaries is given by Equation 3.2.

11.3.1 Heat Transfer Coefficients on the Furnace Side of the Floor

In New Zealand the only furnace test facility is at the Building Research Association (BRANZ) near Wellington. The same furnace is used for wall and floor tests and hence the same emissivity of 0.8 was used.

The dimensionless convective heat transfer coefficient or Nusselt number is a function of the Rayleigh (**Ra**) number raised to a power **b** and multiplied by a coefficient **a**. This is described in Section 3.9.3. The value of the coefficient and the power for a horizontal surface being heated from underneath are higher than those for a vertical plate. Table 11.1 shows the comparative values. The flow regime is turbulent through most of the test. Both Atreya's increase in convection power and Holman's increase in the convection coefficient from 0.1 to 0.15 in the turbulent regime result in about a 50% increase in the overall convection coefficient.

Source	Flow Regime	Walls		Floors	
		a	b	a	b
Gammon (1987)	Laminar	0.555	0.25	N/A	N/A
	Turbulent	0.021	0.4	N/A	N/A
Atreya (1988)	Laminar	0.6	0.2	0.54	0.25
	Turbulent	0.17	0.25	0.15	0.33
Holman (1992)	Laminar	0.59	0.25	0.54	0.25
	Turbulent	0.1	0.33	0.15	0.33

Table 11.1 Values of Convection Coefficients for Walls and Floors

On this basis a higher value for the convection coefficient for floors could be justified, however a sensitivity study showed that little difference would result, so the same value was used for both walls and floors. The value used was based on the assumption of natural convection heat transfer, which is not correct as the convection is forced, and the

values should be higher, however as most of the heat flux is due to radiation this has little effect on the final results.

11.3.2 Heat Transfer Coefficients on the Ambient Side of the Floor

The emissivity of a surface is not affected by its orientation relative to the horizontal so the value for emissivity of 0.6 is used, as was used for the walls.

The value of the convective coefficient and the power for a hot surface being cooled from above are higher than those for a vertical plate. These values are the same as for a cold surface being heated from underneath, given in Section 11.3.1 Once again a sensitivity analysis showed that increasing the value of the convection coefficient had little effect on the result. The same value used for the walls, was used for the floors; 2.2, and 0.33 for the convection coefficient and power respectively on the ambient side.

11.3.3 Heat Transfer Coefficients in the Void

The emissivity of 0.6 used for the walls was also used in the void. The convection coefficient was increased by 50% from 1.0 to 1.5 from that used for the walls. A sensitivity study was carried out varying the emissivity in the void from 0.4 to 0.9 and the convection coefficient from 0.5 to 3.5. The difference in temperature on the ambient side of the void varied by less than $10^{o}C$ and on the ambient side of the floor and within the joist by less than $5^{o}C$.

11.3.4 Final Values for the Heat Transfer Coefficients

The final values used for the emissivity (ε), convection coefficient (β) and convection power (γ) are given in Table 11.2.

Position	ε	β	γ
Fire Side	0.8	1.0	1.33
Lining, Fire Side of Cavity	0.6	1.5	1.33
Lining, Ambient Side of Cavity	0.6	1.5	1.33
Wood Stud Side of Cavity	0.6	1.5	1.33
Ambient Side	0.6	2.2	1.33

Table 11.2 Values Used for the Heat Transfer Coefficients

11.4 Geometry of the Finite Element Mesh

The geometry of the finite element mesh is very similar to that shown in Section 3.10 and Figure 3.30 except the mesh is more widely spaced across the void as the void is wider. The use of a region with fictitious material properties is used as described in Section 3.10 to allow for the contact resistance of the gap between the joist and the gypsum plasterboard.

11.5 Calibration and Validation of the Finite Element Floor Model

After a reasonable range for the appropriate values for the thermal and physical properties of the floor and its component materials were found, the model was calibrated using ISO-834 tests on light timber framed floor systems. Details of the tests used are shown in Table 11.3

Test No.	Test Code	Lining	Joist Depth	Joist Width	Thermocouples			
		(mm)	(mm)	(mm)	Ambient	Cavity	Sheath	Web
1	FR1202	12.5	245	45	8	0	16	0
2	FR1572	12.5	240	67	3	6	7	9
3	FR1369	14.5	240	67	5	2	9	6
4	FR1370	16	240	67	5	2	9	9

Table 11.3 Details of Floor Tests Used

Test FR1202 is a solid joist floor, whereas the other three are Twinaplate floors.

Thermocouples were located on the ambient side of the floor, within the cavity on the immediate underside of the flooring and in contact with the gypsum plasterboard on the ceiling. Sheath thermocouples were located 5 mm from the ceiling lining along the centreline of the joists. The steel webs in the twinaplate floors were instrumented with thermocouples welded to the web in sets of three down the web. The layout of the thermocouples is shown in Figure 11.1.

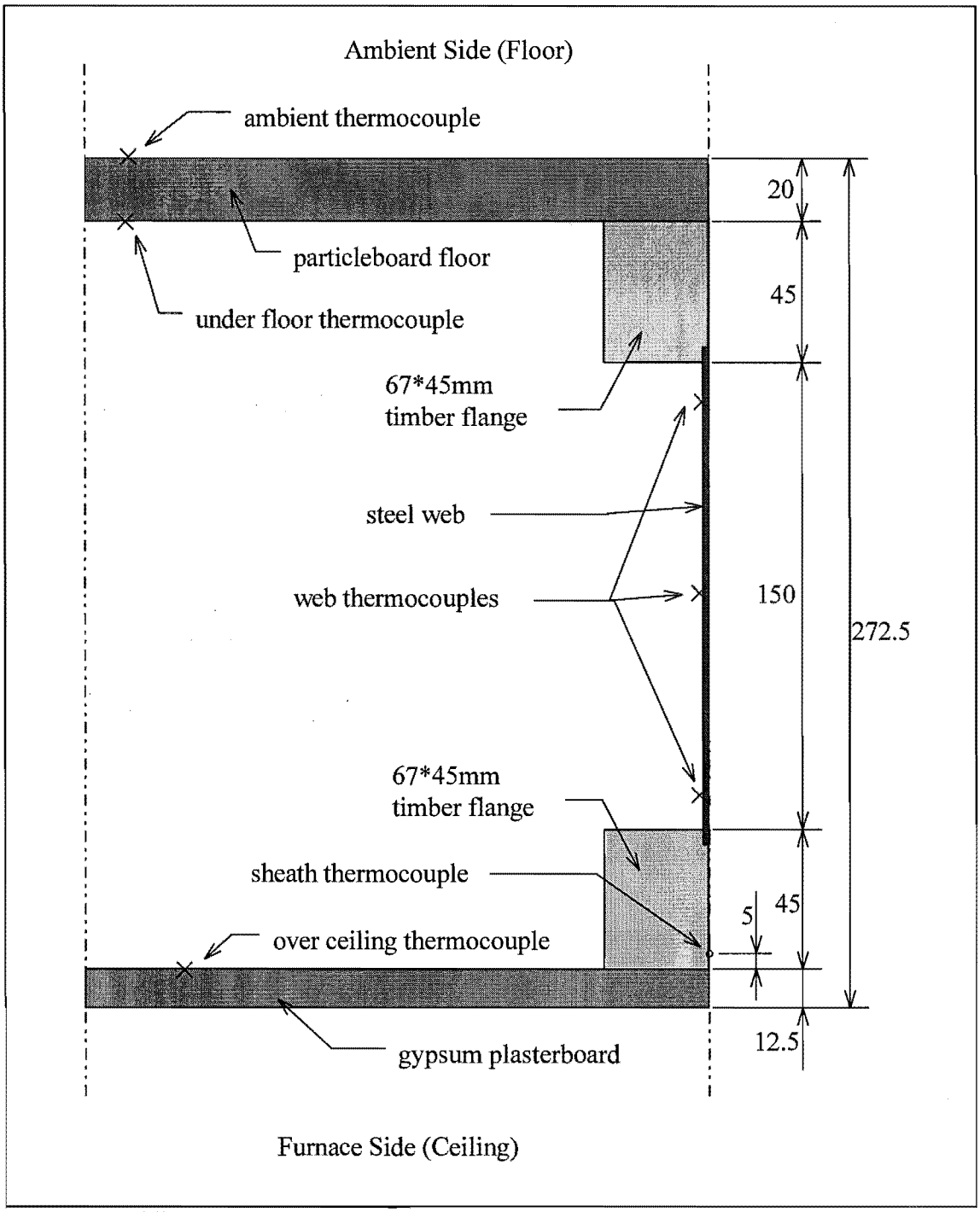

Figure 11.1 "Twinaplate" Floor and Thermocouple Layout

11.5.1 Floor Modelling in ABAQUS

The program TASEF, used for the finite element model of the walls, does not allow for voids with re-entrant angles which occur in Twinaplate floors. ABAQUS, (Hibbitt et al 1994), the general purpose finite element program was used to model the heat transfer in Twinaplate floors. It was first calibrated against the TASEF model of the solid timber floor. The same material properties and heat transfer coefficients were used in both programs. TASEF was used in most instances to model heat transfer as it is a specific

rather than a general purpose program and is faster than ABAQUS, even on a 66 MHz personal computer rather than a 333 MHz 64 bit DEC ALPHA 400 work station.

11.5.1.2 Modelling Void Convection in ABAQUS

ABAQUS does not have routines to calculate the temperature in the void or to vary the convection coefficient with temperature. A user coded sub-routine was written to calculate the convective heat transfer through the void. This routine assumes that the energy required to heat the air is negligible. The mathematical basis is derived as follows.

$$\Delta E_{air} = \Sigma H_c \tag{11.1}$$

where:- ΔE_{air} is the change in energy of the air due to convective heating, this is assumed to be zero

ΣH_c is the sum of the convective heat flux into the void

$$\Sigma H_c = \sum_{i=1}^{n} L_i \beta \left(\Delta T_i\right)^{\gamma} \left(T_{node,i} - T_{air}\right) \tag{11.2}$$

where:- L_i is the tributary length for the node (m)

β is the convection coefficient (dimensionless)

ΔT_i is the temperature difference between the ith node and the void (°C)

γ is the convective power, in this case 0.33 (dimensionless)

$T_{node,i}$ is the temperature of the ith boundary node (°C)

T_{air} is the void temperature (°C)

Since ΔE_{air} is zero then ΣH_c is zero, so Equation 11.2 can be rearranged to give:-

$$\sum_{i=1}^{n} L_i \beta \left(\Delta T_i\right)^{0.33} T_{air} = \sum_{i=1}^{n} L_i \beta \left(\Delta T_i\right)^{0.33} T_{node,i} \tag{11.3}$$

This can be further rearranged to give the value for void air temperature:-

$$T_{air} = \left(\sum_{i=1}^{n} L_i \beta (\Delta T_i)^{0.33} T_{node,i}\right) \Big/ \left(\sum_{i=1}^{n} L_i \beta (\Delta T_i)^{0.33}\right) \quad (11.4)$$

Since ΔT_i is a function of T_{air}, this Equation is solved iteratively to give a value for the void temperature. This method of solving for the void air temperature is also used in TASEF.

User coding also had to be used to define the variable convection conditions on the furnace and ambient side of the floor.

11.5.1.3 Comparison Between the ABAQUS and TASEF Model

The use of the ABAQUS heat transfer model was developed piecemeal. First a model of a solid block with prescribed temperatures at the boundary nodes was modelled in ABAQUS and TASEF and then compared. Then a void with radiation boundary conditions only was modelled. Next the furnace and ambient boundary conditions were modelled with radiation and convective heat transfer. Then a model with fixed boundary temperatures and only convective heat transfer in the void was modelled in both programs and compared. Finally a complete model with convective and radiative heat transfer on both sides and within the void was compared.

The comparison through the floor at the centreline of the void is shown in Figure 11.2.

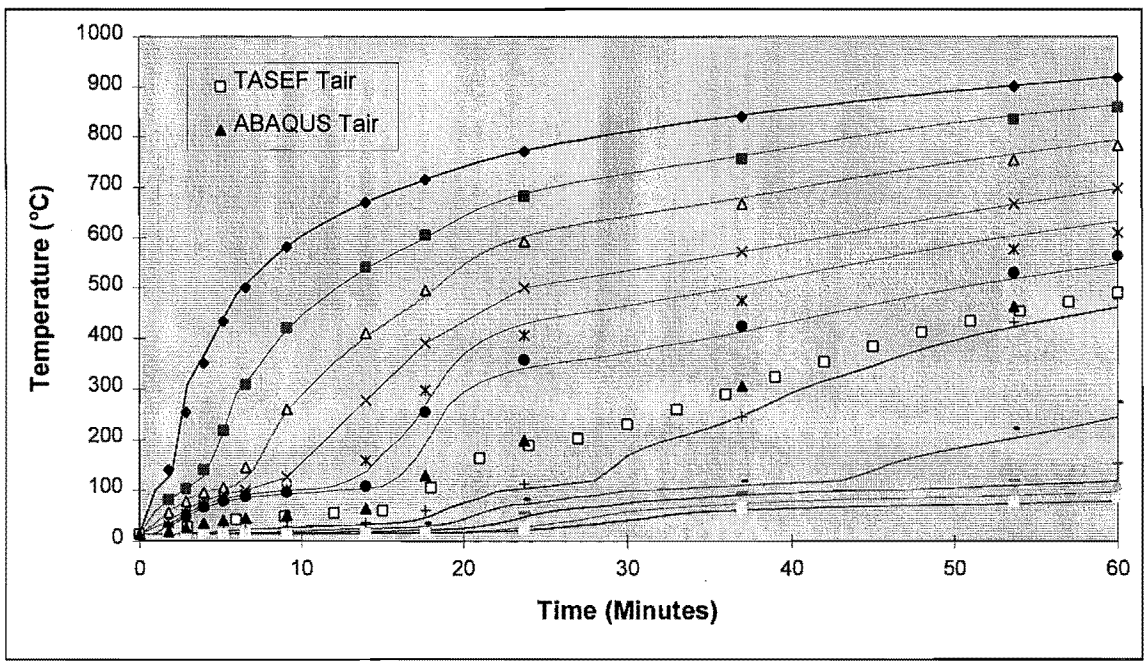

Figure 11.2 Comparison Between the ABAQUS and TASEF Model at the Void Centreline

The symbols are the temperatures on the gridlines through the floor at the centreline of the void from the ABAQUS output. The solid lines are the output from TASEF. The top curve is that at the ceiling level and the lowest on top of the floor on the ambient side (see Figure 11.1).

The two symbols shown in the legend are ABAQUS T_{air}, the air temperature in the void calculated using ABAQUS, and TASEF T_{air} the air temperature in the void calculated using TASEF. The comparison is very good, throughout the wall and within the void. This is to be expected if both programs perform the heat transfer analysis properly as the same heat transfer laws and Equations should govern both programs.

Figure 11.3 shows the comparison between ABAQUS and TASEF through the centreline of the joist. Again the comparison is very good.

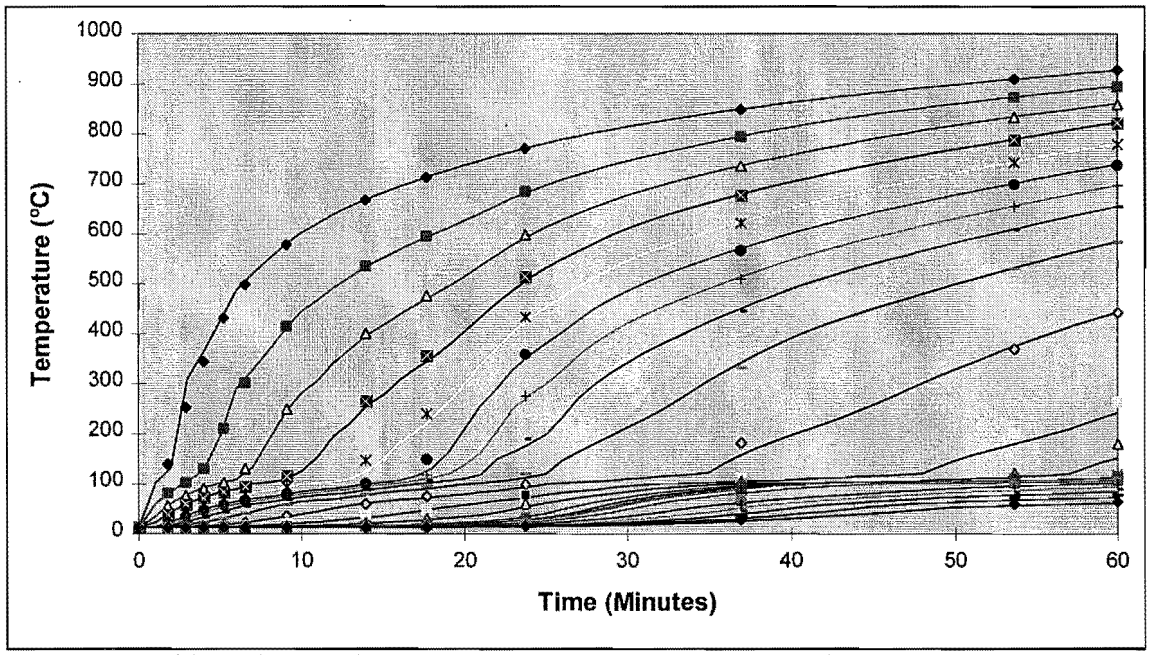

Figure 11.3 Comparison Between the ABAQUS and TASEF Model at the Centreline of the Joist

11.6 Comparison between the Tests and the Model

Once the model had been developed it was compared with test results.

11.6.1 Floor with Solid Joists

Test FR1202 consisted of solid 245*45 mm joists at 400 mm centres and with a 20 mm particleboard flooring. The floor is protected by 12.5 mm "Fyreline" gypsum

plasterboard. The wall has an FRR of 30 minutes. The comparison between the test data and the model is shown in Figure 11.4.

The comparison is at two points, the sheath, 5 mm from the exposed side of the joist (similar to Figure 11.1) and on the ambient side. The comparison is good for the sheath thermocouple points, for the first 30 minutes, after which the ceiling lining started to fall off. The comparison is good on the ambient side, for the duration of the test.

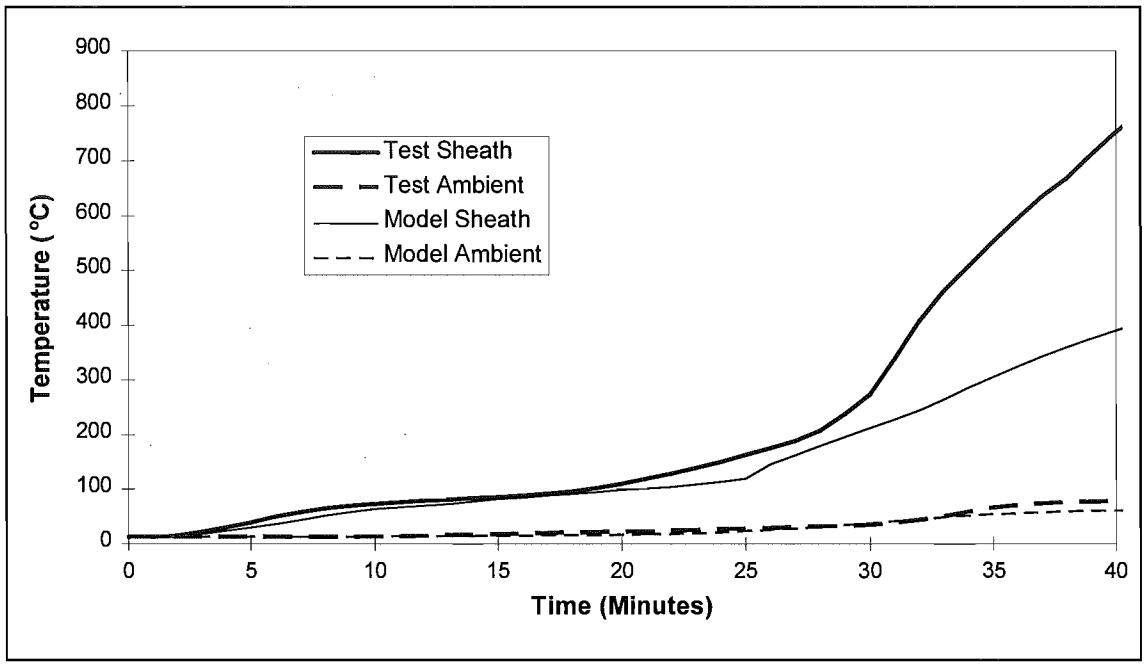

Figure 11.4 Comparison Between Test and Model for Test FR1202

11.6.2 Floors with Twinaplate Joists

For these floors the comparison was very similar to that for the floor with solid joists as shown in Figure 11.5.

These tests were instrumented more thoroughly, and a good comparison was achieved at all instrumented points for all three tests. The comparison between the tests and the model shown in Figure 11.5 is for test FR1572, a "Twinaplate" floor protected with one layer of 12.5 mm "Fyreline" gypsum plasterboard. This floor also has an FRR of 30 minutes. The location of test points is shown in Figure 11.1.

The comparison is very good on the ambient side, reasonable at the point over the ceiling, but is only fair for the sheath thermocouple and under the floor.

The other two tests were also compared but are not illustrated here. The comparison between test FR1369 and the model is much better with good agreement between the sheath and under floor thermocouples. It was very good on the ambient side, but the model underpredicts the temperatures over the ceiling as the test time approaches one hour.

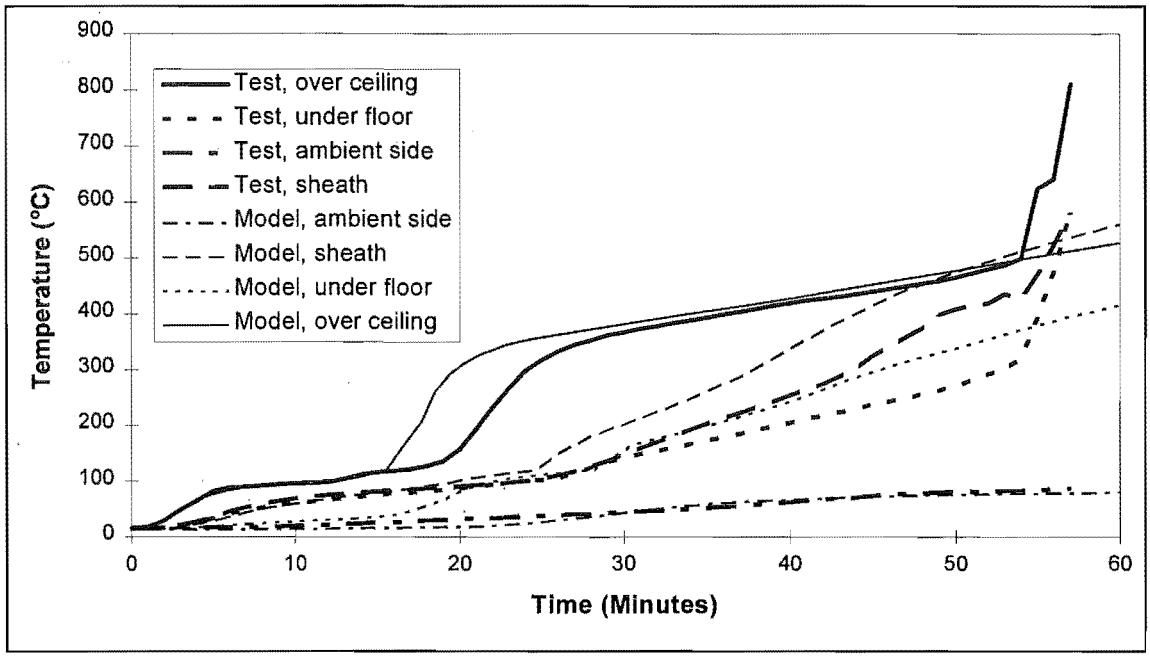

Figure 11.5 Comparison between Model and Floor Test FR1572

For test FR1370, with 16 mm gypsum plasterboard lining is very good on the ambient side, but the model overpredicts the temperatures by a significant amount for the sheath thermocouples and to a lesser extent both over the ceiling and under the floor.

The most important comparison is on the ambient side and that is very good for all three tests.

11.7 Conclusions

A finite element heat transfer model has been developed that compares well with test data. It is identical to that used in Chapters 3 and 4 for walls, except a slightly higher value is used in the cavity for the convective heat transfer coefficient.

TASEF was not suitable for voids with re-entrant corners, so ABAQUS was used for the twinaplate floors.

Both programs, ABAQUS and TASEF give almost exactly the same results, as expected, for solid joist floors.

Chapter 12 Thermal Time Equivalence for Floors

This Chapter describes how the compartment fire model COMPF-2 (Babrauskas 1979) described in Chapter 2 was used to develop time-temperature curves for a range of ventilation factors and fuel loads. The floor model developed in Chapter 11 was then subjected to the time-temperature curves developed using COMPF-2. The maximum temperature values for the insulation, charring and integrity criteria were recorded and an equivalent time deduced from the results from the same floor model exposed to the ISO-834 time-temperature curve. The results were then compared with those found using the CIB and BIA formulae described in Section 1.1

The procedure is the same as that used in Chapter 5 for determining the thermal time equivalence for walls. Sensitivity studies were carried out on significant parameters. Finally the overall results are discussed and conclusions drawn.

The relationship between the calculated and CIB time equivalent formula is reported because the CIB formula is valid for larger ventilation values, which are common in residential buildings in New Zealand and because it has been published in a refereed journal where as the BIA formula has not. The BIA formula is also mentioned because it is specified in the New Zealand code (NZBIA 1992).

12.1 Failure Criteria

The failure of the specimen was determined by using the following three temperature based criteria:-

(i) The time to failure of the floor due to the insulation criterion, that is the time at which the temperature at the unexposed side of the floor (top surface) undergoes an increase of 140°C.

(ii) The time to "structural failure" defined as the time to onset of char in the timber joist, 5 mm from the exposed face on the centreline of the joist, assumed to occur at a temperature of 290°C.

(iii) The time to "integrity failure of the floor" defined as the time at which the underside of the flooring material reaches 320°C. At about this temperature the particleboard flooring softens to such a degree that the loading system penetrates the flooring in furnace tests. The failure criterion may be different for other flooring materials such as plywood. This is not the same definition used in the standard ISO-834 furnace test, but gives an indication of it.

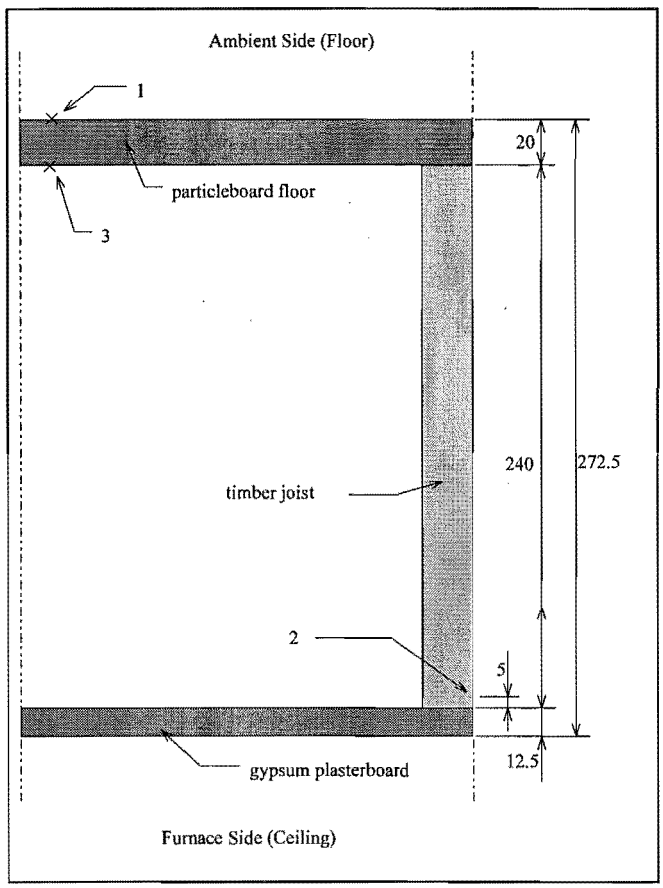

Figure 12.1 Layout of Floor System and Location of Failure Criteria Points

The points at which the temperature was measured are shown in Figure 12.1. The positions 1, 2 and 3 refer to the three failure criteria mentioned above.

The first of these failure criteria is rarely the cause of failure in a load-bearing floor and the second is somewhat conservative. However it will be followed up by a more rigorous study of structural capacity in Chapters 13 and 14. The third is the usual failure mechanism in furnace tests at BRANZ.

12.2 Calculation of Time Equivalence

The calculated time equivalence was found by subjecting the finite element floor model described in Chapter 11 to a compartment fire time-temperature curve derived using COMPF-2. COMPF-2 is described in Chapter 2 and the parameters used in this study are described in Section 5.3.1.

For each combination of ventilation factor and fuel load, the maximum temperature was found at the three locations in the wall assembly defining the charring, insulation, and integrity criteria described in Section 12.1.

The time at which these temperatures were reached in the same three locations, during a model run with the same system exposed to the ISO-834 temperature curve was then found. These three times were defined as the calculated time equivalent for each criterion. In some cases the maximum temperature reached in the floor model when exposed to a compartment fire was higher than the maximum temperature reached during the test. In that case there was no calculated time equivalent and the data point was omitted from subsequent analysis.

12.3 Assumptions and Values Chosen for Variables

The model COMPF-2 was used to derive the compartment fire temperatures. Heat transfer through the floors was modelled using TASEF (Sterner and Wickstrom 1990).

12.3.1 COMPF-2

COMPF-2 is described in Section 2.5. The exact variables used to give the time-temperature curves for the determination of the time equivalence of light timber framed floors are the same as for the light timber framed walls, described in Section 5.3.1 and summarised below:-

(i) A range of opening factors (Equation 5.1) was used as shown Table 12.1.

WINDOW			Opening Factor	Ventilation Factor	Ventilation Factor
Height (m)	Width (m)	Area (m^2)	(Eqn 7) ($m^{1/2}$)	CIB (Eqn 1.2) ($m^{-1/4}$)	BIA (Eqn 1.3) (Dimensionless)
1.0	2.75	2.75	0.025	1.437	1.547
1.5	3.00	4.50	0.050	1.015	1.023
2.0	3.00	6.00	0.077	0.818	0.836
2.0	4.00	8.00	0.103	0.709	N/A
2.0	5.00	10.00	0.129	0.634	N/A
2.0	6.00	12.00	0.154	0.579	N/A

Table 12.1 Ventilation Parameters

(ii) The compartment size chosen is shown in Figure 12.2.

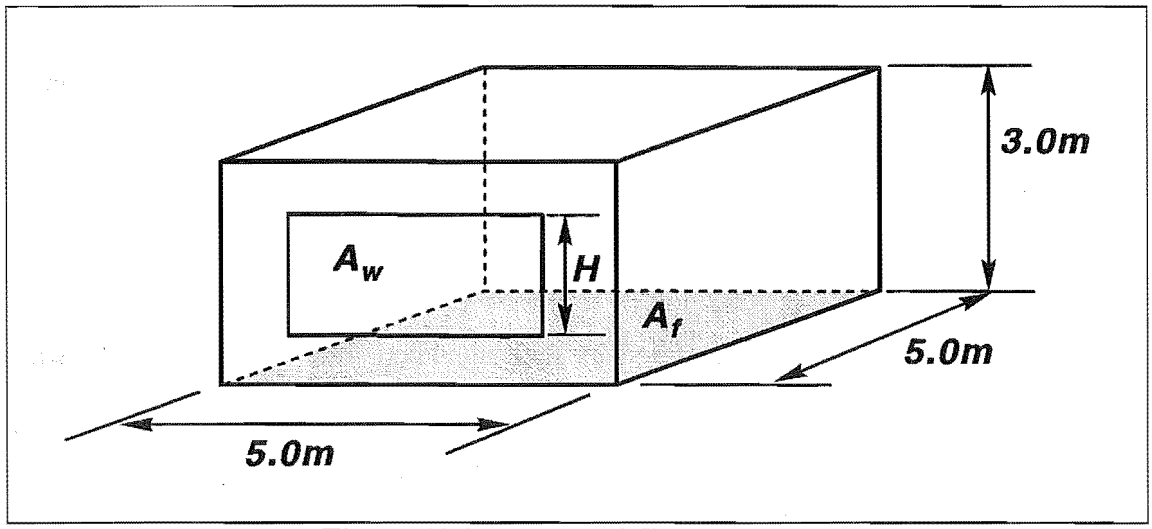

Figure 12.2 Layout of Compartment

The total floor area is 25 m^2 and the total bounding surface area is 110 m^2.

(iii) A range of fuel loads were used, with values of: 100, 200, 300, 400, 500, 600, 800 and 1200 MJ/m^2 of floor area.

(iv) Percentage pyrolysates burnt within the compartment will be 70%.

(v) The fire will be ventilation controlled throughout. This was achieved by using the pessimising option over the pyrolysis rate.

(vi) The initial rate of temperature increase within the compartment was 100^{O}C per minute.

(vii) After the COMPF-2 time-temperature output stops, when the compartment temperature drops below 80^{O}C; the temperature drops to 20^{O}C in 30 minutes and remains at 20^{O}C for 90 minutes.

(viii) A floor/ceiling assembly was chosen for each floor and the thermal properties of the boundary was taken as the average of that of the ceiling (COMPF-2 assumes there is no heat loss through the floor) and the walls, weighted over the relative area of each. Table 12.2 shows the parameters chosen for the three floors.

Test Code	Floor		Wall	
	Joist Depth (mm)	Lining Thickness (mm)	Stud Thickness (mm)	Lining Thickness (mm)
A	240	12.5	90	12.5
B	290	16	140	16
C	140	12.5	70	9.5

Table 12.2 Details of Compartment Boundaries

12.3.2 TASEF

The calculated time equivalence for a floor assembly was based on the maximum temperature found in critical locations in the floor assembly, using TASEF. The time-temperature curves defined above in Section 12.2.1 were used as input time-temperature curves in the TASEF analysis. These are similar to those shown in Figure 5.3 for walls.

Three different floor assemblies were used, with different combinations of joist size and lining thicknesses. The floor assemblies are described in Table 12.3:-

Test Code	Furnace Test Number	Lining Thickness (mm)	Joist Depth (mm)	Joist Width (mm)
A	FR1202	12.5	240	45
B	Not Tested	16	290	45
C	Not Tested	12.5	140	45

Table 12.3 Parameters of Floors Used

The combinations of three floor layouts, six ventilation factors and eight fuel loads give a total of 144 simulations. There were less than 144 data points in the results because some temperature values were higher than those reached in the furnace tests as described in Section 12.2.

12.3.3 Heat Transfer Coefficients

The heat transfer coefficients were altered from those used for the furnace model at the fire exposed underside of the floor, for both radiative and convective heat transfer, as for walls (Section 5.3.4). This was to allow for the differences in the thermal environment between a furnace and a compartment fire. The values used must be the same in COMPF-2 and TASEF. The program COMPF-2 was modified to allow for this.

The compartment gases were assumed to have an emissivity of 1.0. Combining this value with a floor emissivity of 0.9 gives an effective value of 0.9. This was higher than the value of 0.8 used to correlate the floor model undergoing furnace exposure (Chapter 11) because of the differing emission characteristics of the furnace and a compartment fire.

The convection coefficient, β, used was also higher (5.0 compared with 1.0), than that used to calibrate the floor model for furnace exposure (Chapter 11), as the air flow in a burning compartment is not as well defined as in a furnace, and is expected to be more turbulent.

12.4 Matching Variables in the Sub-Models

The time-temperature curves found above for the three different floor assemblies were input into the TASEF finite element model of the floor assemblies. Some parameters must be identical for both models and some parameters must be adjusted in COMPF-2 to allow for differences in the way that the floors were modelled in COMPF-2 and TASEF.

The properties of the timber framed cavity floor had to be modified to mimic those of an equivalent solid floor. The two properties that need to be altered are enthalpy and conductivity.

12.4.1 Enthalpy

Enthalpy is the integral over temperature of the product of specific heat and density and was input as such to COMPF-2. The density term was altered in a relatively simple way. By altering the density term to be a weighted average of density over the thickness of the floor, the enthalpy as a function of temperature for the entire floor remains the same as for the lining with a finite enthalpy and assuming zero enthalpy for the air in the cavity. The same method was used for the walls.

12.4.2 Conductivity

The conductivity also had to be altered, but this is more complex due to the highly non-linear variation in heat transfer, by radiation and convection with respect to temperature within the cavity.

The effective value for the overall conductivity was calculated by multiplying the conductivity by the ratio of the cavity width over the lining thickness (of both sides) and assuming the conductivity does not increase over 300°C. The reasoning behind using this method is described in Section 5.4.2.

12.4.3 Effect on Floor Boundary Temperatures

The temperatures found using COMPF-2 and TASEF on both the exposed and unexposed side of the floors were similar, as was the case for the walls in Section 5.4.3, hence the assumptions made regarding the enthalpy and conductivity of the wall as a homogeneous solid are valid.

12.5 Overall Results

The maximum temperature values for the insulation, charring and integrity criteria were recorded and an equivalent time deduced from the model results. Values for time equivalents were calculated using the CIB formula (Section 1.2.1), with **c** = 0.09, the recommended value for lightweight linings.

12.5.1 Charring Criterion

Figure 12.3 shows the results for the charring analysis using the input values derived in this Chapter.

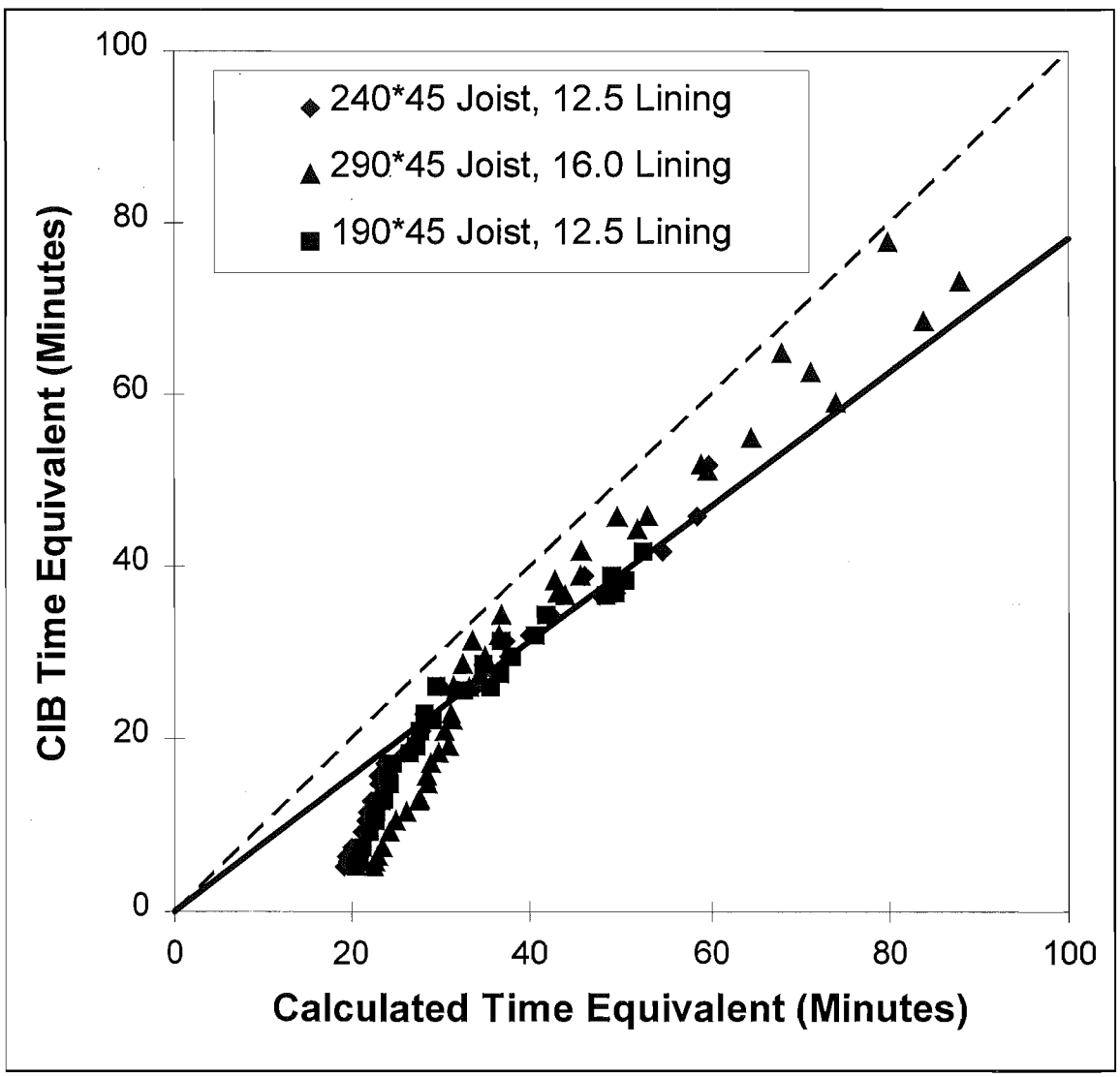

Figure 12.3 CIB Time Equivalent vs. Calculated Time Equivalent for Charring Criterion

The relationship between the calculated time equivalent, for charring, and the CIB time equivalent derived using Equation 1.3 is shown. The symbols are data points for the

three different floor layouts (Table 12.3). The floors with the thicker linings performed better than floors with thinner linings, since their actual time equivalent was shorter relative to the CIB time equivalent. Overall the actual time equivalent was 78% of that calculated using the CIB formula. The regression was forced through zero with a correlation coefficient of 0.88.

12.5.2 Insulation Criterion

Figure 12.4 plots the calculated versus the CIB time equivalent for insulation.

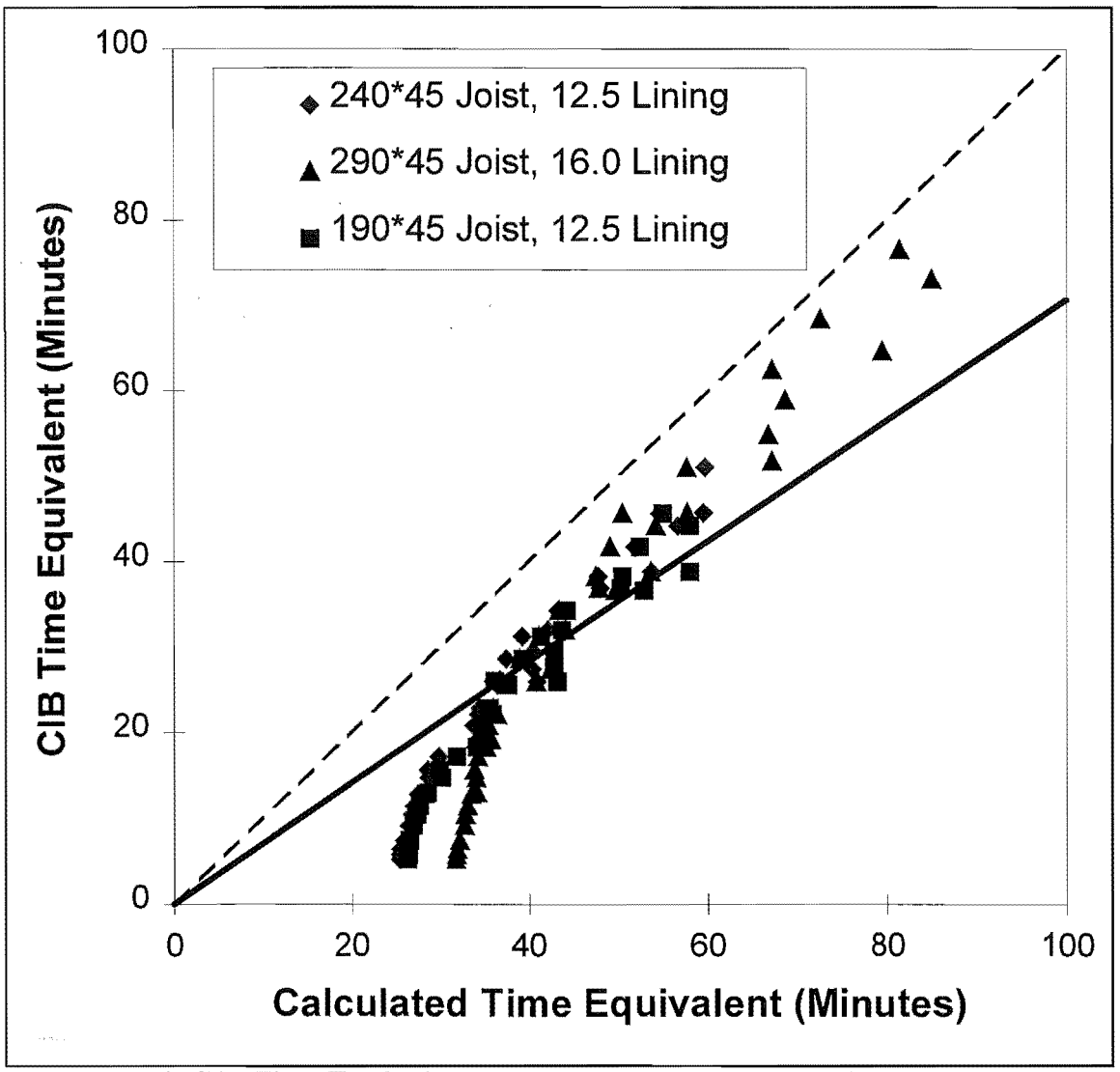

Figure 12.4 CIB Time Equivalent vs. Calculated Time Equivalent for Insulation Criterion

As was the case for the charring criterion, the floors with the thicker linings performed better, since their calculated time equivalent was shorter relative to the CIB time equivalent. Overall the calculated time equivalent was 71% of that calculated using the CIB formula. The correlation coefficient for the regression was 0.77.

12.5.3 Integrity Criterion

Figure 12.5 plots the calculated versus the CIB time equivalent for the integrity criterion.

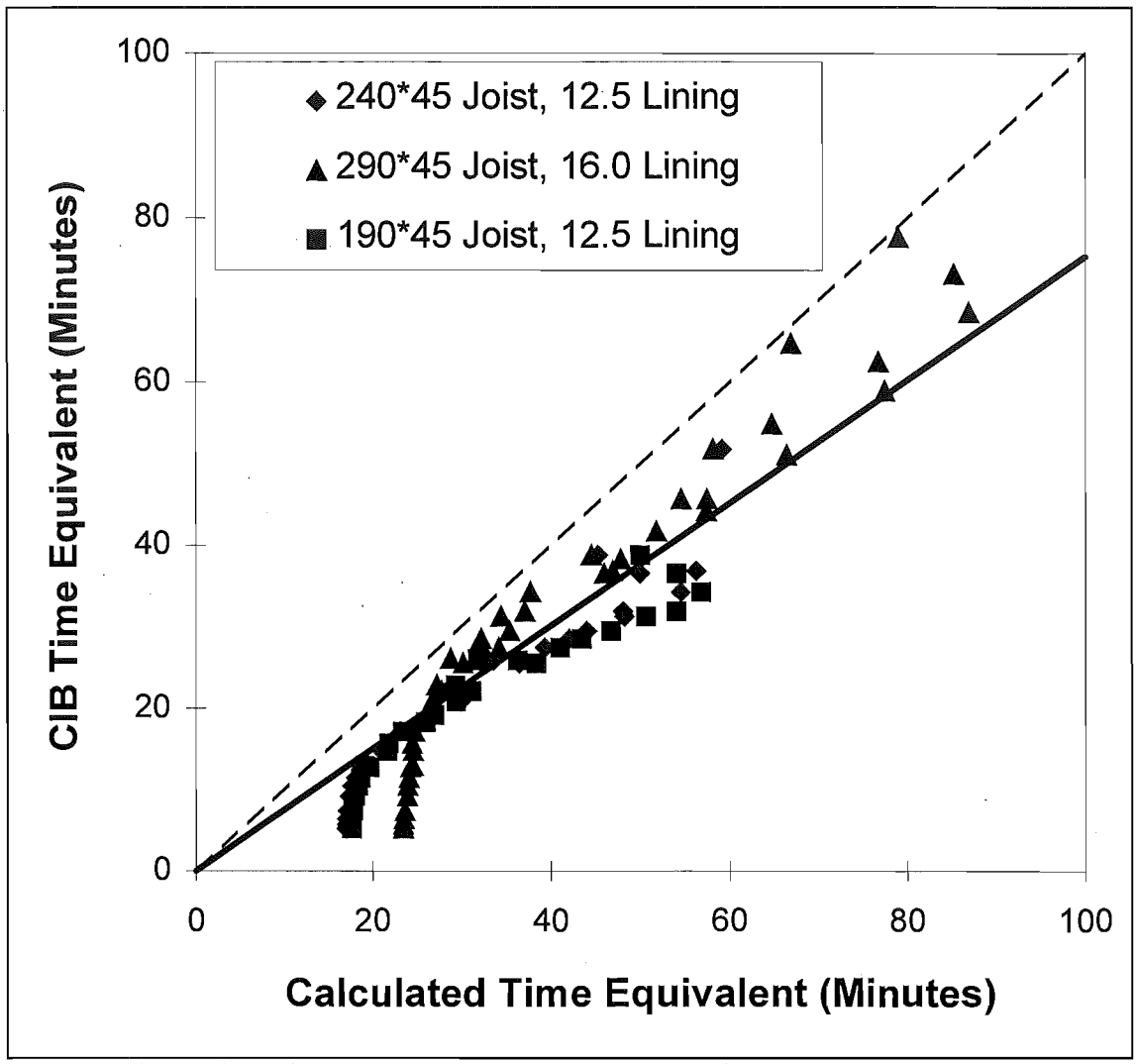

Figure 12.5 CIB Time Equivalent vs. Calculated Time Equivalent for Integrity Criterion

Overall the calculated time equivalent was 75% of that calculated using the CIB formula. The correlation coefficient for the regression was 0.89.

12.5.4 Comparison using the BIA Formula

When the BIA formula is used with a value for **c** of 0.08, the slope is 0.73 with a correlation coefficient of 0.89 for the charring criterion.

The BIA formula results in a slope of 0.64 and a correlation coefficient of 0.83 for the insulation criterion.

For the integrity criterion the BIA formula has a slope of 0.73 and a correlation coefficient of 0.89.

12.5.5 Summary

The correlation between the calculated and CIB time equivalent is good, with a reasonably linear dependence. The CIB formula predicts the trend of the results, but consistently underestimates the values.

12.6 Sensitivity Study

The most critical parameters in the compartment fire sub-model were varied in order to determine their effect on the overall results.

The four parameters are:-

(i) The fraction of fuel burnt within the compartment (Section 12.6.1).

(ii) Modifications to the COMPF-2 time-temperature output (Section 12.6.2).

(iii) The shape of the decay phase of the fire, shown by its effect on the latter part of the time-temperature curves (Section 12.6.3).

(iv) The effect of using the Swedish time-temperature curves (Magnusson and Thelandersson 1970), rather than COMPF-2 output (Section 12.6.4).

The CIB formula is used for this comparison.

12.6.1 Fraction of Fuel Burnt

The most critical parameter in COMPF-2 is the fraction of pyrolysed fuel that is burnt within the compartment, input as "BPF". It can be thought of as the percentage of heat available in the fuel that is released within the compartment. It is always less than 1.0 as the mixing within the compartment is not perfect. The unburnt pyrolysates leave the compartment as a component of smoke. They may burn outside the window or remain unburnt. It also allows for the fact that with charring fuels, not all of the fuel is

pyrolised. COMPF-2 (Babrauskas 1979), recommends a value between 0.7 and 0.9. Values from other sources range from 0.55 to 1.00. The range 0.7 to 0.9 is more reasonable. It is lower for ventilation controlled fires than for fuel bed controlled fires because ventilation controlled fires are oxygen starved. Three sets of computer runs were carried out on one floor layout with one layer of 12.5 mm gypsum plasterboard and 240*45 mm joists, using values of BPF of 0.7, 0.8 and 0.9.

For all three criteria a change from 0.7 to 0.8 increases the peak compartment temperatures by roughly 100°C and decrease the calculated time equivalent by 12 to 14%, but changing to a value of 0.9, the actual time equivalent is 30 to 45% higher than that for a BPF of 0.7 and the peak compartment temperature is about 200°C higher.

The effect was more significant for longer fires. In this study, pessimised pyrolysis was assumed, hence the fires are highly ventilation controlled. In a ventilation controlled regime it is appropriate to use a lower value of BPF and a value of 0.7 was used.

12.6.2 Shortcomings in the COMPF-2 Time-Temperature Output

In Section 12.3.1, two assumptions regarding the initial and final temperature curves during a fire were described. They are:-

The initial rate of temperature increase within the compartment was 100°C per minute.

The time-temperature curves drops from 80°C to 20°C in 30 minutes.

The effect of the first assumption was checked by assuming an instantaneous temperature increase at the start of the fire. The effect of the second assumption was checked by assuming an instantaneous temperature from 80°C at the end of the COMPF-2 run to 20°C in one minute. Having an instantaneous initial temperature rise reduced the calculated time equivalents by 4 to 5%, but having a very rapid drop in temperature at the end had a minimal effect (less than 0.3%).

12.6.3 The Decay Phase

The other parameter that may have had a significant effect on the results was the shape and length of the decay phase of the fire. Two alternative decay phases were investigated:-

(i) The burning rate was kept at the constant ventilation controlled burning rate until two thirds of the fuel was consumed. The burning rate was then assumed to decrease at a rate inversely proportional to the time squared.

(ii) The burning rate was kept at the constant ventilation controlled burning rate until two thirds of the fuel was consumed. The burning rate was then assumed to decrease at a linear time-dependent rate.

These were compared with the standard case, with a constant ventilation controlled burning rate throughout the duration of the fire.

These decay phases and the effect they have on the time-temperature curve are described in Sections 5.6.1 and 5.6.1.1.

The effect that these changes have on the thermal response of the structure was far more important than would be expected from the effect on the time-temperature curve.

For the insulation criterion, assuming either an inverse time squared or linear decay phase results in calculated time equivalents that are less than 3% lower than those assuming pessimised pyrolysis and was not significant.

For the charring criterion, assuming an inverse time squared decay phase results in calculated time equivalents that are 13% lower than those assuming pessimised pyrolysis, and 12% lower if a linear decay phase was assumed.

For the integrity criterion, assuming an inverse time squared decay phase, results in actual time equivalents that are 17% lower than those assuming pessimised pyrolysis, and 16% lower if a linear decay phase was assumed.

Using time-temperature curves that have been developed using COMPF-2 and assuming pessimised pyrolysis is conservative for all three criteria.

When a longer decay phase than the pessimised case is assumed, the fire is of longer duration, but the temperatures after the decay phase starts are lower. The duration of the fire increases by 33% assuming a linear decay phase or 50% assuming a time-squared decay phase. Most of the heat that enters the walls and ceiling is due to radiation. The radiative heat flux is proportional to the fourth power of the absolute temperature, hence

small drops in temperature result in a significant decrease in the level of heat flux. The total energy per unit area that enters the walls and ceiling in the decay phase, that is the integral over time of the heat flux, is less with the longer decay phase, since although the duration is longer the heat flux intensity is lower.

12.6.4 The Swedish Time-Temperature Curves

Tabulated values from the Swedish time-temperature curves were used as input to the floor model and time equivalents found. The tabulated values were for a type G compartment (Magnusson and Thelandersson 1970), that is, one with 80% of the bounding surfaces composed of two 13 mm gypsum plasterboard panels on each side of a 100 mm cavity, supported by steel studs. The other 20% of the bounding surfaces was concrete.

12.6.4.1 Ventilation and Fuel Load Parameters of Curves Used

It was not possible to use the same values for fuel load and ventilation factors in this comparison as was used in the other comparisons. This was because of the problems with interpolating the Swedish time-temperature curves to get curves for intermediate values of the fuel load and the opening factor as described in Section 5.6.3 Twelve combinations of fuel load and ventilation factor were used.

12.6.4.2 Results of the Comparison

For the insulation criterion, using the Swedish time-temperature curves resulted in time equivalents that were 14% longer than those found calculated using time-temperature curves from COMPF-2.

For the integrity and charring criteria, using the Swedish curves resulted in time equivalent that were 10% and 5% shorter than those found using the COMPF-2 output respectively.

The Swedish curves are of different shape to those produced by COMPF-2. They tend to be cooler, but with significantly longer duration. When a floor/ceiling model is subjected to different time-temperature curves it's response will obviously vary.

12.7 Conclusions

12.7.1 Time Equivalence

The CIB (and BIA) time equivalent formula underestimates the equivalent fire severity of light timber framed floors, when considering thermal behaviour. The relationship appears to be roughly linear with correlation coefficients of 0.77, 0.88 and 0.89 for charring, insulation and integrity criteria respectively.

The CIB formula could be modified by the use of a correlation coefficient, with a value of 1.5, to give a better prediction of floor behaviour.

The dependence between time equivalent and total fuel load appears to be slightly less than linear.

12.7.2 Other Conclusions

The percentage of pyrolysates that is burnt within the compartment is significant.

The values used for the emissivity and convection coefficient are not critical, provided that they are within reasonable limits.

Assuming pessimised pyrolysis (that is, ventilation control throughout the fire) is conservative, but not excessively so, (16% or less), compared with time-temperature curves with longer decay phases.

12.7.3 Further Work

It would be desirable to produce design time-temperature curves or standard parameters to model such curves. A curve that is derived assuming that two thirds of the fuel is burnt at a ventilation controlled rate, and then at a decreasing rate proportional to the time squared would be a reasonable choice.

The charring criterion is a first approximation of the structural performance of a floor. The actual structural capacity is of far more significance. Determination of the actual time equivalence for the structural capacity of light timber framed floors will be described in Chapter 13.

Chapter 13 Calibration of the Structural Floor Model

After the development of a structural model for walls, a floor model was developed. The joist in the floor model is very similar to König's tests (Chapter 8), except that the bending moment in the beam varies along the length of the beam and the flooring was loaded, rather than the beam being loaded directly. The timber may exhibit different stress-strain behaviour to the timber used in the beam test because of the species difference. In the floor tests the timber used was radiata pine (pinus radiata), whereas for König's tests the material was Norwegian spruce (picea abies).

13.1 Description of the Floor Tests

The data from five floor tests was supplied by the Building Research Association of New Zealand (BRANZ). Some data was supplied with the permission of Winstone Wallboards Ltd. Three of these tests could not be used in developing the structural model because they were "Twinaplate" floors as described in Chapter 11. These tests are summarised in Table 13.1.

Test Code	Lining Type	Lining Thickness (mm)	Joist Type	Joist Depth (mm)	Joist Width (mm)	Floor Load (kPa)
FR966	Plasterglass	12.5	Solid	240	45	2.4
FR1202	Gibraltar Board	12.5	Solid	240	45	3.0
FR1369	Gibraltar Board	14.5	Twinaplate	240	67	3.0
FR1370	Gibraltar Board	16	Twinaplate	240	67	3.0
FR1572	Gibraltar Board	12.5	Twinaplate	240	67	3.0

Table 13.1 Floor Tests Used for Model Calibration

The test specimens were loaded by using drums filled with water. Each drum has three feet with swivels supported on 100 mm square pieces of particleboard. In all the tests, the floors failed when one of these feet penetrated the particleboard. In test FR966 the lining remained in place throughout the test. The test ended when the loading apparatus penetrated the particleboard. In test FR1202 a portion of the lining fell off after 31

minutes. It was not possible to determine why it fell off. This lining also fell off during the other three tests with Gibraltar Board lining.

13.2 Thermal Model

The thermal model is described in Chapter 11. The thermal model for test FR966 is identical to that for FR1202 except that the enthalpy for the plasterglass lining is based on a density of 1100 kg/m^3 as given in the test report, rather than 747 kg/m^3 for 12.5 mm "Fyreline Gibraltar Board".

In test FR1202 the lining started to fall off after 31 minutes. This was modelled by stopping the thermal analysis and restarting it without the lining on the fire side. The temperatures within the assembly at the start of the second run were obtained from the first run.

The temperatures were not modified to allow for inaccuracies in the thermal model as described in Section 9.2 for walls, because the instrumentation within the floor joists was not of sufficient standard to accurately determine the temperatures within the joists.

13.3 Structural Model

The structural model was developed using the ABAQUS (Hibbitt et al 1994) computer program. The finite element mesh for a cross-section through the floor is shown in Figure 13.1. Symmetry was used to reduce the complexity of the model, hence only one half of the joist cross-section was used. Also only one half of the length of the joist was used. Subsequently, the full cross-section was modelled to check for lateral buckling effects.

The gypsum plasterboard lining underside of the joist was omitted from the structural model. The gypsum plasterboard lining degrades at about 100-120°C, and since these temperatures are reached within the lining within the first five minutes of the test it does not contribute any significant strength to the floor.

The particleboard also degrades between 60°C and 100°C. The floor was modelled without the particleboard, and then it was included for comparison purposes. As the

floor often failed due to the loading apparatus penetrating the floor, the particleboard was also modelled in isolation in order to predict this type of failure.

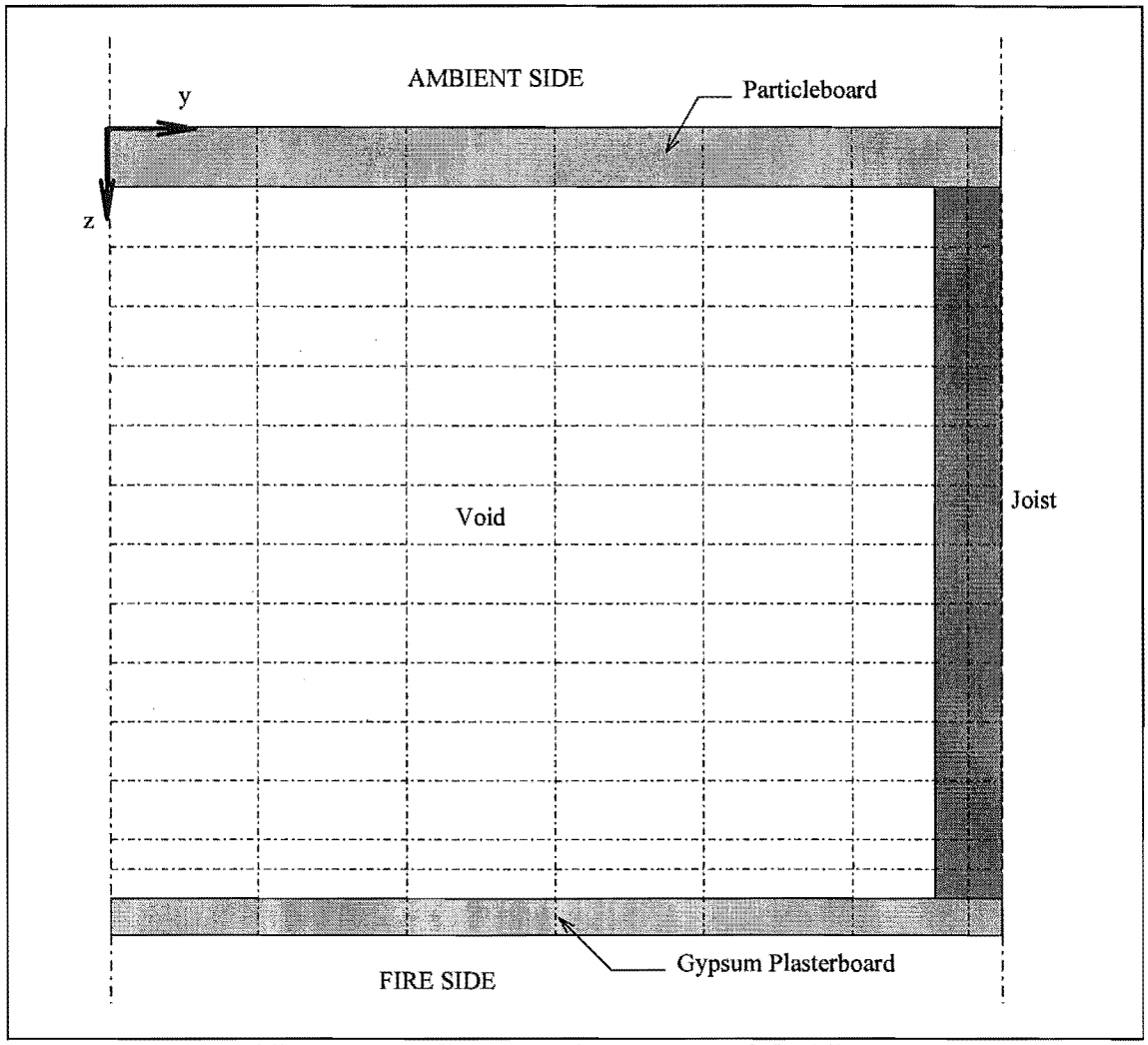

Figure 13.1 Cross-Section of Part of the Floor

13.3.1 Boundary Conditions

Half the length of the joist was modelled, that is, 2.1 metres. The first 100 mm is supported vertically, that is, in the z-direction. The joist is restrained along its centreline in the y-direction and the edge of the particleboard is also restrained in the y-direction (left hand side of assembly in Figure 13.1). When the full cross-section was modelled, only the particleboard at the edges of the model was restrained in the y-direction. The joist was restrained in the longitudinal (x-direction) at midspan.

13.3.2 Loading

The loads were applied to the top edge of the joist as a uniform pressure. The effectiveness of the particleboard in apportioning the load was modelled separately.

13.4 Mechanical Properties

The mechanical properties required are the strength and stiffness parallel to the grain in compression and tension for the timber. These properties vary with temperature, moisture content and time.

13.4.1 Mechanical Properties at Ambient Temperatures

As was the case for the wall tests the mechanical properties at ambient temperature of the timber as tested, were not determined prior to the floor tests. The values had to be assumed from data from other sources.

13.4.1.1 Modulus of Elasticity

The modulus of elasticity used was 7200 MPa, the same as that used for the wall tests (Section 9.4.1.1).

13.4.1.2 Compression

The properties used in compression are the same as for the wall tests in Section 9.4.1.1. An average modulus of rupture of 40 MPa was assumed. Assuming the same relationship between the ultimate tensile strength and the modulus of rupture as in Section 8.2.3 for König's beam tests, gives a value of 24.1 MPa for the compressive strength.

13.4.1.3 Tension

The same relationship between the ultimate tensile strength and the modulus of rupture as in Section 8.2.3 for König's beam tests is used. This gives a value of 47.5 MPa for the tensile strength.

13.4.2 Mechanical Properties at High Temperatures

The effect of high temperature and moisture content on the strength and stiffness of timber is reviewed in Section 8.2.3.1, 8.2.3.2 and 8.2.3.3. The stiffness is assumed to be different in tension and compression. This is because of the "steaming effect" that

causes a very short term creep or relaxation in timber that is exposed to steam at high temperatures. This effect only affects the timber if it is loaded in compression. An "effective stiffness" is used that incorporates this effect, hence the stiffness is lower in compression than tension at higher temperatures.

A summary of available data on mechanical properties of timber at high temperatures is given in Section 8.2.1. Given the problems discussed in Section 8.2.1 associated with accurately determining strength and stiffness as a function of temperature and moisture content in this study, the properties are determined by taking reasonable starting values and modifying them within reasonable limits in order to give a good correlation with the floor and wall tests.

13.4.2.1 Compression

The modulus of elasticity and strength values used are the same as those used for the walls, described in Section 9.4.2.1.

The modulus of elasticity remains constant until 60°C. It then drops to 30% of it's original value at 120°C and remains constant until 295°C. It then drops to effectively zero at 305°C. This is shown in Figure 13.2. The compressive strength remains constant until 120°C is reached and then drops linearly to effectively zero at 300°C, as shown in Figure 13.3. The shape of the curves was derived using data from bending tests between values of about 100°C and 300°C.

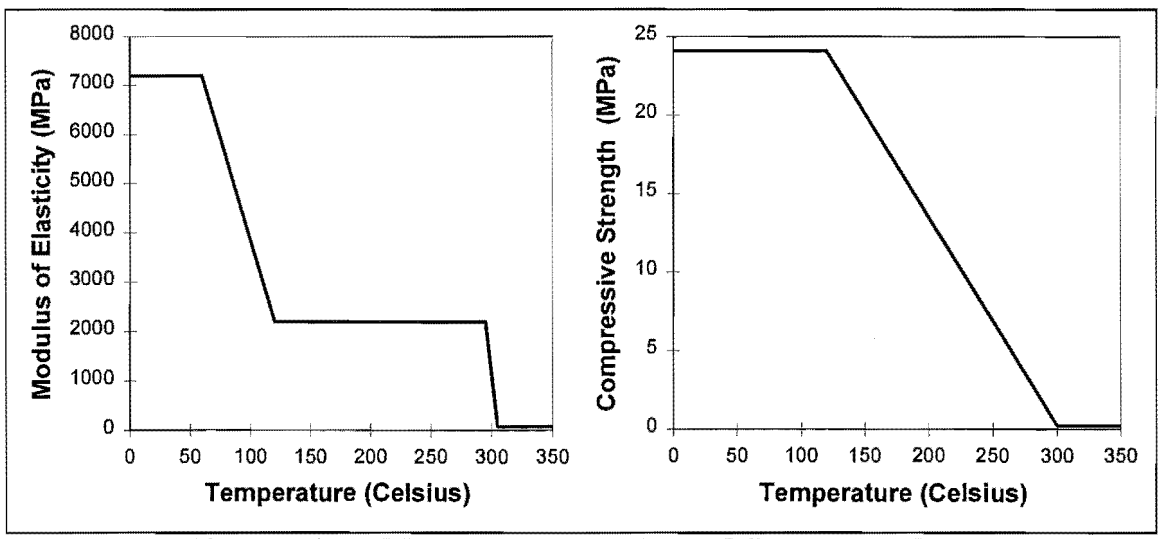

Figures 13.2 and 13.3 Modulus of Elasticity and Strength in Compression

The modulus of elasticity and compressive strength do not reach zero because this causes numerical problems with the model. The effect of the elements at higher temperatures having a close to zero rather than zero strength and stiffness is negligible.

13.4.2.2 Tension

The ratio of strength and stiffness at higher temperatures to that at ambient temperatures in tension are very similar to that used to model König's tests in Section 7.2.3.3 and 7.6.

The modulus of elasticity drops from 7200 at 20°C to about 60% of its original value at 295°C and then drops to effectively zero at 305°C. This is shown in Figure 13.4. The tensile strength remains constant until 80°C is reached and then drops linearly to 30.8% of its ambient value at 295°C and to effectively zero at 305°C, as shown in Figure 13.5. The shape of the curves was derived using data from bending tests between values of about 100°C and 300°C.

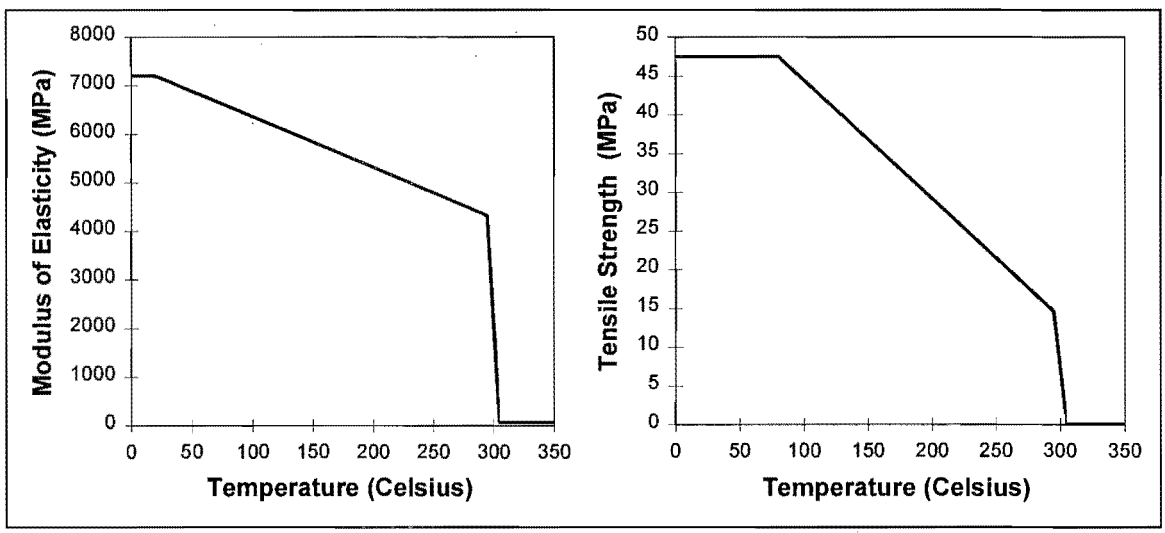

Figures 13.4 and 13.5 Modulus of Elasticity and Strength in Tension

The relationship between the modulus of elasticity and strength in tension and temperature has the same shape as that used in tension for König's tests in Chapter 8. The actual values are lower because the modulus of elasticity and strength at ambient temperatures is lower for pine than for the Norwegian spruce König used.

13.4.3 Stress-Strain Relationship as a Function of Temperature

Combining the values of the modulus of elasticity and the strength in tension and compression as a function of temperature, a stress-strain diagram for specific values of temperature can be compiled. Such a diagram is shown in Figure 13.6.

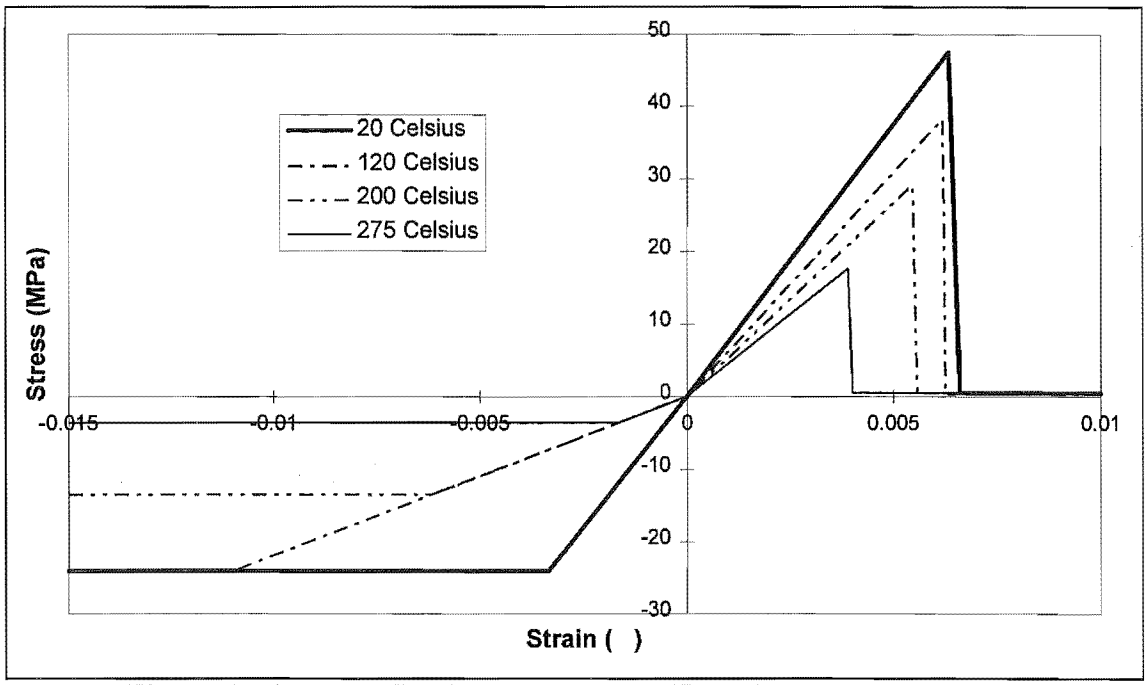

Figure 13.6 Stress-Strain Diagram as a Function of Temperature

13.5 Comparison with Test Data

Since there is only data from two tests available and both failed due to the feet of the loading drums penetrating the floor, rather than the joists failing in bending, it is difficult to compare the structural model with the tests. An examination of the deflections in test FR966 and test FR1202 shows that the deflections were starting to increase very rapidly just before the test was stopped. It would be reasonable to assume that the joists would have failed in bending within the next ten minutes.

Test data from other sources were not used because it would have introduced additional complexity with different species and genotypes of timber. Gypsum plasterboard from different suppliers also has different thermal behaviour.

13.5.1 Comparison of Failure Times

The failure times for the joists in bending were determined as 72.0 and 46.5 minutes respectively for test FR966 and FR1202. The test specimens could still carry load at 75 minutes and 41 minutes respectively, when the particleboard failed.

13.5.2 Particleboard Failure

In both floor tests, the test failed when the leg of a loading drum penetrated the floor. This type of failure was modelled in ABAQUS using a section of particleboard only. The load was applied by 20 drums at 600 mm centres, hence the legs are at about 500 mm centres. In the worst case, the leg would be positioned halfway between adjacent joists. A section 250 mm long was modelled as shown in Figure 13.7.

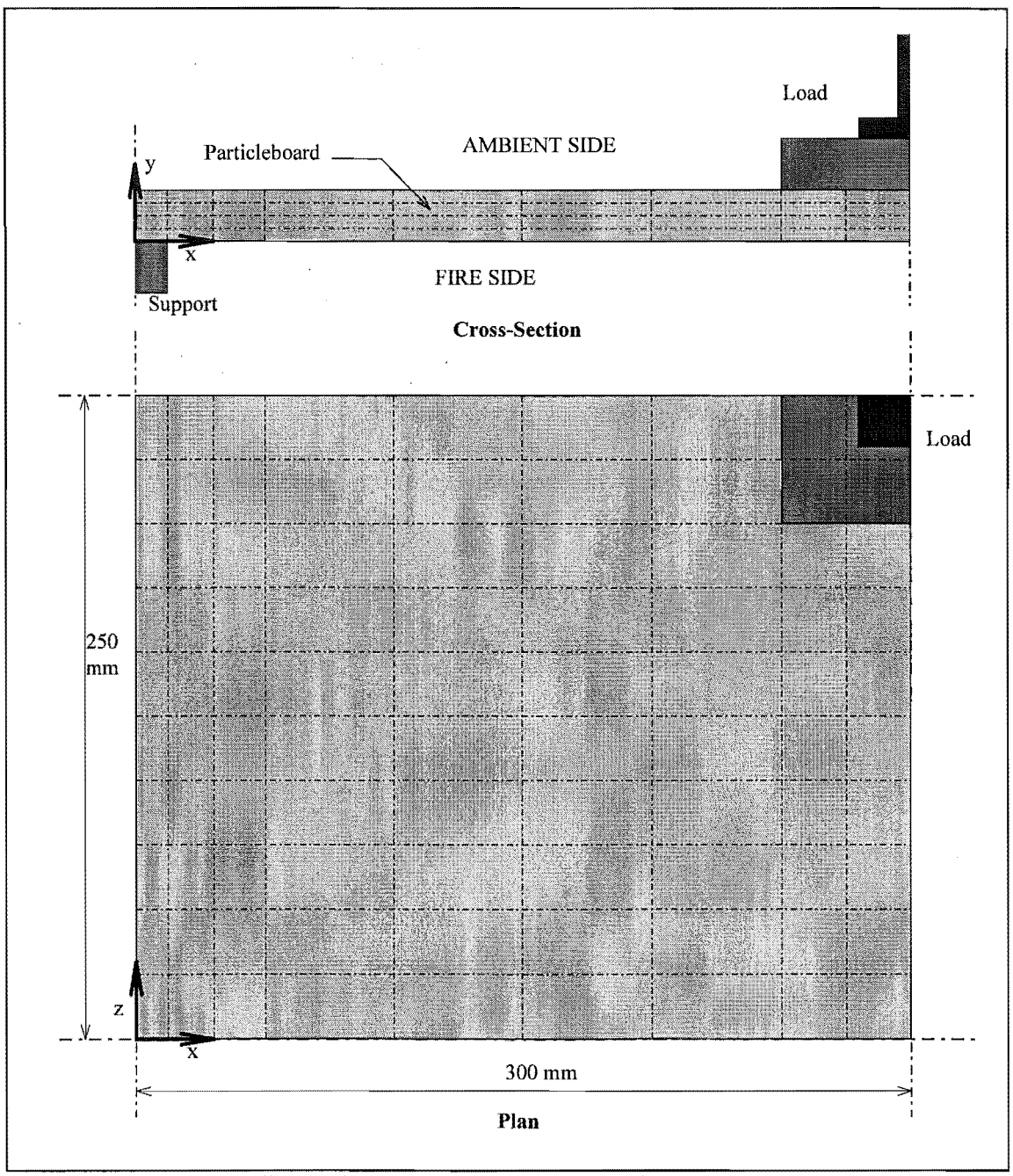

Figure 13.7 Particleboard Flooring Model

The support is 12.5 mm wide for FR966 and 7.5 mm wide for test FR1202 and runs the length (z-direction) of the model. This is the width of the uncharred section of the stud

at the time the particleboard failed. The model is restrained around the four edges shown in the plan, in the x and z directions.

The load applied is equivalent to 2.4 kPa for test FR966 and 3.0 kPa for test FR1202. The actual load per leg is 0.48 kN and 0.6 kN respectively.

13.5.2.1 Mechanical Properties of Particleboard.

At ambient temperatures the modulus of elasticity for particleboard is 2800 MPa and the modulus of rupture 28 MPa. These values are taken from the Timber Use Manual, Section C-3, Panel Products (NZTIF 1989). The ratio between maximum tensile strength, maximum compressive strength and the modulus of rupture is assumed to be the same as for normal timber, as described in Sections 13.4.1.2 and 13.4.1.3. This gives a maximum compressive strength of 15.7 MPa and a maximum tensile strength of 31.7 MPa.

The glue in particleboard, normally urea formaldehyde, softens in the presence of steam and heat (Barber 1994). This process is assumed to start at 60°C and the particleboard is assumed to have effectively no strength at temperatures above 100°C.

The modulus of elasticity and the strength as a function of temperature is shown in Figures 13.8 and 13.9.

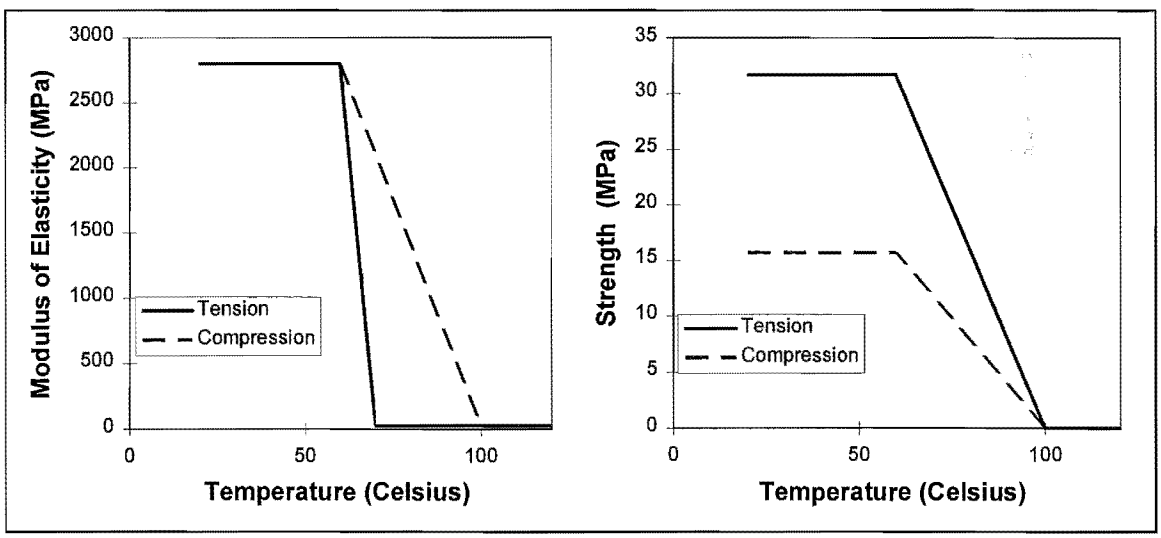

Figures 13.8 and 13.9 Particleboard Strength and Stiffness

The strength of particleboard is assumed to remain constant until 60°C and then reduces to zero at 100°C in both tension and compression. The modulus of elasticity also remains constant until 60°C and then reduce to zero at 70°C in tension and 100°C in

compression. The reason for the faster reduction in stiffness in tension is due to the fact that the softening of the glue has a more severe effect in tension than in compression.

13.5.2.2 Time to Failure of Particleboard

The time to failure of the particleboard in test FR966 was 72 ± 2 minutes and 71.4 minutes for the particleboard model. For test FR1202 the time to failure was 40 minutes in the test and the model prediction was 43.9 minutes.

13.5.3 Effect of Particleboard

In Section 13.5.1 the structural model did not include the particleboard, that is the particleboard was not assumed to contribute to the strength and/or stiffness of the floor as a whole. The effect of this assumption was checked by running the structural model with the particleboard present. The mechanical properties used for the particleboard are those described in Section 13.5.2. As can be seen in Table 13.2, the particleboard does not significantly affect the time to failure for floor FR966, and increases it by 1.9% for floor FR1202.

Test Code	Test Time to Failure	Model Time to Failure	
		No Particleboard	With Particleboard
	(minutes)	(minutes)	(minutes)
FR966	>75	71.4	71.4
FR1202	>41	46.5	46.8

Table 13.2 Effect of Particleboard Strength on the Time to Failure

The particleboard does not significantly affect the strength or stiffness of the floor as a whole during fire exposure. This is because the particleboard degrades very quickly with temperature, and by the time that failure occurs has little residual strength or stiffness. The particleboard was modelled as being fully fixed to the joists. In reality, nail slip occurs, further reducing the effect of the particleboard.

13.5.4 Vertical Deflections

The vertical deflections at the midspan of the floor were measured for both tests. In test FR966 it was only measured midway across the floor. The comparison between the measured deflection and that calculated by the model is shown in Figure 13.10.

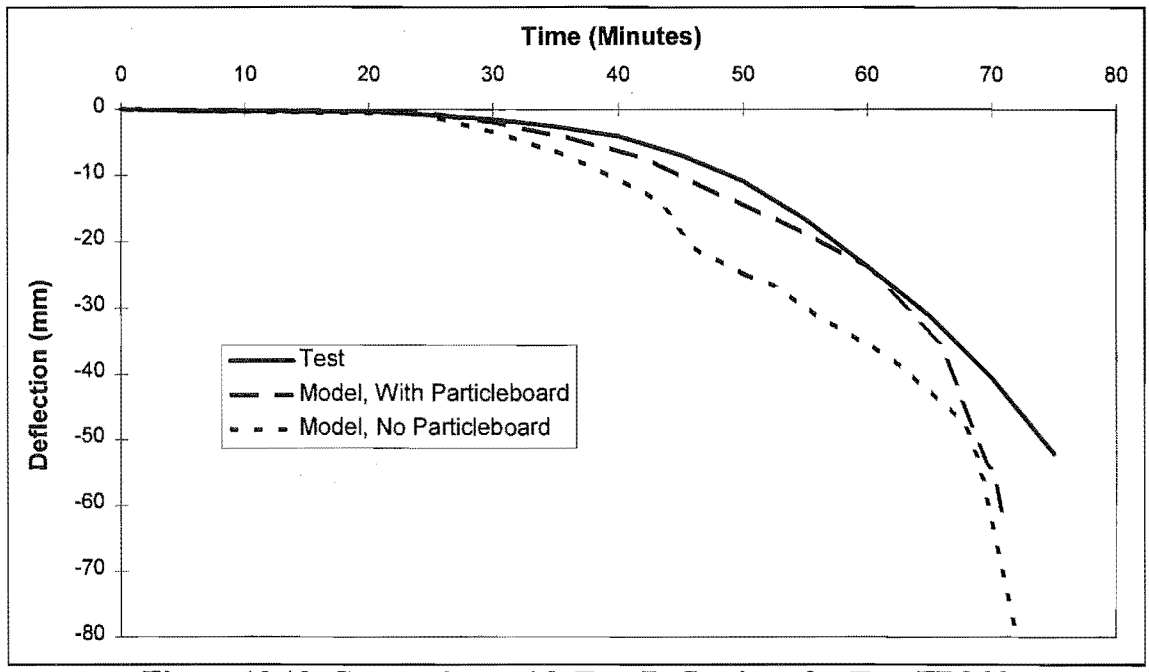

Figure 13.10 Comparison with Test Deflections for Test FR966

Although the model incorporating the contribution of the particleboard does not affect the time to failure, it gives a better comparison with the deflections.

In test FR1202, the deflections were measured at the edges, mid and quarter points across the floor. In Figure 13.11 the average deflection and that midway across the floor is shown. The deflection is at the mid-span of the floor joists.

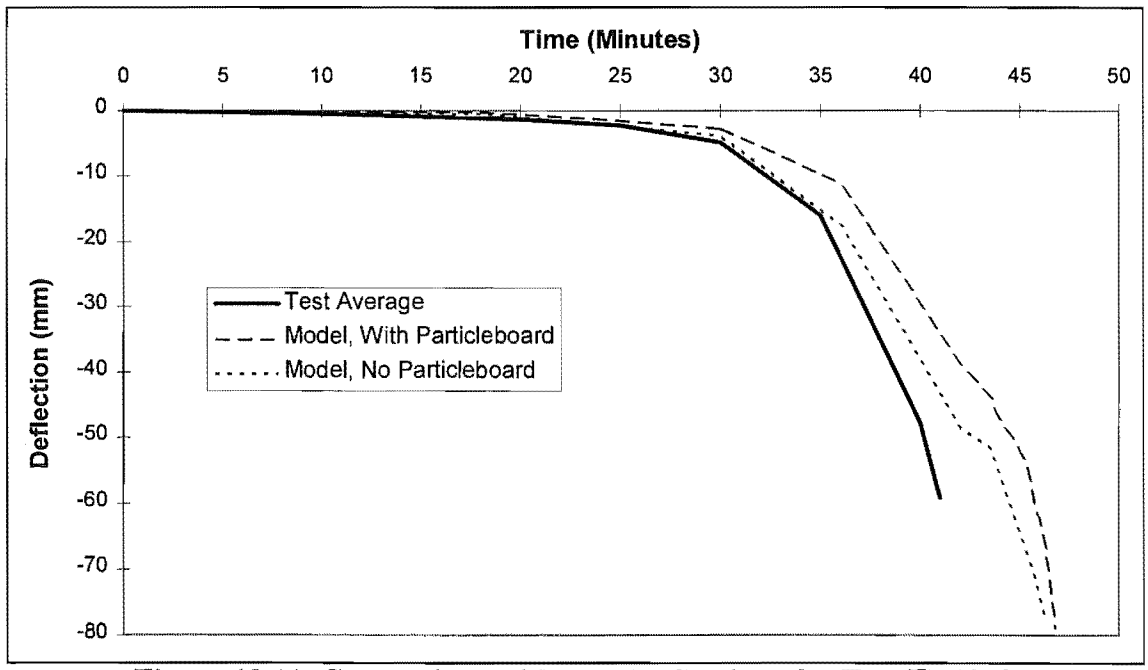

Figure 13.11 Comparison with Test Deflections for Test FR1202

Both of the models (with and without particleboard) predict the deflection well after 30 minutes. This is due to the fact that the lining started to fall off after 31 minutes. Although this was allowed for in the thermal model, the thermal model does not allow

for the effect of flaming timber combustion accelerating the charring of the timber. The decrease in the cross-section of the timber joist is underpredicted by the thermal model, and hence the structural model overpredicts the strength and stiffness of the joist, resulting in smaller deflections in the floor than was the case in the test.

13.5.5 Effect of Model Parameters

Several parameters that may have affected the accuracy of the model were checked for the floor with 12.5 mm gypsum plasterboard (FR1202). They are :-

(1) The size of the finite element mesh.

(2) The size of the time step.

(3) Lateral buckling if the whole cross-section is used and not half the cross-section with a fully restrained plane of symmetry.

13.5.5.1 Effect of the Element Size

The element size was halved across the joist and down the joist. The element size was not halved along the length of the joist as the model would have been too large to run on the computer available. The stress and strain profiles along the joist only varied gradually along the length so further discretisation here would not affect the result. The deflections did not vary by a significant amount as shown in Figure 13.12.

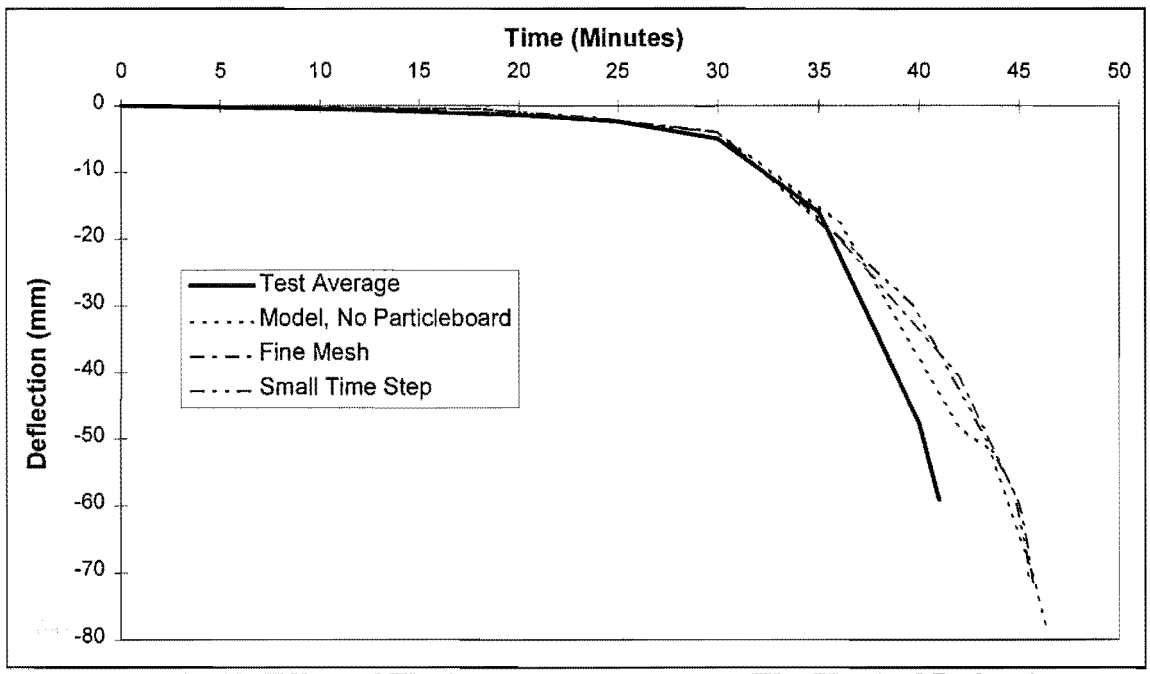

Figure 13.12 Effect of The Model parameters on The Vertical Deflection

The finer model failed at 45.8 minutes compared with 46.8 minutes for the simpler model. The test time to failure was greater than 41 minutes. The difference between the two models was therefore 1.5%, but is on the unconservative side. The deflection plot for the more complex model was smoother than that for the simple model.

A further check on the model by further reducing the element size was not possible. The model would have been too large for the resource limits on the computer being used. It would be expected that a further halving of the element size would result in at most about a further 1% increase in the time to failure, resulting in a total (unconservative) error of 2.5%.

The model is used to calculate time equivalence and the same model is used for both the furnace test runs and the fire test runs so the errors due to the scale of the mesh would cancel to some extent.

13.5.5.2 Effect of Varying the Time-Step

The model was also run with time steps of 0.02 hours rather than 0.1 hours. The time to failure was the 45.5 minutes compared with 46.5 minutes for the coarser time step. This is a difference of 2.2% and is also unconservative. The deflection plot in figure 13.12 is smoother compared to the run with larger time steps as shown in Figure 3.11.

13.5.5.3 Effect of Using Half the Cross-Section

Since only half the cross-section of the joist was used in the model, it was restrained in displacement and rotation down the centreline of the joist. This prevents any lateral buckling of the joist occurring. The model was run with a full cross-section, restrained laterally only at the top edge. This did not affect the time to failure or the deflections, as the top edge restraint was sufficient to prevent lateral buckling.

13.6 Conclusions

The time to failure appears to be reasonably accurately predicted given the limited data.

The deflections appear to be predicted well for the floor with a lining that remains in place.

The particleboard does not significantly add to the time to failure for the floor and hence will be omitted for subsequent analyses. It does however affect the deflections and provides lateral restraint to prevent lateral buckling.

The performance of light timber framed floors could be improved by providing better fixing of the lining to the underside of the joists and the use of a flooring material that can better resist point loads. A material such as plywood or solid timber flooring may avoid the premature failure of the floor due to penetration by point loads.

Despite the fact that data from only two tests were used, the model can be regarded as being more than adequate because the values for the material properties used in the model for compression were also used for structural walls in Chapter 9. The ratio between the tensile mechanical properties at high temperatures and at ambient temperature is the same as those devised to model König's tests in Chapter 8.

Chapter 14 Structural Time Equivalence for Floors

14.1 Introduction

This Chapter is very similar to Chapter 10, Structural Time Equivalence for Walls. It outlines the process involved in determining the structural time equivalence using computer models for floors rather than walls, as in Chapter 10. This Chapter is therefore a brief description of the process and should be read after Chapter 10.

The CIB formula is used for the comparison because it is valid for larger ventilation values, which are common in residential buildings in New Zealand and because it has been published (Law 1977). The relationship between the calculated and BIA time equivalent formula is also mentioned because it is specified in the New Zealand code (NZBIA 1992). Both formulae are described in Section 1.1.

14.2 Methodology

The overall methodology is described in the following five subsections.

14.2.1 Compartment Fire Model

The compartment fire model, COMPF-2 was run for various fuel loads (200, 400, 800 and 1200 MJ/m^2). The window sizes and hence ventilation factor were also varied as shown in Table 14.1.

WINDOW			Ventilation Factor	Ventilation Factor
Height (m)	Width (m)	Area (m^2)	CIB (Eqn 1.3) ($m^{-1/4}$)	BIA (Eqn 1.4) (Dimensionless)
1.0	2.75	2.75	1.437	1.547
1.5	3.00	4.50	1.015	1.023
2.0	3.00	6.00	0.818	0.836
2.0	4.00	8.00	0.709	N/A
2.0	6.00	12.00	0.579	N/A

Table 14.1 Window Sizes and Opening Factors Used in the Model

The two largest of the four openings were out of the range of the BIA formula. The conductivity, density and enthalpy of the compartment boundaries are consistent with the thickness of the wall and ceiling linings and the size of the framing as shown in Table 14.2.

Wall		Floor/Ceiling	
Stud Thickness (mm)	Lining Thickness (mm)	Joist Depth (mm)	Lining Thickness (mm)
90	9.5	240	12.5
90	16.0	290	16.0

Table 14.2 Lining Thickness and Framing Size for the Compartment

The 240*45 mm joists were at 400 mm centres and the 290*45 mm joists were at 600 mm centres.

The method of calculation for the equivalent thermal properties for a homogeneous floor was described in Section 11.2.

14.2.2 Thermal Model of the Floor

The heat transfer model of the floor described in Chapter 11 was subjected to the time-temperature curve from Section 14.2.1. The output was reduced to give the nodal temperatures within the floor joist.

14.2.3 The Structural Model

The load capacity of the joist was found by a systematic trial and error process similar to that described in Section 10.2.3. The model had some time-dependence so the load could not be found directly. The assumption was made that the floor failed due to the joists failing in bending. The common secondary failure (Section 13.5.2) of the foot of the loading apparatus penetrating the floor was ignored. This secondary failure is not a problem when the reduced data set is used as described in Section 14.3.2. It was

assumed that the timber recovered its strength after heating and subsequent cooling. It was also assumed that the lining on the underside (fire side) remained in place throughout the test. The load capacity was determined to the nearest 0.05 kPa. This gives a load step of 0.02 kN/m for the 240*45 mm joists at 400 mm centres and 0.03 kN/m for the 290*45 mm joists at 600 mm centres. The span was 4.1 m for both floors.

The results for the first floor with 240*45 mm joists is shown in Table 14.3.

Opening Factor ($m^{1/2}$)	Fuel Load (MJ/m^2)			
	200	**400**	**800**	**1200**
0.025	5.80	2.48	0.08	0.08
0.05	7.14	3.68	1.14	0.06
0.077	8.46	5.78	2.48	0.14
0.103	8.66	6.62	3.24	1.56
0.154	8.84	7.40	3.40	2.66

Table 14.3 Load Capacities for the 240*45 mm Joist Floor/Ceiling with 12.5 mm Lining (kN/m)

As was the case for the walls, the load capacity decreases with increasing fuel load and with decreasing ventilation. The trend in the load capacity for the other floor was very similar.

14.2.4 Characterising the Capacity - Time Curve for Furnace Exposure

The structural model, with a range of load levels was exposed to the ISO-834 time-temperature curve. A regression of the results was calculated to give the time to failure under ISO-834 exposure as a function of the load. This process is identical to that described in Section 10.2.4 for walls. The form of the regression was the same as for walls and is given in Equation 14.1:-

$$t_e = \frac{a}{\sqrt{p}} + b \qquad (14.1)$$

where: t_e is the time equivalent (minutes)

p is the load (kPa)

a, b are coefficients

Figures 14.1 and 14.2 shows the plot of the load/time data points and the regression.

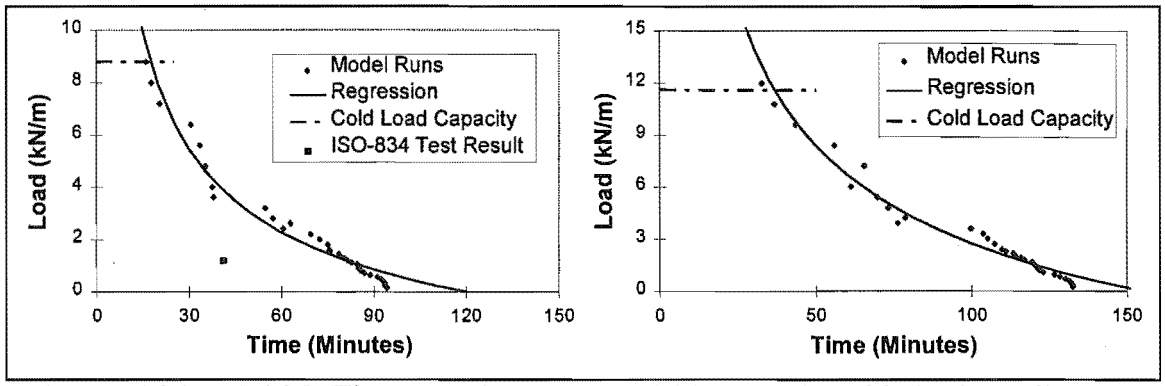

Figures 14.1 and 14.2 Time to Failure for 240*45 mm Joist with 12.5mm Gypsum Plasterboard and 290*45 mm Joist with 16mm Gypsum Plasterboard Respectively

The cold load capacity was calculated using the computer model as 8.80 and 11.6 kN/m respectively for the two floors modelled. When hand calculations were used the calculated capacity was 8.2 and 11.9 kN/m respectively. The minimum load is 0.4 kN/m for the two floors. In Figure 14.1 the test data point is below the model results because in the model it is assumed that the lining stays in place, but in the test if fell off after 31 minutes. The 290*45 mm joist floor does not correspond to a test.

The value of the coefficients **a** and **b** (Equation 14.1) are given in Table 14.4.

Joist Size (mm)	Lining Thickness (mm)	a	b
240*45	9.5	59.82	-5.45
290*45	16.0	136.52	-10.93

Table 14.4 Values for The Regression Coefficients a and b (Equation 14.1)

14.2.5 Calculating the Time Equivalents

The time equivalent was then calculated for each combination of fuel load and ventilation factor by putting the loads found in Section 14.2.3 into the regression from Section 14.2.4. Table 14.5 shows the calculated time equivalent values for the floor/ceiling system with 240*45 mm joists and a 12.5 mm thick lining.

The time equivalent reduces as the ventilation decreases or the fuel load increases. The trends are similar for the other floor system modelled.

Opening Factor ($m^{1/2}$)	Fuel Load (MJ/m^2)			
	200	**400**	**800**	**1200**
0.025	59.2	86.1	N/A	N/A
0.05	51.8	74.6	102.5	N/A
0.077	45.8	59.3	86.1	N/A
0.103	45.0	54.5	78.5	96.9
0.154	N/A	50.5	77.1	84.2

Table 14.5 Calculated Time Equivalents for the 240*45 mm Joist Floor/Ceiling with 12.5 mm Lining

14.3 Results

The CIB time equivalent is plotted against the calculated time equivalent in Figure 14.3.

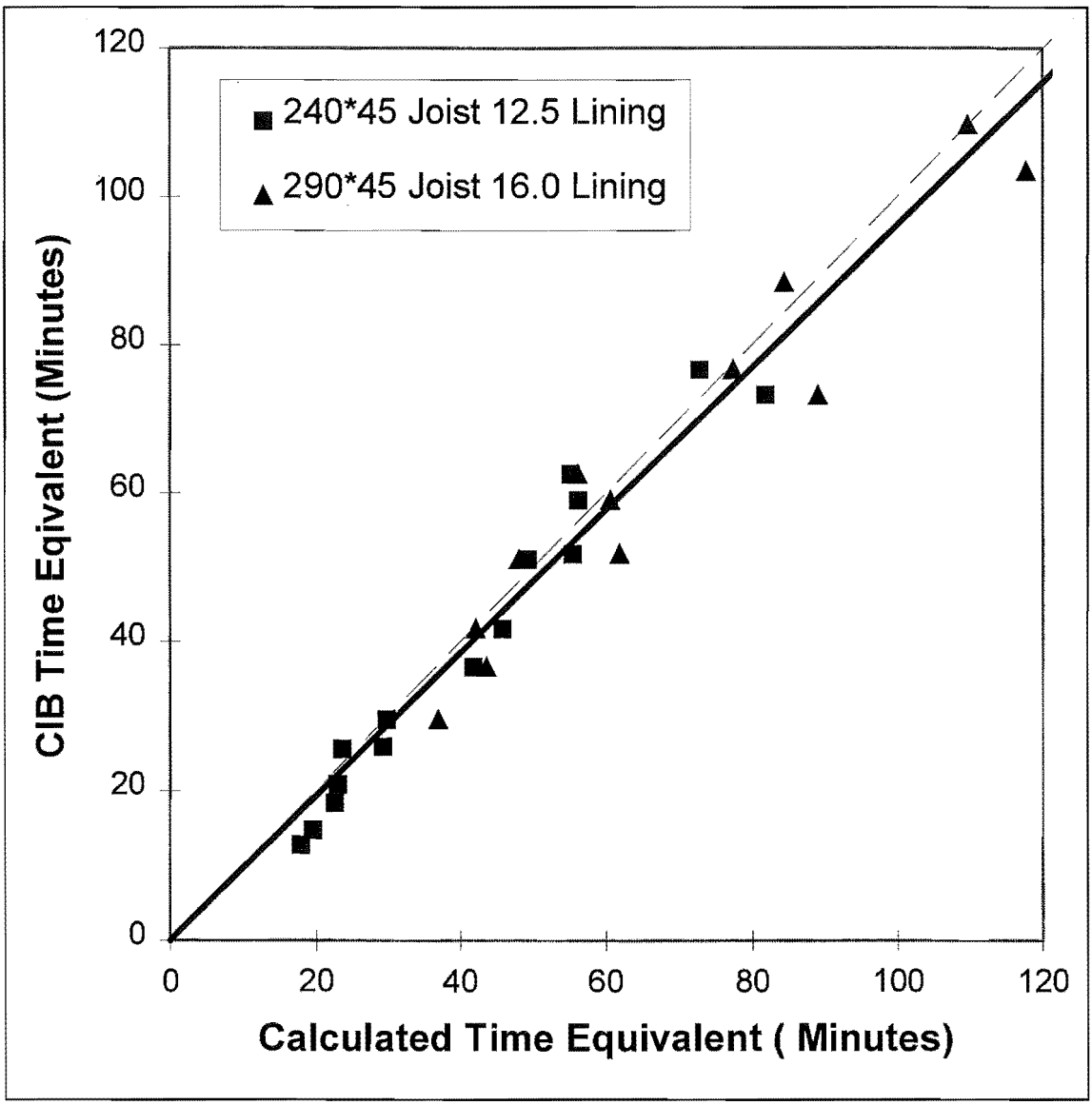

Figure 14.3 CIB Time Equivalents Versus Calculated Time Equivalents

The calculated time equivalent was found using the process outlined in Section 14.2 above.

The dashed line show a 1:1 relationship and the solid line is a regression through the data points.

The formula predicts the time equivalent better than it did for walls. The slope of the regression is 0.96 with a correlation coefficient of 0.96.

14.3.1 Sensitivity Study

It was found when calculating the temperature based time equivalent for the charring criterion for floors (Section 12.6), that two parameters significantly affected the calculated time equivalent. They are the "BPF" or the input value in COMPF-2 (Babrauskas 1979), that specifies the percentage of the fuel that is pyrolysed and subsequently burns within the compartment. Increases this value from 0.7 to 0.9 decreased the slope of the regression through the data points relating the time equivalent calculated using the CIB formula to that calculated using the model by 61%. An increase from 0.7 to 0.8 resulted in a decrease of the slope of the regression of 14%. The first floor (240*45 mm joists and 12.5 mm lining) was run with a BPF of 0.7 and 0.9 for comparison purposes. The comparison is shown in Figures 14.4 and 14.5.

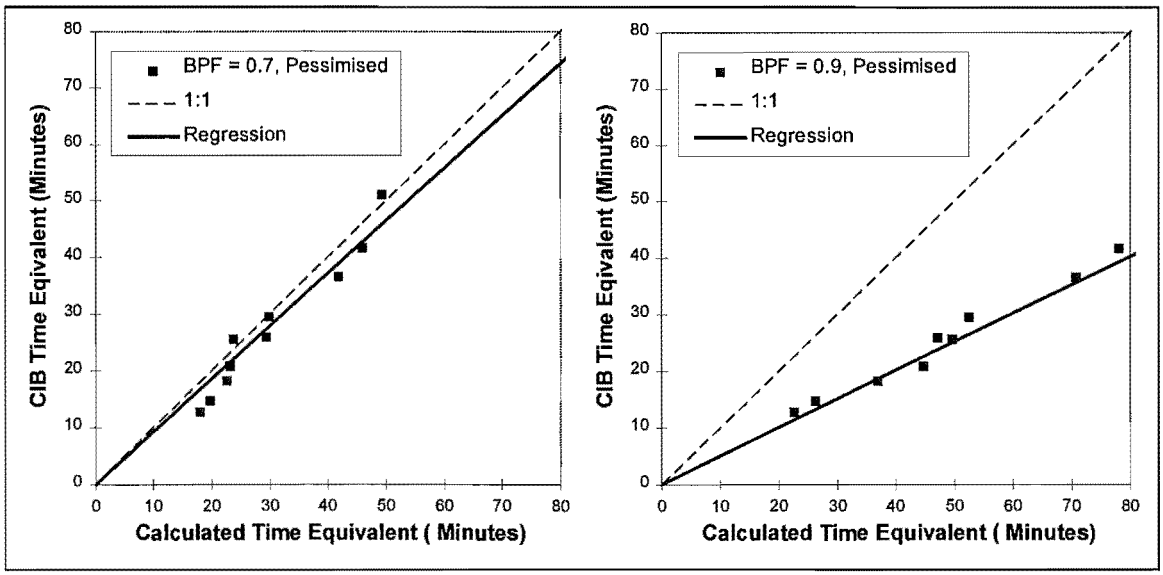

Figures 14.4 and 14.5 Time Equivalents for a BPF of 0.7 and 0.9 Respectively

The slope of the regression has reduced by 46% which is certainly significant, but less than the 61% decrease reported for the charring criterion. The correlation coefficient for the regression has increased slightly. Only points that were within the minimum and maximum load capacity for both runs were used in the comparison.

The other parameter that is significant is the shape of the decay phase. Using a linear or t^2 (Section 5.6.2) decay phase instead of a "pessimised" fire throughout the duration of the fire resulted in an increase in the slope of the regression by 12% and 13% respectively. Figure 14.6 and 14.7 show the comparison for a pessimised fire and a t^2 decay phase.

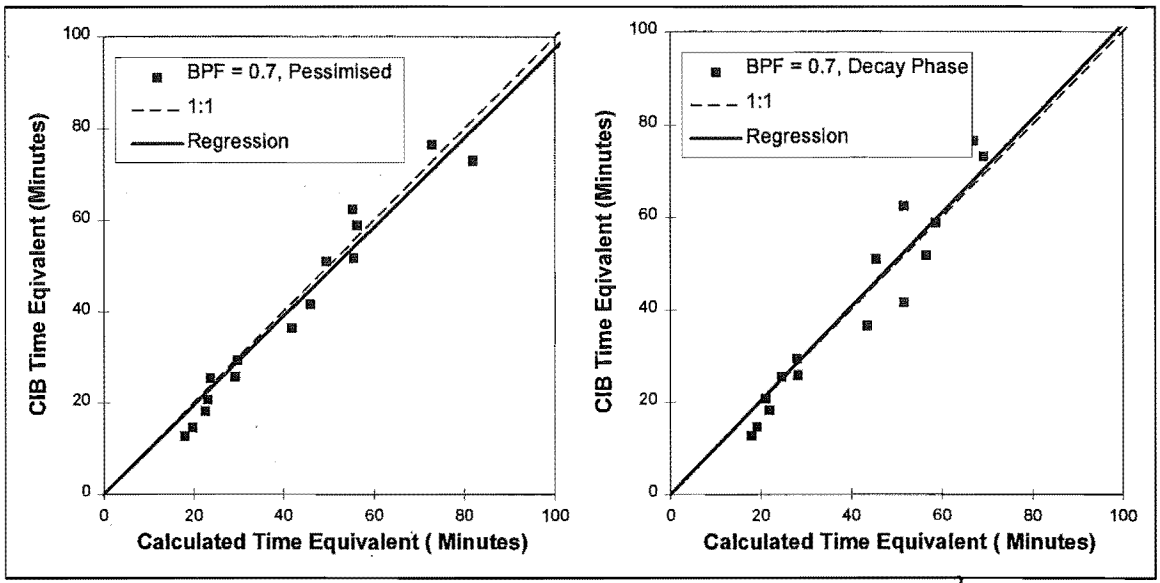

Figures 14.6 and 14.7 Time Equivalents for a Pessimised Fire and a t^2 Decay Phase Respectively

The effect of the assumptions regarding the shape of the time-temperature curve (Section 5.3.1) and the effect of using the Swedish curves (Section 5.6.3) were not checked as their effect was small for the temperature based charring criterion. For some combinations of fuel load and ventilation factor the load capacity actually reduced for the t^2 fire. This is due to the fact that the temperatures may be more even throughout the section for a t^2 fire.

14.3.2 Validity of the Model at High Temperatures

Once charring has occurred over a large enough area of the cross-section it is assumed that this combustion will be self-sustaining even after the compartment fire has gone out (see Section 10.3.2). This always occurs before the secondary failure of the foot of the loading apparatus penetrating the floor (Section 13.5.2). The effect of removing these points has on the regression is shown in Table 14.6.

CIB Formula	All	<300°C	Charring
Slope of Regression	0.96	0.92	0.61
Correlation Coefficient	0.96	0.94	0.88

Table 14.6 Values for the Regression Slope and R^2 for Complete and Reduced Data Sets for the CIB Formula

When points that meet this criterion are removed from the analysis then the slope reduces by 4%. This slope is much higher than that given by the charring, temperature based criterion (with no growth phase). The charring criterion is a highly conservative method of predicting structural failure compared with the reduced (<300°C) structural criterion.

14.3.3 Results from the Comparison with the BIA Formula

Figure 14.8 is similar to Figure 14.3, but shows the BIA rather than the CIB formula.

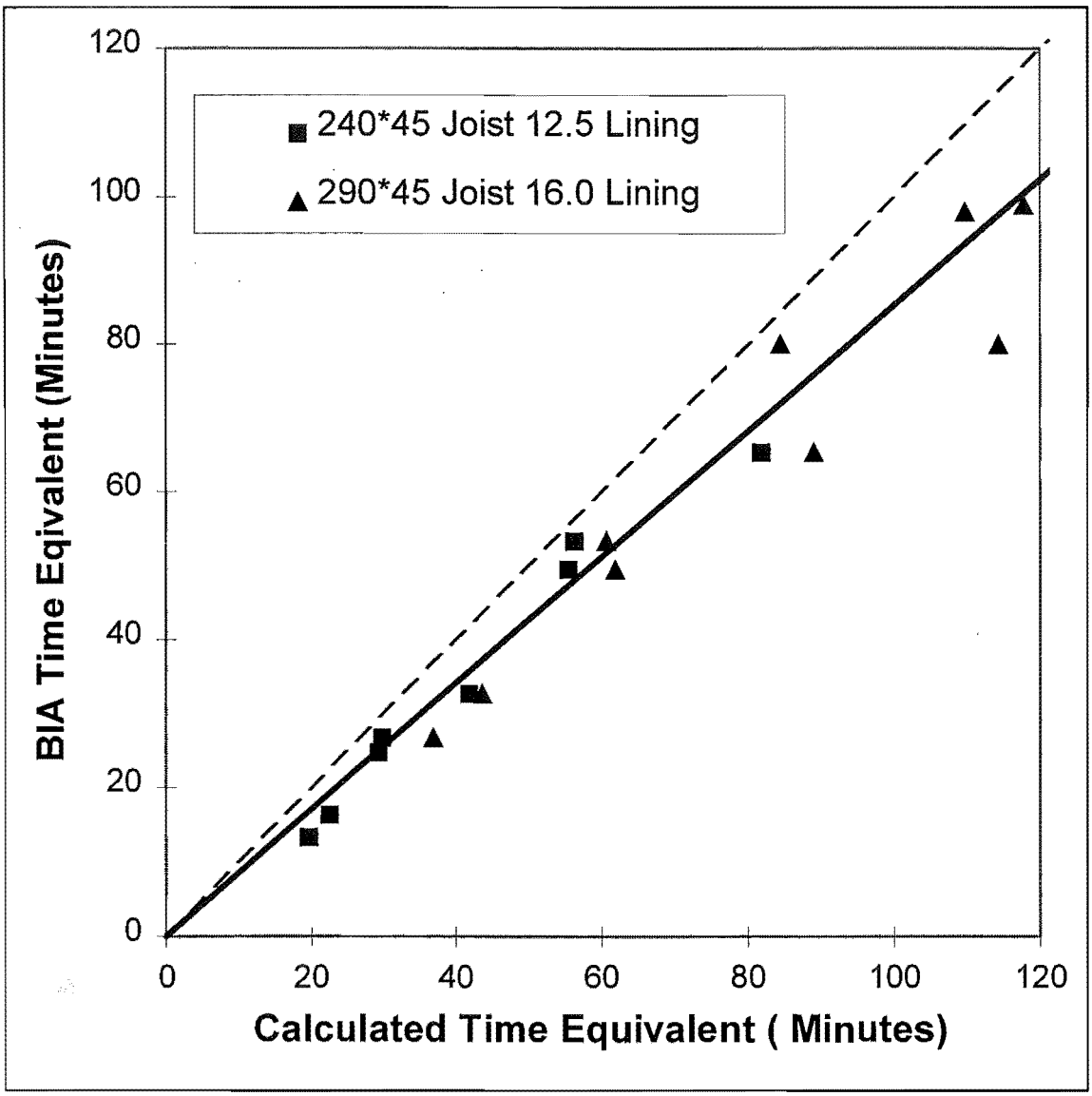

Figure 14.8 BIA Time Equivalents Versus Calculated Time Equivalents

The slope of the regression is less than that for the CIB formula at 0.85, but the correlation coefficient of (0.95) is about the same. In this case the BIA formula is less conservative than the CIB formula.

14.3.3.1 Sensitivity Study

In Section 14.3.1 two parameters were checked for the sensitivity study. They were the fraction of pyrolysates burnt within the compartment (BPF) and the decay phase. When the value of BPF was changed from 0.7 to 0.9 the slope of the regression of the BIA time equivalents compared with the calculated time equivalents decreased by 40%. When the shape of the fire was changed from one with no decay phase to a t^2 decay phase the slope of the regression increased by 4%.

14.3.3.2 Validity of the Model at High Temperatures

The effect of removing floor/ceilings in which charring is likely to continue (Section 14.3.2) is shown in Table 14.7.

BIA Formula	All	<300°C	Charring
Slope of Regression	0.85	0.78	0.60
Correlation Coefficient	0.95	0.96	0.88

Table 14.7 Values for the Regression Slope and R^2 for Complete and Reduced Data Sets for the BIA Formula

The slope of the regression reduces by 8%, but is still much higher than that found for the charring criterion (with no growth phase). The charring criterion is a highly conservative method of predicting structural failure.

14.4 Conclusions

The agreement between the CIB and BIA formula for the structural analysis of floors is good with a good correlation coefficient of over 0.90.

Reducing the data sets does not significantly affect the comparison.

The temperature based charring criterion is a highly conservative method of estimating the structural performance.

The formulae as they stand give a reasonable prediction of structural performance on average.

The effect of the shape of the decay phase and the proportion of pyrolysates burnt within the compartment on the structural time equivalence is less severe than it was for the temperature based criterion.

Chapter 15 Design of Structures for Fire Resistance

In previous Chapters, time equivalents were calculated using thermal criteria for timber walls (Chapter 5), timber floors (Chapters 12) and for steel and concrete structural elements (Chapter 7). The time equivalents were calculated using a structural failure criterion for timber walls (Chapter 10) and timber floors (Chapter 14). The time equivalent formulae described in Section 1.1 were used to find a time equivalent and these values were compared with those calculated using the computer models described previously.

The time equivalent formulae worked well for some structural types and layouts, but were very poor for others. The degree of variation between different materials and layouts is of concern. For some combinations of materials, layout of the structural element and the insulating material, ventilation and fuel load the time equivalent formulae are grossly unconservative.

Following analysis of a number of full scale room fires, Kirby et al (1994) states that "....the equivalent fire severity is not a unique value for a specific set of fire conditions as described in the Eurocode."

This Chapter refers in the main part to the CIB formula not the later BIA formula. The BIA formula is not valid for ventilation area that is greater than 25% of the floor area which precludes its use for most rooms in residential buildings, typical of New Zealand construction. The complexity of the BIA formula is not justified by its level of accuracy.

This Chapter describes how a simplified thermal model could be used for the design of timber structures exposed to fire and how the CIB time equivalent formula could be modified to ensure that it is conservative in most cases.

15.1 Results from Comparisons

Table 15.1 outlines the results from the comparison of the time equivalent found using the CIB formula and that calculated using the models described previously for timber walls and floors for the structural failure criterion. The average slope is that of the regression through the data points comparing the CIB time equivalent and the calculated time equivalent. The "5%ile" column is for the fifth percentile of the regression and R^2 is the correlation coefficient. The type of structure and layout are shown in the Table. The data from the structural model for timber walls and floors is for the reduced data sets (Sections 10.3.2 and 14.3.2).

Type of Structure	Description of Layout	Average Slope	5%ile Slope	R^2
Timber Wall	90*45 mm Stud 9.5 mm Lining	0.95	0.86	0.90
Timber Wall	69*45 mm Stud 12.5 mm Lining	1.69	1.39	0.60
Timber Wall	90*35 mm Stud 16 mm Lining	0.89	0.78	0.79
All Timber Walls		1.10	0.96	0.40
Timber Floor	240*45 mm Joist 12.5 mm Lining	0.90	0.83	0.93
Timber Floor	290*45 mm Joist 16 mm Lining	0.93	0.84	0.83
All Timber Floors		0.92	0.87	0.94
All Timber Walls and Floors		0.90	0.85	0.87

Table 15.1 Comparison of Time Equivalents for Timber Structures

This analysis was similar when the BIA formula was used, but the BIA formula was less conservative with an overall slope of 84%, a fifth percentile slope of 79% and a correlation coefficient of 0.95. The correlation coefficient in Table 15.1 for all timber walls of 0.4 is extremely poor. This shows that the relationship between the CIB formula and the calculated time equivalents varies greatly for different wall layouts.

The CIB formula is unconservative on average by 11%, but when the data are plotted, it is grossly unconservative for some values of fuel load and ventilation (Figures 10.4 and 14.3).

Table 15.2 shows a similar comparison, for steel and concrete structural elements (Chapter 7).

Type of Structure	Description of Layout	Average Slope	5%ile Slope	R^2
Steel Beam	360UB57 with 100 mm slab and 16 mm lining	1.02	0.97	0.94
Steel Column	350UC with 16 mm lining	0.87	0.82	0.89
Steel Beam and Column		0.93	0.90	0.90
Concrete Wall	100 mm slab with D20 bar and 40 mm cover	0.87	0.81	0.88
Concrete Floor	150 mm slab with D20 bar and 20 mm cover	0.81	0.74	0.82
Concrete Wall and Floor		0.83	0.79	0.85
Steel and Concrete		0.88	0.85	0.87

Table 15.2 Comparison of Time Equivalents for Steel and Concrete Structures

This analysis was similar when the BIA formula was used, but the BIA formula was less conservative with an overall slope of 75%, a fifth percentile slope of 72% and a correlation coefficient of 0.89.

There is a significant variation in the slope between the steel beam and steel column. Although the correlation coefficients are reasonably high, a plot of the data (Figures 7.6 and 7.7) shows that the use of a straight line regression through the origin is not supported.

The CIB formula is unconservative on average by 14%, but when the data are plotted, it is grossly unconservative for some values of fuel load and ventilation (Figure 7.6 and 7.7).

Gerlich (1995) found that the use of time equivalence formulae was not an accurate method of predicting the response of light steel stud walls lined with gypsum plasterboard to non-standard furnace tests using time-temperature curves derived using COMPF-2 and supplied by the author. There was no apparent trend.

Both the CIB and BIA formula are overly simplistic, are on average unconservative and grossly unconservative for some examples.

15.2 Proposed Modifications to the CIB Formula

It is proposed to modify the CIB formula to ensure that it is conservative compared with the analysis that has been carried out. A more recent paper by Law (1997) suggests that the BIA formula used in New Zealand is the worst of the time equivalent formula available.

15.2.1 Dependence of the Time Equivalent Formula on Fuel Load

This work has shown that the time equivalence is not linearly dependent on the fuel load. Figure 15.1 shows the time equivalent for a given fuel load divided by the time equivalent for the lowest fuel load analysed (100 MJ/m^2), versus the fuel load divided by the lowest fuel load (100 MJ/m^2). For example if the time equivalent is 45 minutes at a fuel load of 400 MJ/m^2, and the time equivalent is 16 minutes for a fuel load of 100 MJ/m^2 then the value on the x-axis is 400/100 = 4 and on the y-axis 45/16 = 2.81.

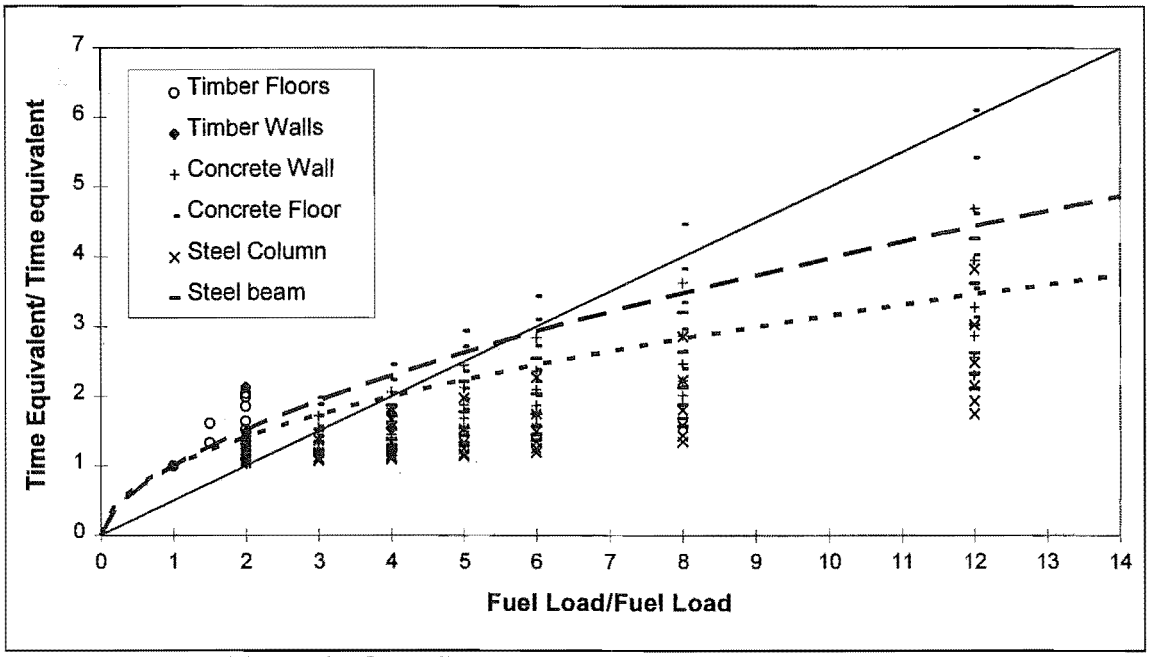

Figure 15.1 Dimensionless Time Equivalent versus Dimensionless Fuel Load

The lines shown on the graph are a 0.5:1.0 relationship and the fuel load/fuel load raised to a power of 0.5 and 0.6. The best fit is with a function of the form of fuel load raised to the power of one half.

It is hardly surprising that the time equivalent is not directly proportional to the fuel load, because of the difference in thermal behaviour of a furnace and a real fire. When the temperatures within a real compartment are compared with an ISO-834 test curve, the ISO curve always increases in temperature whereas the compartment temperatures tend to plateau quite quickly and increase very slowly as the fire progresses. Any surfaces exposed to the compartment fire tend to approach the temperature of the compartment quite quickly, reducing the heat flux between the compartment gases and the surface and so any further increase in temperature is only possible if heat is lost through the solid away from its surface. This is not the case in a furnace, with constantly increasing temperature.

This difference between the heat flux to a wall for a furnace and a compartment fire is shown by the variation in heat flux during a fire or test shown in Figure 7.12. The curves are calculated from the furnace and wall temperatures for the furnace test and given by COMPF-2 for a compartment fire. The heat flux is very high at the start of a fire then drops rapidly. The area under the graph is the total heat energy input to the wall. The longer fire shown has three times the fuel load but the total energy put into the wall was 22 MJ/m^2 which was about double that for the shorter fire (14 MJ/m^2), when the growth phase was excluded. In a furnace the total energy input to the wall is

roughly doubled if the time is doubled, in this case it is 10 MJ/m^2 after 20 minutes and 17 MJ/m^2 after 40 minutes. The heat flux into the wall reduces right from the start of the fire. In the furnace on the other hand the heat flux reaches a peak earlier and then decreases more slowly. In the fire the heat flux reverses as the compartment cools whereas, in the furnace it eventually reaches a value that is almost constant. This effect is even more marked if longer fires are compared, for example a time equivalent of 40 minutes compared with 2 hours.

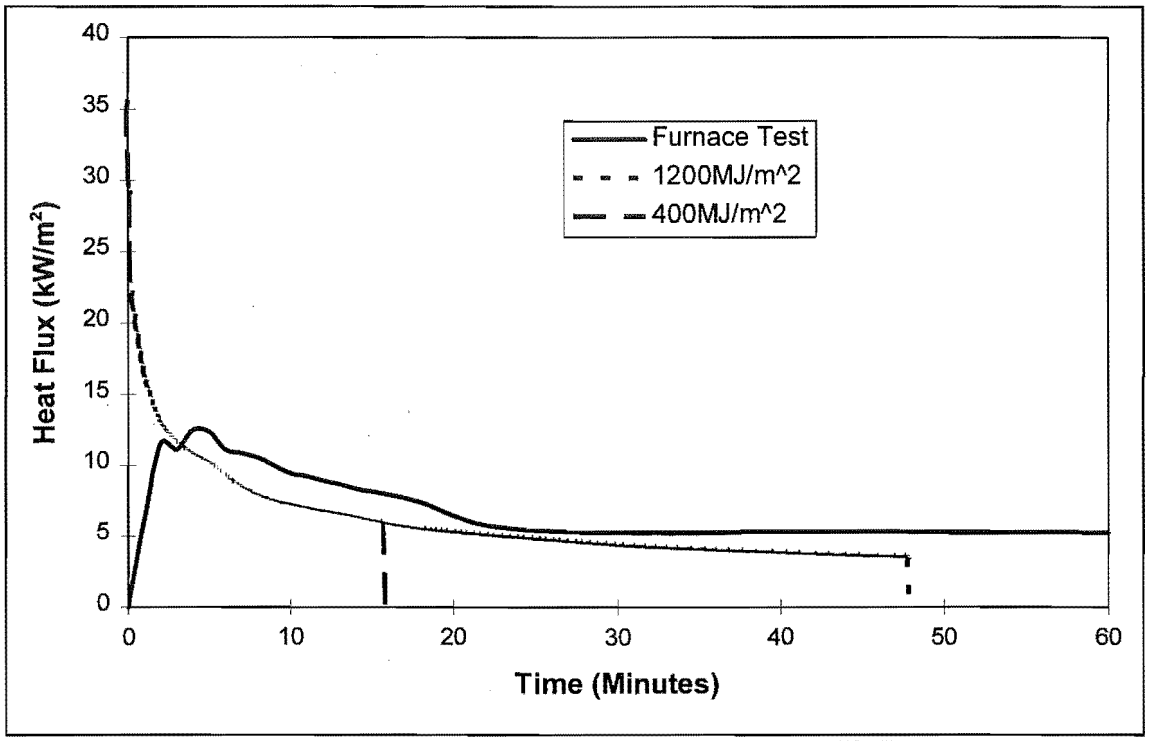

Figure 15.2 Variation in Heat Flux to the Wall

Figure 15.1 shows that the dependence between time equivalent and total fuel load appears to be slightly less than linear, as the CIB and BIA formulae would suggest. In the two formulae it may be more appropriate to use the fuel load raised to a power of less than 1.0, say 0.7. That is, in Equation 12.1, the value of x should be less than 1.0 as is the case at present.

$$t_e = cwQ_f^x \tag{12.1}$$

where:- t_e is the equivalent time of exposure to an ISO-834 test (minutes)

c is a parameter to account for different compartment linings (dimensionless)

w is the ventilation factor (dimensionless)

Q_f is the fuel load in (MJ/m^2 of floor area)

A regression analysis of various values for x showed that there is no difference in accuracy when x was varied from 0.9 to 1.0, but there is a decrease in the correlation coefficient if x is less than 0.9 for the timber walls and floors. For the steel and concrete structures the best correlation was achieved when the value of x was between 0.7 and 0.75, but was not much better than that achieved when x was 0.5 or 1.0. There is insufficient evidence to justify changing the dependence of the time equivalent on the fuel load. The difference in the best value for x for steel and concrete and timber structures does not support the use of one formula for all types of structures.

A complete reanalysis of the time equivalent formula using a power law for each variable, but a more rigorous analysis is recommended and adding yet another time equivalent formula that is more accurate for some circumstances than others will achieve little in the opinion of the Author of this dissertation.

15.2.1 Factors of Safety

Given that the time equivalent formula has been shown to be unconservative for all the structural elements that have been modelled in this study, it is proposed that a factor of safety be applied to the formulae. The calculated time equivalent should be at least below the fifth percentile value and a factor of safety applied. This fifth percentile value used is the value for a normal distribution about the regression line and not the fifth percentile data point.

It could be argued that a factor of safety is unnecessary because fire is a rare occurrence, however the severity of the fire should be based on a "design fire", and this is normally done by assuming a eighty percentile fuel load. for some combinations of fuel load and ventilation the formula are grossly unconservative. Risk factors should be stated explicitly and not buried in a design method.

The factor of safety should reflect the accuracy of the formula for all possible materials and layouts. There is a high degree of scatter and the formula is highly unconservative for some circumstances. A safety factor of at least 1.5 is proposed.

As the term c in Equation 12.1 is poorly defined, it may be appropriate to increase this value in order to produce the appropriate comparison. The values for c from various sources are shown in Table 15.3.

Source	Formula	$\sqrt{k\ \rho\ c}$			
		>2500	720 το 2500	<720	General
CIB W14 (Thomas, P.H. 1986)	CIB	0.050	0.070	0.090	
Eurocode (1993)	Eurocode	0.040	0.055	0.070	0.060
Kirby et al	Eurocode	0.050	0.070	0.090	
FEDG (Buchanan 1994)	Eurocode	0.045	0.055	0.080	0.067

Table 15.3 Values for *c* in the CIB and BIA Formula

It is of interest to note that even if Kirby's proposed values are used the formula is still unconservative by 11% on average.

15.2.2 Proposed Values for the Coefficient *c*

It is proposed that the following *c* values should be used. For the timber and the steel and concrete structural elements the lower 5% average slope is 0.85, hence the value for *c* used should be divided by 0.85. This gives values of 0.059, 0.082 and 0.105 for the three ranges of thermal inertia of the boundaries. If a safety factor of 1.5 is used then these will change to 0.09, 0.12 and 0.16. If these values are used the CIB formula is still unconservative for 3 out of 41 fires for timber structures analysed and 51 out of 193 fires for the steel and concrete structural elements analysed. Most of these 51 fires result in a calculated time equivalent of less than 30 minutes. If those runs were omitted it is still unconservative for 21 of the fires out of 193. It would be conservative for all of Kirby's (1994) tests, but if a safety factor of 1.25 was used it would be conservative for 7 out of Kirby's nine tests.

15.2.2.1 Proposed Values for the Coefficient *c* in the BIA Formula

If the same procedure is applied to the BIA formula the values for *c* should increase by 2.08 times, giving values of 0.094, 0.11 and 0.146. It would be conservative for all of Kirby's tests and all the timber runs. It would be unconservative for 20 out of 96 of the steel and concrete structures and fires analysed. If those runs with time equivalents of less than 30 minutes are omitted it is unconservative for four out of 96 runs.

If a safety factor of 1.25 is used rather than 1.5 the BIA formula is unconservative for two of Kirby's tests 2 out of 24 runs for timber structures and 33 out of 96 for steel and concrete structures.

15.2.3 Recommended Factors of Safety and Formula

It is recommended that the 95% values calculated in this work be used for compartments of similar size or smaller (up to 100 m^3) and a safety factor of 1.25. A minimum time equivalent of 20 minutes should be used because the formulae underestimate the time equivalent at times lower than this and this will allow for local effects of flame impingement directly on elements of structure. For medium sized compartments (say up to 500 m^3) a factor of safety of 1.50 should be used. For larger compartments a value of 2.0 or more should be used. As more published data from larger scale, scientific tests becomes available these values may be reduced. The CIB formula is recommended over the BIA formula as its basis is published. The values that should be used for the coefficient "c" for small compartments are therefore 0.075, 0.10 and 0.13 for the three ranges of thermal inertia and for the safety factor of 1.25. The use of a general *c* value when the thermal inertia of the compartment boundaries is not recommended.

15.3 Alternative Design Procedure

In most cases a thermal or a structural analysis should be carried out to determine the likelihood of a structural element surviving a fire.

The time equivalent formulae (with coefficients from Section 15.2.2) should only be used for small structures where more rigorous analysis is not justified.

The scope of the time equivalent formulae should be restricted to values for the ventilation factor, the coefficient *c*, fuel load and room size and geometry that it has been validated for, however this information is not readily available.

Making the formula more conservative will also encourage the development of more accurate methods of determining the fire resistance of structures.

The author proposes that the following could be used as an alternative to the use of time equivalent formulae:-

(i) The compartment parameters are determined, that is, the size of the compartment and the openings, and the design fuel load.

(ii) A time-temperature curve is developed for the compartment assuming a ventilation controlled pyrolysis rate. When two thirds of the fuel is consumed at time T_1 a decay phase is assumed that is inversely proportional to the square of the remaining time. This decay phase continues for a time T_2, where T_2 is $1.5*T_1$.

(iii) The structural element to be assessed is analysed as a two-dimensional finite element heat transfer model, or for simpler elements as a one-dimensional lumped thermal mass. This model is subjected to the time-temperature curve found in (ii).

(iv) The strength of a concrete or steel element can then be calculated , based on the elevated temperatures and applied load. A conservative method of assessing the possibility of failure of a timber member is outlined in Section 15.4.

(v) Alternatively, if the temperatures at critical locations do not exceed those in a test, before failure of the test specimen, then the element would be deemed to be satisfactory.

It is possible to develop a series of design fire curves using this method in order to alleviate the need to model the heat balance within the compartment and there are programs available to do this.

This approach is similar to that devised by Petersson (1973), but computer models are used instead of design charts to calculate temperature.

15.4 Simplified Design Method for Timber Structures

The method developed in this thesis to assess the structural performance of walls and floors is too complex for use in design. It is proposed that a simplified method based on temperature and hence thermal analysis be used. An attempt was made to develop a simplified structural model, but it was not possible for the range of walls and floors studied in this thesis.

In order to be certain that a timber wall or floor will not collapse after the compartment fire has gone out it is essential to ensure that the timber stops charring. If the depth of charring is small enough, then the combustion of the wood is not self-supporting. The heat loss is too great compared with the energy released and hence the charring will stop.

It can therefore be assumed that if the charring does not exceed a minimum depth, in this case 10 mm on the centreline of the stud or joist, then the structure will survive the fire. The time at which a temperature of 300°C was reached in all the furnace tests for walls and floors the lining on the furnace side of the specimen was always intact and failure (integrity, insulation or structural) had not occurred.

This failure criterion and one where charring only reached 5 mm is compared with the structural failure criterion for various levels of load at 40% and 70% of the cold load capacity. The comparison for one wall is shown in Table 15.2, with the totals for all floor and wall runs that were valid (Sections 10.2.4 and 14.2.4) in the last row.

Opening Factor	Fuel Load	Temperature over 300°C @		Fails at % of Cold Load	
$m^{1/2}$	MJ/m^2	5 mm	10 mm	40%	70%
0.025	200	n	n	n	n
0.025	400	y	y	n	y
0.025	800	y	y	y	y
0.025	1200	y	y	y	y
0.05	200	n	n	n	n
0.05	400	n	n	n	n
0.05	800	y	y	y	y
0.05	1200	y	y	y	y
0.075	200	n	n	n	n
0.075	400	n	n	n	n
0.075	800	y	y	n	y
0.075	1200	y	y	y	y
0.103	200	n	n	n	n
0.103	400	n	n	n	n
0.103	800	y	n	n	n
0.103	1200	y	y	y	y
0.154	200	n	n	n	n
0.154	400	n	n	n	n
0.154	800	n	n	n	n
0.154	1200	y	y	n	n
Total Runs that Fail Criterion		10	11	14	12
Total All Walls and Floors		43	52	75	68

Table 15.2 Failure Criteria for 90*45 mm Stud Wall with 16 mm Lining

In no case did the wall or floor fail structurally if this temperature criterion was failed.

The charring at 10 mm depth criterion is conservative in all cases, but predicts a "failure" in 16 cases out of 68, where structural failure did not occur. In these cases however, structural failure may occur due to ongoing charring of the timber.

Using this temperature-based method, failure can be conservatively predicted. A one-dimensional thermal model could be used to predict the failure. Such a model is being developed at BRANZ (Collier 1996).

15.5 The Insulation Criteria

In Chapters 5 and 12 the validity of the time equivalent formulae in predicting insulation failures was tested. The CIB and BIA formulae underpredict the equivalent time to failure of walls and floors based on the insulation criterion of an average temperature rise of 140°C on the unexposed side of the specimen.

If the value for c of 0.09 in the CIB formula is divided by 0.75, the fifth percentile slope of the regression and multiplied by a safety factor of 1.5 to give a value of 0.18, it is still unconservative for 40 out of 238 combinations of fires and structures analysed.

If the value for c of 0.08 in the BIA formula is divided by 0.68, the fifth percentile slope of the regression and multiplied by a safety factor of 1.5 to give a value of 0.18, it is still unconservative for 8 out of 99 combinations of fires and structures analysed.

Neither formula give a good prediction of the insulation failure, due to the large amount of scatter in the results. Time equivalent formulae are not a good predictor of insulation failure.

15.6 Conclusions

The time equivalent formulae used at present are highly unconservative for some combinations of fuel load and ventilation factor and should be modified by increasing the coefficient c, applying a safety factor. The scope of application of the formula should be severely restricted.

The resistance of structural elements to fire is too complex to be determined by a simple formula.

Factors of safety have to be devised for design, that are consistent with the level of risk and the accuracy of the method.

Any reduction in the factor of safety due to the low risk of a fire occurring should be explicit in a design method and not hidden in a formula.

A conservative temperature based failure criterion for structural performance has been devised.

A multi-level approach is proposed for the design of structures exposed to fire. As the methods increase in complexity, the level of conservatism reduces.

Having a simple, conservative and a more accurate complex approach is consistent with the New Zealand design philosophy for earthquakes. In earthquake design, the design load is not well known and a likely "design earthquake" is chosen. In earthquake design smaller structures may be analysed using a simple equivalent static analysis and for larger structures the more sophisticated spectral modal response is required. The fire problem is similar so a "design fire" should be chosen based on ventilation, fuel load and boundary conditions. The structure can then be analysed using a finite element model and either compared with test results using a calculated time equivalent or by using a temperature dependent structural analysis.

Chapter 16 Conclusions

Overall this work has shown that computer modelling can be used to determine the thermal and structural performance of light timber frame walls and floors exposed to fire. The time equivalent formulae used to predict the response of structures to fire in terms of an equivalent time of exposure to a standard fire test are inadequate to describe this highly complex and variable problem.

The rest of the conclusions relates to particular aspects of the work.

16.1 Compartment Fire Model

The time-temperature curves derived by Magnusson and Thelandersson (1970) are conservative for concrete lined compartments and unconservative for gypsum plasterboard lined compartments. Many of the assumptions inherent in their curves, especially during the decay phase of the fire can not be justified. The compartment fire tests used to develop this model lacked measurement of fundamental data such as mass loss rate. The heat balance is simplified and the bounding surfaces are assumed to be semi-infinite slabs.

COMPF-2 is a more sophisticated model and the coding is freely available, so it can be readily modified. It is too complex for general use. The time-temperature curve produced by COMPF-2 is very sensitive to the assumption made about the fraction of fuel burnt within the compartment. A value of 0.7 is suitable for ventilation controlled fires. Modifications can be made to the decay phase to produce a longer decay phase, which is typical for real fires as they switch from ventilation to fuel-bed controlled at the start of the decay phase. The geometry and size of the fuel significantly affects the time-temperature curve for fires that are not ventilation controlled throughout the duration of the fire.

The variation in temperature between the side and middle of the compartment tested during the house burn suggests that the thermal exposure of a structural element isolated

in the middle of a room is more severe than the exposure of an element such as a wall or floor.

16.2 Thermal Model

The thermal model developed using the program TASEF is very good for predicting the temperatures through the cavities of walls and floors and on the ambient side. It gives a good prediction of the temperatures within wall studs. There was insufficient data to determine the accuracy of the prediction within timber floor joists. The values of the heat transfer coefficients on the fire side of the wall are not significant within a reasonable range. The values of some properties have been manipulated to some extent to overcome the limitations of the model such as the movement of moisture through the wall or floor.

Thermal analysis using ABAQUS, a general purpose finite element program compared very well with analysis using TASEF.

The thermal model does not predict failures due to a loss of integrity. In most cases these can be prevented by good detailing and ensuring structural elements are built to specification.

16.3 Structural Model

The structural model developed using the program ABAQUS predicts the structural response of walls very well and floors adequately. It gave good results in comparison with the test series of single joists exposed to fires carried out by König. The mechanical properties at elevated temperatures used in the model were "effective" properties, incorporating time-dependent effects, such as creep due to the presence of steam in the timber. The mechanical properties were manipulated within a reasonable range to provide good comparison with test data. There appears to be some species dependence of the mechanical properties, especially in compression. The mechanical properties used in the structural model may not be accurate for species other than pinus radiata and for picea abies loaded in bending.

The structural model can be extrapolated for longer walls and floors and different boundary conditions.

The structural model is too complex for use in design, so a simpler and conservative temperature based failure criterion is proposed. Simplified structural design methods were considered, but were found to be unreliable for all the walls and floors used in the analysis.

16.4 Time Equivalence

The use of time equivalence formulae to predict insulation failure of walls and floors is not supported because of the high degree of scatter and the ease at which it can be determined using two-dimensional heat transfer analysis. One-dimensional analysis using an equivalent solid homogeneous wall as described in this thesis is also more accurate than a time equivalent formula.

The time equivalent formula have been compared with results derived using validated computer models and some tests. Unfortunately accurate test data on full size compartments in well designed scientific tests is lacking, especially for compartments with light-weight boundaries.

The performance of structures when exposed to fires is too complex a phenomenon to be described by one formula. The comparison between calculated time equivalents and those derived using formula shows that the time equivalent is not independent of the material, or the size and layout of structural elements and insulation materials. These time equivalents have only been tested for a limited range of structural types and fire parameters. The BIA formula is not valid for high levels of ventilation that are common in residential buildings. There is a high degree of scatter within the results, which needs to be accounted for by the use of a safety factor. The formula of choice is the CIB formula as it has been published in refereed journals , but its use should be restricted to small buildings where more extensive analysis is not justified. Safety factors need to be chosen that reflect the level of risk and the accuracy of the design method.

16.5 Alternative Design Methods

Four different design methods are proposed, in increasing order of complexity and reducing order of conservatism for all materials.

(i) A time equivalent formula (with appropriate safety factor) could be used to determine the required FRR for a building for which does not warrant more sophisticated analysis.

(ii) A temperature based criterion can be used for design of structural elements, with heat transfer analysis.

(iii) A temperature based time equivalent could be calculated using heat transfer analysis and used to predict structural and other failure modes.

(iv) A full-scale structural analysis, utilising temperature based mechanical properties and the positive effect of surrounding structural elements. This will result in a more economic design than the simpler methods.

This tiered approach is consistent with the engineering philosophy of reducing the level of conservatism as the accuracy of the analysis improves.

16.6 Further Work

A user-friendly computer model needs to be developed to predict time-temperature curves for compartment fires.

More scientific compartment fire tests, with instrumentation to record all important parameters need to be carried out, especially in compartments with light-weight linings.

More compartment tests on loaded structural elements are necessary.

A two dimensional heat transfer model could be developed to predict the thermal behaviour of light timber framed walls and floors with only the basic geometry required to be input by the user.

More testing needs to be carried out to determine the mechanical properties of timber at elevated temperatures.

The development of a simple structural model to describe the behaviour of light timber frame walls and floors when exposed to fire is highly desirable, but may not be possible.

The structural model described here should be extended to predict behaviour for different boundary conditions and different size members with validation against further tests.

Acknowledgments

I would like to sincerely thank the following people for their assistance and advice during the production of this work.

My supervisors, Athol Carr, Charley Fleischmann and Peter Moss, but especially Andy Buchanan, who not only provided the idea for this project, but came up with funding, provided invaluable technical advice and assistance, provided an environment where I could concentrate fully on my work.

I would also like to thank other staff in this department and others who helped me along the way, such as the secretaries, particularly Catherine Price, the department draughtsman, Val Grey and the computer technicians, Peter Coursey and Brandon Hutchison.

The librarians in the Engineering Library, especially the reference librarian Pat Roddick.

Marc Janssens and Jonathan Barnett for their encouragement and advice, particularly at the start of the project.

Jürgen König of Trätek in Sweden for test data and advice. Peter Collier of BRANZ for test data and willingness to answer my questions regarding tests whenever I asked. Hans Gerlich of Winstone Wallboards for permission to use test data from the furnace tests they paid for. Paul Clancy for results and advice.

Also the University of Canterbury for providing a doctoral scholarship and the Foundation for Research Science and Technology for funding for the project.

The other students from this department and from other parts of the university, for friendship and support during my doctorate.

Finally, I would like to thank my wife Joanne for her support, understanding and encouragement during this project.

References

Andersson, L. and Jansson, B. 1987. Analytical Fire Design with Gypsum - A Theoretical and Experimental Study. Institute of Fire Safety Design. Lund. Sweden.

ASTM. 1985. E-119 83. Standard methods of Fire Tests of Building Construction and Materials. American Society for Testing and Materials. Philadelphia. United States.

Atreya, A. 1988. Convection Heat Transfer. The SFPE Handbook of Fire Protection Engineering. Section 1. Chapter 4. Society of Fire Protection Engineers/National Fire Protection Association. Boston. United States.

Babrauskas, V. 1979 COMPF2, A Program for Calculating Post-Flashover Fire Temperatures. U.S. Department of Commerce/National Bureau of Standards. NBS Technical Note 991. Gaithersburg. United States.

Babrauskas, V. and Williamson, R. B. 1975. Post - Flashover Compartment Fires. Fire Research Group, University of California- Berkeley. Report Number UCB FRG 75-1.

Babrauskas, V. and Williamson, R. B. 1978a. Post - Flashover Compartment Fires - Basis of a Theoretical Model. Fire and Materials. Volume 2. Number 2. pp 39-53.

Babrauskas, V. and Williamson, R. B. 1978b. Temperature Measurement in Fire Test Furnaces. Fire Technology. Volume 14. Number 3. pp 226-238

Babrauskas, V. and Williamson, R. B. 1978c. The Historical Basis of Fire Resistance Testing - Part I. Fire Technology. Volume 14. Number 3. pp 184-205.

Babrauskas, V. and Williamson, R. B. 1978d. The Historical Basis of Fire Resistance Testing - Part II. Fire Technology. Volume 14. Number 4. pp 304-316

Babrauskas, V. and Williamson, R. B. 1979. Post - Flashover Compartment Fires - Application of a Theoretical Model. Fire and Materials. Volume 3. Number 1. pp 1-7

Barber, D. J. 1994. Fire Resistance of Epoxied Steel Rods in Glulam Timber. Department of Civil Engineering. University of Canterbury. Research Report Number 94-1. Christchurch. New Zealand.

Barnett, J. R. 1989. The Development of an Analytical Methodology for the Design of Steel Frame Structures Exposed to Fire. Ph.D Dissertation. Worcester Polytechnic Institute. U.M.I. Dissertation Services. United States.

Barnett, J. R. 1991. A New Design Approach For Steel Structures Exposed to Fires. Journal of Fire Protection Engineering Volume 3 Number 1. pp 1-8.

Bodig, J. and Jayne, B.A. 1982. Mechanics of Wood and Wood Composites. Van Nostrand Reinhold. New York. pp 303-306.

Bohm, B. 1977. Fully Developed Polythene and Wood Compartment Fires with Application to Structural Design. Technical University of Denmark. Laboratory of Heating and Air Conditioning.

Buchanan, A. H 1990. Bending Strength of Lumber. Journal of Structural Engineering. Volume 116. Number 5. American Society of Civil Engineers.

Buchanan, A. H 1994 (Editor). Fire Engineering Design Guide. Centre for Advanced Engineering. University of Canterbury. Christchurch. New Zealand.

Clancy, P, Young, S. and Leicester, R. 1994. Modelling of Timber-Framed Barriers in Real Fires. Pacific Timber Engineering Conference. Gold Coast, Australia. pp 273-282.

Clancy, P. 1996. A Model for Predicting the Probability of Failure of Wood Framed Walls and Floors in Real Fire. Wood and Fire Safety. Third International Scientific Conference. Slovak Republic.

Collier, P. C. R. 1991a. Design of Loadbearing Light Timber Frame Walls for Fire Resistance:Part 1. Study Report Number 36. Building Research Association of New Zealand.

Collier, P. C. R. 1991b. Design of Light Timber Framed Walls and Floors for Fire Resistance. Technical Recommendation Number 9. Building Research Association of New Zealand.

Collier, P. C. R. 1992. Design of Loadbearing Light Timber Frame Walls for Fire Resistance: Part 2. Study Report Number 43. Building Research Association of New Zealand.

Collier, P. C. R. 1994. Fires Resistant Light Timber Framed Walls. Pacific Timber Engineering Conference. Gold Coast, Australia. pp 248-254.

Collier, P. C. R. 1996. A Model for Predicting the Fire-Resisting Performance of Small-Scale Cavity Walls in Realistic Fires. Fire Technology. Volume 32. Number 2. pp 120-136.

Collins, M. J. 1983. Density Conversions for Radiata Pine. Forest Research Institute. Rotorua. New Zealand.

Cramer, S. 1995. Fire Endurance Modelling of Wood Floor/Ceiling Assemblies. Proceedings Fire and Materials Conference. Washington D.C. pp 105-114.

CRC. 1991. CRC Handbook of Chemistry and Physics. 71st. Edition. Lide, D. R. Editor.

Currier, P. F. 1993. Development of a Two-Dimensional Fire Endurance Model for Gypsum-Board/Wood-Stud Walls. Forintek Canada Corporation.

Drysdale, D. 1985. An Introduction to Fire Dynamics. John Wiley and Sons. Chichester. United Kingdom.

EUROCODE 5. 1993. Part 1.2. Structural Fire Design. Final Draft.

Fang, J. B. 1981. Repeatibility of Large-Scale Room Fire Tests. Fire Technology Volume 17. Number 1. pp 5-16.

Fredlund, B. 1988. A Model for Heat and Mass Transfer in Timber Structures During Fire, A Theoretical, Numerical and Experimental Study. Department of Fire Safety Engineering. Institute of Science and Technology. Lund University. Sweden.

Fredlund, B. 1993. Modelling of Heat and Mass Transfer in Wood Structures During Fire. Fire Safety Journal. Volume 20. Number 1. pp 39-69.

Fuller, J. J. 1990. Predicting the Thermo-Mechanical Behaviour of A Gypsum-to-Wood Nailed Connection. Master's Thesis. Oregon State University. United States.

Gammon, B. W. 1987. Reliability Analysis of Wood-Frame Assemblies Exposed to Fire. Ph.D. Dissertation. University of California, Berkeley. U.M.I. Dissertation Services. United States.

Gerhards, C. C. 1982. Effect of the Moisture Content and temperature on the Mechanical Properties of Wood: An Analysis of Immediate Effects. Wood and Fibre. Volume 14. Number 1. pp 4-36.

Gerlich, H. 1995. Personal Communication, Hans Gerlich, Winstone Wallboards Limited. Wellington. New Zealand.

Glos, P. and Henrici, D. 1991. Bending Strength and MOE of Structural Timber (Picea abies) at Temperatures up to 150°C. HOLZ ALS ROH-UND WERKSTOFF. v.49 (1991) pp 417-422. Translated from German by, USDA Forest Service. Forest Products Laboratory Library. Madison. Wisconsin. United States.

Groves, A. W. 1958. Gypsum and Anhydrite. Overseas Geological Surveys, Mineral Resources Division, Her Majesty's Stationary Office, London. p 28.

Harmathy, T. Z. 1979. Design to Cope with Fully Developed Files. National Research Council of Canada. DBR Paper Number 854, Division of Building Research. (Reprinted from American Society of Testing and Materials. Special Technical Publication Number 685, 1979)

Harmathy, T. Z. 1981. The Fire Resistance Test and its Relation to Real-World Fires. Fire and Materials. Volume 5. Number 3. pp 112-122.

Harmathy, T. Z. 1983. Fire Severity: Basis of Fire Safety Design. National Research Council of Canada. DBR Paper Number 1148, Division of Building Research. (Reprinted from Fire Safety of Concrete Structures, American Concrete Institute, SP-80. 1983

Harmathy, T. Z. 1988. Properties of Building Materials. The SFPE Handbook of Fire Protection Engineering. Section 1 Chapter 26. Society of Fire Protection Engineers/National Fire Protection Association. Boston. United States.

Harmathy, T. Z. and Mehaffey, J. R. 1982. Normalized Heat Load: A Key Parameter in Fire Safety Design. Fire and Materials. Volume 6. Number 1. pp 27-31.

Harmathy, T. Z. and Mehaffey, J. R. 1983. Post-Flashover Compartment Fires. Fire and Materials. Volume 7 Number 2. pp 49-61.

Harmathy, T. Z. and Mehaffey, J. R. 1987. The Normalized Heat Load Concept and it's Use. Fire Safety Journal Volume 12 Number 1. pp 75-81.

Harmathy, T. Z. and Sultan, M. A. 1988. Correlation between the Severities of The ASTM E119 and ISO 834 Fire Exposures. Fire Safety Journal. Volume 13. Number 3. pp 163-168

Hibbitt, Karlsson and Sorensen Inc. 1994. ABAQUS User Manuals. Version 5.4. Pawtucket. Rhode Island. United States.

Holman, J. P. 1992. Heat Transfer. Edition 7 (S.I. Units). McGraw-Hill. New York. United States.

Ince, N. Z. and Launder, B. E. 1989. On the Computation of buoyancy Driven Flows in Rectangular Enclosures. International Journal of Heat and Fluid Flow. Volume 10 Number 2. pp 110-117.

ISO-834. 1975. Fire Resistance Tests - Elements of Construction. (International Standards Organisation).

Janssens, M. 1994. Thermo - Physical Properties for Wood Pyrolysis Models. Pacific Timber Engineering Conference. Gold Coast, Australia. pp 607-618.

Kawagoe, K. and Sekine, T. 1963. Estimation of Time temperature Curves in Rooms. B.R.I. Occasional Report Number 11. Building Research Institute. Ministry of Construction, Japanese Government.

Keltner, N. R. and Moya, J. L. 1990. Defining The Thermal Environment in Fire Tests. Fire and Materials. Volume 14. Number 4. pp 133-138.

Kirby, B. R, Wainman, D. E.., Tomlinson, L.N., Kay, T.R. and Peacock, B.N. 1994. Natural Fires in Large Scale Compartments - A British Steel Technical, Fire Research Station Collaborative Project. British Steel Technical. Swinden Laboratories. United Kingdom.

König, J. 1991. Modelling the Effective Cross-Section of Timber Frame Members Exposed to Fire. International Council for Building Research Studies and Documentation. Working Commission W18A - Timber Structures Meeting 24. Oxford, United Kingdom. September 1991.

König, J. 1994. Axially Loaded Timber Framed Walls Exposed to Fire on One Side. Pacific Timber Engineering Conference. Gold Coast, Australia. pp 263-272.

König, J. 1995. Fire Resistance of Timber Joists and Load Bearing Wall Frames. Institutet for Trateknisk Forskning (TRÄTEK). Stockholm. Sweden.

König, J. and Kallsner, B. 1988. The Influence of the Support Conditions on the Loadbearing Capacity of Axially Loaded Wood Studs Under Simulated Fire Exposure. Proceedings of the 1988 International Conference on Timber Engineering. Seattle. United States. pp 423-431.

König, J. and Noren, J. 1991 Fire Tests on Timber Frame Members in Pure Bending. International Conference on Timber Engineering. London. United Kingdom. pp 4.75-4.82.

Law, M. 1977. A Relationship Between Fire Grading and Building Design and Contents. Fire Research Station. Fire Research Note Number 877. United Kingdom.

Law, M. 1997. A Review of Formula for T - Equivalent. Proceedings of The Fifth International Symposium on Fire Safety Science. Melbourne. Australia.

Lie, T. T. 1988. Fire Temperature-Time Relations. The SFPE Handbook of Fire Protection Engineering. Section 3 Chapter 5. Society of Fire Protection Engineers/National Fire Protection Association. United States.

Lie, T. T. 1992. (Editor). Structural Fire Protection. American Society of Civil Engineers. Manuals and Reports on Engineering Practice Number 78.

Magnusson, S. E. and Thelandersson, S. 1970. Temperature-Time Curves of Complete Process of Fire Development, Theoretical Study of Wood Fuel Fires in Enclosed Spaces. Acta Polythechnica Scandinavica. Civil Engineering and Building Construction Series Number 65.

Mehaffey, J. R. 1991. Development of Fire Endurance Models for Wood Stud Walls - Progress Report. Forintek Canada Corporation.

Mehaffey, J. R., Cuerrier, P. and Carisse, G. 1994. A model for Predicting heat Transfer Through Gypsum-Board/Wood-Stud Walls Exposed to Fire. Fire and Materials. Volume 18. pp 297-305.

Nilsson, L. 1974. Time Curve of Heat Release for Compartment Fires with Fuel of Wooden Cribs. Lund Institute of Technology. Division of Structural Mechanics and Concrete Construction. Bulletin 36. Lund. Sweden.

NZBIA. 1992. New Zealand Building Code and Approved Documents. New Zealand Building Industry Authority. Wellington. New Zealand.

NZTIF. 1989. Timber Use Manual. Editor Buchanan, A. H. New Zealand Timber Industry Federation. Wellington. New Zealand.

S.A.N.Z. 1990. (Standards Association of New Zealand) N.Z.S. 3604:1990. Code of Practice for Light Timber Frame Buildings Not Requiring Specific Design. Wellington. New Zealand.

S.A.N.Z. 1993. (Standards Association of New Zealand) N.Z.S. 3603:1993. Timber Structures Standard. Wellington. New Zealand.

S.A.N.Z. 1995. (Standards Association of New Zealand) N.Z.S. 3101:1995. Concrete Structures Standard:Part 1 and Part 2. Wellington. New Zealand.

Schleich, J.B. 1993. (Chairman). Fire Engineering Design of Steel Structures: State of The Art. International Iron and Steel Institute.

Stanish, A.J. 1994. Mechanical Properties of Gypsum Plasterboard. Third Professional Year Research Project Report. Department of Civil Engineering. University of Canterbury. Christchurch. New Zealand.

Sterner, E. & Wickstrom, U. 1990. TASEF - Temperature Analysis of Structures Exposed to Fire. Fire Technology SP Report 1990:05. Swedish National Testing Institute.

Sultan, M. A., Harmathy, T. Z. and Mehaffey, J. R. 1986. Heat Transmission in Fire test Furnaces. Fire and Materials. Volume 10. Number 1. pp 47-55.

Thomas, G. C. 1991. The Feasibility of Multistorey Light Timber Frame Buildings. Department of Civil Engineering. Research Report Number 91-2. University of Canterbury.

Thomas, P. H. 1986. (Co-ordinater). Design Guide - Structural Fire Safety. Fire Safety Journal. Volume 10. Number 2. pp 75-138.

Tien, C. L., Lee, K. Y. and Stretton, A. J. 1988. Radiation Heat Transfer. The SFPE Handbook of Fire Protection Engineering. Section 1 Chapter 5. Society of Fire Protection Engineers/National Fire Protection Association. Boston. United States.

Tsehaye A. and Buchanan A.H. 1996. Characteristic Design Stresses for Radiata Pine Grown In Canterbury. Paper to be Published. (Department of Forestry. University of Canterbury. Christchurch. New Zealand.)

Walford, B. 1994. Preliminary Results of an In-Grade Evaluation of Juvenile Radiata Pine. Pacific Timber Engineering Conference. Gold Coast, Australia. pp 725-730.

Williamson, R.B. and Buchanan, A.H. 1972. A Heat Balance Analysis of the Standard Fire Endurance Test. A paper presented at the meeting of Commission W14 of the Conseil International du Bâtiment. Stockholm. Sweden.

Winstones 1989. Twinaplate Structural Beams. Product Brochure. Winstone Litewall Systems. Auckland. New Zealand.

Winstones 1992. Gib Board. Fire Rated Systems. Winstone Wallboards Limited.

Wellington. New Zealand.

Young, S. A and Clancey, P. 1996. Compression Load-Deformation of Timber Walls in Fire. Proc. Wood and Fire Safety. Third International Scientific Conference. Slovak Republic.

Notation

Symbol	Description	Units
a, b	are coefficients used seperately in several equations	( )
A_f	floor area of the compartment	m^2
A_h	total area of horizontal openings	m^2
A_t	total area of the bounding surfaces of the compartment	m^2
A_v	total area of vertical openings	m^2
A_w	total window area	m^2
B	extinction coefficient	m^{-1}
b_v	function of the ratio of vertical openings' area to floor area	( )
c	accounts for different compartment linings	( )
C_p	specific heat	kJ/kg.K
g	gravitational acceleration	m^2/s
Gr	Grashof number, ratio of buoyancy forces to viscous forces	( )
h	convective heat transfer coefficient	$W/m^2.K$
H_c	compartment height	m
H_v	effective height of the vertical openings	m
k	thermal conductivity	W/m.K
k_{air}	conductivity of air	W/m.K
k_w	conductivity of wood	W/m.K
l	characteristic dimension	m

Symbol	Description	Units
L	mean path length	m
NE	total number of elements	( )
NE_y	number of elements across the model or the bandwidth	( )
NN	total number of nodes	( )
Nu	Nusselt number, dimensionless heat transfer coefficient	( )
p	axial load	kN
P	floor pressure	kPa
Pr	Prandtl number, ratio diffusion of momentum to heat diffusion	( )
q	rate of heat transferred	kW/m^2
Q	internally generated heat	kW/m^3
Q_f	fuel load	MJ/m^2
Ra	Rayleigh number	( )
R_{max}	maximum rate of fuel consumption	kg/min
T	absolute temperature	K
t	time	s
T_{air}	temperature of the void	K
T_c	temperature in celsius	^oC
t_e	equivalent time of exposure to an ISO-834 test	min
T_f	flame temperature	K
T_g	gas temperature	K
$T_{node,i}$	temperature of ith node	K
T_s	surface temperature	K

Symbol	Description	Units
T_t	thermocouple temperature	K
T_w	fluid temperature next to wall surface	K or ^{O}C
T_x	furnace wall temperature	K
T_∞	bulk fluid temperature	K or ^{O}C
u	moisture content	( )
V	opening factor	$m^{1/2}$
W	ventilation factor	$m^{-1/4}$
x	a spatial co-ordinate	m
y	a spatial co-ordinate	m
z	a spatial co-ordinate	m

Greek Symbols

Symbol	Description	Units
α	thermal diffusivity	m^2/s
α_h	ratio of horizontal openings area to floor area	( )
α_v	ratio of vertical opening area to floor area	( )
β	convection coefficient	W/m^2
Δc	correction to specific heat of wood to allow for bound moisture	( )
ΔE_{air}	change in energy of the air in the void	MJ/m
ΔT_i	temperature differance between ith node and void	K
ε	resultant emissivity of the gas and the boundary	( )
ε_1	emissivity of one surface	( )
ε_2	emissivity of another parallel surface	( )

Symbol	Description	Units
ε_{CO_2}	emissivity of carbon dioxide	( )
ε_{eff}	overall effective emissivity	( )
ε_f	the flame emissivity	( )
ε_g	the gas emissivity	( )
ε_{H_2O}	the emissivity of water	( )
ε_s	the emissivity of soot	( )
ε_w	the emissivity of wood	( )
ε_x	the furnace wall emmisivity	( )
γ	convection power, usually 1.33	( )
Γ	thermal inertia of a material	$Ws^{1/2}/m^2K$
ρ	density	kg/m^3
σ	Stefan -Boltzmann constant ($5.67*10^{-8}$)	W/m^2K^4
$\sum H_c$	sum of convective heat flux over length	MJ/m